



Investigating biological features of
Type IV pili in *Clostridioides difficile*

Ziyi Wang

Supervisor: Dr Paula Salgado

Thesis submitted for the degree of Doctor of Philosophy

Newcastle University Biosciences Institute

February 2023

Abstract

Clostridioides difficile is a Gram-positive multidrug-resistant pathogen, capable of releasing toxins and colonising the gut. *C. difficile* infections (CDI) lead to symptoms ranging from mild diarrhoea to toxic megacolon and pseudomembranous colitis and, in some severe cases, death. Recurrent CDI episodes are also a considerable issue and one of the main reasons for the burden on healthcare systems caused by *C. difficile*.

Type IV pili (TFP) are protein filaments that extrude from bacterial cells and are found in Gram-positive and Gram-negative pathogens. TFP have been shown to enhance virulence and described functions include bacterial motility, colonisation, biofilm formation and DNA up taking.

In this work, genes in the primary cluster encoding TFP proteins, particularly PilA1, the major pilin composing TFP, and PilD1, one of the pre-pilin peptidases, and the minor pilin PilJ were studied in detail.

Mutagenesis studies of PilA1, PilD1 and PilJ (a minor pilin) were performed and their role in *C. difficile* TFP biosynthesis, biofilm formation and motility was investigated. Interestingly, PilD1 and PilJ are not required in TFP biosynthesis in cell growth, unlike previous observations for other TFP, but PilD1 seems to be important on solid media. Surprisingly, flagella expression is affected in the mutants suggesting a potential crosstalk between twitching and swimming motility beyond c-di-GMP regulation.

This work furthers current understanding of biological features of *C. difficile* TFP. It raises new research questions regarding the interplay between *C. difficile* TFP and flagella. Together, this provides a deeper understanding of mechanisms involved in CDI that could be explored as novel therapeutic targets.

Acknowledgements

Firstly, I would like to thank my supervisor Dr Paula Salgado for offering me the opportunity to do a PhD, supporting and mentoring with patience and warmth, through all the circumstances I have been through during my PhD, especially changing project and being away during COVID-19. Beyond science and research, I have gained philosophical thinking and new attitudes to continue exploring life and the world. I will always appreciate being Dr Paula Salgado's student, who inspired me with her positivity, intelligence and open mind.

Thanks to all past and current members of Salgado, Waldron and Hirt groups. A special thank you to Dr Anna Barwinska-Sendra, Dr Marcin Dembek and Dr Emma Tarant for always being patient and supportive with their wisdom and skills and teaching me how to overcome many experimental problems I had, especially in the early stages. Thanks to Dr Paola Lanzoni-Mangutchi for being a friendly and enthusiastic peer, who always come up with cheerful chats, entertainments and wonderful Brazilian food. Also, thanks to Dr Henrik Strahl's group for help with microscopy and to the Fagan, Tamayo and Sievers groups for sharing helpful protocols and materials.

I would like to thank my friends who made me feel at home during my PhD, occasionally celebrated Chinese festivals together and cooked a bit of taste of home: Dr Yiling Zhu, Effy Mu, Dr Chun Chen, Amelia Lu, Ian Fairclough, Carol Fan, Peiran Shen, Dr Yuetao Li, Dr Alyson Dawn, Mengran Cai, Liangxun Xie, Angela Wong, Koon Wai, Dr Gewei Zhu, Dr Yao Hao and Dr Xuefei Yu. As well as my friends back in China, who supported me across the distance and during COVID-19 when I was back with them: Shengmeng Hou, Zitong Chen, Haozheng Yang and Hanwen Xue. Especially, Shengmeng for always standing with me and sharing all my thoughts and feelings.

I will always be grateful to my parents, who supported me on everything I would love to do with their unconditional love and anything they own. Thanks to my cousins Xingming and Zike, who provided room and space for me to study during COVID-19, as well as my grandparents, aunt Xiuying and cousin-in-law Ning.

I would never been able to do this without you all!

Table of Contents

Chapter 1: Introduction	1
1.1. <i>Clostridioides difficile</i>	1
1.1.1. <i>Life Cycle</i>	1
1.1.2. <i>Strain characterisation</i>	4
1.1.3. <i>Infection and Pathogenesis</i>	5
1.2. Type IV Pili	7
1.2.1. <i>Components of Type IV Pili</i>	8
1.2.2. <i>Type IV Pili in Clostridia species</i>	14
1.3. TFP in <i>C. difficile</i>	16
1.3.1. <i>C. difficile TFP Gene Clusters</i>	16
1.3.2. <i>Induction of TFP in C. difficile</i>	21
1.3.3. <i>Functions of TFP in C. difficile</i>	24
1.4. c-di-GMP and flagella ON-/OFF-phase	26
1.5. Aims and objectives	30
Chapter 2: Materials and Methods	31
2.1. Bacterial strain and Growth Conditions	31
2.1.1. <i>Culturing Escherichia coli</i>	31
2.1.2. <i>Culturing C. difficile</i>	31
2.1.3. <i>Storage of Strains</i>	32
2.1.4. <i>Transformation of E. coli</i>	32
2.1.5. <i>Plasmid DNA Conjugation into C. difficile</i>	33
2.2. Bioinformatics	34
2.2.1. <i>DNA, Gene and Protein Analysis</i>	34
2.3. DNA Manipulation	34
2.3.1. <i>Genomic DNA Extraction</i>	34
2.3.2. <i>Purification of Plasmid DNA</i>	34
2.3.3. <i>Polymerase Chain Reaction (PCR) and Primers</i>	35
2.3.4. <i>Agarose Gel Electrophoresis</i>	35
2.3.5. <i>Purification of PCR Products</i>	36
2.3.6. <i>Restriction Digests</i>	36
2.3.7. <i>DNA Ligation</i>	36
2.3.8. <i>Gibson Assembly</i>	37
2.3.9. <i>Allele Exchange Mutagenesis</i>	37
2.3.10. <i>Vector Construction</i>	38

2.4.	Protein Manipulation	39
2.4.1.	<i>Protein Expression in C. difficile</i>	39
2.4.2.	<i>Tri-Chloroacetic Acid Precipitation of Protein</i>	39
2.5.	SDS-PAGE and Immunoblotting.....	39
2.5.1.	<i>Cell lysate Preparation</i>	39
2.5.2.	<i>SDS-PAGE and Coomassie Staining</i>	40
2.5.3.	<i>Immunoblotting</i>	40
2.6.	Phenotypic Analysis.....	41
2.6.1.	<i>Growth Curves</i>	41
2.6.2.	<i>Flagella Motility Assays</i>	41
2.6.3.	<i>Twitching Motility Assays</i>	41
2.6.4.	<i>Biofilm Assays</i>	41
2.6.5.	<i>Phase Contrast Microscopy</i>	42
2.6.6.	<i>Statistical analysis</i>	42
Chapter 3:	c-di-GMP Impact on Cell Growth and TFP Expression.....	43
3.1.	Introduction.....	43
3.2.	Effects of c-di-GMP on <i>C. difficile</i> Cell Growth and TFP expression	44
3.2.1.	<i>dccA induction and CD630 growth and cell morphology</i>	44
3.2.2.	<i>TFP expression in C. difficile 630 under optimised ATc concentration</i>	50
3.3.	Impact of TFP Proteins on Cell Growth	52
3.3.1.	<i>pilA1 expression in ΔpilA1 mutant and complement strains</i>	52
3.3.2.	<i>Effect of PilA1 in growth and cell morphology</i>	56
3.3.3.	<i>TFP expression in 630ΔpilD1</i>	59
3.3.4.	<i>Effect of pilD1 in cell growth</i>	62
3.3.5.	<i>Role of pilD1 in cell morphology</i>	63
3.3.6.	<i>TFP expression in 630ΔpilJ</i>	65
3.3.7.	<i>Effect of PilJ in growth</i>	67
3.3.8.	<i>Effects of PilJ in cell morphology</i>	68
3.4.	<i>Effects of c-di-GMP induction and TFP proteins in biofilm formation</i>	70
3.4.1.	<i>Biofilm formation in CD630</i>	70
3.4.2.	<i>Biofilm formation in ΔpilA1</i>	71
3.5.	Discussion	72
Chapter 4:	Motility in <i>C. difficile</i>	74
4.1.	Introduction.....	74
4.2.	Motility in <i>C. difficile</i> 630.....	75

4.2.1.	<i>Twitching Motility of CD630</i>	75
4.2.2.	<i>Expression of PilA1 in 1.8% agar</i>	76
4.2.3.	<i>Flagella Expression in CD630 in 1.8 % agar</i>	78
4.2.4.	<i>Swimming Motility of CD630</i>	80
4.3.	Motility in CD630 $\Delta pilA1$ mutant	81
4.3.1.	<i>Effects of PilA1 in CD630 Twitching Motility</i>	81
4.3.2.	<i>TFP and flagella Expression in $\Delta pilA1$ mutant and complement strains grown on 1.8% agar</i>	84
4.3.3.	<i>Effects of PilA1 on Swimming Motility</i>	86
4.3.4.	<i>Flagella Expression in $\Delta pilA1$ mutant and complement strains</i>	87
4.4.	Motility in CD630 $\Delta pilD1$ mutant	88
4.4.1.	<i>Effects of PilD1 on Twitching Motility</i>	88
4.4.2.	<i>Expression of pilA1 in $\Delta pilD1$ and complement strains on 1.8% agar</i>	91
4.4.3.	<i>Effects of PilD1 on Swimming Motility</i>	93
4.4.4.	<i>Flagella Expression in pilD1 mutant and complement strains</i>	94
4.5.	Motility in CD630 $\Delta pilJ$ mutant	96
4.5.1.	<i>Effects of PilJ on Twitching Motility</i>	96
4.5.2.	<i>Expression of pilA1 in $\Delta pilJ$ and complement strains on 1.8% agar</i>	98
4.5.3.	<i>Effects of PilJ on Swimming Motility</i>	100
4.5.4.	<i>Flagella Expression in $\Delta pilJ$ mutant and complement strains</i>	101
4.6.	Discussion	102
Chapter 5: Discussion and future work		106
5.1.	c-di-GMP effects on pili, flagella and cell division	106
5.2.	Genetic diversity of TFP genes in <i>C. difficile</i>	108
5.3.	Factors affecting colony and cell morphology	111
5.4.	The role of pre-pilin peptidases	112
References		114
Appendix A		129
Appendix B		136
Appendix C		147
Appendix D		150
Appendix E		153

List of figures

Figure 1-1. <i>C. difficile</i> spores	2
Figure 1-2. Life cycle of <i>C. difficile</i> during infection	3
Figure 1-3. The pathogenicity locus (PaLoc)	6
Figure 1-4. <i>C. difficile</i> transferase (CDT) locus (CDTloc).....	7
Figure 1-5. Gram-negative and Gram-positive TFP assembly.....	8
Figure 1-6. Crystal structure of full-length PilE1 from <i>N. gonorrhoeae</i>	9
Figure 1-7. Movements and functions of PilB and PilT ATPase	11
Figure 1-8. Type VI Pili gene loci in <i>C. perfringens</i>	15
Figure 1-9. Type VI Pili gene loci in <i>C. difficile</i>	17
Figure 1-10. Crystal structure of PilA1 from <i>C. difficile</i>	18
Figure 1-11. PilA1 and PilJ localisation on <i>C. difficile</i> TFP	20
Figure 1-12. Crystal structure and incorporation of subunits in <i>C. difficile</i> TFP	21
Figure 1-13. Predicted secondary structure of Cdi2_4 c-di-GMP-II riboswitch-mediated transcription regulator.....	22
Figure 1-14. c-di-GMP induces TFP formation	24
Figure 1-15. TFP-mediated surface motility stimulated by c-di-GMP	25
Figure 3-1. <i>C. difficile</i> growth under varying ATc concentrations.....	45
Figure 3-2. <i>C. difficile</i> CD630 cell morphology under varying ATc concentrations.....	46
Figure 3-3. <i>C. difficile</i> 630_pASF85 cell morphology under ATc concentrations.....	47
Figure 3-4. <i>C. difficile</i> 630_pECC17 cell morphology under ATc concentrations.....	48
Figure 3-5. <i>C. difficile</i> growth with and without ATc supplementation.....	49
Figure 3-6. <i>C. difficile</i> cell morphology with and without ATc supplementation	50
Figure 3-7. Immunoblot detection of PilA1 in <i>C. difficile</i> extracts.....	52
Figure 3-8. Colony PCR for pZGW005 and pZGW006 plasmids	53
Figure 3-9. Immunoblot detection of PilA1 in <i>C. difficile</i> 630 $\Delta pilA1$ and complement strains.....	55
Figure 3-10. CD630 and $\Delta pilA1$ growth curves and rates	57
Figure 3-11. Effects of <i>pilA1</i> in cell morphology	58
Figure 3-12. Screening of $\Delta pilD1$ mutants and complementation	60
Figure 3-13. Immunoblot detection of PilA1 in <i>C. difficile</i> 630 <i>pilD1</i> mutant and its complement strain.....	61

Figure 3-14. CD630 and $\Delta pilD1$ growth curves and rates.....	63
Figure 3-15. Effect of <i>pilD1</i> in cell morphology	64
Figure 3-16. Screening of $\Delta pilD1$ mutants and complementation.....	66
Figure 3-17. Immunoblot detection of PilA1 in CD630 $\Delta pilJ$ mutant and its complement strain	67
Figure 3-18. CD630 and $\Delta pilJ$ growth curves and rates.....	68
Figure 3-19. Effects of PilJ in cell morphology.....	69
Figure 3-20. CD630 biofilm formation.....	70
Figure 3-21. CD630 and $\Delta pilA1$ biofilm formation	71
Figure 4-1. CD630 colony size and morphology on 1.8% agar	76
Figure 4-2. Immunoblot detection of PilA1 in CD630 on 1.8% agar	77
Figure 4-3. Immunoblot detection of FliC	79
Figure 4-4. Colony diameter variation in 0.3% agar	80
Figure 4-5. Colony morphology on 0.3% agar	81
Figure 4-6. Effect of PilA1 on colony diameter in 1.8% agar	82
Figure 4-7. Effect of <i>pilA1</i> on colony morphology on 1.8% agar	83
Figure 4-8. Immunoblot detection of PilA1 in $\Delta pilA1$ and complement strains on 1.8% agar	84
Figure 4-9. Immunoblot detection of FliC in 630 $\Delta pilA1$ mutant and complement strains on 1.8% agar	85
Figure 4-10. $\Delta pilA1$ and complement strains colony diameter variation in 0.3% agar.....	86
Figure 4-11. Immunoblot detection of FliC in $\Delta pilA1$ mutant and complement strains...	88
Figure 4-12. Effect of PilD1 in colony diameter in 1.8% agar	89
Figure 4-13. Effect of PilD1 and complement colonies on 1.8% agar	90
Figure 4-14. Immunoblot detection of PilA1 in 630 $\Delta pilD1$ and complement strains on 1.8% agar	91
Figure 4-15. Immunoblot detection of FliC in <i>C. difficile</i> 630 $\Delta pilD1$ and complement strains on 1.8% agar	93
Figure 4-16. Variations in colony diameter for 630 $\Delta pilD1$ and complement strains grown in 0.3 % agar	94
Figure 4-17. Immunoblot detection of FliC in <i>C. difficile</i> 630 $\Delta pilD1$ and complement strains	95

Figure 4-18. Effect of PilJ on colony diameter in 1.8 % agar	96
Figure 4-19. $\Delta pilJ$ and complement colonies on 1.8% agar plates	97
Figure 4-20. Immunoblot detection of PilA1 in 630 $\Delta pilJ$ and complement strains on 1.8% agar.....	98
Figure 4-21. Immunoblot detection of FliC in 630 $\Delta pilJ$ and complement strains on 1.8% agar.....	99
Figure 4-22. Effect of <i>pilJ</i> on colony diameter in 0.3 % agar	100
Figure 4-23. Immunoblot detection of FliC in <i>C. difficile</i> 630 $\Delta pilJ$ and complement strains	102
Figure 5-1. Sequence similarity of riboswitch Cdi2_4 and primary TFP cluster genes from 47 <i>C. difficile</i> isolates.....	109
Figure 5-2. Phylogenetic tree of <i>C. difficile pilA1</i> genes	110
Figure A-1. Plasmid map of pECC17 containing inducible region.....	133
Figure A-2. Plasmid map of pECC109 containing inducible region.....	133
Figure A-3. Screening of putative $\Delta pilA1$ mutant	134
Figure A-4. Screening of pECC109 in $\Delta pilA1$ mutant	134
Figure A-5. Plasmid map of pZGW005 containing inducible region	135
Figure A-6. Plasmid map of pZGW006 containing inducible region	135
Figure B-1. $\Delta pilA1$ growth curves and rates with vector control.....	136
Figure B-2. $\Delta pilA1$ cell morphology with vector control.....	136
Figure B-3. $\Delta pilD1$ growth curves and rates with vector control.....	137
Figure B-4. $\Delta pilD1$ cell morphology with vector control.....	137
Figure B-5. <i>pilJ</i> growth curves and rates with vector control.....	138
Figure B-6. <i>pilJ</i> cell morphology with vector control.....	138
Figure B-7. $\Delta pilD1$ biofilm formation	139
Figure B-8. <i>pilJ</i> biofilm formation	139
Figure B-9. <i>C. difficile</i> 630 colony size and morphology on 1.8 % agar	140
Figure B-10. $\Delta pilA1$ and complement colonies on 1.8 % agar plates	141
Figure B-11. Colony diameter in 1.8% agar of 630 $\Delta pilA1$ and vector control.....	142
Figure B-12. Colony diameter variation in 0.3 % agar of $\Delta pilA1$ and complement strains	142
Figure B-13. $\Delta pilD1$ and complement colonies on 1.8 % agar plates	143

Figure B-14. Colony diameter in 1.8 % agar of 630 Δ <i>pilD1</i> and vector controls.....	144
Figure B-15. Colony diameter variation in 0.3 % agar of Δ <i>pilD1</i> and complement strains	144
Figure B-16. Δ <i>pilJ</i> and complement colonies on 1.8 % agar plates.....	145
Figure B-17. Colony diameter in 1.8 % agar of 630 Δ <i>pilJ</i> and vector controls.....	146
Figure B-18. Colony diameter variation in 0.3% agar of Δ <i>pilJ</i> and complement strains.....	146
Figure D-1. <i>C. difficile</i> TFP platform proteins.....	150
Figure D-2. <i>C. difficile</i> TFP minor pilins.....	151
Figure D-3. <i>C. difficile</i> TFP pre-pilin peptidases.....	151
Figure D-4. <i>C. difficile</i> predicted TFP platform proteins on the secondary gene cluster	152
Figure D-5. <i>C. difficile</i> TFP minor pilins on other gene loci.....	152

List of Tables

Table 1-1. Current grouping of selected <i>C. difficile</i> strains.....	5
Table 2-1. <i>Clostridioides difficile</i> Defined Medium (CDMM) composition.....	32
Table 2-2. <i>C. difficile</i> 630 strains used in biological assays in this study.....	33
Table A-1. Primers used in this study.....	129
Table A-2. Plasmids used in this study.....	132
Table A-3. Antibodies used in this study.....	132
Table C-1. Nucleotide similarities of 47 <i>C. difficile</i> isolates by BLAST.....	147
Table C-2. Template genes for nucleotide similarity BLAST.....	148
Table C-3. References of isolates used in nucleotide similarity analysis.....	149
Table E-1. Quantified band intensity of PilA1 signals from <i>C. difficile</i> 630 in Figure 3-7	153
Table E-2. Quantified band intensity of PilA1 signals from <i>C. difficile</i> 630 <i>pilA1</i> mutant and complement strains in Figure 3-9.....	154
Table E-3. Quantified band intensity of PilA1 signals from <i>C. difficile</i> 630 <i>pilD1</i> mutant and complement strains in Figure 3-13.....	155
Table E-4. Quantified band intensity of PilA1 signals from <i>C. difficile</i> 630 <i>pilJ</i> mutant and complement strains in Figure 3-17.....	155
Table E-5. Quantified band intensity of FliC signals from <i>C. difficile</i> 630 in Figure 4-3...	156
Table E-6. Quantified band intensity of PliA1 signals from <i>C. difficile</i> 630 <i>pilA1</i> mutant and	

complement strains on 1.8% agar in Figure 4-8	156
Table E-7. Quantified band intensity of FliC signals from <i>C. difficile</i> 630 <i>pilA1</i> mutant and complement strains on 1.8% agar in Figure 4-9	157
Table E-8. Quantified band intensity of FliC signals from <i>C. difficile</i> 630 <i>pilA1</i> mutant and complement strains in culture in Figure 4-11	158
Table E-9. Quantified band intensity of PilA1 signals from <i>C. difficile</i> 630 <i>pilD1</i> mutant and complement strains on 1.8% agar in Figure 4-14	159
Table E-10. Quantified band intensity of FliC signals from <i>C. difficile</i> 630 <i>pilD1</i> mutant and complement strains on 1.8% agar in Figure 4-15	159
Table E-11. Quantified band intensity of FliC signals from <i>C. difficile</i> 630 <i>pilD1</i> mutant and complement strains in culture in Figure 4-17	159
Table E-12. Quantified band intensity of PliA1 signals from <i>C. difficile</i> 630 <i>pilJ</i> mutant and complement strains on 1.8% agar in Figure 4-20	160
Table E-13. Quantified band intensity of FliC signals from <i>C. difficile</i> 630 <i>pilJ</i> mutant and complement strains on 1.8% agar in Figure 4-21	160
Table E-14. Quantified band intensity of FliC signals from <i>C. difficile</i> 630 <i>pilJ</i> mutant and complement strains in culture agar in Figure 4-21	160

List of abbreviations

ATc	Anhydrotetracycline
BHIS	Braine heart infusion - supplemented
bp	Basepair
CDI	<i>Clostridioides difficile</i> infection
c-di-GMP	3'-5' cyclic diguanosine monophosphate
CD630	<i>Clostridioides difficile</i> strain 630
CDMM	<i>C. difficile</i> minimal medium
cm	Centimeter
DMSO	Dimethylsulfoxide
DNA	Deoxyribonucleic acid
dNTPs	Deoxyribonucleotide triphosphate
DTT	Dithiothreitol
EDTA	Ethylenediaminetetraacetic acid
g	Gravitational constant
gDNA	Genomic DNA
kb	Kilobase
kDa	KiloDalton
LB	Luria broth
min	Minute
mg	Milligram
mM	Millimolar
mm	Millimeter
ml	Milliliter
mw	Molecular weight
MLST	Multilocus sequence typing
ng	Nanogram
nm	Nanometer
OD ₅₉₅	Optical density at 595nm
OD ₆₀₀	Optical density at 600nm
O/N	Overnight
PBS	Phosphate-buffered saline

PCR	Polymerase chain reaction
rpm	Revolutions per minute
RT	PCR-ribotyping or room temperature
SDS	Sodium dodecyl sulphate
SDS-PAGE	Sodium dodecyl sulphate polyacrylamide gel electrophoresis
TAE	Tris base, acetic acid and EDTA
TBS	Tris-buffered saline
TBST	Tris-buffered saline with Tween
TBSTM	Tris-buffered saline with Tween and milk
TCA	Tri-chloroacetic acid
TEMED	N, N, N', N'-tetramethylethane-1,2-diamine
TFP	Type VI pili
UV	Ultraviolet
WT	Wild type
W/V	Weight / volume
µg	Microgram
µl	Microliter

Chapter 1: Introduction

1.1. *Clostridioides difficile*

Clostridioides difficile is a Gram-positive, anaerobic, and opportunistic human pathogen. When the normal gut microbiota is disrupted, *C. difficile* colonises the gut epithelium, releases toxins, and leads to inflammation, known as *C. difficile* infection (CDI). Disruption of normal gut microbiota is largely due to broad-spectrum antibiotic treatments that also kill non-virulent bacteria in the gut microbiota. Gut microbiota can protect the host from CDI by competing for nutrition, activating immunity, producing antibiotics, or modifying metabolic products (Horvat and Rupnik, 2018; Rosa et al., 2018). Gut microbiota is composed by diverse species, but major phyla are *Firmicutes*, *Bacteroidetes*, *Actinobacteria*, *Proteobacteria* and *Verrucomicrobia* (Tap et al., 2009). It has also been demonstrated that gut microbiota processes bile salts and inhibits *C. difficile* growth (Buffie et al., 2015; Studer et al., 2016), *Bacteroides thetaiotaomicron* cleaves sialic acid and competes with *C. difficile* growth and expansion (Martens et al., 2008; Ng et al., 2013). Members of the gut microbiota can also produce bacteriocins which kill *C. difficile*, such as thuricin CD that causes *C. difficile* cell lysis (Mathur et al., 2017), Ruminococcin C1 which inhibits nucleic acid synthesis in Gram-positive bacteria (Chiumento et al., 2019). The disruption of gut microbiota creates an opportunity for *C. difficile*, as a multidrug resistant pathogen, to proliferate in the bowel.

Symptoms of CDI can range from mild to severe diarrhoea, pseudomembranous colitis, and potentially fatal toxic megacolon (Sayedy et al., 2010). In the last 10 years, more than 10,000 cases of CDI were reported annually in England, with 15,919 cases reported from July 2021 to July 2022 (Public Health England, 2022). CDI is also a highly recurrent infection, it has been reported a second recurrence occurs in 40 % of patients, and further recurrence reported in 45 % - 60 % of patients (Song and Kim, 2019).

1.1.1. Life Cycle

As an anaerobic species, *C. difficile* is very sensitive to oxygen, however, *C. difficile* forms endospores (referred to as spores) before entering the aerobic environment (Figure 1-1). In

the spores, DNA transferred from the mother cell is protected by small acid-soluble proteins, calcium-chelated dipicolinic acid and reduced water content (Setlow, 2007).

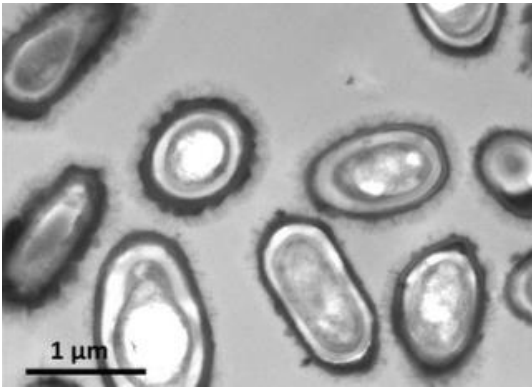


Figure 1-1. *C. difficile* spores

The figure shows purified spores visualised by transmission electron microscopy (TEM). Bar scale: 1 μm. Adapted from Pizarro-Guajardo *et al.* (2020).

Once the spores are released into the environment, they can persist for long periods of time and wait until encountering the next host (Figure 1-2). When the spores enter the digestive system of a host, either animal or human, they can germinate to produce vegetative cells. During this irreversible process, the spores rehydrate, and its cortex is degraded (Vincent and Manges, 2015).

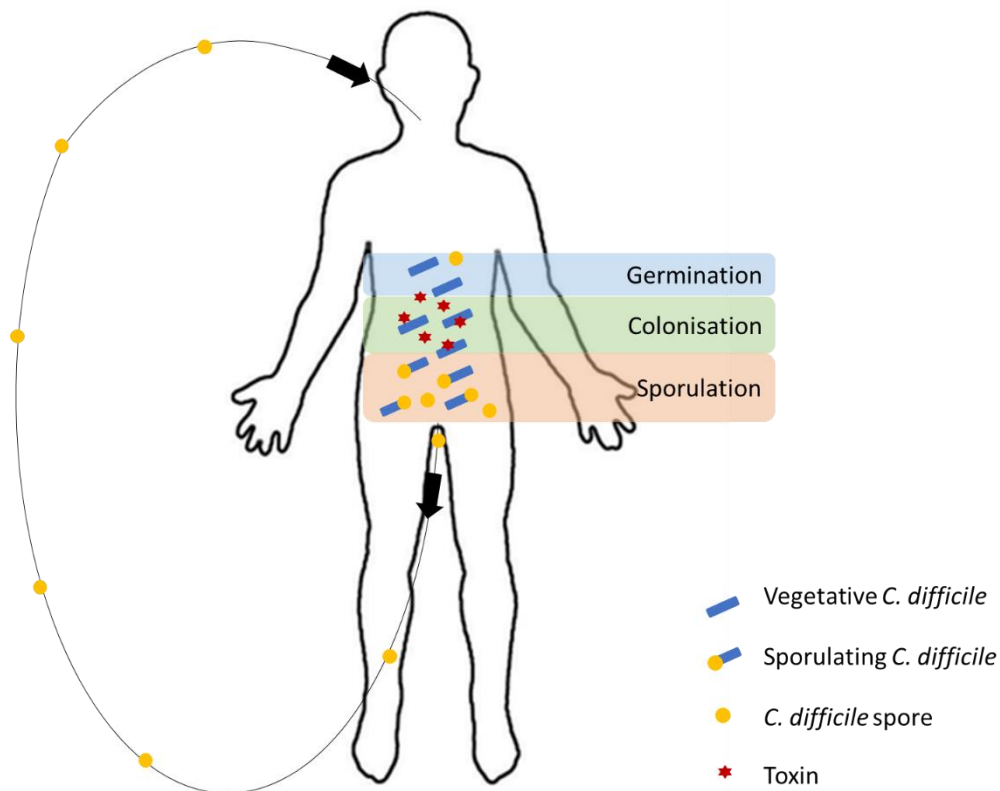


Figure 1-2. Life cycle of *C. difficile* during infection

The figure shows the life cycle of *C. difficile* during infecting a host. Spores (yellow) are ingested from aerobic environment and germinate to vegetative cells in the anaerobic environment when stimulated by germinants such as bile salts. Vegetative cells (blue) colonise the gut epithelia, form biofilms and release toxins (red) to disrupt the lining of epithelial cells which results in the clinical symptoms. Spores are produced when exposed to oxygen or deprived of nutrients. The highly resistant dormant spores are released into the aerobic environment and will enter other or the same host.

A CDI patient will shed spores during and after the infection, where *C. difficile* can then be found in the immediate environment, particularly in hospitals (Barra-Carrasco and Paredes-Sabja, 2014). Spores are found on the shoes of hospital workers and can survive on disinfected surfaces and gowns (Dyer et al., 2019; Janezic et al., 2018).

The initiation of germination occurs when spores bind to germinants, for example, bile salts and amino acids (Setlow, 2003; Setlow et al., 2017). Though the receptor of binding has not been identified, a germination-specific protease, CspC, may function as a signalling node to sense germinants and/or transduce germinant signal (Lawler et al., 2020; Rohlfing et al., 2019). Primary bile salts, cholate and chenodeoxycholate, are found in the large intestine.

These bile salts can be conjugated with taurine, producing taurocholate or taurochenodeoxycholate, which promote *C. difficile* spore germination. Cholate and chenodeoxycholate can be metabolised by the normal gut microbiota and produce secondary bile salts, deoxycholate and lithocholate, that prevent *C. difficile* spore germination, chenodeoxycholate can also prevent the growth of vegetative *C. difficile* (Sorg and Sonenshein, 2010, 2009; Vincent and Manges, 2015).

1.1.2. Strain characterisation

In molecular epidemiological studies of CDI, a range of techniques has been widely used. The genome of *C. difficile* strain 630 was firstly sequenced completely and annotated in 2006 (Sebahia et al., 2006), which has become the benchmark strain used in research, including this work. Interestingly, *C. difficile* genomes have been documented with a high proportion of mobile genetic elements, with an ultra-low level of genetic conservation across strains (16 %-32 %) (Janvilisri et al., 2009; Knight et al., 2016; Scaria et al., 2010; Stabler et al., 2006).

PCR-ribotyping is one of the popular methods in *C. difficile* genomic studies and is also a useful diagnostic tool to track outbreaks and understand *C. difficile* epidemiology. For example, several ribotypes (RT027, RT078, RT017, RT053) have been identified during *C. difficile* outbreaks in hospital, and are therefore considered virulent strains that can lead to infections (Goorhuis et al., 2008; Kabała et al., 2021; Kuijper et al., 2008; Loo et al., 2005; McDonald et al., 2005; Moloney et al., 2021; Pépin et al., 2004; Waterfield et al., 2022). PCR-ribotyping targets the intergenic spacer region (ISR) between the 16S and 23S rRNA genes (Bidet et al., 1999). By PCR amplifying 16S – 23S rRNA ISRs, a primer pair results in a pattern of bands unique to a specific PCR-ribotype (RT) (range from 200 to 700 bp) due to the difference in lengths in the ISRs (Bidet et al., 1999; Janezic and Rupnik, 2010). The mechanisms behind the variation in the 16S – 23S rRNA ISRs are proposed to be slipped-strand mispairing and intra- and possibly interchromosomal homologous recombination (Indra et al., 2010).

Using multilocus sequence typing (MLST), six distinct phylogenetic lineages (clades 1-5 and C-I) were recognised (Eyre et al., 2013; Griffiths et al., 2010; Janezic and Rupnik, 2015; Stabler et al., 2012) (Table 1-1). Clade 1 is heterogeneous and includes clinically toxigenic and non-

toxigenic MLST sequence types (STs) and PCR-ribotypes (RTs) (Janezic and Rupnik, 2015; Wu et al., 2019). A hypervirulent PCR-ribotype, RT027, is representative of clade 2, which has been causing severe outbreaks, especially in Europe and North America (Kabała et al., 2021; Kuijper et al., 2008; Lim et al., 2014; O'Connor et al., 2009; Tickler et al., 2014; Waterfield et al., 2022). RT023 belonging to clade 3 was isolated from humans in Europe and China (Bauer et al., 2011). RT017 from clade 4 caused outbreaks in Europe and North America (Alfa et al., 2000; Kuijper et al., 2001, 2007; Moloney et al., 2021) and is also responsible for the most CDI cases in Asia (Collins et al., 2013). Clade 5 is also highly heterogeneous, containing a diverse collection of sources from clinical, animal, and food worldwide (Collins et al., 2013; Suo et al., 2017). Clade C-I contains non-toxigenic strains only. This clade is identified as highly divergent from other clades by phylogenetic tree analysis, which was even speculated to be a novel species (Dingle et al., 2014).

Table 1-1. Current grouping of selected *C. difficile* strains

Clade	Number of STs	Prominent strains		Other PCR ribotypes represented within these STs
		PCR ribotype	MLST - ST	
1	104	RT001	ST3	RT009, RT055, RT072, RT77, RT115, RT262, RT268, RT305 RT030, RT038, RT046, RT104, RT159
	115	RT002	ST8, ST35, ST48, ST146	
		RT012	ST54	-
		RT014	ST2, ST13, ST14, ST49, ST50, ST132	RT007, RT020, RT025, RT076, RT095, RT129, RT169, RT220
		RT015	ST10, ST44	RT116, RT062
		RT018	ST17	RT052
2	19	RT027	ST1	RT016, RT036, RT176
	14	RT106	ST41, ST42, ST135	RT118, RT135, RT156, RT174, RT194, RT208, RT321
		RT244	ST41	RT156, RT208
3	4	RT023	ST5, ST22, ST25	RT063, RT212, RT122
	4			
4	13	RT017	ST37, ST86	RT047
	16			
5	3	RT078	ST11	RT033, RT045, RT066, RT126, RT127, RT193, RT237, RT280, RT281
	3			
	5	ND	ST177, ST178, ST179, ST180, ST181	-

1.1.3. Infection and Pathogenesis

C. difficile toxin A and B

The key virulence factors of *C. difficile* are the large clostridial cytotoxins (LCCs), TcdA and TcdB, encoded by *tcdA* and *tcdB* genes (Just and Gerhard, 2004). Both genes are located in the Pathogenicity Locus (PaLoc), together with three additional genes, *tcdR*, *tcdE* and *tcdC* (Figure

1-3) (Hammond and Johnson, 1995). A small fragment of an endolysin gene, *tcdL*, has been found downstream of *tcdE* in recent years (Mehner-Breitfeld et al., 2018). *tcdR* encodes an RNA polymerase σ factor, which positively regulates toxin expression (Mani and Dupuy, 2001). A bacteriophage holin, which is essential for toxin secretion, is encoded by *tcdE* (Govind and Dupuy, 2012). *tcdC* encodes a negative regulator of *tcdR*, that downregulates toxin production and reduces pathogenicity (Matamouros et al., 2007). TcdL is proposed to bind to TcdB to facilitate toxin secretion, losing the function as an endolysin (Mehner-Breitfeld et al., 2018). The PaLoc is found in the same genomic location across strains, except in non-toxigenic strains, where it is replaced by a highly conserved 115/75 base pair (bp) non-coding region (Braun et al., 1996; Dingle et al., 2014).

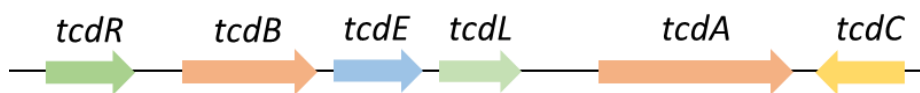


Figure 1-3. The pathogenicity locus (PaLoc)

The figure shows that the PaLoc (19.6kb) contains genes encoding the large clostridial toxins A (TcdA) and B (TcdB), the positive regulator TcdR, the negative regulator TcdC, the holin TcdE and the endolysin fragment TcdL. Adapted from Shanon *et al.* (2022).

TcdA and TcdB enter the gut epithelial cells by receptor-mediated endocytosis and lead to tight junction collapse and apoptosis. Two glycoproteins, sucrase-isomaltase (SI) and soluble glycoprotein 96 (gp96), have been reported as TcdA receptors (Na et al., 2008; Pothoulakis et al., 1996). Multiple classes of protein receptors, chondroitin sulphate proteoglycan 4 (CSPG4), Frizzled 1 (FZD1), FZD2, FZD7 and Nectin 3 (i.e., poliovirus receptor-like protein 3, PVRL3), have been reported for TcdB (LaFrance et al., 2015; Tao et al., 2016; Yuan et al., 2015).

Binary toxin

Between 17 % and 23 % of *C. difficile* strains produce an additional toxin, *C. difficile* transferase (CDT, or binary toxin), which belongs to a family of bipartite ADP-ribosylating clostridial toxins (Gerding et al., 2014; Popoff et al., 1988). Based on its prevalence in epidemic sequence types, it has been suggested to promote the severity of CDI (Bacci et al., 2011; Barbut et al., 2005; Stewart et al., 2013). The genes encoding CDT are located at the CDT locus (CDTloc), which

includes 3 genes: *cdtA*, *cdtB* and *cdtR* (Figure 1-4) (Metcalf and Scott Weese, 2011). CDTa and CDTb compose CDT. The phosphorylation of CdtR activates the transcription of *cdtA* and *cdtB* (Bilverstone et al., 2019; Lyon et al., 2016). Unlike the PaLoc, no gene in CDTloc is found to be associated with pore-forming mechanisms. The mechanism of secretion of CDT from *C. difficile* is currently unknown (Metcalf and Scott Weese, 2011).



Figure 1-4. *C. difficile* transferase (CDT) locus (CDTloc)

The figure shows that the CDTloc (6.2kb) contains genes encoding CDT, *cdtA* and *cdtB*, and the positive regulator CdtR. Adapted from Shanon *et al.* (2022).

CDTa consists of ADP-ribosyltransferase (ADPRT) and pseudo-ADPRT (pADPRT) domains (Perelle et al., 1997; Sundriyal et al., 2009). CDTb is structurally and functionally homologous to anthrax toxin protective antigen (Anderson et al., 2020; Krantz et al., 2005). CDTb binds to lipolysis-stimulated lipoprotein receptor on the host cell surface (Anderson et al., 2020; Genisyuerek et al., 2011). CDTb then binds to CDTa and forms pores on host cells, which allows CDT to enter the host cell via endosome. (Barth *et al.*, 2004; Sheedlo *et al.*, 2020; Anderson *et al.*, 2020; Xu *et al.*, 2020). The enzymatic ADPRT domain of CDTa catalyses the ADP-ribosylation of globular actin, which prevents polymerisation of F-actin. Furthermore, the depolymerisation leads to microtubule protrusion on the host cell surface. These outgrowths of microtubules enhance adherence of *C. difficile* to the colonic epithelial cells, which causes pro-inflammatory responses and leads to detachment of the tight junction connecting cells. (Popoff et al., 1988; Sheedlo et al., 2020; Wegner and Aktories, 1988).

1.2. Type IV Pili

Bacterial pili are long, hair-like structures on the surface of bacterial species. They were first identified in 1949 (Anderson, 1949). Since then, several types of pili have been discovered across various species, including *Escherichia coli*, *Klebsiella sp.*, *Salmonella sp.* and more (Brinton, 1959). Pili are classified by identifying their assembly pathways, such as chaperone-

usher pili, curli and fap fibers, sortase-mediated pili, conjugative and type VI secretion pili, type IV pili, type V pili, (Lukaszczyk et al., 2019). Type IV pili (TFP) is the focus of this thesis and is described in detail.

1.2.1. Components of Type IV Pili

The key components of TFP are mostly shared in Gram-negative and Gram-positive bacteria. This constitutes the main filament proteins known as pilins, the core and platform proteins, peptidases and the assembly and retraction ATPases. To allow the pilin filament to be exported through the outer membrane in Gram-negative bacteria, a secretion channel is required, which is not found in Gram-positive bacteria TFP (Figure 1-5).

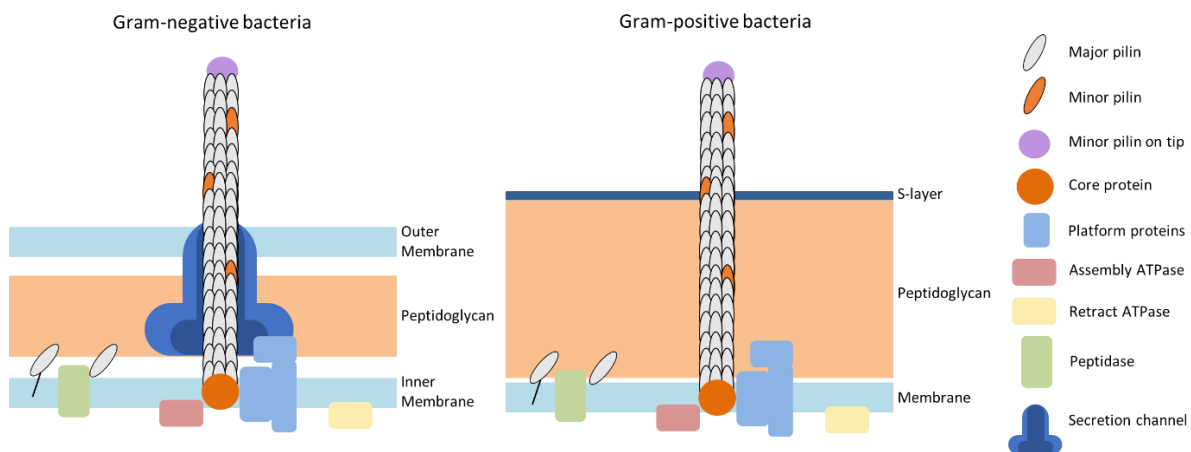


Figure 1-5. Gram-negative and Gram-positive TFP assembly

The figures show the predicted assembly of Gram-negative (left) and Gram-positive (right) bacterial TFP. The major pilins (grey) are expressed on the cytosolic side of the cell membrane (inner membrane in Gram-negative bacteria) and translocated across the membrane while pre-pilin residues are cleaved from the N-terminus by peptidase (green). The assembly ATPase (pink) is required to allow pilin filament to probe the membrane and extend the filament. Retraction of the pilin filament is dependent on the retraction ATPase (yellow). The base of the pilin filament is associated with a core protein (orange), and accessory membrane proteins (platform proteins; blue). In Gram-negative bacterial (left), a secretion channel (navy) is required to allow the filament through the outer membrane. Minor pilins (purple or orange) may decorate along the pilin filament, which may contribute to surface adhesion and filament capping. Adapted from Melville and Craig (2013).

Pilins

The type IV pilus filament is assembled by protein subunits, which are known as pilins. There is one type of pilin making up the main structure, known as major pilin. Some various types of minor pilins present seldom and decorate the pilus filament. They play a variety of roles in the TFP system (Giltner et al., 2010a). The nomenclature of pilins is variable between species.

Type IV pilins share a basic structure but have been classed into either Type IVa or Type IVb, depending on their size and sequence in Gram-negative bacteria. Type IVa pilins have a total size of approximately 150 amino acids, while Type IVb pilins have a total size either significantly shorter (less than 100 amino acids) or longer (approximately 200 amino acids) (Craig et al., 2004). All Type IV pilins are initially synthesised as pre-pilins, which have a type III signal peptide at the N-termini (Giltner et al., 2012). The signal peptide ends with a glycine residue and is positively charged (Pelicic, 2008). It is around 5-7 amino acids in length on Type IVa pilins and approximately 15-30 amino acids long on Type IVb pilins (Craig et al., 2004). The signal peptide is cleaved by pre-pilin peptidase(s) to produce the mature pilin.

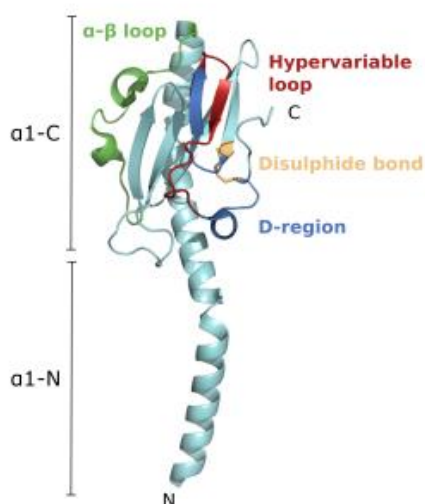


Figure 1-6. Crystal structure of full-length PilE1 from *N. gonorrhoeae*

The structure of full-length PilE1 has distinct domains: an N-terminal hydrophobic helix ($\alpha 1$; cyan), an α - β loop (green) and D-region (blue). The $\alpha 1$ domain is responsible for polymerisation. The D-region is delimited by a disulphide bond that links the termini of the D-region (yellow), but also contains a hyper-variable loop (Red). Adapted from Crawshaw *et al.* (2019)

Following the signal peptide at the N-terminal, an hydrophobic α -helix about 30 amino acids in length is the most homologous domain between pilins (Craig et al., 2004). In Type IVa pilins, the first residue of the N-terminal α -helix is phenylalanine (Craig et al., 2004), whereas in Type IVb pilins, the first residue could be methionine, leucine, or valine (Craig et al., 2004). The hydrophobic N-terminal helix targets pre-pilins into the Sec translocase system and inserts it

into the cytoplasmic membrane, which then forms a transmembrane structure (Francetic et al., 2007).

Compared to the N-terminal, the C-terminal domain is much more variable across pilins (Burrows, 2012a). The C-terminal generally shows a hydrophilic globular structure composed of both α -helix and β -sheet (Craig et al., 2004). The $\alpha\beta$ -loops linking the structures are extremely variable across species, and may have a wide diversity of functions (Giltner et al., 2012). The D-region is the most variable part of the core structure, but it has a disulphide bond generally conserved across Type IVa and Type IVb pilins (Giltner et al., 2012).

Type IV pilins assemble into pilus filaments via their hydrophobic N-terminal tails, which bind together by hydrophobic forces (Craig et al., 2004). The hydrophilic C-terminal heads face out and cover the hydrophobic tails in the central shaft. An individual pilus can be composed of several thousands of major pilins (Giltner et al., 2012).

Minor Pilins

TFP systems also contain other proteins less abundant than the major pilin and therefore termed minor pilins (Giltner et al., 2010b). Minor pilins can play various roles, and certain minor pilins are required for TFP biosynthesis (Carbounelle et al., 2005). Minor pilins may exist on the tips or the base of TFP filament, or incorporated into the filament (Linke et al., 2010; Quigley et al., 2009; Smith et al., 2010). Some are required in attachment and adherence, such as PilC1, PilC2 and PilX in *Neisseria meningitidis* (Hélaine et al., 2005; Morand et al., 2009). An example of different functions is the minor pilin ComP in *Neisseria* which binds to DNA at species-specific DNA Uptake Sequences, so that the extracellular DNA is taken up into the bacterial cell via TFP (Berry et al., 2013; Cehovin et al., 2013). A chemosensory PilJ is found in *P. aeruginosa*, which activates the Chp signalling cascade and results in retraction of TFP (Persat et al., 2015). Some genes encoding minor pilins may be located elsewhere in the genome, outside the main TFP operon, as has demonstrated in *P. aeruginosa* (Belete et al., 2008; Burrows, 2012a; Leighton et al., 2015).

Pre-Pilin Peptidase

During the assembly of the pilus filament, the signal peptide of the pre-pilins is cleaved by the

pre-pilin peptidase, PilD. PilD proteins form a family of membranous aspartyl peptidases, which sit at the cytoplasmic side of the cell membrane (LaPointe and Taylor, 2000). There are two active sites found in most PilD peptidases, which function differently. One of the active sites cleaves the type III signal peptide pre-pilins, while the other methylates the phenylalanine residue on the N-terminal of type IVa (Strom et al., 1993). It has been demonstrated that the cleavage of signal peptides is essential for TFP biosynthesis, but the methylation of N-terminal residues is not (Pepe and Lory, 1998).

Assembly ATPase

Pilins assemble into a pilus filament by pilin polymerisation, which is driven by an assembly ATPase, PilB (PilF in *Neisseria*) (Turner et al., 1993). PilB is a Walker Box-containing ATPase, and it presents as hexamers in the cytoplasm at the site of pilus biosynthesis (Crowther et al., 2004). A crystal structure of PilB has been obtained from *Geobacter metallireducens*, (McCallum et al., 2017). During pili biosynthesis, PilB may interact with the TFP platform protein, PilC, at the conserved pore of the hexamer (McCallum et al., 2017) (Figure 1-7). PilB rotates clockwise with ATP hydrolysis, which in turn leads to a rotation of PilC clockwise (McCallum et al., 2017). PilA1, the main pilin, directly binds to PilC and is pushed out of membrane, where it polymerises to form the helical pili structure.

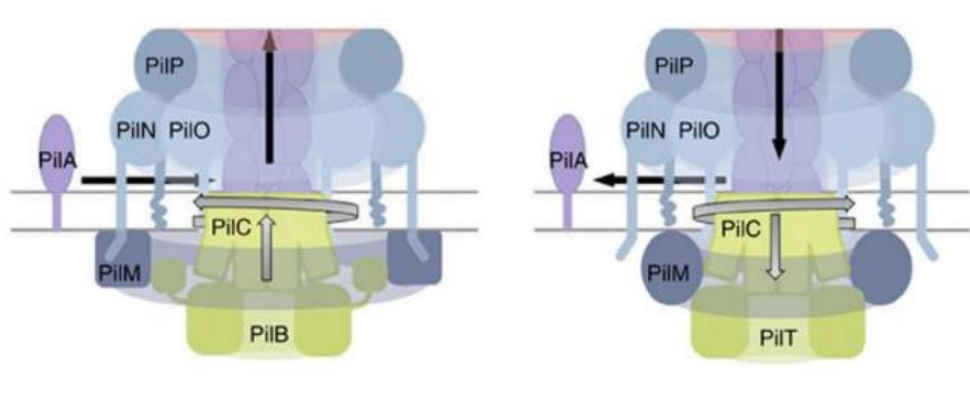


Figure 1-7. Movements and functions of PilB and PilT ATPase

A model of the molecular mechanism of the PilB and PilT motor. PilB is proposed to thrust PilC upwards towards the membrane and rotate to facilitate major pilin polymerisation. PilT is suggested to wrench downward towards the cytoplasm and rotate to facilitate major pilin depolymerization. From McCallum *et al.* (2017).

Retraction ATPase

The retraction of TFP is driven by the depolymerisation of the pili filaments, which is achieved by a retraction ATPase, PilT (Sheetz et al., 2000). In *Pseudomonas aeruginosa*, there is a second retraction ATPase, PilU, while, in *Neisseria meningitides*, there are 3 retraction ATPase, PilT, PilU and PilT2 (Brown et al., 2010). However, some TFP (especially TFPb) are not able to retract the pili filament due to the lack of retraction ATPases (Burrows, 2012b).

Retraction ATPases belong to the same family as the assembly ATPase, PilB, and contain Walker boxes. Similarly, retraction ATPases are localised on the inner side of cytoplasmic membrane as hexamers (Satyshur et al., 2007). A crystal structure of a PilT monomer from *Aquifex aeolicus* shows that the N-terminal domain interacts with the C-terminal domain of the next monomer when forming a hexamer (Satyshur et al., 2007). Although the crystal structure of PilT indicates the ATPase forms a homohexamer, bacterial two-hybrid studies show the three retraction ATPases of *N. meningitides* may interact with each other, and even with the assembly ATPase (Georgiadou et al., 2012).

Similar to PilB, PilT also goes through rotation, but anticlockwise, which may turn PilC and depolymerise the pili (McCallum et al., 2017) (Figure 1-7).

Platform Protein

PilC is known as a platform protein of TFP (PilG in *Neisseria*) (Figure 1-7). PilC is composed of 3 transmembrane helices, likely inserted at the cytoplasmic membrane, a cytoplasmic N-terminus and a periplasmic/extracellular C-terminus (Berry and Pelicic, 2015). The role of PilC can be varied across species and it was recently found to be necessary for surface-dependent signalling in *Pseudomonas aeruginosa* (Kuchma and O'Toole, 2022).

Accessory Membrane Proteins

There are three or four other membrane-associated proteins forming a transmembrane complex at the base of TFP (Figure 1-7). A cytoplasmic, actin-like protein, PilM, interacts with PilN, which is a monotopic membrane protein (Karuppiah and Derrick, 2011). PilN has a large periplasmic/extracellular C-terminal domain, but a small cytoplasmic N-terminus

(Sampaleanu et al., 2009). On the N-terminus, a conserved INLLP amino acid motif can interact with PilM (Tammam et al., 2013). In some TFP systems, PilM and PilN are fused into a single protein, such as BfpC from *E. coli*. PilM is shown to interact with the assembly ATPase and may contribute to transmitting signals (Yamagata et al., 2012).

PilO is an accessory membrane protein. Similarly to PilN, PilO has a larger periplasmic/extracellular domain and a short cytoplasmic domain (Sampaleanu et al., 2009). PilO and PilN interact on their periplasmic domain and form heterodimers (Sampaleanu et al., 2009).

Another accessory membrane protein, PilP, is a periplasmic inner membrane lipoprotein of Gram-negative bacteria (Drake et al., 1997). PilP is not found in Gram-positive bacteria (Melville and Craig, 2013). The N-terminal domain of PilP interacts with the PilNO complex and forms a PilNOP heterotrimer (Tammam et al., 2011).

Secretin

The TFP systems in Gram-negative bacteria must reach out through the outer membrane (Figure 1-5, navy). A multimeric protein complex, known as secretin, forms a pore on the outer membrane to allow the pilus filament to pass through. Secretins are commonly found in the inner and outer membrane of Gram-negative bacteria as part of the Type III Secretion System (Hodgkinson et al., 2009). In the TFP system, the secretin is known as PilQ. Each secretin complex is composed of 12-15 PilQ monomers forming a symmetrical circle as the pore on the outer membrane (Lieberman et al., 2015).

PilQ monomers interact with each other via their extracellular C-termini and form β -barrels in the outer membrane (Lieberman et al., 2015). The periplasmic N-terminal contains four discrete domains, two of them close to the N-terminal side vary across species, and are known as 'species specific', SS1 and SS2, domains. The rest are highly conserved and known as NO and N1 (Tammam et al., 2013). The NO domain can interact with the C-terminal β -domain of PilP, while PilP interacts with PilNO by its N-terminus, therefore, a trans-envelope complex PilMNOPQ is comprised (Tammam et al., 2013). The study also shows that PilA can interact with the N-terminal domains of PilQ.

Because the width of the secretin pore may disrupt the integrity of the outer membrane in the absence of pili, the pore is gated by two gates from a secretin complex (Gold et al., 2015). Gate 1 is at the outer membrane, while Gate 2 is at the base of the secretin. During the passage of a pilus filament, the secretin undergoes conformational changes to open the gates and form a pore (Gold et al., 2015).

Secretin Pilotin

Secretin pilotin is found in Gram-negative bacteria, known as PilF in *P. aeruginosa*, or PilW in *N. meningitidis*. PilF is a lipoprotein at the outer membrane, which promotes the transport of PilQ monomers to pass through the periplasm and formation of multimeric secretin complexes (Koo et al., 2008).

1.2.2. Type IV Pili in Clostridia species

TFP was first identified and was initially thought to be exclusive to Gram-negative species (Melville and Craig, 2013). The first TFP-like structures were observed on Gram-positive species in *Streptococcus sanguinis*, in 1985 (Fives-Taylor and Thompson, 1985). However, due to the lack of genome sequencing and bioinformatics tools at the time, TFP was not identified from their works. The production of TFP by a Gram-positive species, *Ruminococcus albus*, was finally confirmed in 2002 (Rakotoarivonina et al., 2002). Further, TFP was identified in *Clostridium perfringens*, which became the model to study TFP in *Clostridia* species (Varga et al., 2006a). *C. perfringens* is a pathogen that can also release toxins, causing food poisoning and attacking the nerve system (Wioland et al., 2013).

Melville and Craig identified two TFP gene clusters in the *C. perfringens* genome: the primary cluster encodes all key genes for TFP assembly while the secondary cluster encodes another set of *pilB* and *pilC* and a pilin (Figure 1-8). A *pilT* gene is found in another independent locus (Melville and Craig, 2013).

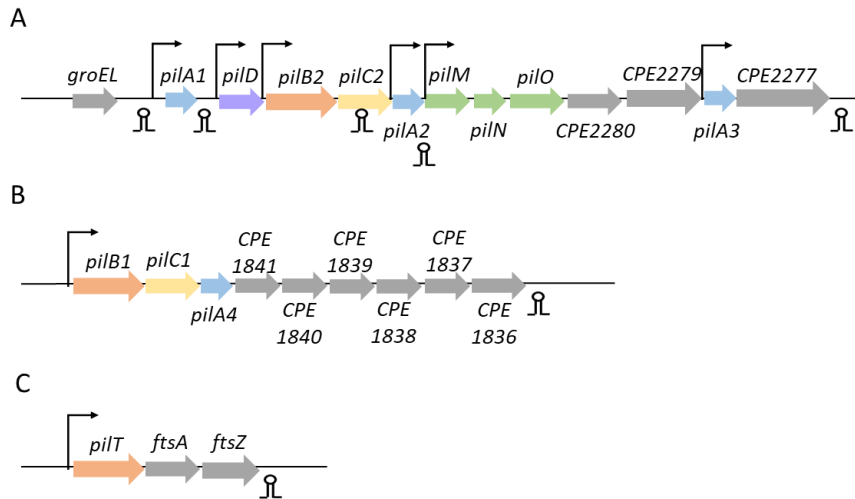


Figure 1-8. Type VI Pili gene loci in *C. perfringens*

(A) Operon map of TFP primary gene cluster. (B) Operon map of TFP secondary gene cluster. (C) *pilT* gene is located separately on an operon with *ftsA* and *ftsZ*. Genes encoding pilins are shown in blue, ATPases in orange, core proteins in yellow, membrane platform proteins are coloured green, the peptidase is in purple and genes not relevant to TFP in grey. Arrows indicate the location of promoters, circles and stems represent the p-independent terminators. Adapted from Soncini *et al.* (2020).

Both PilA1 and PilA2 were observed on the cell surface of *C. perfringens*, PilA2 was demonstrated to be the major pilin assembling the pilus filament, whereas PilA1 is predicted to act more like a pseudopilin, which is a type II secretion system with a piston-like structure (Varga *et al.*, 2006a). From a mutagenesis study, *C. perfringens* lost 84 % of adherence in a *pilA2* mutant, while a *pilA4* mutant led to a loss of 42 %, but no reduced adherence was observed in a *pilA3* mutant (Soncini *et al.*, 2020).

A study in *C. perfringens* revealed that PilB1 loses its pole localisation in cells in a *pilC1* mutant and suggests that PilC1 primarily localises on the poles and attracts PilB1 to export pilus (Hartman *et al.*, 2011). However, this dependency is not observed between PilC2 and PilB2 (Hendrick *et al.*, 2017).

The bacterial secondary messenger 3'-5' cyclic diguanosine monophosphate (c-di-GMP) plays multiple roles in bacterial physiology and virulence, such as regulation of bacterial motility, biofilm formation and virulence-related gene expression (Hengge, 2009; Pratt *et al.*, 2007; Römling *et al.*, 2013). In Gram-negative bacteria, TFP ATPases are found to bind c-di-GMP and up-regulate TFP polymerisation (Roelofs *et al.*, 2015; Wang *et al.*, 2016). In *C. perfringens*, PilB2

binds to c-di-GMP at the N-terminal domain, but the efficiency of ATPase activity is not affected when binding to c-di-GMP (Hendrick et al., 2017). However, in increased levels of c-di-GMP, both PilB2 and PilC2 are essential for PilA2 polymerisation and exportation (Hendrick et al., 2017).

Compared to TFP in Gram-negative species, TFP in *C. perfringens* have the same TFP assembly genes, but miss *pilF*, *pilP* and *pilQ* (Varga et al., 2006a) as it is not necessary to sustain secretin genes in Gram-positive species with one cytoplasmic membrane. Interestingly, transcription of the retraction ATPase PilT is dependent on temperature: it increases at higher temperatures and decreases in lower temperatures (Soncini et al., 2020).

1.3. TFP in *C. difficile*

1.3.1. *C. difficile* TFP Gene Clusters

Apart from TFP in *C. perfringens*, Varga *et al* demonstrated that TFP genes are encoded in other Clostridial species (Varga et al., 2006b). Although there is some diversity between species, they are all predicted to express TFP (Varga et al., 2006). *C. perfringens*, *C. beijerinckii*, *C. difficile* and *C. thermocellum* contain genes that encode additional pilins and repeated TFP proteins with the same function, whereas fewer genes encoding essential TFP proteins are found in *C. tetani*, *C. botulinum* and *C. acetobutylicum* (Varga et al., 2006). Recent studies have focused on TFP in *C. perfringens* and *C. difficile*, there is not much biological investigation on TFP in other Clostridial species.

The first whole genome sequencing (WGS) for *C. difficile* strain 630 was done in 2006 (Sebaihia et al., 2006). Genes encoding TFP in *C. difficile* were discovered by Varga *et al.*, and gene names were formalized by Maldarelli *et al.* (Maldarelli et al., 2014; Varga et al., 2006a). Like in *C. perfringens*, two gene clusters were found (Figure 1-9). However, there are differences between the two species.

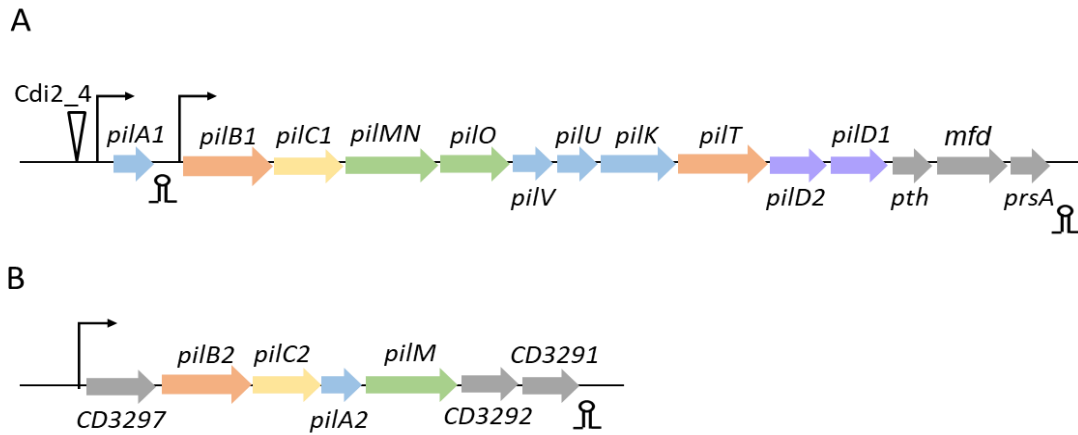


Figure 1-9. Type VI Pili gene loci in *C. difficile*

(A) Operon map of TFP primary gene cluster. (B) Operon map of TFP secondary gene cluster. Genes encoding the pilins are shown in blue, ATPases in orange, core proteins are coloured yellow, membrane platform proteins in green, peptidase in purple and genes non-relevant to TFP in grey. Arrows indicate the location of promoters, triangle points the location of the c-di-GMP riboswitch (*Cdi2_4*), circles and stems represent the ρ -independent terminators.

In the primary gene cluster, a gene encoding pilin, *pilA1*, at the start of this gene cluster is predicted to be the major pilin (Maldarelli et al., 2014). A c-di-GMP riboswitch, regulating the expression of *PilA1*, is found in the upstream region of *pilA1*.

The structure of *PilA1* from *C. difficile* R20291 and CD630 were previously determined in our lab (Crawshaw, 2016). The constructs folded into distinct domains, characteristic of pilin structures: an N-terminal helix that is involved in pili formation (Crawshaw et al., 2020), an α - β loop that connects α 1 helix and an antiparallel β -sheet. The variable D-region which is mostly composed of flexible loops contains a shorter α -helix (Figure 1-10).

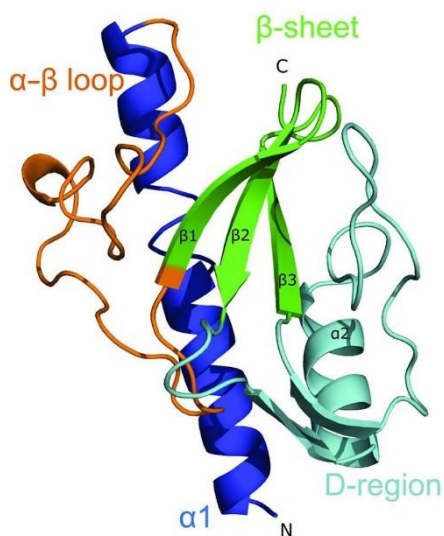


Figure 1-10. Crystal structure of PilA1 from *C. difficile*

Cartoon representation of the structure of PilA1 from R20291 lacking part of the N-terminal long helix characteristic of TFP pilins. N-terminal helix (α_1 ; dark blue), α - β loop (orange), an antiparallel β -sheet (green) and variable D-region (cyan). Adapted from Crawshaw *et al.* (2020).

Following *pilA1*, genes encoding an assembly ATPase (*pilB1*), the core protein (*pilC*) and platform proteins (*pilMN*, *pilO*) are located in the primary gene cluster (predicted protein structures in Figure D-1, Appendix D). Gene *pilMN* was initially named *pilM*, however, this *pilM* in *C. difficile* is much larger in size in other Gram-negative or Gram-positive species (1713 bp, encoding a 510 amino acid protein in *C. difficile* 630, compared to 1155 bp/ 384 aa in *C. perfringens* strain 13, 1065 bp/ 354 aa in *P. aeruginosa* strain PA01 or 1116 bp/ 371 aa in *N. meningitidis* strain ATCC 13091). *C. difficile* is claimed not to contain an independent *pilN* gene in its genome. An analysis using TMHMM, a membrane protein topology prediction method based on a hidden Markov model (Krogh *et al.*, 2001), suggested that the *C. difficile pilM* gene in the TFP primary gene cluster contains a transmembrane helix, whereas PilM is known to locate in the cytoplasm in other species (Martin *et al.*, 1995). As PilM attaches to the cytoplasmic N-terminal domain of the monotopic membrane protein PilN and forms a membrane-anchored complex, this primary cluster *pilM* gene in *C. difficile* is proposed to be a *pilM-pilN* fusion (Ayers *et al.*, 2009; Karupiah and Derrick, 2011). The hypothesis was confirmed by BLAST analysis as the gene product identifies both PilM (at the N-terminus) and PilN (at the C-terminus) domains within the protein (Couchman, 2016; Melville and Craig, 2013). Interestingly, BLAST analysis also suggested that the C-terminus might contain an amidase domain, which might help to re-order the peptidoglycan cell wall to allow TFP to pass through (Couchman, 2016).

Following genes encoding the platform proteins, three genes encoding minor pilins (*pilV*, *pilU* and *pilK*), the retraction ATPase (*pilT*) and two pre-pilin peptidases (*pilD2* and *pilD1*) are found in the primary gene cluster (predicted proteins structures in Figure D-2 and D-3, Appendix D).

Mutagenesis studies of all primary cluster genes encoding TFP proteins, apart from *pilD1*, showed that only PilT is not essential for PilA1 filament biosynthesis, as assessed by presence of extracellular PilA1 (Couchman, 2016). The assembly ATPase PilB1, membrane proteins PilC, PilMN and PilO and minor pilins PilK, PilV and PilU all led to failure to detect PilA in the supernatant.

Three genes (*pth*, *mfd* and *prsA*) are found downstream of *pilD1* gene but seem to be part of the operon, even though they appear to have no relation to TFP. Gene *pth* encodes a peptidyl-tRNA hydrolase protein, which hydrolyses the amide bonds between peptide and tRNA within peptidyl-tRNA molecules released from stalled ribosomes (Das and Varshney, 2006). The accumulation of peptidyl-tRNA inhibits protein synthesis, and *pth* is confirmed to be essential for survival of *E. coli* (Das and Varshney, 2006). Gene *mfd* encodes the Mutation Frequency Decline (Mfd) protein, which is a transcription-repair coupling factor, releasing RNA polymerase complexes during transcription at locations of DNA damages and recruiting the DNA repair factor UvrA (Hanawalt and Spivak, 2008). *mfd* gene is not essential for bacterial survival, but the loss of this gene leads to an increased rate of mutation (Hanawalt and Spivak, 2008). Work carried out by our collaborators showed that *mfd* is not required for TFP biosynthesis (Couchman, 2016). The final gene within the cluster is *prsA*, which encodes lipoprotein PrsA a chaperone that catalyses the folding of exported proteins (Hyyryläinen et al., 2010). It is unclear what, if any, these genes have in relation to TFP in *C. difficile*.

The secondary cluster contains genes encoding additional assembly ATPase (*pilB2*), the core protein (*pilC2*), a second copy of the major pilin (*pilA2*) and platform protein (*pilM*) (Maldarelli et al., 2014). The other three genes are predicted to encode monotopic membrane proteins using TMHMM, and no homologue is identified using BLAST (Couchman, 2016). Interestingly, the final two genes (*CD3291* and *CD3292*) encode analogous to PilN and PilO, which indicates the secondary cluster may encode a full complement of TFP membrane proteins (Couchman, 2016) (Predicted protein structures in Figure D-4, Appendix D). However, no study has further

investigated these genes. PilB2 has been proved to not be required for TFP biosynthesis in the mutagenesis studies carried out by our collaborators (Couchman, 2016).

Four other putative TFP-like genes were identified in the *C. difficile* genome: *CD2305*, known as *pilW*, *CD0755* or *pilJ*, *CD1242* - *pilX* and *CD630_1245*, labelled *pilA3*, based on predicted secondary structure homologies with type IVa pilin structures of *Neisseria gonorrhoeae*, *Pseudomonas aeruginosa*, and *Dichelobacter nodosus*, as well as the structure of pseudopilin PulG from *Klebsiella pneumoniae* (Melville and Craig, 2013). These genes are proposed to encode minor pilins. PilJ has been confirmed to be a minor pilin and forms heteropolymeric pili, with the crystal structure solved by Piepenbrink *et al.* (2014) (Figure 1-11). A recent study also determined the structure of PilW and suggested the protein assembly of PilA1, PilJ and PilW (Figure 1-11) (Ronish *et al.*, 2022). The α 1-N helical regions of the three proteins are similar in sequence and are modelled with identical backbone into the fibre. The conserved interaction residues lysine in position 30 (K30) and its proposed equivalent residues, E75 on PilA1, D85 on PilW, and E76 on PilJ, are suggested to maintain certain structural motifs when incorporating into TFP filament (Figure 1-11) (Ronish *et al.*, 2022). PilW is nearly identical to PilA1 in size, but due to its extended $\alpha\beta$ loop, is wider from the helical axis of the TFP filament, while the C-terminal domain of PilJ extends out from the pilus filament (Figure 1-11). The predicted protein structures of the rest of minor pilins are shown in Figure D-5 in Appendix D. Additionally, although CD3297 on the TFP secondary gene cluster is not yet reported as a predicted minor pilin, the predicted structure shows a similar shape to PilJ, with an extended C-terminal domain.

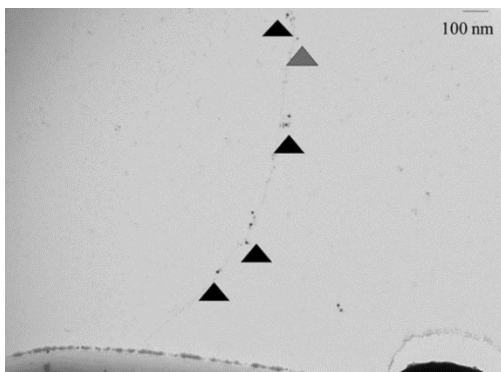


Figure 1-11. PilA1 and PilJ localisation on *C. difficile* TFP

An electron micrograph with immunogold-labelled PilA1 and PilJ on a TFP filament of *C. difficile*. Detected PilA1 is pointed by grey triangles, PilJ is pointed by black triangles. A *C. difficile* R20291 cell can be observed on the bottom left. From Piepenbrink *et al.* (2014).

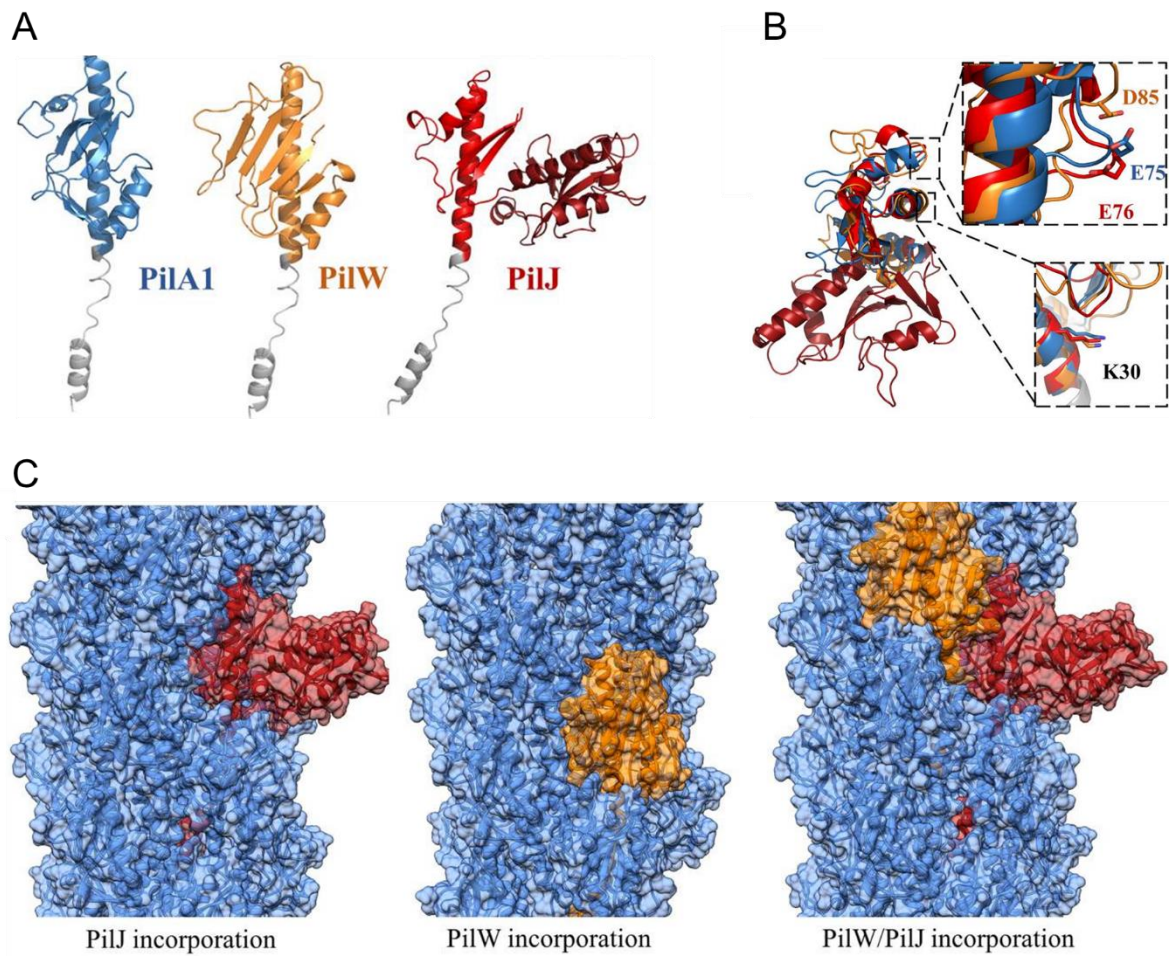


Figure 1-12. Crystal structure and incorporation of subunits in *C. difficile* TFP

(A) Full-length models of PilA1, PilW, and PilJ based on X-ray crystal structures of the soluble domains with α 1-N regions removed (grey). (B) Superimposition of PilA1, PilW and PilJ. Insets show zoomed region at the conserved interaction residues K30 and its proposed salt-bridge residues: E75 on PilA1, D85 on PilW, and E76 on PilJ. (C) Heterologous model of TFP filaments showing the incorporation of PilW and PilJ into the filament. Blue indicates PilA1, yellow indicates PilW, red indicates PilJ. Adapted from Ronish *et al.* (2022).

1.3.2. Induction of TFP in *C. difficile*

The first direct evidence of c-di-GMP regulation of TFP-mediated twitching motility was found in *P. aeruginosa* (Huang *et al.*, 2003). In *C. difficile*, an increased level of c-di-GMP was observed to regulate TFP-mediated motility and aggregation (Purcell *et al.*, 2012). Twitching motility is a form of surface-associated bacterial movement usually mediated by pili. Twitching motility requires attaching the tip of a pilus to the surface and pulling the bacteria to move by

retracting and shortening the pilus.

The levels of c-di-GMP are sensed by specific intracellular receptors (Chou and Galperin, 2016). A c-di-GMP riboswitch (Cdi2_4), located directly upstream of the *pilA1* gene regulates TFP biosynthesis in *C. difficile* (Bordeleau et al., 2015).

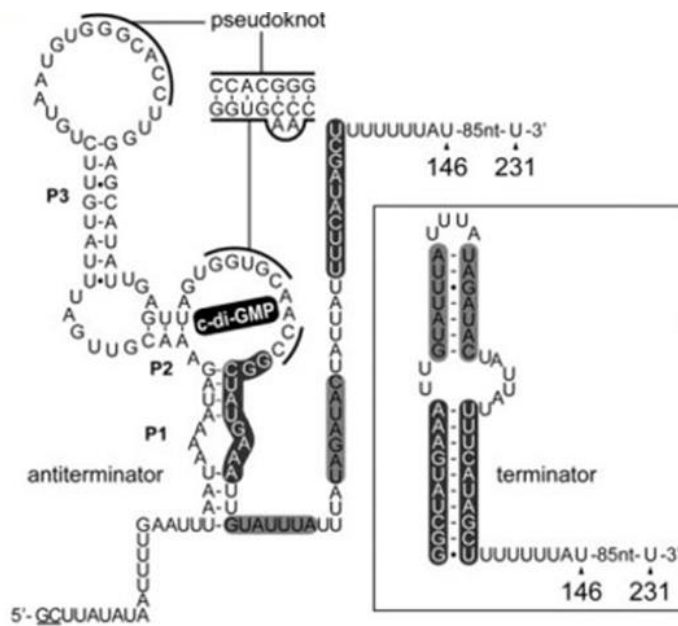


Figure 1-13. Predicted secondary structure of Cdi2_4 c-di-GMP-II riboswitch-mediated transcription regulator

The predicted terminator structure is shown in the box. Upon c-di-GMP binding, an anti-terminator forms at P1 and P2 stems. Positions 231 and 146 correspond to the last nucleotides of the full-length transcript and the predicted terminated transcript, respectively. GC nucleotides (underlined) were added to the template for transcription priming using GC dinucleotides. Edited from Bordeleau *et al.*, 2015.

Riboswitches are encoded in the 5' leader sequence (untranslated region, UTR) of some messenger RNAs (mRNAs), and fold to adopt a structure that binds a specific ligand (Sherwood and Henkin, 2016). Ligand binding causes the formation of an alternate, exclusive RNA structure that affects the accessibility of the ribosome binding site and influences the translation of the downstream coding sequences. Therefore, riboswitches can act as 'on' or 'off' switches in the response to ligand binding, which promotes or prevents gene expression. The predicted structures of Cdi2_4 is shown in Figure 1-13. The predicted terminator structure

is shown in the box in Cdi2_4 under a c-di-GMP free condition. When c-di-GMP binds to the aptamer, the P1 stem folds and sequesters nucleotides for the formation of the terminator, which becomes an anti-terminator.

Two classes of c-di-GMP specific riboswitches have been identified: class I and class II (Sudarsan et al., 2008). While most riboswitches bind to ligands that typically play a role as feedback mechanism for that specific metabolite, c-di-GMP riboswitches are unusual, as they rarely control c-di-GMP metabolic genes. Instead, C-di-GMP riboswitches have been identified upstream of genes known or predicted to be involved in motility, chemotaxis, adherence or other processes.

The genome of *C. difficile* 630 contains 12 class I and 4 class II c-di-GMP riboswitches, but only 11 of them are functional (Lee et al., 2010; Robert W. McKee et al., 2018; Soutourina et al., 2013; Sudarsan et al., 2008).

The level of c-di-GMP is controlled by two groups of enzymes with antagonistic activities, diguanylate cyclases (DGCs) and c-di-GMP phosphodiesterases (PDEs). The DGCs contain a GGDEF amino acid sequence motif and synthesise c-di-GMP from two GTP molecules, whereas the PDEs contain EAL or HDxGYP sequence motifs and hydrolyse c-di-GMP into linear 5'-phosphoguanylyl-(3',5')-guanosine (pGpG) or two GMP molecules (Ryjenkov et al., 2005; Schmidt et al., 2005; Simm et al., 2004; Tamayo et al., 2005).

In the genome of *C. difficile* 630, 18 confirmed or putative DGCs and 17 confirmed or putative PDEs have been determined (Bordeleau et al., 2011; Gao et al., 2014). This is considerably more than in other Clostridial genomes such as in *C. perfringens* or *C. botulinum*, which has 9 predicted DGCs and 16 predicted PDEs (Mendez et al., 2008; Skarin et al., 2011). Gene *CD1420* encodes the smallest DGC in *C. difficile*, and the product has been confirmed to have enzymatic activity (Bordeleau et al., 2011). Purcell *et al.* demonstrated that the overexpression of this gene results in elevated intracellular c-di-GMP levels. They also named the gene as diguanylate cyclase from *Clostridium* A (*dccA*) (Purcell et al., 2012).

The riboswitch regulating *pilA1*, Cdi2_4, is one of the functional class II riboswitches, and PilA1 expression is increased in higher levels of intracellular c-di-GMP (Bordeleau et al., 2015). Expression of *dccA* leads to higher c-di-GMP levels and production of TFP (Figure 1-14).

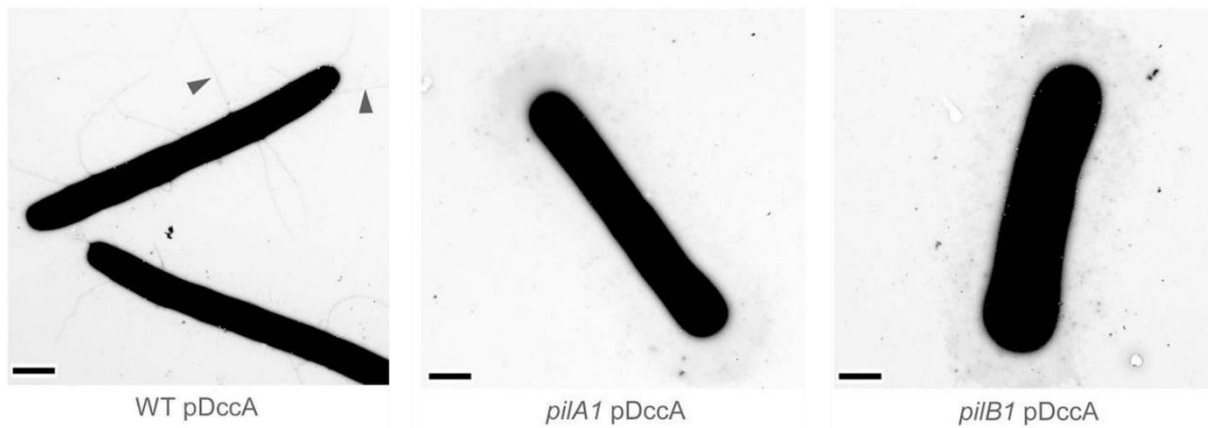


Figure 1-14. c-di-GMP induces TFP formation

Transmission electron microscopy of *C. difficile* 630 Δ *erm* strain (wild type; WT pDccA), *pilA1* (*pilA1* pDccA) and *pilB1* (*pilB1* pDccA) mutants with elevated level of c-di-GMP achieved by expressing *dccA* from a plasmid. Triangles point TFP. Scale bar indicated 1 μ m. Disappearance of TFP in both *pilA1* and *pilB1* mutants. Edited from Bordeleau et al. (2015)

In the work presented in this thesis, *dccA* is used for elevating intracellular level of c-di-GMP by introducing a plasmid carrying the *dccA* gene under an inducible promoter into *C. difficile* cells.

1.3.3. Functions of TFP in *C. difficile*

Since it has been shown that high level of intracellular c-di-GMP can induce PilA1 expression and enhance twitching motility, biofilm formation and adherence, the link between TFP and these biological functions has been investigated (Purcell et al., 2017).

Purcell et al. have shown that increased level of c-di-GMP promotes aggregation in *C. difficile* R20291, a RT027 strain (Purcell et al., 2012). A study further reveals that *pilA1* and *pilB1* mutants show deficiencies in aggregation (Bordeleau et al., 2015). Both mutants lead to disappearance of TFP from *C. difficile* cell surface, under the condition of elevated level of c-

di-GMP (Figure 1-14) (Bordeleau et al., 2015). Later studies show that strains carrying both mutations have a reduced adhesion to host epithelial cells *in vivo* (Robert W McKee et al., 2018).

Twitching motility

From the first observation of TFP-mediated twitching motility in R20291 by Purcell *et al.* (2016), branched, tendril-like shapes were observed on the edges of the colonies (Figure 1-15). When the level of intracellular c-di-GMP increases, the branched shapes are enriched compared to a normal colony and move further on the surface from the centre of the colony. The branched shapes and surface mobility are lost in *pilB1* mutant both with and without elevated c-di-GMP levels (Purcell et al., 2016).

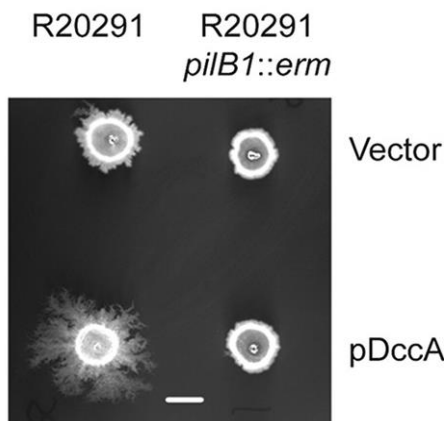


Figure 1-15. TFP-mediated surface motility stimulated by c-di-GMP
Colony morphology of *C. difficile* R20291 wild type (R20291) and *pilB1* mutant (R20291 *pilB1::erm*). Colonies in the top row bear empty vectors (Vector), while the bottom row bears plasmid expressing *dccA* (pDccA) to elevate the level of intracellular c-di-GMP. Disrupting *pilB1* gene results in loss of the branchy shapes on colony edges. The branchy shapes are enhanced under DccA expression. The scale bar indicates 5 mm. Edited from Purcell *et al.* (2016).

Biofilm formation

The relevance between TFP and biofilm formation in Gram-positive bacteria was firstly revealed in *C. perfringens* (Varga et al., 2008). *C. difficile* also forms biofilm (Đapa et al., 2013; Dawson et al., 2012). The first investigation between *C. difficile* TFP and biofilm revealed that *pilA1* and *pilJ* gene transcripts are remarkably increased during biofilm growth, including aggregate biofilm and colony biofilm, compared to planktonic cell growth (Maldarelli et al., 2016). The same study also observed a deficiency of initiating biofilm formation in a *pilA1* mutant (Maldarelli et al., 2016). Later, higher levels of *pilT*, *pilB2* and *pilM* transcripts were detected in aggregate biofilms in contrast to colony biofilms (Brauer et al., 2021). Similar to what was observed when investigating twitching motility, *pilA1* and *pilB1* mutants show a

deficiency in biofilm formation under high levels of c-di-GMP (Purcell et al., 2016). A recent study from Ronish *et al.* (2022) also reveals loss and deficiency in biofilm formation when mutating *pilA1*, *pilW* and *pilJ* genes (Figure 1-16).

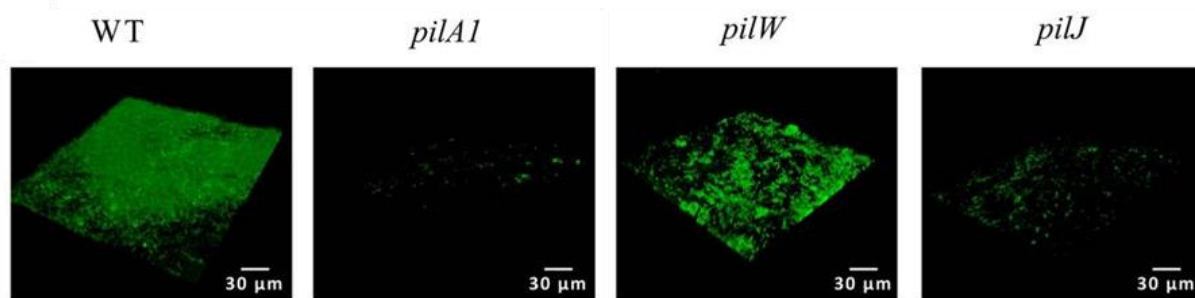


Figure 1-16. Biofilm formation by *C. difficile* R20291 and mutants

Confocal laser scanning microscopy images of *in vitro* biofilms of *C. difficile* R20291 (WT) and pilin mutants (*pilA1*, *pilJ*, and *pilW*). Less biofilm signals are detected from mutants compared with WT. 3D reconstructions of biofilms generated from z-stacks. Cells were incubated with stainless washers for 7 days prior to imaging. On the 7th day, stainless washers were washed and cells stained aerobically, followed with 48h freezing as preparation for imaging. Adapted from Ronish *et al.* (2022).

1.4. c-di-GMP and flagella ON-/OFF-phase

As discussed in section 1.3.2., higher levels of intracellular c-di-GMP switch on PilA1 expression via a class II riboswitch Cdi2_4, which leads to increased level of twitching motility, aggregation, and biofilm formation. *C. difficile* also encodes for flagella and shows flagella-mediated motility, adherence, and colonisation (Baban et al., 2013; Dingle et al., 2011; Stabler et al., 2009; Stevenson et al., 2015; Twine et al., 2009). Therefore, as the aim of this project was to investigate TFP-mediated biological features, it was important to compare it with flagella-mediated motility.

The proteins involved in the early steps of flagellar biosynthesis, such as flagellar hook, basal body, MS ring, motor and other assembly proteins are encoded in the *flgB* operon (Twine et al., 2009). A class I riboswitch, Cd1 (also named Cdi1_3), is found in the 5' UTR of the *flgB* operon (Sudarsan et al., 2008). It has been demonstrated that the increased level of intracellular c-di-GMP inhibits *flgB* operon expression (Purcell et al., 2012). Later, a truncated RNA corresponding to the riboswitch-mediated termination product was detected by

northern blot (Anjuwon-Foster and Tamayo, 2017; Soutourina et al., 2013).

Together with the studies on TFP (Anjuwon-Foster and Tamayo, 2017; Purcell et al., 2016, 2012; Soutourina et al., 2013), this indicates that, under increased level of c-di-GMP, TFP expression is activated by a class II riboswitch, Cd2_4, while the expression and biosynthesis of flagella is inhibited by a class I riboswitch, Cd1_3 (Figure 1-17).

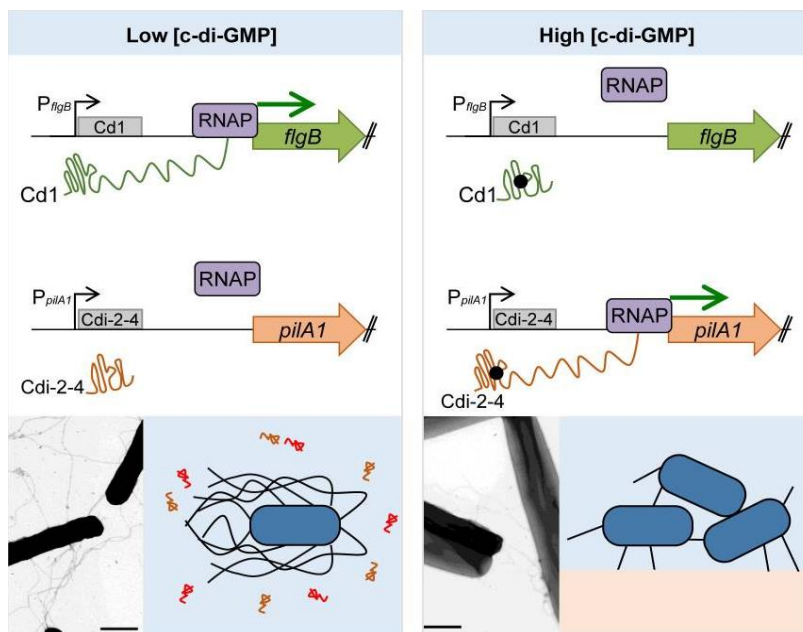


Figure 1-17. Model for c-di-GMP-mediated transition between flagella 'on' and 'off' states in *C. difficile*

(Left) Under low intracellular c-di-GMP conditions, the riboswitch Cd1 forms a structure conducive to transcription of the downstream *flgB* operon. Riboswitch Cd2_4 assumes a structure that includes a transcription terminator, precluding transcription of downstream TFP genes.

Together, low level of c-di-GMP favours flagellated, free-living and swimming bacteria, producing toxins TcdA and TcdB (red and orange symbols). (Right) Increased level of intracellular c-di-GMP (black dots) binding to riboswitches Cd1 and Cd2_4 results in mRNA conformational changes and termination of the transcription of the *flgB* mRNA but promotion of the transcription of *pilA1*. High levels of c-di-GMP results in non-flagellated, non-toxicogenic, pillated bacteria with increased aggregation and biofilm formation. From Tamayo (2019).

A sigma factor, σ_D , is also encoded in *flgB* operon. σ_D is found in many Gram-negative and Gram-positive bacteria, and positively regulates the expression of flagellar genes, allowing the assembly of the flagellum (Chilcott and Hughes, 2000; Colland et al., 2001; Helmann and Chamberlin, 1987; Prouty et al., 2001). In *C. difficile*, σ_D not only coordinates flagellar gene expression but also activates the transcription of *tcdR*, which encodes another sigma factor required for toxin TcdA and TcdB expression (McKee et al., 2013). Increased level of c-di-GMP inhibit *flgB* expression and lead to an inhibition of the expression of toxins. Therefore, under a lower level of intracellular c-di-GMP, *C. difficile* expresses flagella and toxins, while the cells

have higher abilities in swimming motility and disease development, which is identified as flagella 'on' phase. In the opposite, flagella 'off' phase, *C. difficile* expresses TFP instead and shows higher abilities in twitching motility and biofilm formation (Figure 1-17). In terms of disease development, during the early stage of CDI infection, *C. difficile* are under flagella 'on' phase and relies on flagella for swimming motility. *C. difficile* cells are 'free' to move in the gut lumen, towards intestinal cells. As they approach the mucus-rich layers, a signalling cascade leads to an increased level of c-di-GMP, switching flagella 'off' phase and decreasing swimming motility. *C. difficile* cells use TFP to attach to other host and bacterial cells and initiate colonisation and biofilm formation, which protects them from gut movement and antibiotic treatment (Frostid et al., 2021).

To identify the roles of switching 'on' and 'off' phases in infection stages, some work has investigated flagella and TFP adhesion to host cells. McKee *et al.* infected mice with *C. difficile* 630 Δ erm *pilA1* and *pilB1* mutants and counted spores from patient mice faeces (Robert W McKee et al., 2018). The results show that *pilA1* and *pilB1* mutants do not lead to phenotypes during the first 3 days of infection, however, no spore was detected on the 7th day of infection (McKee *et al.*, 2018). This indicates that TFP is a crucial factor in long-term infection and could help to strengthen colonisation and biofilm (McKee *et al.*, 2018). Studies on flagella demonstrated that *fliC* and *fliD* mutants of *C. difficile* R20291 shows decreased adherence to Caco-2 cells, whereas these mutants in *C. difficile* 630 Δ erm shows increased adherence to Caco-2 cells (Baban et al., 2013; Dingle et al., 2011). These studies suggest that the factor mediating adhesion may vary from strain to strain (Dingle et al., 2011).

To distinguish TFP-mediated twitching motility from flagella-mediated swimming motility, previous studies have used motility assays. Flagella-mediated motility of *C. difficile* is generally studied using 0.3% motility agar on petri dish plates or glass test tubes (Anjuwon-Foster and Tamayo, 2017; Purcell et al., 2012). Purcell *et al.* (2016) optimised a protocol to investigate TFP-mediated motility in *C. difficile* with a range of concentration of agar in the media (Figure 1-18), which demonstrated incubation on 1.8% agar gives the most appropriate observation of TFP-mediated twitching motility. Along with qRT-PCR to measure the *pilA1* transcription abundance, they confirmed that the motility is TFP-mediated.

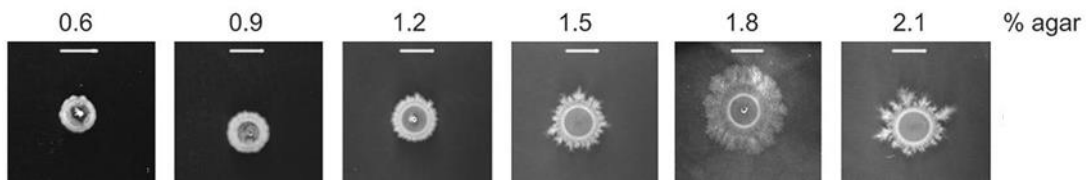


Figure 1-18. *C. difficile* migrates across agar surface using TFP-mediated twitching motility

The figure shows the migration of *C. difficile* on varying concentrations of agar (0.6 %, 0.9 %, 1.2 %, 1.5 %, 1.8% and 2.1%) after 120h incubation at 37°C. The white scale bars indicated 5mm. Edited from Purcell *et al.* (2016).

Further, work published by Garrett *et al.* (2016) suggested that restreaked colonies from branched edges of twitching motility colonies on 1.8% agar shows more branched shapes than the colonies restreaked from the centre (Figure 1-19, panel A) (Garrett *et al.*, 2019). Conversely, colonies restreaked from 0.3% agar no longer show branched colony morphologies on 1.8% agar (Figure 1-19, panel B) (Garrett *et al.*, 2019).

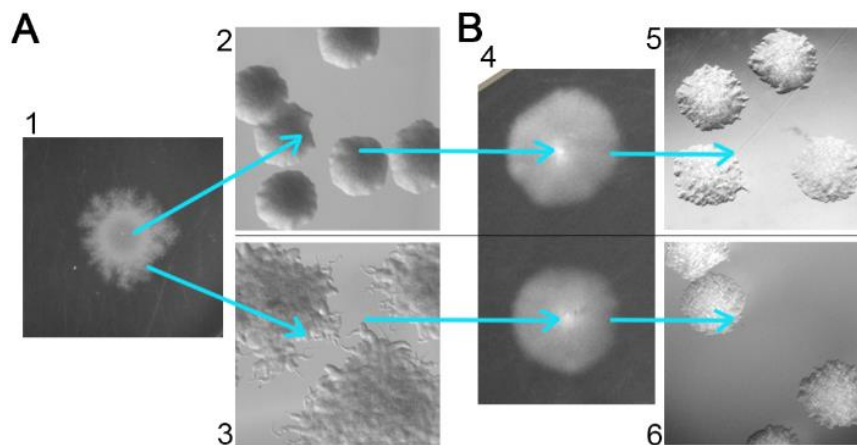


Figure 1-19. Distinct colony morphotypes with different motility phenotypes

(A) *C. difficile* R20291 was spotted on 1.8% agar and allowed to spread (panel 1). Bacteria collected from the centre of a spot yielded mostly smooth colonies (panel 2), whereas bacteria from the edge yield almost exclusively rough colonies (panel 3). (B) Rough and smooth colony isolates obtained as in (A) were passaged in 0.3% agar (panel 4). Both rough and smooth colony isolates only gave rise to smooth colonies (panels 5 and 6). Adapted from Garrett *et al.* (2016).

This study proposes that branched colony morphologies are characteristic of twitching motility and can be used to distinguish it from swimming motility.

1.5. Aims and objectives

To contribute to further the understanding of TFP in *C. difficile*, this work aimed to investigate the effects of c-di-GMP in TFP expression and related flagella-linked motility. Optimisation of *dccA* induction to appropriate increased levels of c-di-GMP was undertaken to then study the effects on TFP and flagella expression, cell and colony morphology, twitching and swimming motility.

We also aimed to complete and revisit previous mutagenesis studies on individual pilins. The roles of *C. difficile* major pilin PilA1, the pre-pilin protease PilD1 and the minor pilin PilJ were investigated.

Chapter 2: Materials and Methods

2.1. Bacterial strain and Growth Conditions

2.1.1. *Culturing Escherichia coli*

E. coli strains were grown on LB agar (VWR) or in LB broth (VWR). All media were supplemented where appropriate with antibiotics chloramphenicol (15 µg/ml). *E. coli* NEB5α cells (NEB) were used as recipient strain in cloning procedures. *E. coli* CA434 (provided by Dr Anna Barwinska-Sendra in Dr Salgado's lab) was used as the donor strain for conjugation of plasmids into *C. difficile*. Cultures were grown O/N with agitation (180 rpm) at 37°C.

2.1.2. *Culturing C. difficile*

Plated cultures of *C. difficile* strains were grown on BHIS agar (brain-heart infusion (Oxoid) agar supplemented with 0.1% L-cysteine (Sigma) and 5 mg/ml yeast extract (Bacto)) or *Clostridioides difficile* Defined Medium (CDMM) (Karasawa et al., 1995). A list of CDMM component recipe is shown in Table 2-1.

Liquid cultures were grown in BHIS or TY broth (3% tryptose, 2% yeast extract (Bacto)). Cultures were supplemented where appropriate with antibiotics thiamphenicol (15 µg/ml), cycloserine (250 µg/ml). Cultures were grown in an anaerobic cabinet (Don Whitley Scientific) at 37 °C, in an atmosphere of 10% CO₂, 10% H₂ and 80% N₂. Media were pre-reduced in the anaerobic cabinet before inoculation.

Table 2-1. *Clostridioides difficile* Defined Medium (CDMM) composition

Component	Stock concentration (mg/ml)	Final concentration (mg/ml)
Amino acids (5X)		
Casamino acids	50	10
L-Tryptophan	2.5	0.5
L-Cysteine	2.5	0.5
Salts (10X)		
Na ₂ HPO ₄	50	5
NaHCO ₃	50	5
KH ₂ PO ₄	9	0.9
NaCl	9	0.9
Glucose (20X)		
D-Glucose	200	10
Trace salts (50X)		
(NH ₄) ₂ SO ₄	2	0.04
CaCl ₂ · H ₂ O	1.3	0.026
MgCl ₂ · 6H ₂ O	1	0.02
MnCl ₂ · 4H ₂ O	0.5	0.01
CoCl ₂ · 6H ₂ O	0.05	0.001
Iron (100X)		
FeSO ₄	0.4	0.004
Vitamins		
D-Biotin (1000X)	1	0.001
Calcium-D-panthothenate (1000X)	1	0.001
Pyridoxine (1000X)	1	0.001

2.1.3. Storage of Strains

All strains produced as part of this thesis were catalogued in the Salgado lab strain collection. 1 ml of an overnight LB or BHIS culture for *E. coli* strains and *C. difficile* strains, respectively, of the sequence-verified isolate was mixed with 1 ml of sterile 50% glycerol and frozen at -80 °C.

2.1.4. Transformation of *E. coli*

Plasmid DNA were transformed into competent *E. coli* cells by heat-shock in strain constructions. Competent cells (15 µl of NEB5α, 50 µl of CA434) were thawed on ice. 40-200

ng of intact plasmid DNA or ligation/Gibson assembly reaction mixture was added to the cells which were then incubated on ice for 30 mins. Cells were heat-shocked for 45 sec at 42°C and returned on ice for incubation 5 mins. 150 µl of LB broth was then added to the cells which were then incubated at 37°C for 1 hr, following which 100 µl of the transformation product was spread onto LB-agar plates supplemented with appropriate antibiotic.

2.1.5. Plasmid DNA Conjugation into *C. difficile*

pMTL960-based shuttle plasmids were transformed into *E. coli* CA434 (described in 1.1.4) and conjugated into *C. difficile* as described previously (Purdy et al., 2002). Briefly, 1 ml of *E. coli* O/N culture (donor) was spun down (1 min at 3,000 x g), washed gently with sterile phosphate-buffered saline (PBS) and mixed with 200 µl of O/N *C. difficile* culture (recipient). The resulting mixture was spotted onto nonselective BHIS agar and incubated anaerobically for 8h. The resulting growth was resuspended in 1 ml of sterile PBS and spread out on BHIS agar supplemented with thiamphenicol (15 µg/ml) to select for pMTL960-based plasmids and either cycloserine (250 µg/ml) or cefoxitin (16 µg/ml) to counterselect against *E. coli*. Transconjugants were re-streaked onto selective BHIS and CDDM plates. Colonies were patch-plated on selective and nonselective BHIS plates, growing on only nonselective plates were screened as the final constructs. A detailed list of *C. difficile* strains used or constructed throughout this project is provided in Table 2-2.

Table 2-2. *C. difficile* 630 strains used in biological assays in this study

Strain	Descriptive	Source/Reference
630	Wild-Type Strain	Mullany et al., 1990
630Δ <i>pilA1</i>	<i>pilA1</i> deleted from 630 using <i>codA</i> Allele Exchange Mutagenesis	Dr. E Couchman (Imperial College London)
630Δ <i>pilD1</i>	<i>pilD1</i> deleted from 630 using <i>codA</i> Allele Exchange Mutagenesis	This work
630Δ <i>pilJ</i>	<i>pilJ</i> deleted from 630 using <i>codA</i> Allele Exchange Mutagenesis	This work

2.2. Bioinformatics

2.2.1. DNA, Gene and Protein Analysis

C. difficile genome sequences were obtained from NCBI. Plasmid and DNA fragment maps were constructed and visualised using Geneious Prime 2019 (Biomatters Ltd., New Zealand). Genes encoding TFP proteins in *C. difficile* strains were determined by mapping *C. difficile* 630 TFP genes to *C. difficile* genomes in Geneious Prime 2019. *C. difficile* TFP genes throughout strains were compared by NCBI BLAST (<https://blast.ncbi.nlm.nih.gov/Blast.cgi>). Phylogenetic trees were generated in Geneious Prime 2019 and edited in iTOL (<https://itol.embl.de/>). All DNA sequencing was performed by Sanger sequencing from Eurofins Genomics. Sequences were aligned using Geneious Prime 2019. Protein molecular mass is predicted by Expasy ProtParam (<https://web.expasy.org/protparam/>).

2.3. DNA Manipulation

2.3.1. Genomic DNA Extraction

Genomic DNA (gDNA) of *C. difficile* was extracted from the cells using DNA Mini Kit (QIAamp), according to the manufacturer's guidelines. Briefly, 15 – 20 ml of overnight culture was centrifuged at 4,000 rpm for 15 min, followed by resuspending in Buffer ATL and incubating with Proteinase K at 56 °C for an hour, treated by vortex every 10 min. Buffer AL was added and vortexed, followed by incubating at 70 °C for 10 min and mixed with ethanol. The sample was transferred into a column and spun down at 6,000 xg for 1 min. After the column being washed in Buffer AW1 and AW2, gDNA was eluted in 50 µl of Buffer AE twice at centrifuge 6,000 xg for 1 min.

2.3.2. Purification of Plasmid DNA

DNA preparations for routine colony screening were extracted using 5% (w/v) Chelex 100 resin (Bio-Rad). Colonies were suspended in 5 % Chelex, boiled for 10 min at 100 °C and pelleted at 10,000 xg for 1 min. Supernatants containing DNA were used further analysis.

Plasmid DNA was extracted from *E. coli* using a mini-prep kit (Sigma or NEB) according to

manufacturer's protocol. Briefly, 5 ml cultures were centrifuged at 4,000 xg for 15 min and the resulting pellets were re-suspended in 200 μ l of Resuspending buffer. An equal volume of Lysis buffer was added, and mixture was incubated for 1 min at room temperature. 350 μ l of Neutralise buffer was added, the sample was centrifuged at 13,000 xg for 10 min. The supernatant was applied to a column and centrifuged at 13,000 xg for 1 min. The column was washed with 700 μ l of washing buffer. Residual buffer was removed by centrifuging once more at 13,000 xg for 2 min. DNA was eluted by adding 30 - 50 μ l of nuclease-free water, incubating for 1 min at room temperature and centrifuging at 10,000 xg for 1 min.

2.3.3. Polymerase Chain Reaction (PCR) and Primers

Routine screening PCR and colony PCR were carried out using Quick-Load Taq polymerase Mix (NEB) according to manufacturer's guidelines in a total volume of 20 μ l (1x Quick-Load Taq polymerase Mix, 0.2 μ M forward and reverse primers, 1 μ l of plasmid DNA from Chelex extraction). Initial denaturation was at 95 °C for 3 min followed by thirty cycles of denaturation at 95 °C for 30 s, annealing at the lower primer temperature for 30 sec and extension at 68 °C for 1 min per kb. A final extension at 68 °C for 5 min was included to ensure completion of DNA synthesis.

PCR reactions requiring higher stringency for inverse PCR and amplification of gDNA fragments during cloning were carried out using Phusion polymerase (NEB) according to manufacturer's guidelines in a total volume of 50 μ l (1x Phusion HF, 0.2 mM dNTPs, 0.5 μ M forward and reverse primers, 3 % DMSO, 0.4 ng – 0.6 ng of template DNA). Initial denaturation was at 98 °C for 30 sec followed by 30 cycles of denaturation at 98 °C for 10 s, annealing at the lower primer temperature for 30 s and extension at 72 °C for 15 s per kb. A final extension at 72 °C for 10 min was included to ensure completion of DNA synthesis. Primers used throughout this study were synthesised by Euorfin Genomics and are listed in Appendix A, Table A-1.

2.3.4. Agarose Gel Electrophoresis

Agarose gels were prepared by melting 1.5 % (w/v) agarose powder (Invitrogen) in 1 x TAE (40 mM Tris-Acetate, 2 mM Na₂EDTA pH 8.3). Agarose gel was cast on a horizontal perspex plate

supplemented with 1/ 10,000 volume of SybrSafe DNA stain (NEB). DNA samples were mixed with 1/4 volume of DNA loading buffer (NEB) and loaded into the gel wells. Electrophoresis was performed at approximately 10V cm⁻¹ in 1 x TAE buffer. DNA was visualised by Bio-Rad.

2.3.5. Purification of PCR Products

PCR-amplified DNA fragments were purified using the PCR Clean-up kit (Sigma-Aldrich) according to manufacturer's guidelines. PCR reaction was mixed with Binding Solution in 1:5 of volume and centrifuged at 13,100 *xg* for 1 min. Following with washing in Wash solution, DNA was finally eluted with 30 – 50 µl of water.

DNA was extracted from agarose gels using the PCR Gel Extraction kit (Sigma-Aldrich) according to manufacturer's guidelines. Briefly, bands were excised using a scalpel, weighed and mixed with 3 volumes of neutralise buffer. Following 10 min incubation at 56 °C. 1 volume of isopropanol was added, and the resulting samples were applied onto a column and centrifuged at 13,000 *xg* for 1 min. The column was washed with 800 µl of washing buffer (13,000 *xg* for 1 min). DNA was eluted by adding 30 - 50 µl of nuclease-free water, incubating for 1 min at RT and centrifuging at 13,000 *xg* for 1 min.

2.3.6. Restriction Digests

All restriction endonuclease digest were carried out using enzymes provided by New England Biolabs (NEB) according to manufacturer's guidelines. Vector plasmid was then mixed with 2 µl of DpnI and 4 µl of CutSmart buffer in a final volume of 40 µl and incubated at 37 °C for 2 hours, followed by PCR clean-up. DNA inserts and digested vector were then incubated with 1 µl each BamHI-HF, SphI, and 1X CutSmart buffer in a final volume of 34 µl at 37 °C for 1-2 hours.

2.3.7. DNA Ligation

Digested vector plasmid was dephosphorylated by Antarctic phosphatase (NEB), according to manufacturer's guidelines. Ligation reactions were carried out for 15 min at RT using

QuickStick ligase (Bioline) as per manufacturer's guidelines in a total volume of 20 μ l (50 ng of DNA in nuclease-free water, 1x Quick Stick ligase buffer, 1 μ l QuickStick ligase). For routine cloning a 2:1 or 3:1 or 5:1 insert:vector molar ratio was used, the amounts of DNA inserts were calculated by NEBioCalculator (<http://nebiocalculator.neb.com>). Restriction digested enzymes were phosphorylated using 1 μ l of T4 polynucleotide kinase (NEB) prior to ligation.

2.3.8. Gibson Assembly

Assembly of vector plasmid and DNA inserts in some mutant cloning was performed using Gibson Assembly Master Mix (NEB). Primers used to amplify DNA inserts were designed using NEBuilder (<http://nebuilder.neb.com/>). Linearised vector and DNA inserts were mixed in 1:2 or 1:3 or 1:5 molar ratio, using 100 - 200 ng of vector and the amounts of inserts was calculated according to manufacturer's instructions. DNA mixture was incubated with 1X Gibson Assembly Mater Mix at 50 °C for an hour, followed by transforming in to NEB5 α cells as described in 1.1.4.

2.3.9. Allele Exchange Mutagenesis

ACE mutants were generated in *C. difficile* 630 as described by Ng et al. (2013) (Ng et al., 2013). Briefly, mutated alleles carrying in-frame deletions were generated by cloning PCR-amplified 750 bp upstream and downstream homology regions into pMTL960 derived plasmids using Gibson Assembly or restriction sites according to manufacturer's instructions. The resulting plasmids were conjugated into *C. difficile* as described in 1.1.5. Following two passages on BHIS agar supplemented with 5 μ g ml⁻¹, 15 μ g ml⁻¹ thiamphenicol and 250 μ g ml⁻¹ cycloserine or 16 μ g ml⁻¹ cefoxitin, colonies that were noticeably larger (indicative of plasmid integration) were screened by colony PCR to identify single-crossover mutants using primers flanking the upstream and downstream homology regions and one of these primers in conjunction with a plasmid-specific primer to amplify across the integration junction. Single crossover mutants were streaked onto *C. difficile* minimal medium (CDMM) supplemented with 5 μ g ml⁻¹ uracil and 2 mg ml⁻¹ 5-fluoroorotic acid (FOA) to select for plasmid excision. The isolated FOA resistant colonies were screened by PCR. Double-crossover mutants in which the mutated

allele was successfully integrated yielded products smaller than those seen in WT revertants. The resulting colonies were then patch plated onto non-supplemented and selective BHIS agar to select for thiamphenicol prototrophic indicating successful allele exchange, as plasmid-borne thiamphenicol resistance released from the gDNA. Thiamphenicol-sensitive colonies were screened by colony PCR and sequenced by Eurofins Genomics for confirmation.

2.3.10. Vector Construction

As explained in 1.3.9, construction of plasmids for allele-exchange mutagenesis started from inserting amplified gene homology regions into a linearised pseudo-suicide vector pMTL-SC7315, or pJAK112 by Gibson Assembly or BamHI/SacI restriction sites.

A *pilD1* deletion plasmid was constructed using primers oZGW030/oZGW031 to amplify the upstream region and oZGW032/oZGW033 to amplify the downstream region. Vector pMTL-SC7315 was linearised by primers oZGW028/oZGW029. Amplified upstream and downstream regions of *pilD1* were assembled into the linearised vector, yielding plasmid pZGW001. Assembly clones were screened by colony PCR using primers oZGW001/oZGW002.

A *pilD1* complementation plasmid was constructed using primers oZGW058/ oZGW059 to amplify *pilD1*, which was inserted into linearised vector pECC76 via BamHI/SphI restriction sites, yielding plasmid pZGW007. Assembly clones were screened by colony PCR using primer oZGW056/oZGW057. Vector pECC76 was linearised using primers oZGW062/oZGW063.

A *pilJ* deletion plasmid was constructed using primers oZGW040/oZGW041 to amplify the upstream region and oZGW042/oZGW043 to amplify the downstream region, which were then assembled into vector pJAK112 using BamHI/SacI restriction sites, yielding plasmid pZGW002. Assembly clones were screened by colony PCR using primers oZGW001/oZGW002.

A *pilJ* complementation plasmid was constructed using primers oZGW060/ oZGW061 to amplify *pilJ*, which was inserted into linearised pECC76 via BamHI/SphI restriction sites, yielding plasmid oZGW008. Assembly clones were screened by colony PCR using primers oZGW056/oZGW057.

pilA1 complementation plasmids pZGW005 and pZGW006 were synthesised by GENEWIZ (Azenta Life Sciences, US). Plasmid pZGW005 contains *Ptet* promoter regulating *dccA*, followed by a terminator and *pilA1* with its own promoter region from *C. difficile* 630 genomic DNA. Plasmid pZGW006 is based on pZGW005, but contains a riboswitch *Cdi2_4* between the

terminator and *pilA1* promoter region. Both plasmids were transformed into NEB5 α and clones confirmed by colony PCR using primers oZGW077/oZGW078.

A full list of plasmids used in this study can be found in Table A-2 in Appendix A.

2.4. Protein Manipulation

2.4.1. Protein Expression in *C. difficile*

Overnight growth was sub-cultured into pre-reduced BHIS to a resultant OD₆₀₀ of 0.1 and grow until reaching late log-phase (OD₆₀₀ of approximately 1.8). The culture was centrifuged at 17,000 $\times g$ for 10 min in Eppendorf tubes. The supernatant was kept for TCA extraction. The cell pellets were washed in PBS and centrifuged once again, followed by freezing at -20 °C.

2.4.2. Tri-Chloroacetic Acid Precipitation of Protein

C. difficile culture supernatant was harvested by centrifugation (17,000 $\times g$ for 10min). Tri-chloroacetic acid (TCA) was added into *C. difficile* culture supernatant to a final concentration of 10 %. Samples were vortexed briefly, incubated on ice for 30 min on shaker and centrifuged at 4,000 for 10 min. The sample was precipitated with ice-cold 90 % acetone for 15 min on shaker and centrifuged at 17,000 $\times g$ for 3 min and vortex, followed by repeating precipitate and centrifuge two more times. Protein pellets were incubated at room temperature overnight to evaporate any residual liquid and resuspended to OD₆₀₀ of 100.

2.5. SDS-PAGE and Immunoblotting

2.5.1. Cell lysate Preparation

Cell pellets were thaw on ice and resuspended to OD₆₀₀ of 100, followed by incubation with 12 $\mu g ml^{-1}$ of DNase and 20 $\mu g ml^{-1}$ of CD27L for 1 hour. 60 % w/v of 0.1 mm beads were added into the cell pellets, vortexed for 10 min and mixed with 10 % SDS. Both cell proteins and TCA extracted proteins were mixed with 1X Loading buffer (100 mM Tris base pH 8.8, 4 % SDS, 20 % glycerol, 0.2 % bromophenol blue, 200 mM DTT).

2.5.2. SDS-PAGE and Coomassie Staining

Denaturing sodium dodecyl sulphate (SDS) polyacrylamide gel electrophoresis (PAGE) was used throughout to identify and verify the quality of protein samples. Samples were mixed with 2X SDS-sample buffer prior to loading on a 12% SDS-PAGE gel (12% Bis-acrylamide, 375mM Tris base (pH8.8), 0.1% SDS, 0.1% ammonium persulphate, 0.05% TEMED). SDS-PAGE was performed at 180 V for 45 - 60 mins depending upon the mass of the sample. Proteins were stained with InstantBlue (Expedeon), followed by destaining in water overnight. Gels were scanned using Bio-Rad ChemiDoc and verified molecular weight using PageRuler protein ladder (ThermoFisher Scientific).

2.5.3. Immunoblotting

Following SDS-PAGE, proteins were transferred onto nitrocellulose membranes by semi-dry transfer. The transfer stack was assembled as follows. Two pieces of Whatman 3 mm filter paper soaked in Anode buffer I (300 mM Tris-HCl in 10 % methanol, pH 10.4), followed by one piece of filter paper soaked in Anode buffer II (25 mM Tris-HCl in 10% methanol, pH 9.4), followed by nitrocellulose membrane wet with Anode buffer II, followed by the gel soaked in Cathode buffer 40 mM glycine; 25 mM Tris-HCl in 10 % Methanol, pH 9.4) followed by three pieces of filter paper soaked in Cathode buffer. Transfer was carried out for 20 - 25 min at a constant voltage of 15V. Following protein transfer, membranes were blocked in TBSTM buffer (3 % milk, 0.01 % Tween-20, 1X TBS) for 1 hour at 4 °C and incubated with primary antibodies in TBSTM buffer for 1 hour in 4 °C. After washing the membrane with TBST buffer (0.01 % Tween-20, 1X TBS) for 10 min and repeating twice, secondary antibodies were applied in TBSTM buffer and incubated as above. The membranes were washed with TBST buffer two more times and rinsed by 1X TBS buffer and developed using chemiluminescence substrate (Bio-Rad). Signal was detected using Bio-Rad ChemiDOC. Immunoblots were performed in at least biological triplicates. Data for quantitative analysis was collected with Fiji and processed in Excel. A complete list of primary and secondary antibodies used throughout this study is provided in Appendix A, Table A-3.

2.6. Phenotypic Analysis

2.6.1. Growth Curves

Overnight cultures of *C. difficile* were sub-cultured into pre-reduced BHIS to resultant OD₆₀₀ at 0.05. The cultures were incubated for several hours, and OD₆₀₀ was measured hourly either manually in a spectrometer or using a Cerillo plate reader. For statistical analysis, each assay was performed in technical duplicates with biological triplicates.

2.6.2. Flagella Motility Assays

Overnight cultures of *C. difficile* were sub-cultured into pre-reduced BHIS to resultant OD₆₀₀ at 0.1, and grow until reaching log phase (OD₆₀₀ ~ 0.8). Flagella motility was assessed by inoculating a plate of 0.3 % motility agar (0.5X BHIS, 0.3 % agar) with 1 µl of cultures. The rest of culture was used for western blot analysis as described in 2.4. Motility zones were measured 24 and 48 hours after inoculation. Each assay was performed in technical duplicates with biological duplicates.

2.6.3. Twitching Motility Assays

Overnight cultures of *C. difficile* were sub-cultured into pre-reduced BHIS to resultant OD₆₀₀ at 0.1, and grow until reaching log phase (OD₆₀₀ ~ 0.8). Twitching motility was assessed by spotting 5 µl of cultures onto plates of 1.8 % agar (1X BHIS, 1.8 % agar) supplemented with antibiotics. Colony size was measured every 24 hours for 7 days. When harvesting from the plate, cells were resuspended in 1 ml of BHIS by L-spreader and transferred in to Eppendorf tubes by pipetting. Assays were performed in technical triplicates with biological triplicates.

2.6.4. Biofilm Assays

Overnight cultures were inoculated in 1:100 into pre-reduced BHIS in 24-well plates. After incubation in cabinet for 7 days, culture liquid was taken out by pipettes and washed by PBS,

followed by staining in 0.2 % of crystal violet for 30 min. Biofilm in each well was then washed in PBS twice. Stains on biofilm were dissolved in absolute methanol for 30 min and absorbance at 595nm was measured by using plate reader (Biotek, UK). Assays were performed in technical triplicates with biological triplicates.

2.6.5. Phase Contrast Microscopy

Overnight growth was sub-cultured into pre-reduced BHIS to a resultant OD₆₀₀ of 0.1 and grown until reaching late log-phase (OD₆₀₀ of approx. 1.8). Cells were harvested by centrifuging at 4,000 *xg* for 3 min and washed in PBS buffer and repeat centrifuge. Cells were resuspended in PBS buffer to OD₆₀₀ 10 and 1 μ l was spotted onto an agarose pad (1.5 % agarose, 1 μ g ml⁻¹ FM 4-64, 1 μ g ml⁻¹ Hoechst, 0.5 % DMSO) on a microscope slide (VWR), covered with cover glass after agarose pad absorbing the culture. Cells were visualised in a Nikon Ti microscope. Microscopy images were taken at 4 random fields from biological triplicates. Cell lengths were measured with 10 random cells from each image.

2.6.6. Statistical analysis

Statistical analysis was carried out in GraphPad Prism v.12. For cell length, biofilm formation and motility diameters one-way ANOVA tests were used, while for cell growth a two-way ANOVA was carried out. Significance is indicated as * ($p < 0.1$), ** ($p < 0.01$), *** ($p < 0.001$) and **** ($p < 0.0001$).

Chapter 3: c-di-GMP Impact on Cell Growth and TFP Expression

3.1. Introduction

At a high intracellular level of c-di-GMP, c-di-GMP binds to riboswitch Cdi2_4 and induces *pilA1* expression. To control the level of c-di-GMP in our experiments, *dccA*, the diguanylate cyclase (DGC) responsible for c-di-GMP synthesis, was introduced into *C. difficile* via an inducible plasmid vector.

The overexpression of *dccA* when under the control of P_{cwp2} , a constitutively active promoter, resulted in an uncontrolled high level of c-di-GMP, which lead to elongated cell shapes (Couchman, 2016). Therefore, a tetracycline-inducible promoter, P_{tet} , was used to control *dccA* expression (Appendix Figure A-1). When supplementing anhydrotetracycline (ATc) during incubation, the P_{tet} promoter is activated to induce *dccA* expression, which increases the level of c-di-GMP and triggers *pilA1* expression via binding to the riboswitch Cdi2_4.

The first aim in this chapter was to optimise DccA levels by investigating a range of ATc concentrations. An ideal level of induction to elevate intracellular c-di-GMP should switch on *pilA1* expression but avoid leading to long abnormal cell morphologies, as reported for constitutive *dccA* expression (Couchman, 2016).

In previous work, genes encoding TFP proteins in the primary gene cluster, apart from one of the pre-pilin peptidases, *pilD1*, had been deleted for mutagenesis studies. In this chapter, strains lacking *pilD1* and *pilJ* were constructed and characterised, in order to complete that work (Couchman, 2016). Investigation of cell growth and morphology, *pilA1* expression and biofilm formation in these strains was the second aim of the work described in this chapter.

3.2. Effects of c-di-GMP on *C. difficile* Cell Growth and TFP expression

3.2.1. *dccA* induction and CD630 growth and cell morphology

As described above, expression of *C. difficile* TFP requires a high level of intracellular c-di-GMP, while avoiding forming long-chain cell shape phenotype. An inducible copy of the *dccA* gene was introduced into cells via plasmid pECC17 with a regulatory promoter P_{tet} . First, a range of anhydrotetracycline (ATc) concentrations, from 0 to 100 ng ml⁻¹, was supplemented into *C. difficile* growth culture and cell growth was examined in the wild-type strain 630 (CD630), vector control 630_pASF85 and *dccA* inducible strain 630_pECC17. The vector pASF85 contains the P_{tet} promoter region and *slpA* terminator without the *dccA* gene.

Cell growth was followed from 0 to 11 hours of culture growth by manually collecting a sample at one-hour intervals and measuring the OD_{600nm} in a spectrometer, as described in section 2.6.1. There was no phenotype observed in strains CD630 (Figure 3-1, panel A and B) and 630_pASF85 (Figure 3-1, panel C and D). However, in 630_pECC17, addition of ATc to the culture lead to slower growth rates, particularly at 75 and 100 ng ml⁻¹ of ATc (Figure 3-1, panel E and F).

During growth measurements, microscopy samples were taken from incubated cultures after 7 hours of growth, which is in the middle of log phase approximately. From the results, CD630 (Figure 3-2) and vector control 630_pASF85 (Figure 3-3) do not show obvious difference in cell morphology under 0 – 100 ng ml⁻¹ of ATc supplementation. This indicates neither addition of ATc from 0 – 100 ng ml⁻¹ nor introducing the empty vector have any effect on cell morphology. When inducing *dccA* expression in 630_pECC17, longer cell shapes are observed as ATc concentration increases (Figure 3-4).

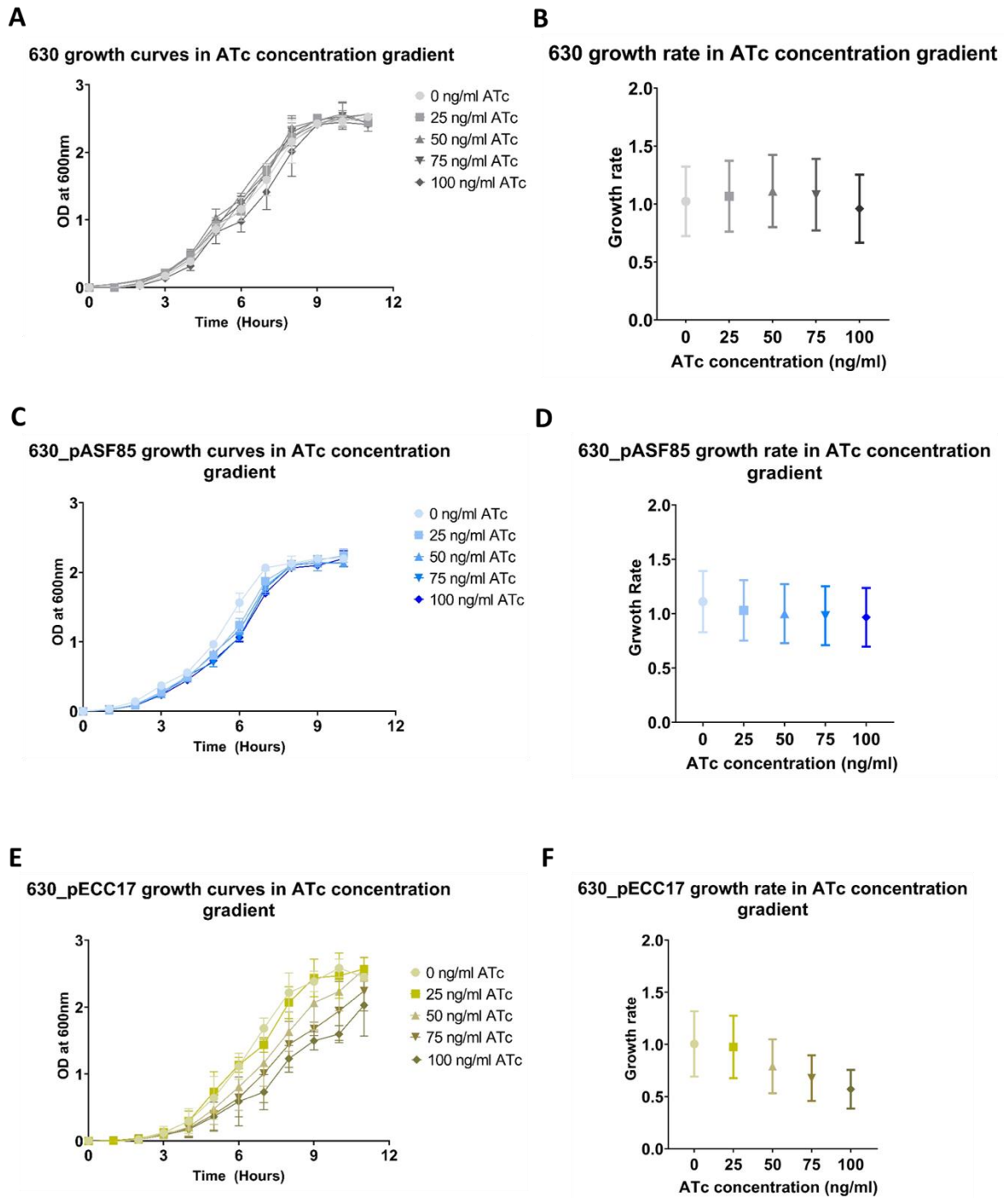


Figure 3-1. *C. difficile* growth under varying ATc concentrations

Growth curves of *C. difficile* strain CD630 (A), vector control 630_pASF85 (C) and *dccA* inducible strain 630_pECC17 (E) were measured hourly by spectrometry absorbance at 600nm during 11 h incubation in BHIS with 0, 25, 50, 75 or 100 ng ml⁻¹ of ATc supplementation. The corresponding growth rates are shown in panels B, D and F. Data analysed via 2-way ANOVA performed by GraphPad Prism.

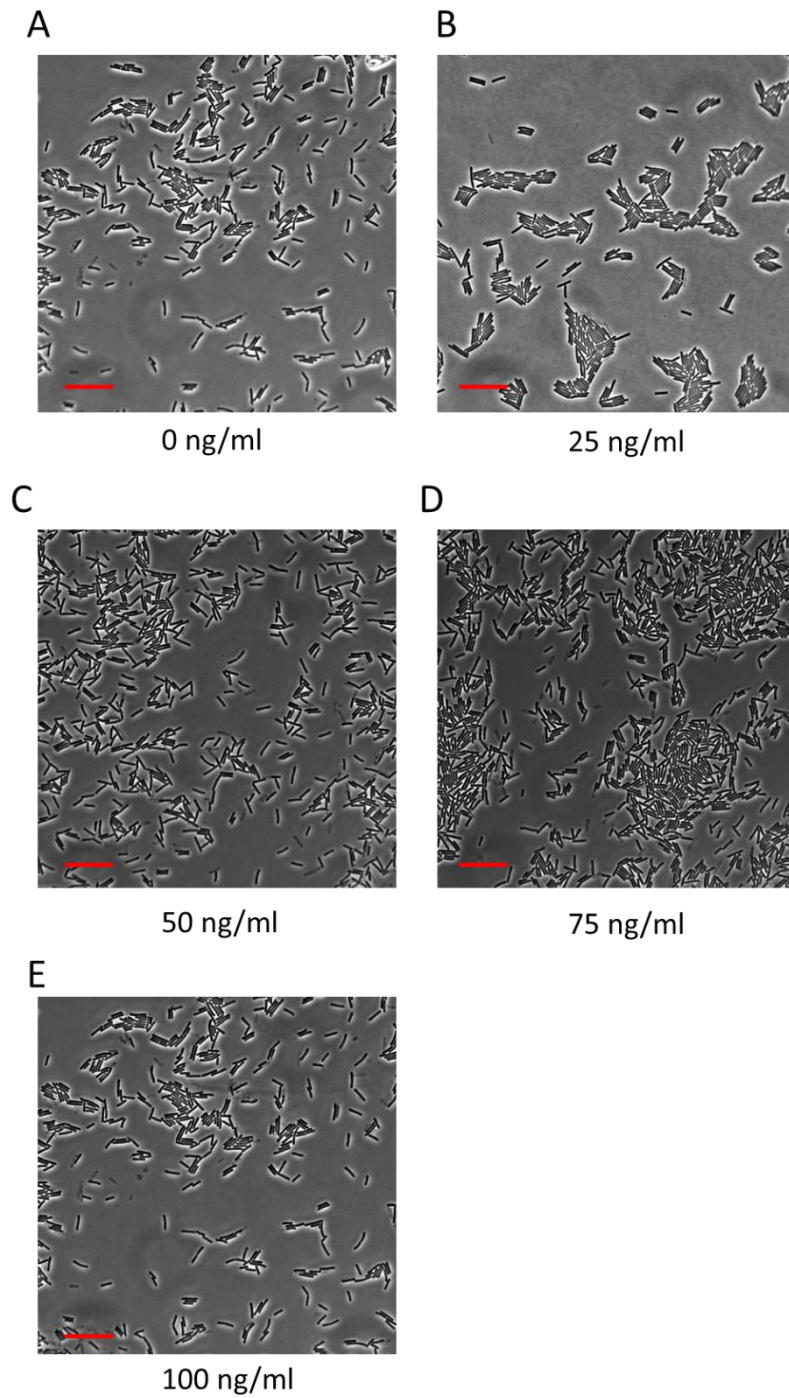


Figure 3-2. *C. difficile* CD630 cell morphology under varying ATc concentrations

Phase contrast microscopy showing CD630 cells incubated in BHIS culture for 7 hours with 0, 25, 50, 75, 100 ng ml^{-1} (A-E) of ATc supplementation. Red bar indicates 10 μm .

630_pASF85

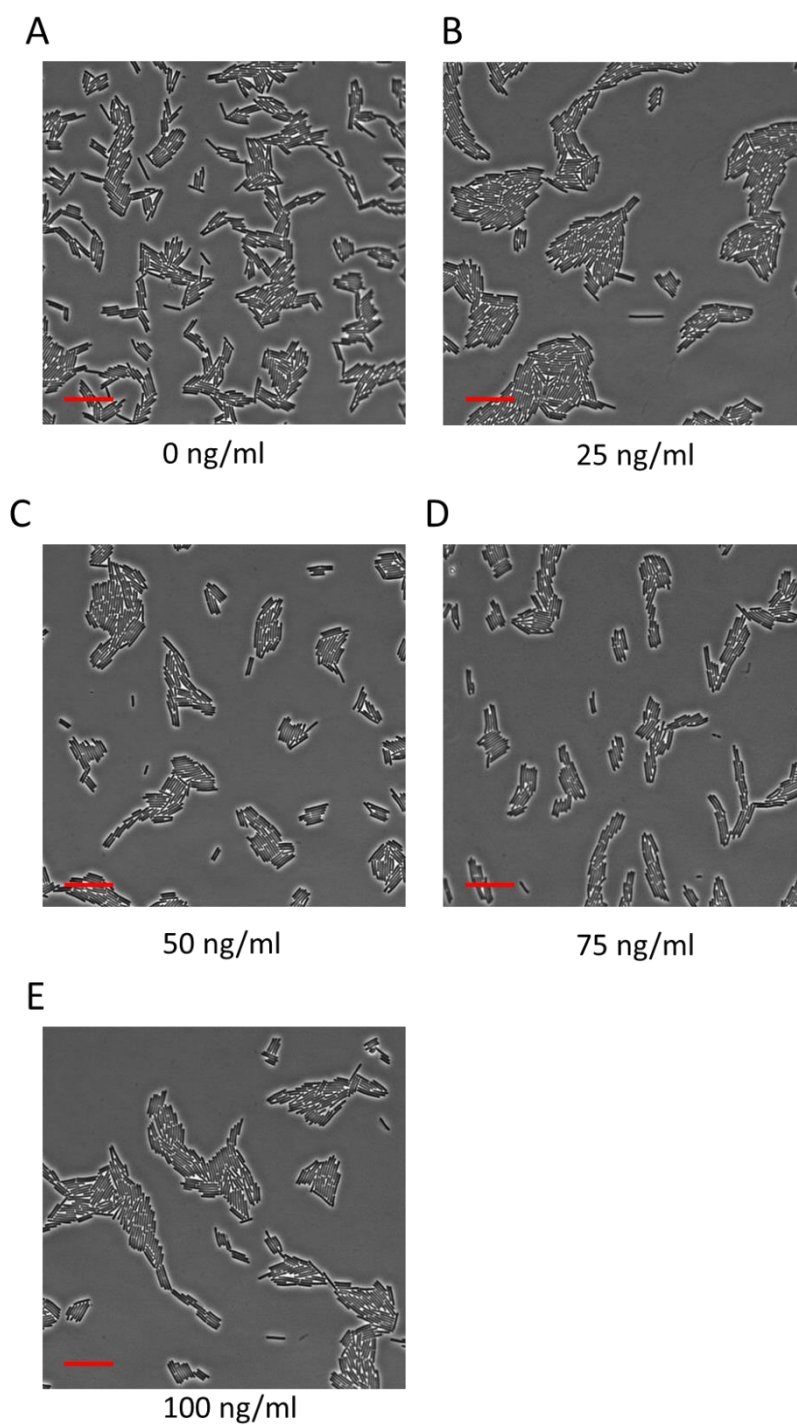


Figure 3-3. *C. difficile* 630_pASF85 cell morphology under ATc concentrations

Phase contrast microscopy figures showing *C. difficile* 630_pASF85, the vector control strain, cells incubated in BHIS culture for 7 hours with 0, 25, 50, 75, 100 ng ml⁻¹ (A-E) of ATc supplementation. Red bar indicates 10 μ m.

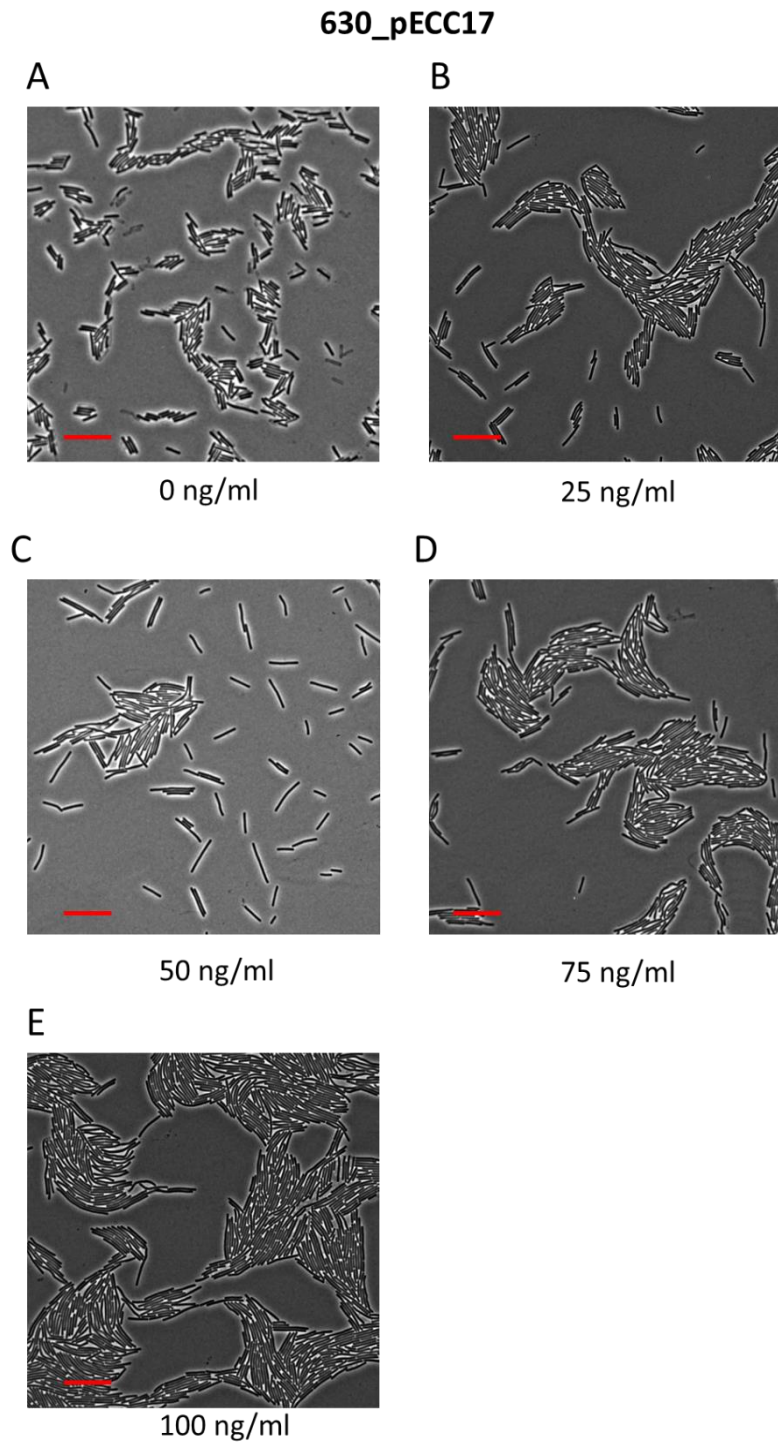


Figure 3-4. *C. difficile* 630_pECC17 cell morphology under ATc concentrations

Phase contrast microscopy figures showing *C. difficile* 630_pECC17, *dccA* inducible strain, cells incubated in BHIS culture for 7 hours with 0, 25, 50, 75, 100 ng ml⁻¹ (A-E) of ATc supplementation. Red bar indicates 10 µm.

Analysis of the growth curves and examination of cell morphology showed that concentrations higher than 50 ng ml⁻¹ of ATc lead to significant defects in 630_pECC17 so this was the concentration used to analyse the effects of *dccA* induction in more detail.

Growth of the three *C. difficile* strains, CD630, vector control 630_pASF85 and *dccA* inducible strain 630_pECC17, under 0 or 50 ng ml⁻¹ of ATc supplementation was further analysed (Figure 3-5). One-way ANOVA analysis showed no significant difference on growth rates in the presence or absence of 50 ng ml⁻¹ of ATc in all three strains, confirming that this is a suitable concentration of ATc to use in our studies (Figure 3-5).

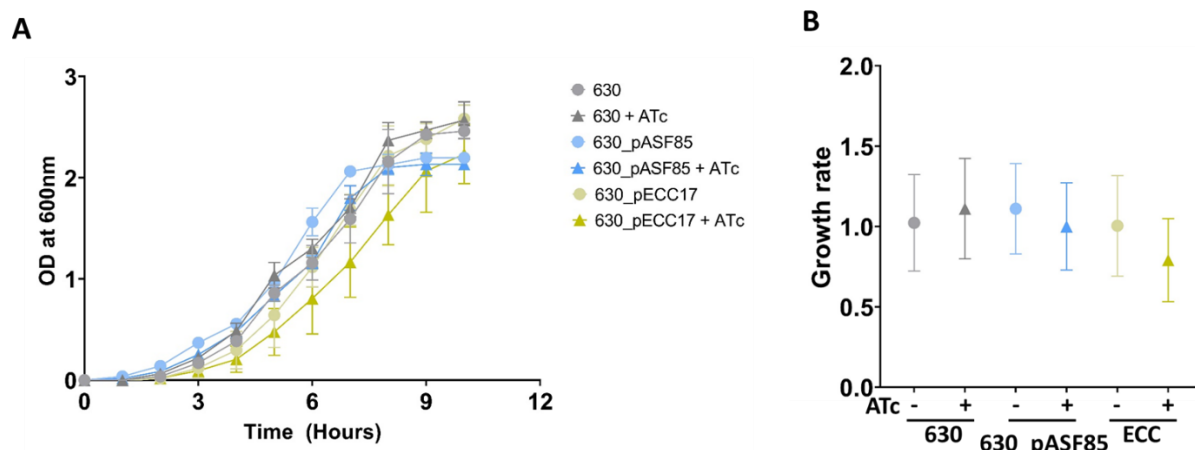


Figure 3-5. *C. difficile* growth with and without ATc supplementation

The growth of *C. difficile* strains CD630 (grey), vector control 630_pASF85 (blue) and *dccA* inducible strain 630_pECC17 (ECC; yellow) with 0 (circle) or 50 (triangle) ng ml⁻¹ of ATc supplementation from 0 – 11 hours of growth are presented by growth curves (A) and growth rates (B). OD is measured by absorbance at 600nm. Figure and one-way ANOVA analysis performed using GraphPad Prism.

The cell morphology was investigated in more detail by phase contrast microscopy, and cell length was measured. In CD630 and vector control 630_pASF85, there is no significant difference in cell length when adding 0 or 50 ng ml⁻¹ of ATc (Figure 3-6, panel A, B and D). There is also no significant difference between these two strains. This confirms that addition of 50 ng ml⁻¹ of ATc or introducing the empty vector does not lead to changes in cell morphology. Compared to CD630 and 630_pASF85 or absence of ATc, 630_pECC17 cells grow to a longer cell shape when *dccA* expression is induced (Figure 3-6, panel C and D), suggesting that higher c-di-GMP levels lead to a phenotype related to cell division/growth. It should be noted that strain 630_pECC17 contains multiple copies of the inducible plasmid and the effect of addition of ATc is therefore amplified when compared to insertion of an inducible gene on the chromosome.

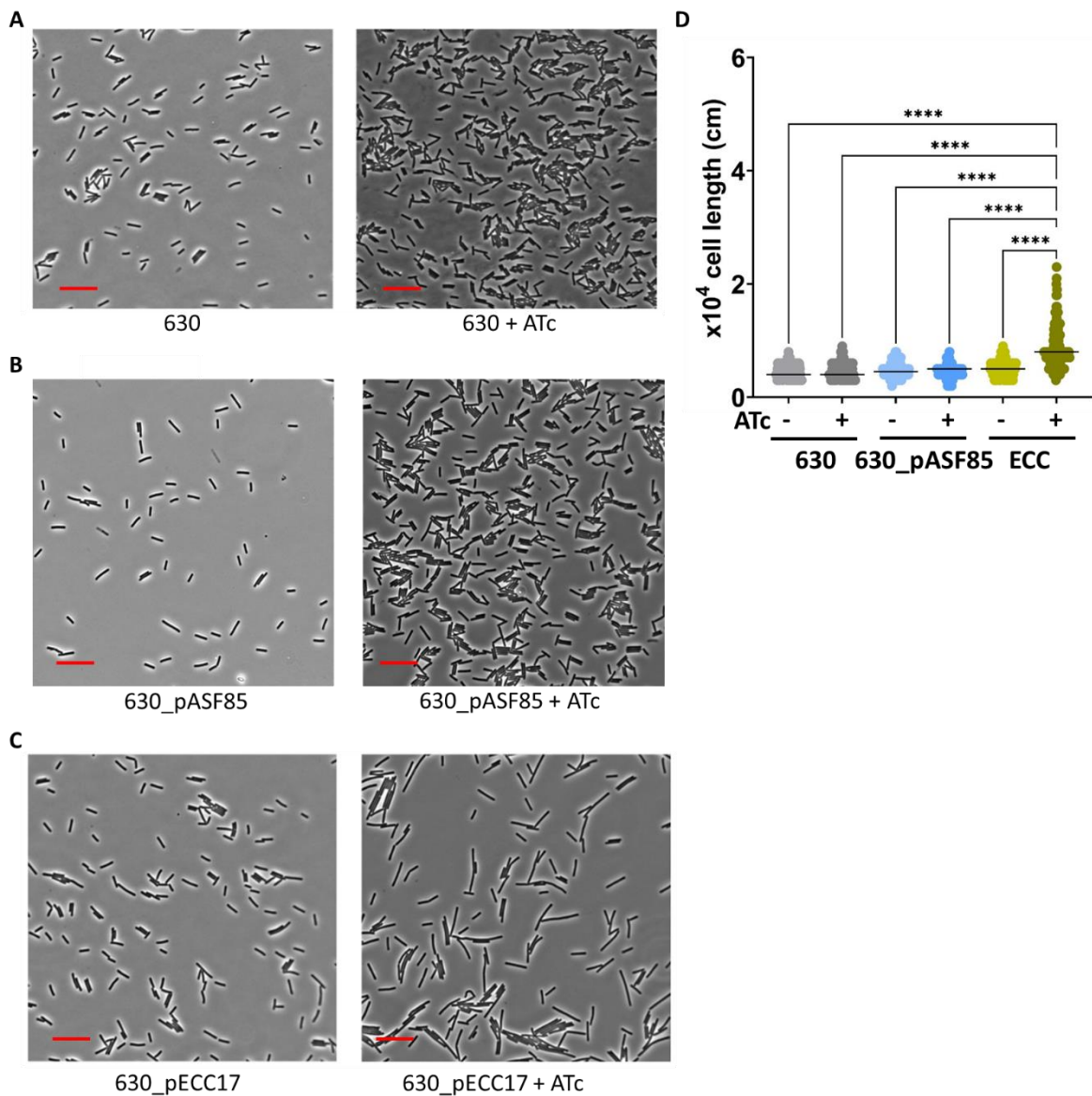


Figure 3-6. *C. difficile* cell morphology with and without ATc supplementation

Phase contrast microscopy figures showing *C. difficile* CD630 (A), 630_pASF85 (B) and 630_pECC17 (C). Samples were incubated in BHIS for 7 hours with (+ ATc) or without (- ATc) 50 ng ml⁻¹ ATc supplementation. Red bar indicates 10 μm. (D) Dot plots show the data of measured cell lengths of CD630 (grey), 630_pASF85 (blue) and 630_pECC17 (ECC yellow). 120 cells were randomly picked and measured. Horizontal lines indicate the median. ‘****’ indicates P<0.0001. Figure generated and one-way ANOVA analysis performed by GraphPad Prism.

3.2.2. TFP expression in *C. difficile* 630 under optimised ATc concentration

After selecting the optimised concentration of ATc, we then investigated whether TFP expression is up regulated by induction of *dccA*, by immunoblot analysis of cell extracts and supernatant fractions of CD630, 630_pASF85 and 630_pECC17 cultures. After harvesting cells

as described in section 2.4.2., the culture supernatants were kept for tri-chloroacetic acid (TCA) protein precipitation to investigate the proteins exported on cell surfaces, while cells were lysed for investigating the cytosolic proteins. Each strain was incubated with and without 50 ng ml⁻¹ of ATc supplementation, and samples were run side by side on western blots, as described in section 2.5.3.

Comparing the western blot results shown in Figure 3-7, no PilA1 signal is detected from CD630 cultures, from neither TCA nor lysate samples with only a very faint signal observed in secreted fractions (Figure 3-7, panel A). In 630_pASF85 vector control, small amounts of PilA1 are detected from lysate samples in both plain and ATc supplemented conditions (Figure 3-7, panel B). However, very enhanced *pilA1* expressions are detected in ATc-induced 630_pECC17 samples from both cell lysate and culture supernatant (TCA samples), and PilA1 polymers are clearly observed in the TCA sample, while smaller amount of PilA1 signals is also detected in uninduced 630_pECC17 but no PilA1 polymers were detected. (Figure 3-7, panel C).

The results indicate that PilA1 is efficiently expressed and exported to assemble into polymers only when *dccA* is induced by supplementing with ATc. As DccA is a key enzyme in c-di-GMP synthesis, these results indicate that *pilA1* expression is regulated by the level of c-di-GMP. The PilA1 signals detected in uninduced 630_pECC17 might be due to leakage of the *P_{tet}* promoter, which is also observed by other groups (Loew et al., 2010).

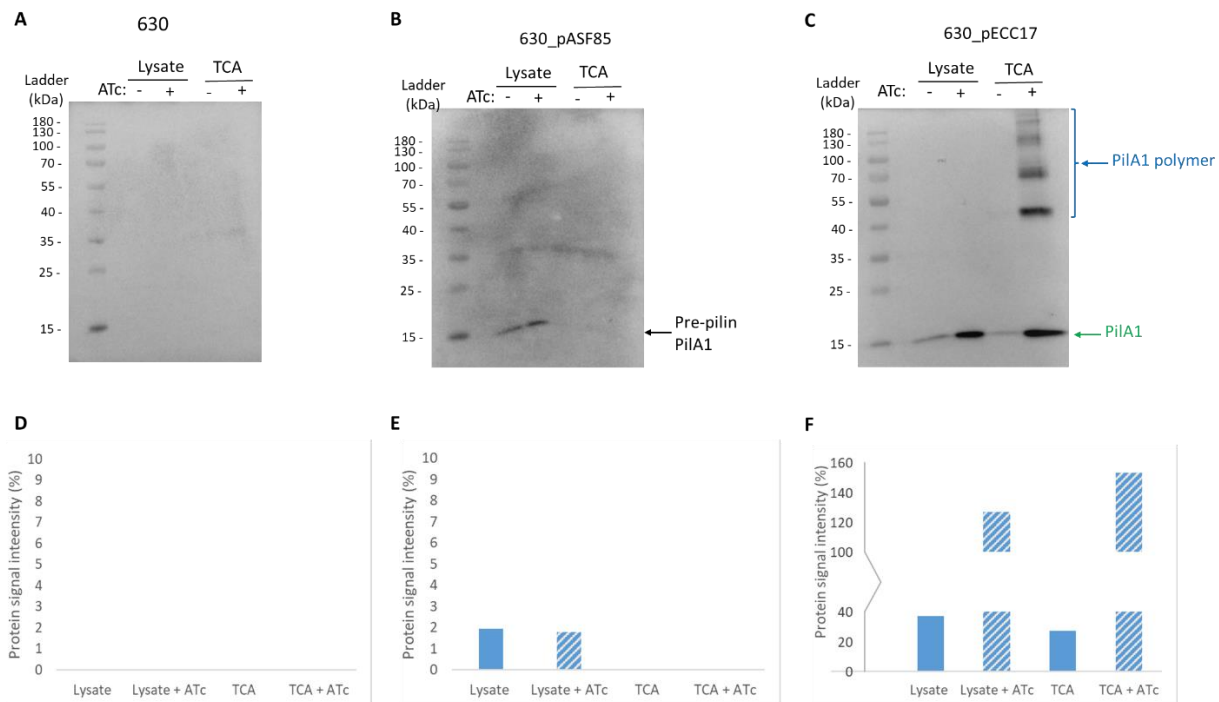


Figure 3-7. Immunoblot detection of PilA1 in *C. difficile* extracts

PilA1 signals detected by western blots using anti-PilA1 antibodies in cultures from strains CD630 (A, D), vector control 630_pASF85 (B, E), and *dccA* inducible strains 630_pECC17 (C, F) after 7 hours growth in BHIS with 0 ('-') or 50 ('+') ng ml⁻¹ of ATc. Secreted proteins present in the culture supernatant were extracted with TCA, while cytosolic proteins were analysed from the cell lysate. Quantified intensity of bands is shown in (D), (E), and (F), slash colours indicate ATc supplementation, raw data presented in Appendix E-1. Predicted molecular weight of pre-pilin PilA1 is 18.2 kDa (black arrow), mature pilin PilA1 (green arrow) is 17.2 kDa. PilA1 polymers (blue arrow) were detected in TCA fractions of induced 630_pECC17.

3.3. Impact of TFP Proteins on Cell Growth

3.3.1. *pilA1* expression in $\Delta pilA1$ mutant and complement strains

PilA1 is known as the major pilin assembling into pili filaments and is therefore a surface protein being exported and functioning outside the cell. A *pilA1* mutant ($\Delta pilA1$) and complemented strain where the *pilA1* gene was inserted via a pECC17-derived plasmid, downstream of *dccA* regulated by *P_{tet}* promoter (*P_{tet}* – *dccA* – *pilA1* – plasmid pECC109, see Appendix Figure A-2) had successfully been constructed by our collaborator Dr Couchman as detailed in section 2.1.5. Both deletion and complemented strains were confirmed by PCR (Appendix Figure A-3 and A-4).

In the plasmid pECC109, both *dccA* and *pilA1* genes are under direct regulation of the P_{tet} promoter, rather than *pilA1* being under c-di-GMP riboswitch control. This means that characterisation of the 630_pECC109 under ATc supplementation corresponds to an artificially high *pilA1* expression. Therefore, we designed two other complementation plasmids, based on pECC109 but containing a terminator sequence between the *dccA* and *pilA1* sequences. In one plasmid, pZGW006, we also included the riboswitch Cdi2_4 and predicted promoter regions of CD630 genomic *pilA1* ($P_{tet} - dccA - term - cdi2_4 - P_{pilA1} - pilA1$, Appendix Figure A-5). In this plasmid, *dccA* expression is regulated by the P_{tet} promoter, the level of c-di-GMP is increased and it then binds the Cdi2_4 sequence, switching on *pilA1* expression from the plasmid.

Complementation plasmid pZGW005 contains the terminator between *dccA* and *pilA1* without the riboswitch or *pilA1* promoter regions ($P_{tet} - dccA - term - pilA1$), and the *pilA1* expression is not expected to be up regulated by increased level of c-di-GMP (Appendix Figure A-6).

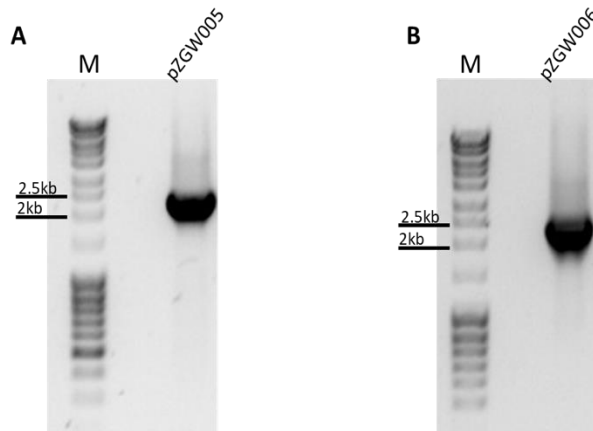


Figure 3-8. Colony PCR for pZGW005 and pZGW006 plasmids

Agarose gel to analyse products of colony PCR using primers oZGW077/oZGW078. Lane 'M' indicates marker. Both plasmids were synthesised and used as $\Delta pilA1$ complementation. (A) PCR product of pZGW005, expected band size is 2145bp. (B) PCR product of pZGW006, expected band size is 2253bp.

To confirm if $\Delta pilA1$ and complemented strains are aligned with our hypothesis when designing our complement vectors, levels of PilA1 were analysed by immunoblotting as described above. As we had previously established that expression of detectable levels of PilA1 requires increased c-di-GMP via *dccA* induction (section 3.2.), all further investigations were done in the 630_pECC17 strain background, where we can control c-di-GMP levels by addition of ATc.

Expression of PilA1 in CD630 with *dccA*-inducible plasmid (630_pECC17), $\Delta pilA1$ (630 $\Delta pilA1$ _pECC17) and complement strains 630 $\Delta pilA1$ _pECC109, 630 $\Delta pilA1$ _pZGW005 and 630 $\Delta pilA1$ _pZGW006 were studied (Figure 3-9). When *dccA* expression is not induced by addition of ATc, no PilA1 signal can be detected from cell lysates or supernatants from any of these strains. Upon *dccA* induction, PilA1 signals are detected in the cell lysates from 630_pECC17 and 630 $\Delta pilA1$ _pZGW006 (Figure 3-9, panel A) and in culture supernatants from 630_pECC17, 630 $\Delta pilA1$ _pECC109 and 630 $\Delta pilA1$ _pZGW006 (Figure 3-9, panel B and C).

The complement strain 630 $\Delta pilA1$ _pZGW006 was expected to show similar levels of PilA1 as 630_pECC17, as *pilA1* gene expression is regulated by increased binding of c-di-GMP to Cdi2_4 riboswitch. However, in the western blots, 630 $\Delta pilA1$ _pZGW006 expresses a much higher amount of PilA1, as indicated by the strong signal detected (Figure 3-9, panel B). This could be due to the multiple copies of plasmids pZGW006 containing *cdi2_4* and *pilA1* genes in a 630 $\Delta pilA1$ _pZGW006 cell, where only a single copy of *cdi2_4* and *pilA1* genes are present in the genome of a 630_pECC17 cell.

To better compare the levels of PilA1 detected in 630_pECC17 and 630 $\Delta pilA1$ _pECC109, the membrane was imaged at higher contrast and the strong signals of 630 $\Delta pilA1$ _pZGW006 were omitted from the analysis (Figure 3-9, panel C). Higher levels of PilA1 were detected in 630 $\Delta pilA1$ _pECC109 than in 630_pECC17 as the *P_{tet}* promoter induces *pilA1* expression directly as well as indirectly by induction of *dccA* and subsequent binding of c-di-GMP to the riboswitch, further increasing *pilA1* expression.

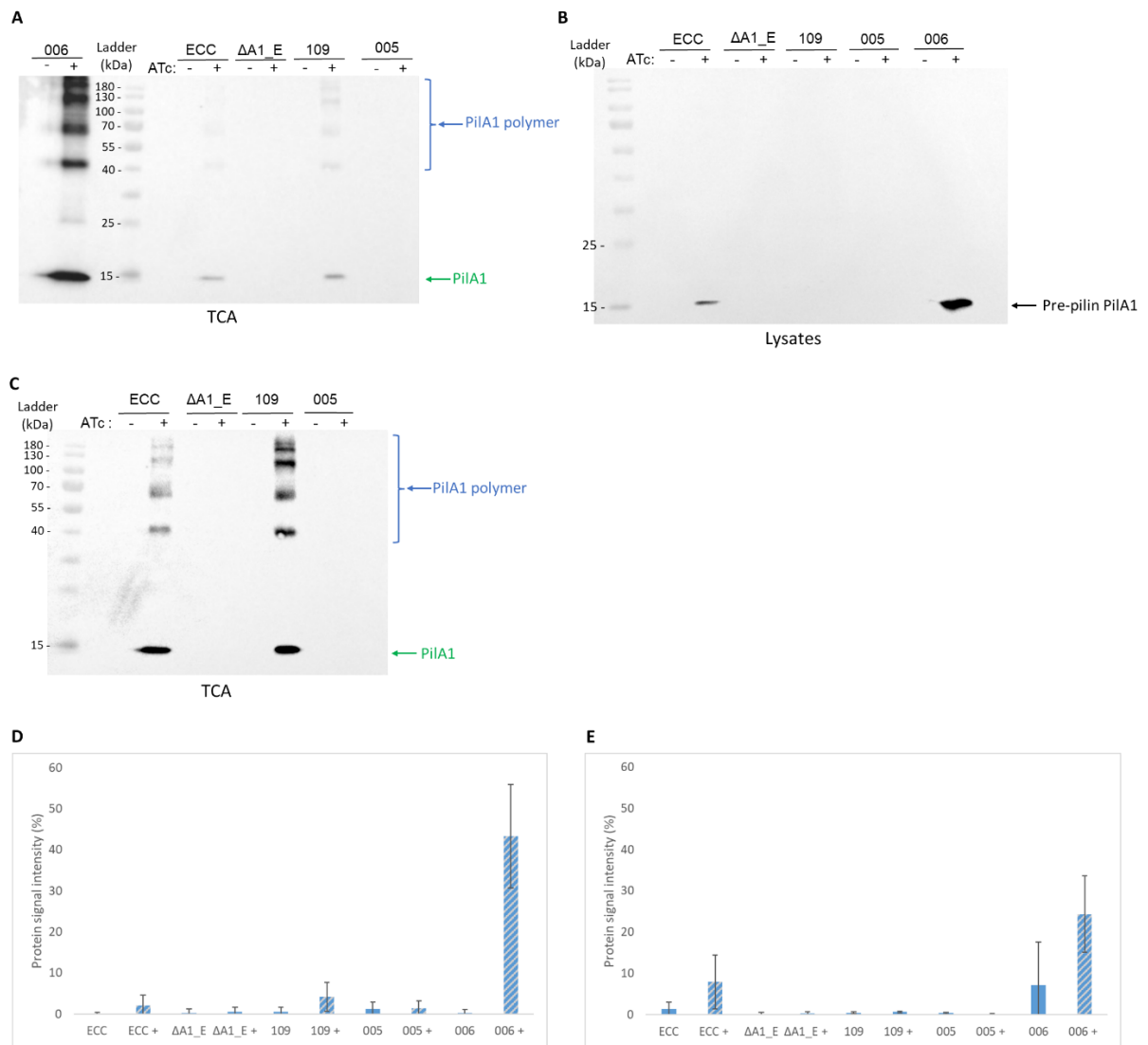


Figure 3-9. Immunoblot detection of PilA1 in *C. difficile* 630 $\Delta pilA1$ and complement strains

PilA1 signals detected by western blots using anti-PilA1 antibodies in cultures from strains 630_pECC17 (ECC), 630 $\Delta pilA1$ _pECC17 ($\Delta A1_E$) and complement strains 630 $\Delta pilA1$ _pECC109 (109), 630 $\Delta pilA1$ _pZGW005 (005) and 630 $\Delta pilA1$ _pZGW006 (006) after 7 hours growth in BHIS with (+ ATc) or without induction (- ATc) of *dccA* induction by ATc supplementation. (A) Secreted proteins present in the culture supernatant were extracted with TCA. (B) Cytosolic proteins were analysed from the cell lysates. (C) High exposure of the membrane seen in (A) to better analyse the bands for samples from 630_pECC17 (ECC), 630 $\Delta pilA1$ _pECC17 ($\Delta A1_E$), 630 $\Delta pilA1$ _pECC109 (109) and 630 $\Delta pilA1$ _pZGW005 (005) cultures, with lanes corresponding to 630 $\Delta pilA1$ _pZGW006 samples removed for clarity. Quantified PilA1 signals are shown for samples in TCA (D) and lysates (E), slash colours representing ATc supplementation, raw data presented in Appendix E-2. Predicted molecular weight of pre-pilin PilA1 is 18.2 kDa (black arrow), mature pilin PilA1 (green arrow) is 17.2 kDa. PilA1 polymers (blue arrow) were detected in TCA fractions of induced 630_pECC17, 630 $\Delta pilA1$ _pECC109 and 630 $\Delta pilA1$ _pZGW006.

Conversely, *pilA1* expression in 630 Δ *pilA1*_pZGW005 is similar to that seen in CD630, as this plasmid lacks both the riboswitch, the *pilA1* promoter regions and the gene is found after the terminator sequence within the plasmid.

These results confirm that *dccA* regulates PilA1 expression via the c-di-GMP riboswitch Cdi2_4 and that little to no of PilA1 are produced when c-di-GMP levels are low. Moreover, it shows that, in order to analyse complementation of a *pilA1* deletion, careful plasmid design is needed to replicate gene regulation mechanisms. It should be noted that complementation in the chromosome would have been ideal, but this was beyond the scope of this work.

3.3.2. Effect of PilA1 in growth and cell morphology

After analysing *pilA1* expression in *C. difficile* Δ *pilA1* and complement strains, the impact of the lack of PilA1 in cell growth and morphology were investigated in both CD630, 630_pECC17 and 630_pASF85 background. Growth measurements were performed at an OD of 595nm using a plate reader. From the growth curves shown on Figure 3-10, there is no significant difference between CD630 and Δ *pilA1* (Figure 3-10). Similarly, no difference is seen between 630_pECC17 and 630 Δ *pilA1*_pECC17 or when introducing the empty vector pASF85 (Appendix figure B-1).

We then compared the effect of addition of ATc in the growth of strains lacking *pilA1* and complemented with the different plasmids described above. When *dccA* is induced by adding ATc, neither deletion nor re-introduction of the *pilA1* gene leads to a phenotype when compared to the parent strain (Figure 3-10). Therefore, *pilA1* expression does not affect growth under increased levels of c-di-GMP. Complementation of the *pilA1* deletion with the pZGW006 plasmid seems to have a slower growth than other strains under both uninduced and induced conditions (Figure 3-10) but two-way ANOVA analysis shows that this not a statistically significant difference.

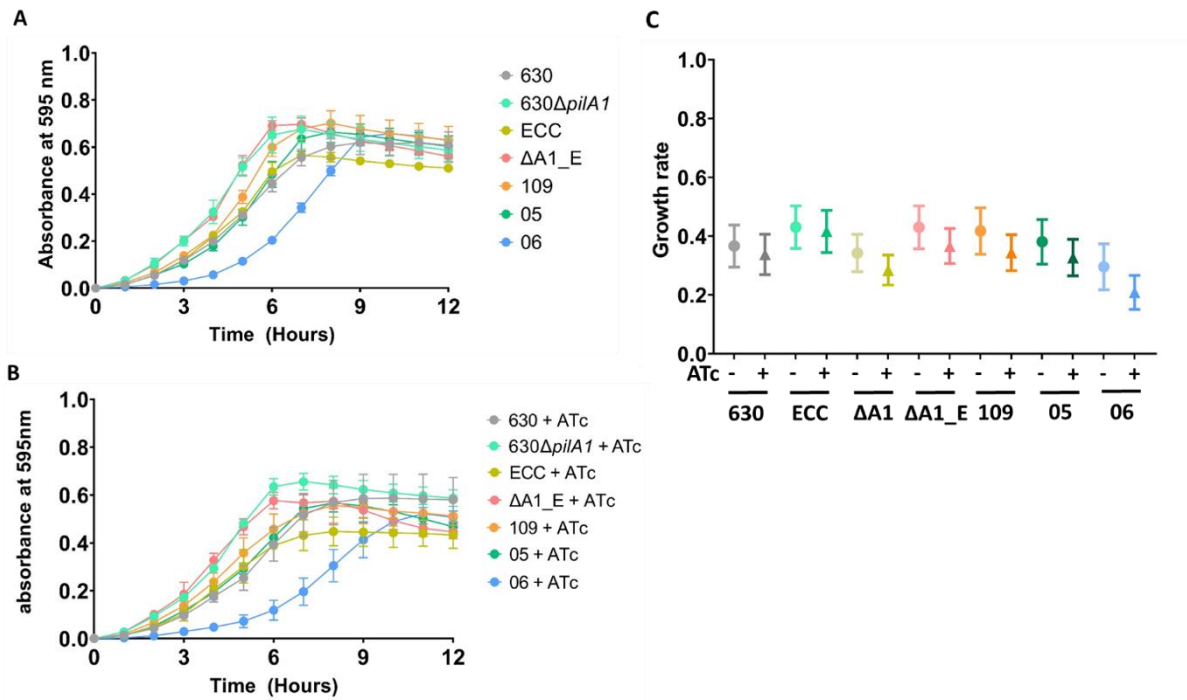


Figure 3-10. CD630 and Δ *pilA1* growth curves and rates

Growth of CD630 (grey), 630 Δ *pilA1* (Δ A1; cyan), 630_pECC17 (ECC; yellow), 630 Δ *pilA1*_pECC17 (Δ A1_E; pink) and complementation strains 630 Δ *pilA1*_pECC109 (109; orange), 630 Δ *pilA1*_pZGW005 (05; green) and 630 Δ *pilA1*_pZGW006 (006; blue) was measured hourly by spectrometry absorbance at 595 nm in a plater reader during 12 hour incubation in BHIS. (A) Growth curves without ATc supplementation. (B) Growth curves under 50 ng ml⁻¹ of ATc supplementation. (C) Growth rates of all strains under either 0 (-, dots) or 50 ng ml⁻¹ (+, triangles) of ATc supplementation. No significant difference reported after one-way ANOVA analysis performed by GraphPad Prism.

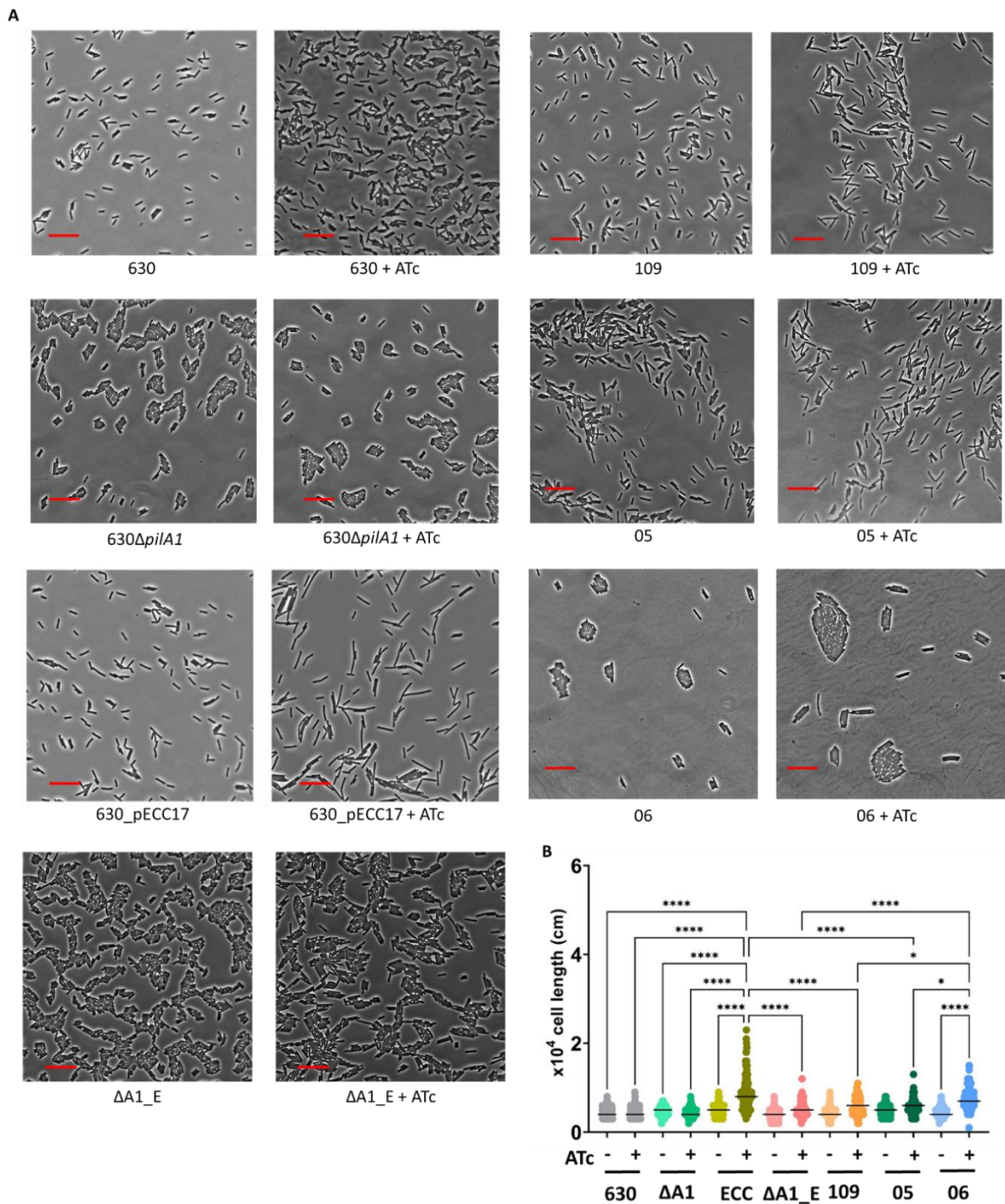


Figure 3-11. Effects of *pilA1* in cell morphology

CD630 (grey), 630 Δ *pilA1* (Δ A1; cyan), 630_pECC17 (ECC; yellow), 630 Δ *pilA1*_pECC17 (Δ A1_E; pink) and complementation strains 630 Δ *pilA1*_pECC109 (109; orange), 630 Δ *pilA1*_pZGW005 (05; green) and 630 Δ *pilA1*_pZGW006 (06; blue) incubated either with (+) or without (-) ATc supplementation. Samples were collected after incubating in BHIS for 7 hours. (A) Phase contrast microscopy. Red bar indicates 10 μ m. (B) Dot plots show the data of measured cell length. 120 cells were randomly picked and measured. Data from samples under ATc supplementation is coloured in darker shades. Horizontal lines indicate the median. '*' represents $P < 0.1$, '****' represents $P < 0.0001$. Figure generated and one-way ANOVA analysis performed in GraphPad Prism.

To investigate whether *pilA1* expression affects cell morphology, *C. difficile* cells were examined by phase contrast microscopy and cell length was measured (Figure 3-11). There was no difference in cell morphology or length between CD630 and $\Delta pilA1$ cells (Figure 3-11). Therefore, deleting *pilA1* gene has no significant effect on CD630 cell growth and morphology. Similarly, introducing the empty vector pASF85 or pECC17 plasmid into $\Delta pilA1$ shows no phenotype when compared to the strains containing an intact *pilA1* gene or CD630 (Appendix Figure B-2). Moreover, complementation of the *pilA1* deletion with pECC109, pZGW005 or pZGW006 also did not cause any changes in the absence of ATc.

As reported in section 3.2.1., upon *dccA* induction, 630_pECC17 shows longer cell shapes. Interestingly, these long cell shapes were not observed in $\Delta pilA1$ upon *dccA* induction (Figure 3-11). When *pilA1* was re-introduced into cells by complementation, the long cell shapes are not restored in 630 $\Delta pilA1$ _pECC109 and 630 $\Delta pilA1$ _pZGW005 but are observed in 630 $\Delta pilA1$ _pZGW006 strain (Figure 3-11). *PilA1* expression in 630 $\Delta pilA1$ _pZGW006 strain is regulated by riboswitch *Cdi2_4*, while the other two complement strains are either regulated by *P_{tet}* promoter or not activated. This result confirms that increased level of c-di-GMP leads to the long cell shapes, but also suggests that *pilA1* expression could be linked to the changes in cell morphology.

3.3.3. TFP expression in 630 $\Delta pilD1$

In the *C. difficile* 630 genome, genes encoding TFP proteins are mainly located into two gene clusters, the primary and secondary gene clusters. In the primary gene cluster, two peptidases, *PilD1* and *PilD2*, were predicted to modify pre-pilin *PilA1* to generate the mature major pilin. As discussed in section 1.3.1., in the previous study from our collaborators all genes in the TFP primary gene cluster of CD630 have been deleted and their role in pilin formation investigated, apart from *PilD1* (Couchman, 2016). Here, a *pilD1* mutant ($\Delta pilD1$) was successfully constructed, as detailed in 2.3.10. (Figure 3-12, panel A). The mutant was also complemented with plasmid pZGW007 and the *dccA*-inducible plasmid pECC17 also introduced in the 630 $\Delta pilD1$ strain, as described in 2.3.10. (Figure 3-12, panel B).

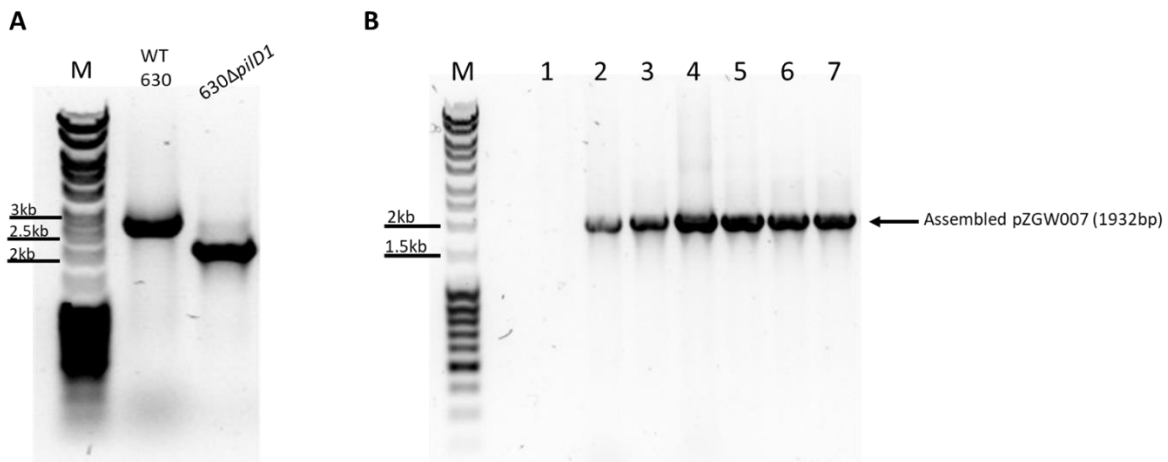


Figure 3-12. Screening of $\Delta pilD1$ mutants and complementation

(A) Colony PCR using primer pair oZGW036/oZGW037 to confirm deletion of *pilD1*. PCR product band size of CD630 strains is 2423bp. A smaller band of 1895bp is seen in $630\Delta pilD1$, confirming successful deletion. (B) Colony PCR using primers oZGW001/oZGW002 to confirm complementation of 630 $\Delta pilD1$ with plasmid pZGW007 (expected size 1932bp). Lane 'M' indicates marker, lane '1-7' indicate PCR products of assembly clones. Clones of lane '2-7' contain the plasmid for *pilD1* complementation.

After confirming deletion, the strains $630\Delta pilD1$ and $630\Delta pilD1_pASF85$ (vector control) were firstly tested under conditions of without and with ATc supplementation, results are shown in Appendix figure B-3. The *dccA* inducible plasmid was then introduced into the $\Delta pilD1$ mutant strain, and a complement plasmid was constructed and introduced into the mutant as described in 2.3.10.

We then investigated if deletion of *pilD1* would affect the levels of detectable PilA1. Proteins on the cell surface were extracted by TCA precipitation, whereas cytosolic proteins were examined from the cell lysates, as described above for the $\Delta pilA1$ and complement strains. Figure 3-13 shows the western blots of supernatant extracts and cell lysates from 630_pECC17, $\Delta pilD1$ ($630\Delta pilD1_pECC17$) and the complemented strain ($630\Delta pilD1_pZGW007$). PilA1 signal was detected in both cell lysates and supernatant extracts from all strains when *dccA* expression is induced, although at seemingly lower levels in the $\Delta pilD1$ and complement strains. PilA1 polymers are detected from supernatant extracts, which shows PilA1 is assembled into pilin filaments.

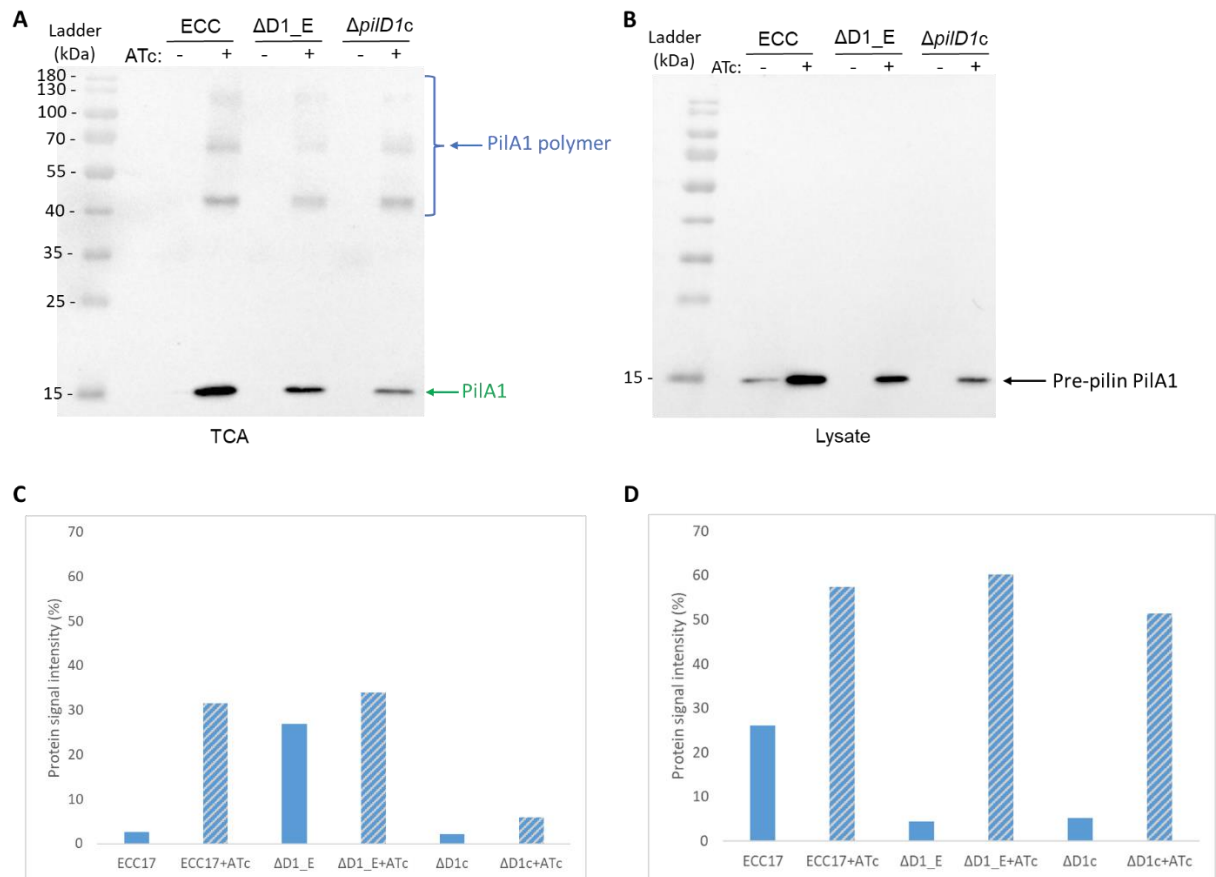


Figure 3-13. Immunoblot detection of PilA1 in *C. difficile* 630 *pilD1* mutant and its complement strain

PilA1 signals detected by western blots using anti-PilA1 antibodies from strains 630_pECC17 (ECC), 630 Δ *pilD1*_pECC17 (Δ D1_E) and 630 Δ *pilD1*_pZGW007 (Δ *pilD1c*) cultures after 7 hours growth in BHIS with (+ ATc) or without (- ATc) *dccA* induction by ATc supplementation. (A) Secreted proteins present in the culture supernatant were extracted via TCA extraction, signal bands were quantified (C), slash colours representing ATc supplementation, quantification data in Appendix E-3. (B) Cytosolic proteins were analysed from the cell lysates, signal bands were quantified (D), slash colours representing ATc supplementation, quantification data presented in Appendix E-3. Cathode/Anode buffers were applied in western blot, transfer was performed at 15V for 23 minutes onto nitrocellulose membranes. Predicted molecular weight of pre-pilin PilA1 is 18.2 kDa (black arrow), mature pilin PilA1 (green arrow) is 17.2 kDa. PilA1 polymers (blue arrow) were detected in TCA fractions of all strains with *dccA* induced background.

Interestingly, a small amount of PilA1 is detected in the cell lysate of 630_pECC17 without induction, but this is not seen in cell lysates from either Δ *pilD1* or the complemented strains. As previously mentioned, P_{tet} is a leaky promoter and some induction of *dccA* is likely to occur even without the addition of ATc, which would explain the detection of PilA1 in uninduced 630_pECC17. Together with lower levels of PilA1 detected upon *dccA* induction in Δ *pilD1* strains, including in pilin polymers, this suggests that, although not essential for expression

and export of PilA1, PilD1 might play a role in full processing of the pre-pilin. As demonstrated by Couchman in his previous work, the other pre-pilin peptidase in the primary gene cluster, PilD2, is essential for detection of PilA1 and therefore TFP biosynthesis. Taken together, these results suggest that PilD1 is not the main pre-pilin peptidase, although some level of redundancy is possible, and it could be implicated only under certain conditions. Further work is required to fully understand the role of this peptidase.

3.3.4. Effect of pilD1 in cell growth

We then investigated the role of *pilD1* in cell growth. $\Delta pilD1$ was examined in both CD630 and 630_pECC17 backgrounds, together with the complemented strain (Figure 3-14). Comparing *pilD1* mutant (630 $\Delta pilD1$) with wild type CD630 or 630_pECC17, no significant difference is observed, which indicates deleting *pilD1* gene does not lead to a change in growth (Figure 3-14). It was also tested whether introducing the vector and supplementing ATc lead to any changes in cell growth, results show there is no significant phenotype (Appendix figure B-3). Similarly, under *dccA* induced conditions, no significant phenotype was observed in 630 $\Delta pilD1$ _pECC17 and the complement strain 630 $\Delta pilD1$ _pZGW007 (Figure 3-14). These results indicate that absence of *pilD1* does not affect cell growth, even at higher levels of c-di-GMP.

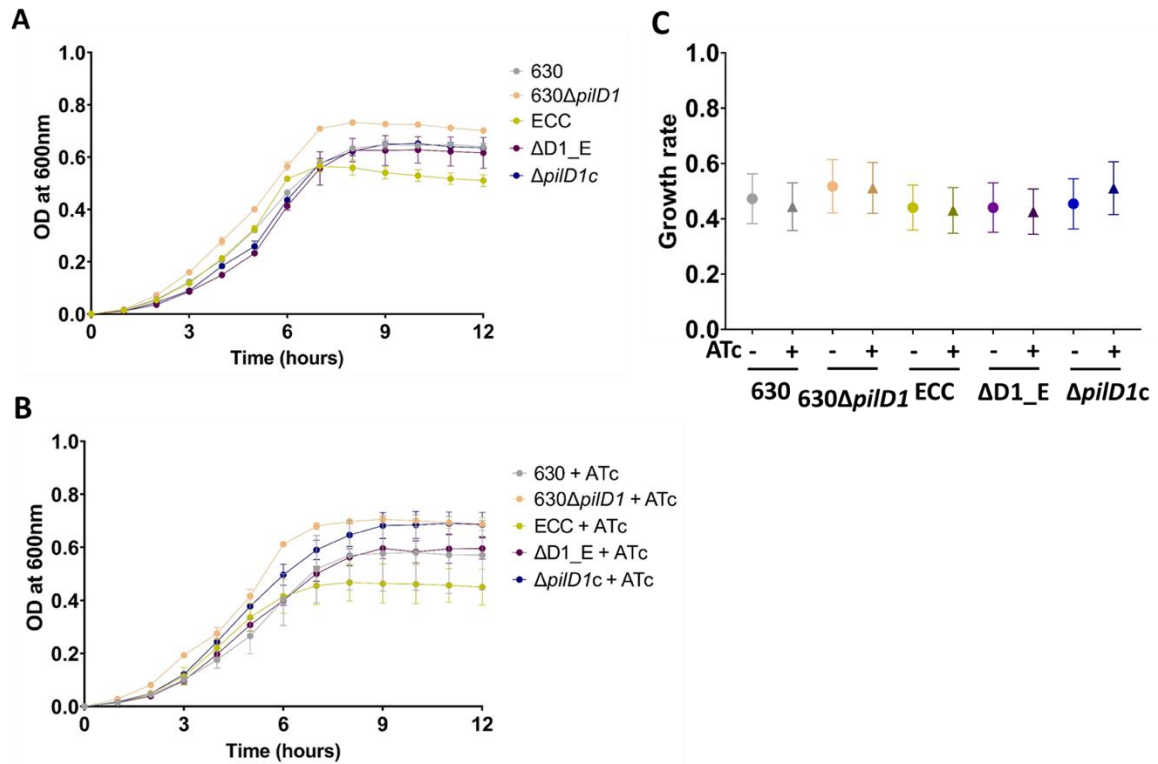


Figure 3-14. CD630 and $\Delta pilD1$ growth curves and rates

Growth of CD630 (grey) and 630 $\Delta pilD1$ (orange), 630_pECC17 (ECC; yellow), 630 $\Delta pilD1$ _pECC17 ($\Delta D1_E$; purple) and 630 $\Delta pilD1$ _pZGW007 ($\Delta pilD1c$; navy) was measured hourly by spectrometry absorbance at 595 nm in a plate reader, for 12h incubation in BHIS. (A) Growth curves without ATc supplementation. (B) Growth curves under 50 ng ml⁻¹ of ATc supplementation. (C) Growth rates under either 0 (dots) or 50 ng ml⁻¹ (triangles) of ATc supplementation. No significant differences were reported after one-way ANOVA analysis in GraphPad Prism.

3.3.5. Role of *pilD1* in cell morphology

As with the $\Delta pilA1$, the cell morphology was examined in $\Delta pilD1$ strains by phase contrast microscopy and cell length measurements (Figure 3-15). Interestingly, the longer cell shapes seen in 630_pECC17 are occasionally observed in 630 $\Delta pilD1$, even though this phenotype was not observed in $\Delta pilA1$ (Figure 3-15). No phenotype was shown by introducing the empty vector (Appendix Figure B-4).

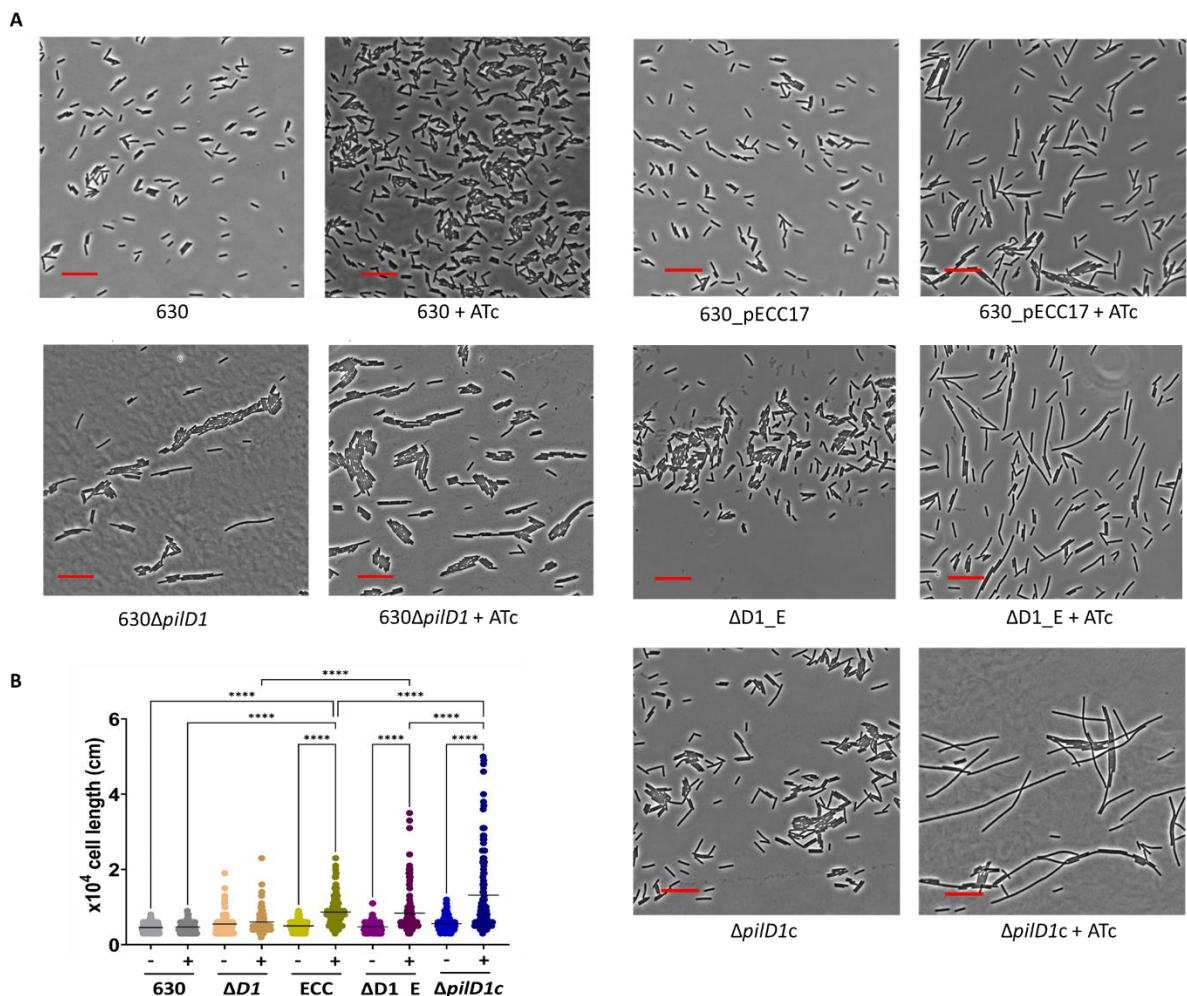


Figure 3-15. Effect of *pilD1* in cell morphology

CD630 (grey), 630Δ*pilD1* (Δ*D1*; orange), 630_pECC17 (ECC; yellow), 630Δ*pilD1*_pECC17 (Δ*D1_E*; purple) and 630Δ*pilD1*_pZGW007 (navy) incubated either with (+, darker shades) or without (-) ATc supplementation. Samples were collected after incubating in BHIS for 7 hours. (A) Phase contrast microscopy. Red bar indicates 10 μm. (B) Dot plots representing measured cell length of 120 cells were randomly picked for each strain. Horizontal lines indicate the median. ‘****’ indicates P<0.0001. Figure generated and one-way ANOVA analysis performed in GraphPad Prism.

Further, CD630, Δ*pilD1* and its complement strain were then assessed upon induction of *dccA*. Surprisingly, the extended cell length seen in 630_pECC17 strain and hypothesised to be due to high c-di-GMP levels, is also observed in the corresponding Δ*pilD1* mutant strain (630Δ*pilD1*_pECC17), where *pilA1* is expressed and exported to form TFP (see section 3.3.3. above). As discussed above, the longer cell length phenotype seen in 630_pECC17 supplemented with ATc is likely due to an increased level of c-di-GMP. However, this phenotype is not observed in 630Δ*pilA1*_pECC17, even upon *dccA* induction, suggesting a

direct effect of *pilD1* rather than an effect on *pilA1* maturation, as immunoblotting showed this is not affected in these strains (see above).

Unexpectedly, this phenotype was also observed in $\Delta pilD1$ complement strain, where cell lengths are even longer than those detected in 630_pECC17 and 630 $\Delta pilD1$ _pECC17 (Figure 3-15). It should be noted that the plasmid to complement *pilD1* deletion was designed in a similar way to pECC109: the *pilD1* gene was introduced in the pECC17 plasmid, downstream of *dccA*, under direct control of the P_{tet} promoter, as well as indirectly upregulated by the elevated c-di-GMP levels due to *dccA* induction. Together with the fact that pZGW007 is a multi-copy plasmid, *pilD1* complement strain is likely to express PilD1 at considerably higher levels than CD630 and 630_pECC17.

Taken together, these results suggest that both absence and overexpression of *pilD1* can lead to longer cell shapes and further work is required to understand the effect of *pilD1* on cell division.

3.3.6. TFP expression in 630 $\Delta pilJ$

As discussed in section 4.1., previous work has shown that a higher level of *pilJ* transcription was found in biofilm culture than in planktonic culture (Maldarelli et al., 2016). PilJ is known as a minor pilin, but the encoding gene is not located in either the primary or secondary TFP clusters. Previous work showed by immunogold-labelled microscopy that PilJ decorates the PilA1 filament (Piepenbrink et al., 2014).

Here, a *pilJ* mutant (630 $\Delta pilJ$) was constructed and investigated. The *dccA* inducible plasmid was also introduced into $\Delta pilJ$, and a complement plasmid was constructed and introduced into $\Delta pilJ$ strain, as described in 2.3.10 (Figure 3-16).

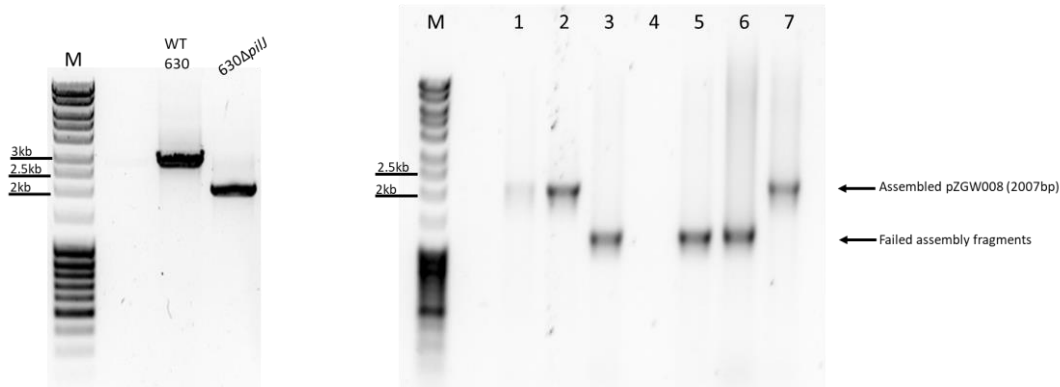


Figure 3-16. Screening of $\Delta pilD1$ mutants and complementation

(A) Colony PCR using primers oZGW038/oZGW039 to confirm deletion of *pilD1*. PCR product band size of CD630 strains is 2606 bp. A smaller band of 1821bp is seen in 630 $\Delta pilJ$, confirming successful deletion. (B) Colony PCR using primers oZGW001/oZGW002 to confirm complementation of 630 $\Delta pilD1$ with plasmid pZGW008 (expected size 2073 bp). Lanes '1-7' indicate PCR products of assembly clones. Clones of lane 2 and 7 contain construct plasmid for *pilJ* complementation. Lane 'M' indicates marker.

PilA1 expression in $\Delta pilJ$ and the complement strains containing the inducible dccA plasmid was then analysed, using the same procedures as described above. For completion, strains lacking the plasmid were also tested (Figure 3-16). From the results shown in Figure 3-17, no obvious difference was detected in the cell lysate across all strains. However, PilA1 polymers were not detected in the complemented strain in the supernatant fraction, while they were found in both 630_pECC17 and $\Delta pilJ$. As the complementation plasmid is derived from pECC17, *pilJ* is under direct activation of ATc, so it is possible that there is an excess PilJ which might disrupt PilA1 assembly into polymers.

These results indicate PilJ is not required for expression and export of PilA1 to form TFP filaments.

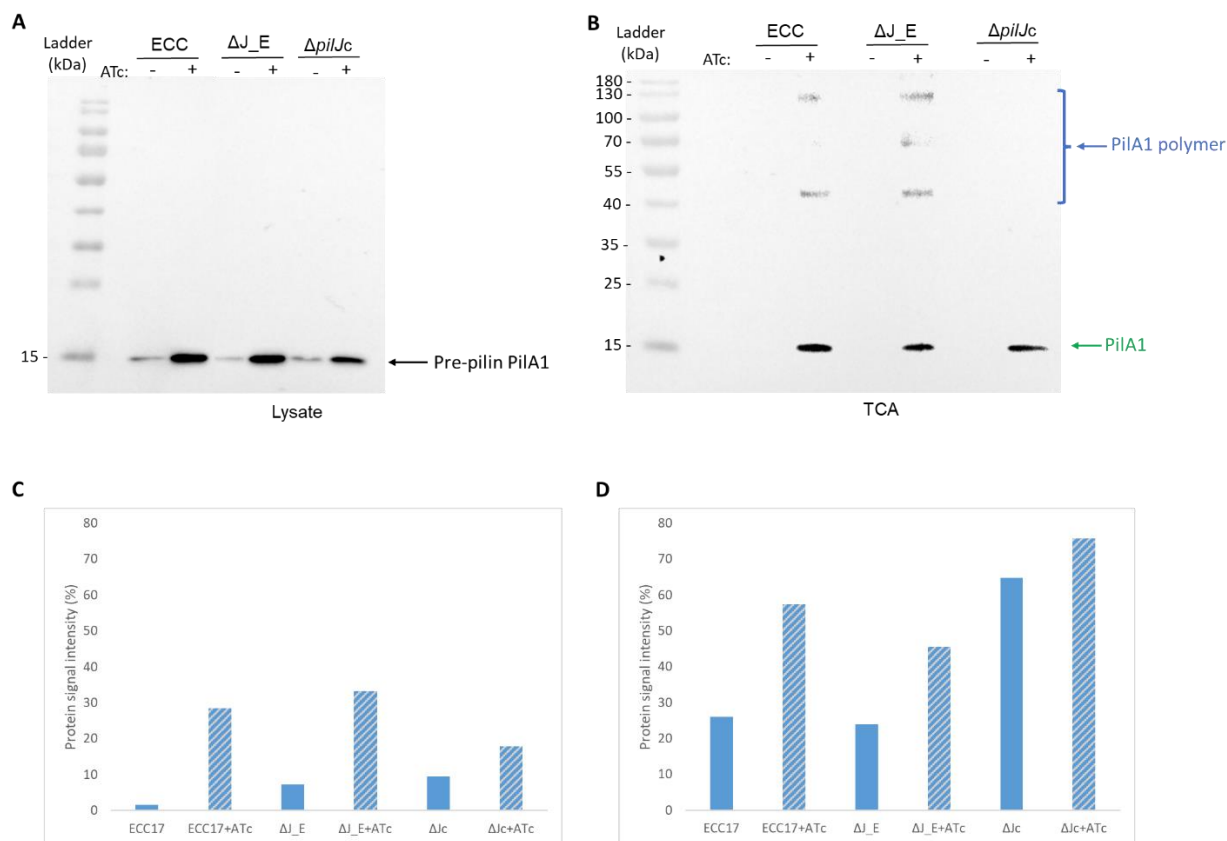


Figure 3-17. Immunoblot detection of PilA1 in CD630 $\Delta pilJ$ mutant and its complement strain

PilA1 signals detected by anti-PilA1 western blots from strains 630_pECC17 (ECC), 630 $\Delta pilJ$ _pECC17 ($\Delta pilJ$) and 630 $\Delta pilJ$ _pZGW008 ($\Delta pilJ_c$) cultures after 7 hours growth in BHIS with (+ ATc) and without (- ATc) *dccA* induction by ATc supplementation. (A) Secreted proteins present in the culture supernatant were extracted via TCA extraction, signal bands were quantified and plotted in (C), slash colours representing ATc supplementation, quantification data can be found in Appendix E-4. (B) Cytosolic proteins were analysed from the cell lysates, signal bands were quantified and plotted in (C), slash colours representing ATc supplementation, quantification data can be found in Appendix E-4. Cathode/Anode buffers were applied in western blot, transfer was performed at 15 V for 23 minutes onto nitrocellulose membranes. Predicted molecular mass of pre-pilin PilA1 (black arrow) is 18.2 kDa, mature pilin PilA1 (green arrow) is 17.2 kDa. PilA1 polymers (blue arrow) were detected in TCA fractions of all strains with *dccA* induced background.

3.3.7. Effect of PilJ in growth

Following our workflow for other strains, we then investigated if deletion would affect cell growth. CD630, $\Delta pilJ$ and its complement strain with and without inducible *dccA* were analysed over 12 h incubation.

The resulting growth curves and corresponding growth rates show no significant difference among any of the strains, regardless of the presence or absence of the plasmid, with and without ATc supplementation (Figure 3-18 and Appendix Figure B-5). These results indicate that deleting *pilJ* does not lead to a change in growth.

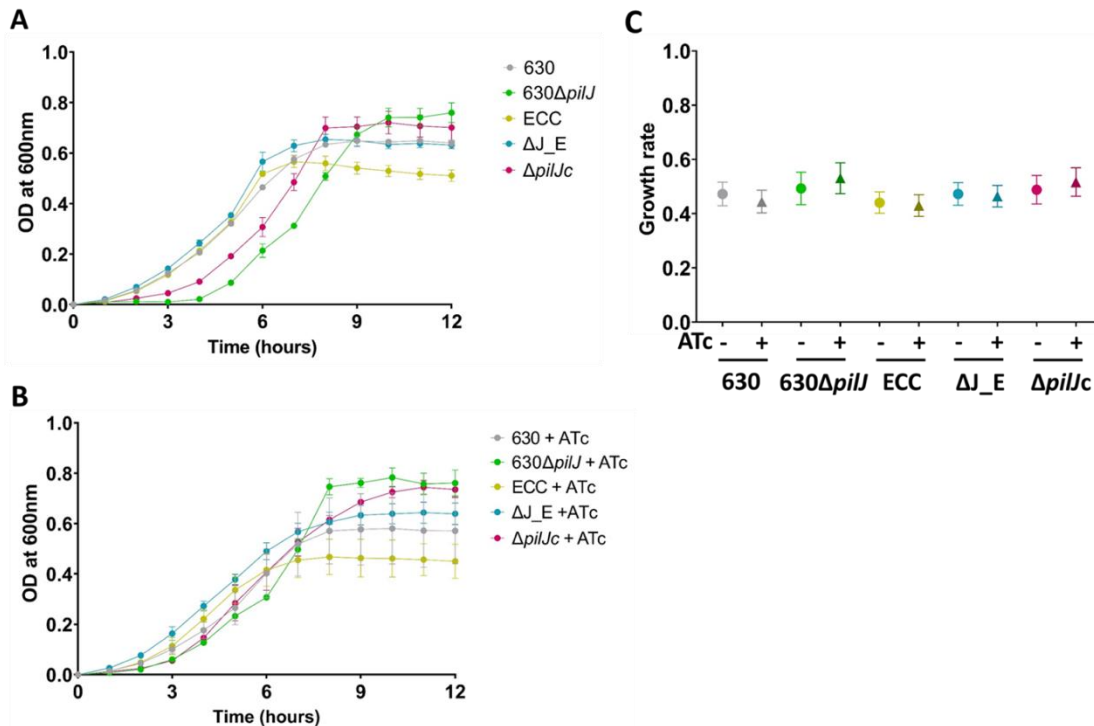


Figure 3-18. CD630 and $\Delta pilJ$ growth curves and rates

Growth of CD630 (grey) and 630Δ*pilJ* (orange), 630_pECC17 (ECC; yellow), 630Δ*pilJ*_pECC17 (Δ*J_E*; blue) and 630Δ*pilJ*_pZGW008 (Δ*pilJc*; pink) was measured hourly by spectrometry absorbance at 595nm using a plate reader during 12h incubation in BHIS without (A) and with (B) ATc supplementation. (C) Growth rates of all strains under either 0 (- ATc, dots) or 50 ng ml⁻¹ (+ ATc, triangles) of ATc supplementation. No significant difference reported after one-way ANOVA analysis performed using GraphPad Prism.

3.3.8. Effects of *PilJ* in cell morphology

Cell morphology was then examined by phase contrast microscopy and cell length measured. There is no significant phenotype observed when comparing CD630 to 630Δ*pilJ* (Figure 3-19) which indicates deleting *pilJ* does not cause a phenotype in cell morphology.

CD630, Δ*pilJ* and its complement strain with inducible *dccA* background were then examined, after confirming introducing the empty vector and adding ATc caused no phenotype

(Appendix figure B-6). Interestingly, in $\Delta pilJ$ and complement strains, cell shapes are slightly longer under *dccA* induction, although this phenotype is less pronounced in these strains than in 630_pECC17.

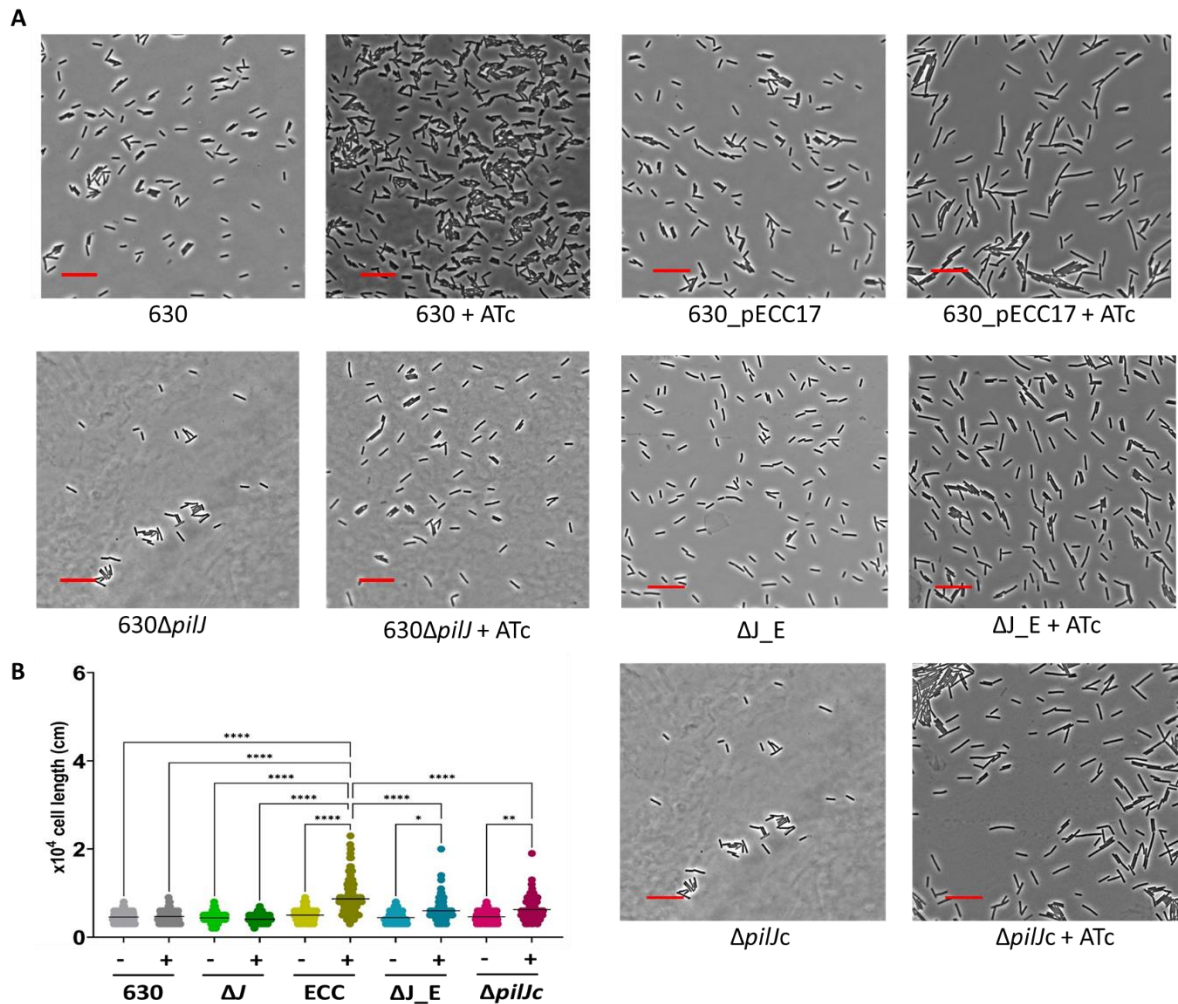


Figure 3-19. Effects of PilJ in cell morphology

CD630 (grey), 630 $\Delta pilJ$ (green), 630_pECC17 (ECC; yellow), 630 $\Delta pilJ$ _pECC17 (ΔJ_E ; blue) and 630 $\Delta pilJ$ _pZGW008 (pink) incubated either with (+) or without (-) ATc supplementation. Samples were collected after incubating in BHIS for 7 hours. (A) Phase contrast microscopy images. Red bar indicates 10 μ m. (B) Dot plots of cell length of 120 cells randomly picked and measured for each strain. Data from samples under ATc supplementation is coloured in darker shades. Horizontal lines indicate the median. '*' represents $P < 0.1$, '**' represents $P < 0.01$, '***' represents $P < 0.0001$. Figure generated and one-way ANOVA analysis performed by GraphPad Prism.

3.4. Effects of c-di-GMP induction and TFP proteins in biofilm formation

3.4.1. Biofilm formation in CD630

TFP may contribute to biofilm formation which allows *C. difficile* to survive under antibiotic treatments and causing longer term disease. After optimising *dccA* induction and examining cell growth and morphology, biofilm formation assays were carried out.

Following the protocols described in 2.6.4., CD630 was first tested, compared with vector control (630_pASF85) and *dccA*-inducible plasmid 630_pECC17 (Figure 3-20). Our assays showed that supplementing ATc or introducing the vectors has no effect on CD630 biofilm formation.

Based on previous work, we hypothesised that inducing *dccA* would lead to increased biofilm formation by raising TFP and we would observe higher absorbance from 630_pECC17 upon *dccA* induction. However, expression of *dccA* induced in 630_pECC17 had no significant effect on biofilm formation, which suggests a high level of c-di-GMP does not contribute to biofilm formation, in contradiction to previous work (Purcell et al., 2007). It is worth noting that despite extensive protocol optimisation with a range of plates, media and washup volumes, there was considerable variability across assay replicates, which could mask biological significant differences.

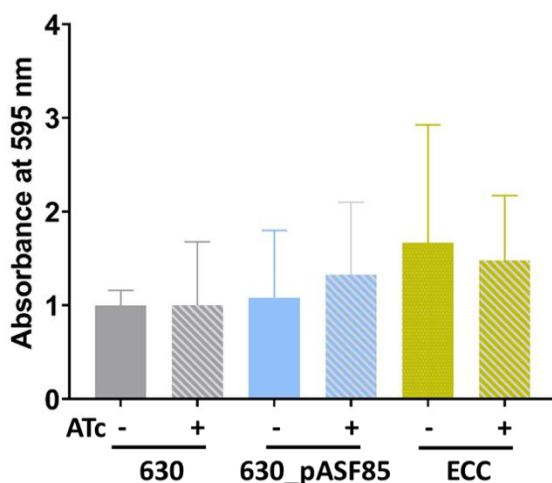


Figure 3-20. CD630 biofilm formation

Biofilm formation was quantified by absorbance at 595 nm of CD630 (grey), 630_pASF85 (blue) and 630_pECC17 (ECC; yellow) upon cell culture precipitation after 7-day incubation in 24-well plates either without (- ATc) or with (+ ATc) 50 ng ml⁻¹ of ATc supplementation. Strip shades indicated samples under ATc supplementation. Significance analysed with one-way ANOVA in GraphPad Prism.

3.4.2. Biofilm formation in $\Delta pilA1$

According to previous studies discussed in 1.3.3., a deficiency of biofilm formation is observed in $\Delta pilA1$ from *C. difficile* strain R20291 (Maldarelli et al., 2016; Ronish et al., 2022). We wanted to examine whether the same phenotype is observed in CD630.

The biofilm formation assay was carried out on $\Delta pilA1$ mutants in CD630 and 630_pECC17 background and three complement strains described in section 3.3.1. From the result, there is no significant phenotype between the wild type and respective $\Delta pilA1$ strains (Figure 3-21), which suggests deleting *pilA1* does not lead to a phenotype in biofilm formation.

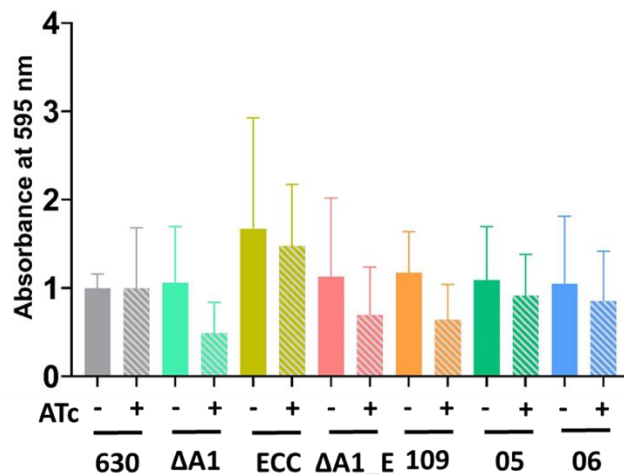


Figure 3-21. CD630 and $\Delta pilA1$ biofilm formation

Biofilm formation is quantified by absorbance at 595 nm of CD630 (grey), 630 $\Delta pilA1$ ($\Delta A1$; cyan), 630_pECC17 (ECC; yellow), 630 $\Delta pilA1$ _pECC17 ($\Delta A1_E$; pink), 630 $\Delta pilA1$ _pECC109 (109; orange), 630 $\Delta pilA1$ _pZGW005 (05; green) and 630 $\Delta pilA1$ _pZGW006 (06; blue) cultures after 7-day incubation in 24-well plates either without (- ATc) or without (+ ATc, strips) 50 ng ml⁻¹ of ATc supplementation. Significance analysed with one-way ANOVA in GraphPad Prism.

Similarly, no statistically significant phenotype was detected despite the observation of a minor deficiency in the mutant, which was not restored in any of the complement strains (Figure 3-21). A similar minor, not statistically significant, reduction of biofilm formation upon *dccA* induction was observed. Unlike the observation in *C. difficile* strain R20291, absence of *pilA1* in CD630 does not seem to lead to a significant deficiency in biofilm formation.

Biofilm assays were also carried out for $\Delta pilD1$ and $\Delta pilJ$ strains, but the results were even more variable and no clear conclusion could be drawn from this work, as shown in Appendix Figure B-7 and B-8.

3.5. Discussion

To investigate TFP, the *dccA* gene was introduced into *C. difficile* cells via plasmid vectors, in order to induce higher levels of intracellular c-di-GMP and 'switch on' *pilA1* expression as excess c-di-GMP binds to Cdi2_4 riboswitch upstream of *pilA1*. In these plasmids, the expression of *dccA* is regulated by the *P_{tet}* promoter, which is activated by ATc.

In this chapter, the ATc supplementation was optimised. When the level of c-di-GMP is increased by inducing *dccA* expression, we observed long *C. difficile* cells indicating that cell division might be influenced under a higher level of c-di-GMP. Lately, studies of *C. difficile* riboswitches suggest that Cdi6 regulates an operon, which contain genes related to colony and cell morphologies (Garrett et al., 2019; Sekulovic et al., 2018). Those genes encode proteins which were named as colony morphology regulator RST (CmrRST) (Garrett et al., 2019). The study demonstrated CmrRST expression is regulated by c-di-GMP, and that CmrR and CmrT are responsible for forming bacterial chains (Garrett et al., 2019). The observed phenotype in our work when inducing *dccA* and increasing c-di-GMP is likely due to activation of these genes. This could be investigated by qRT-PCR of these genes in our strains, with and without ATc supplementation, to confirm if CmrRST genes are elevated in our experimental conditions.

C. difficile cell growth and morphology were examined in $\Delta pilA1$, $\Delta pilD1$ and $\Delta pilJ$ mutants. Interestingly, mutagenesis studies of PilA1 and PilD1 show phenotypes in cell length, with the long cell shapes observed in wild type under a higher level of c-di-GMP not detected in $\Delta pilA1$ mutant. Conversely, cells grow to even longer size in *pilD1* mutant and complement strains. To our knowledge, this cell size phenotype associated with specific TFP proteins has not been reported before and it would be important to further investigate a potential link between TFP and cell division.

PilA1 expression was investigated in CD630 under *dccA* induction, and in $\Delta pilA1$, $\Delta pilD1$ and $\Delta pilJ$ strains. It was confirmed that CD630 only expresses PilA1 and forms PilA1 polymers on the cell surface under a higher level of c-di-GMP. The three *pilA1* complement strains show different levels of PilA1. As predicted, when complementing without Cdi2_4 riboswitch, PilA1

is not being expressed even under an increased level of c-di-GMP, confirming that Cdi2_4 riboswitch is involved in *pilA1* expression control.

Interestingly, one of the pre-pilin peptidases in the TFP primary gene cluster, PilD1, is not required for *pilA1* expression and polymer assembly, which is different to the other pre-pilin peptidase, PilD2, in the same operon. There is a possibility that PilD1 functions as a pre-pilin peptidase cleaving PilA2, which is encoded in the TFP secondary cluster and contains an N-terminal signal peptide. Future work would require exploring the function of PilD1.

PilJ had been observed to decorate the PilA1 filament, although the absence of PilJ does not affect PilA1 assembling into polymers. Surprisingly, complementation of *pilJ* gene in a multi-copy, inducible plasmid, leads to a failure in detecting PilA1 polymers. There might be a higher level of PilJ in the complemented strain than the wild type and *pilJ* mutant and PilA1 assembly might be affected by excess levels of PilJ. To confirm this hypothesis, anti-PilJ western blot could be applied in future studies. It is not clear what signals induce *pilJ* expression as it does not possess a c-di-GMP riboswitch so it would be interesting to explore regulation of this minor pilin and its role in TFP in more detail.

In this chapter, biofilm formation assays were carried but due to considerable experimental variability, only limited interpretation of the results is possible. Compared to previous work by Purcell *et al.*, biofilm formation assays were carried out in 24-well culture plates and stained with 0.1% crystal violet (Purcell *et al.*, 2017, 2015). *C. difficile* R20291 culture was incubated for 24 or 48 hours before staining to investigate the early phase of biofilm formation in this previous work, whereas *C. difficile* 630 was incubated for 7 days in this work. While 24-well culture plates were pre-reduced in the anaerobic cabinet for 72 hours in previous work, they were pre-reduced for overnight in this work. Interestingly, pH 7.5 sodium phosphate buffer was introduced in one of Purcell *et al.*'s work (Purcell *et al.*, 2017), which may also help with the stability of biofilm in the assays. Confocal laser scanning microscopy has been recently applied to study *C. difficile* biofilm formation (Ronish *et al.*, 2022) and it would be interesting to apply this method to the strains studied in this work.

Chapter 4: Motility in *C. difficile*

4.1. Introduction

C. difficile expresses both TFP and flagella, which both contribute to bacterial motility. The expression of PilA1, as the major pilin of TFP, and the *flgB* operon to assemble flagella are regulated by c-di-GMP specific riboswitches (Bordeleau et al., 2015; Purcell et al., 2012). Expression of PilA1 is regulated by a class II c-di-GMP specific riboswitch, Cdi2_4, located upstream of *pilA1* gene. Like other class II riboswitches, gene transcription is 'switched on' under a higher intracellular level of c-di-GMP by binding of the ligands and subsequent conformational changes (Sherwood and Henkin, 2016). Conversely, *flgB* operon is regulated by a class I c-di-GMP specific riboswitch, Cdi1_3, which 'switches off' gene transcription under a higher level of c-di-GMP (Purcell et al., 2012; Sudarsan et al., 2008). Therefore, when we elevate the level of c-di-GMP by inducing *dccA* expression, PilA1 is expected to be expressed and assembled into TFP, while the expression of *flgB* operon is downregulated. When investigating the motility features of *C. difficile*, it should be considered that TFP motility can be observed under a higher level of c-di-GMP, whereas under a lower level of c-di-GMP, flagella-mediated swimming motility takes place.

The expression of *flgB* operon also activates the expression of toxins TcdA and TcdB in *C. difficile* (McKee et al., 2013) indicating that at a lower level of c-di-GMP, *C. difficile* moves in the host gut lumen via flagella and enters host intestinal tissue with toxin secretion. As the bacterial cell invades the tissue, it no longer needs swimming motility and twitching movement using TFP is preferred.

In this chapter, both twitching and swimming motilities were investigated and distinguished by using different densities of agar. A rigid agar (1.8%) is used to observe TFP-mediated twitching motility, which allows the TFP to attach and grab, then retract the pili filament by disassembly of the pilin polymers and pull the bacteria toward the attaching site. Conversely, a soft agar (0.3%) is used to observe flagella-mediated swimming motility, which allows flagella to rotate, and bacteria can penetrate the agar to move. The expression of TFP and flagella under different c-di-GMP conditions were examined in *C. difficile* strain 630 and TFP

mutants by immunoblotting.

4.2. Motility in *C. difficile* 630

4.2.1. Twitching Motility of CD630

From the results in the previous chapter, in wild type CD630, PilA1 is only expressed under elevated levels of c-di-GMP, which is achieved by inducing *dccA* from the plasmid vector pECC17. We hypothesised that we would observe a higher level of motility in CD630 with induced *dccA* than the wild type strain.

In order to investigate twitching motility, the diameter of colonies spotted on 1.8% agar was monitored over time. Changes in diameter between day 1 and day 3 were calculated and analysed, as these two time points were representative of the biggest difference in colony expansion.

Comparing CD630, vector control 630_pASF85, and 630_pECC17, there is no significant difference across the strains. Similarly, no significant difference was detectable after ATc supplementation (+ ATc), which indicates induction of *dccA* does not seem to increase twitching motility, contrary to our hypothesis (Figure 4-1).

Observation of colony morphology shows branching on the edges of the colonies of all strains (Figure 4-1, panel C), which is characteristic of twitching motility mediated by TFP (Purcell et al., 2016). Interestingly, even though the overall diameter is similar, the branches seem to be more pronounced in 630_pECC17 in the presence of ATc when compared to absence of inducer. This suggests that increasing c-di-GMP is indeed producing an enhanced twitching phenotype, despite the lack of significant changes in colony diameter.

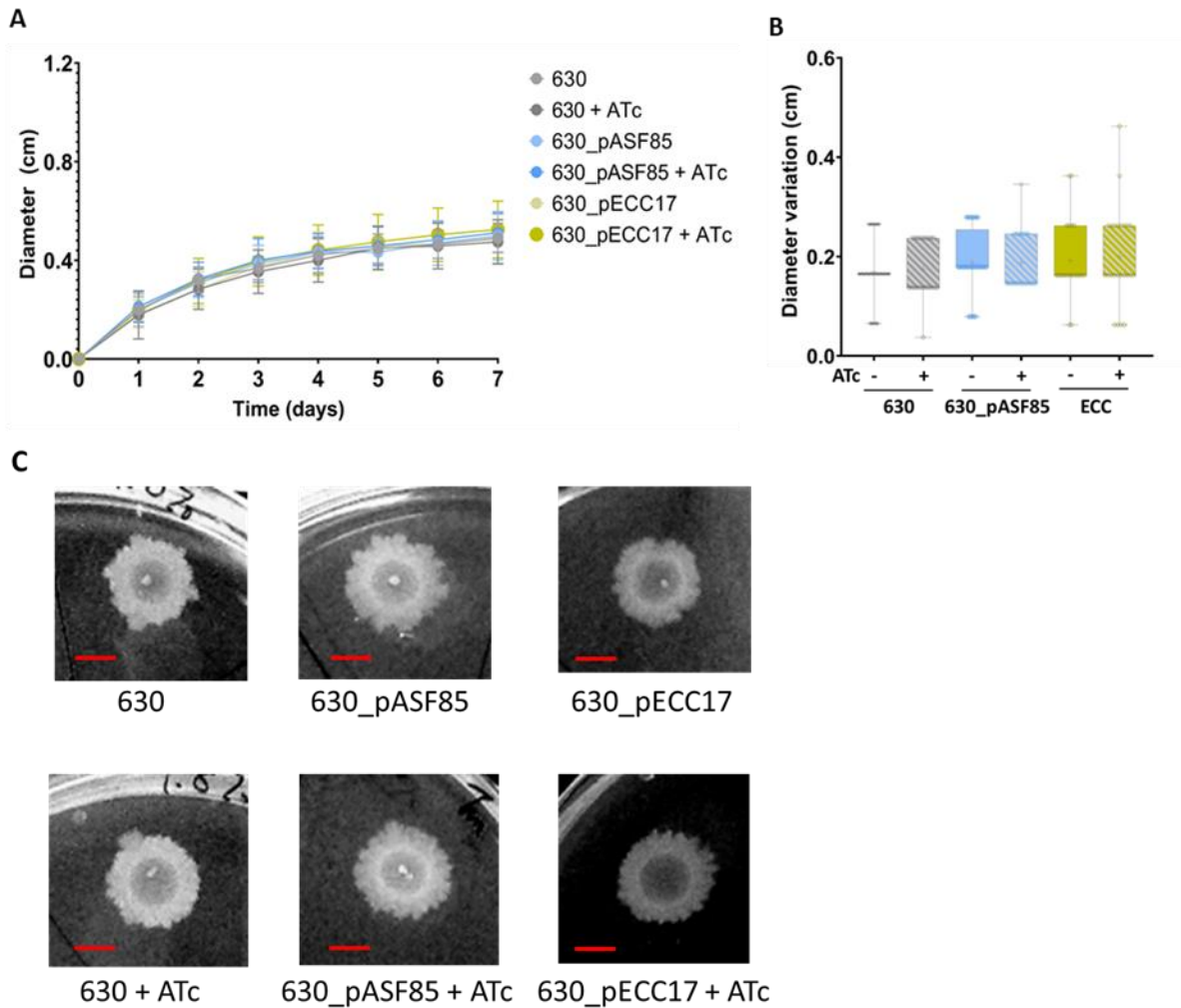


Figure 4-1. CD630 colony size and morphology on 1.8% agar

C. difficile CD630 (grey), vector control 630_pASF85 (blue) and 630_pECC17 (yellow) samples were incubated with (+ ATc) or without (- ATc) 50 ng ml⁻¹ of ATc on 1.8% agar plates. (A) Colony diameters were measured every 24 hours for 7 days. (B) Changes in colony diameter between Day 1 and Day 3 post-inoculation, with (solid colour) and without ATc (strips). Values from each replicate (diamonds) are included. One-way ANOVA analysis performed by Graphpad Prism. (C) Examples of colony morphology on 1.8% agar plates. Red bars indicate 0.6 cm. Images of the entire plates are shown in Appendix B-9.

4.2.2. Expression of *PilA1* in 1.8% agar

We then tested if *pilA1* is expressed by extracting bacteria from 1.8% agar 3 days after inoculating the plates and analysing them via immunoblotting. Samples were treated as described in sections 2.4.2 and 2.5.1.

4.2.3. Flagella Expression in CD630 in 1.8 % agar

We then investigated if inducing the expression of *dccA* and subsequent increased c-di-GMP levels would lead to a decreased level of expression from *flgB* operon via the regulatory Cdi1_3 riboswitch when grown in 1.8 % agar. Samples were treated as described above, with surface proteins extracted by TCA precipitation and cytosolic proteins presented in the cell lysates analysed using anti-FliC antibodies (see section 2.4.2 and 2.5.1. for details).

FliC is detected both with and without ATc supplementation in CD630 and the empty vector control (Figure 4-3). There is a slight reduction in external FliC and corresponding increase in cytosolic protein in these strains, possible due to a natural reduction of flagella production when swimming motility is not possible or required.

Importantly, there is a clear reduction in FliC detectable in the TCA samples and even almost missing in the cell lysate upon ATc supplementation of 630_pECC17. This indicates that increasing c-di-GMP level causes a reduction in *fliC* expression and assembly of flagella at the surface, as reported previously (Purcell et al., 2016; Sudarsan et al., 2008).

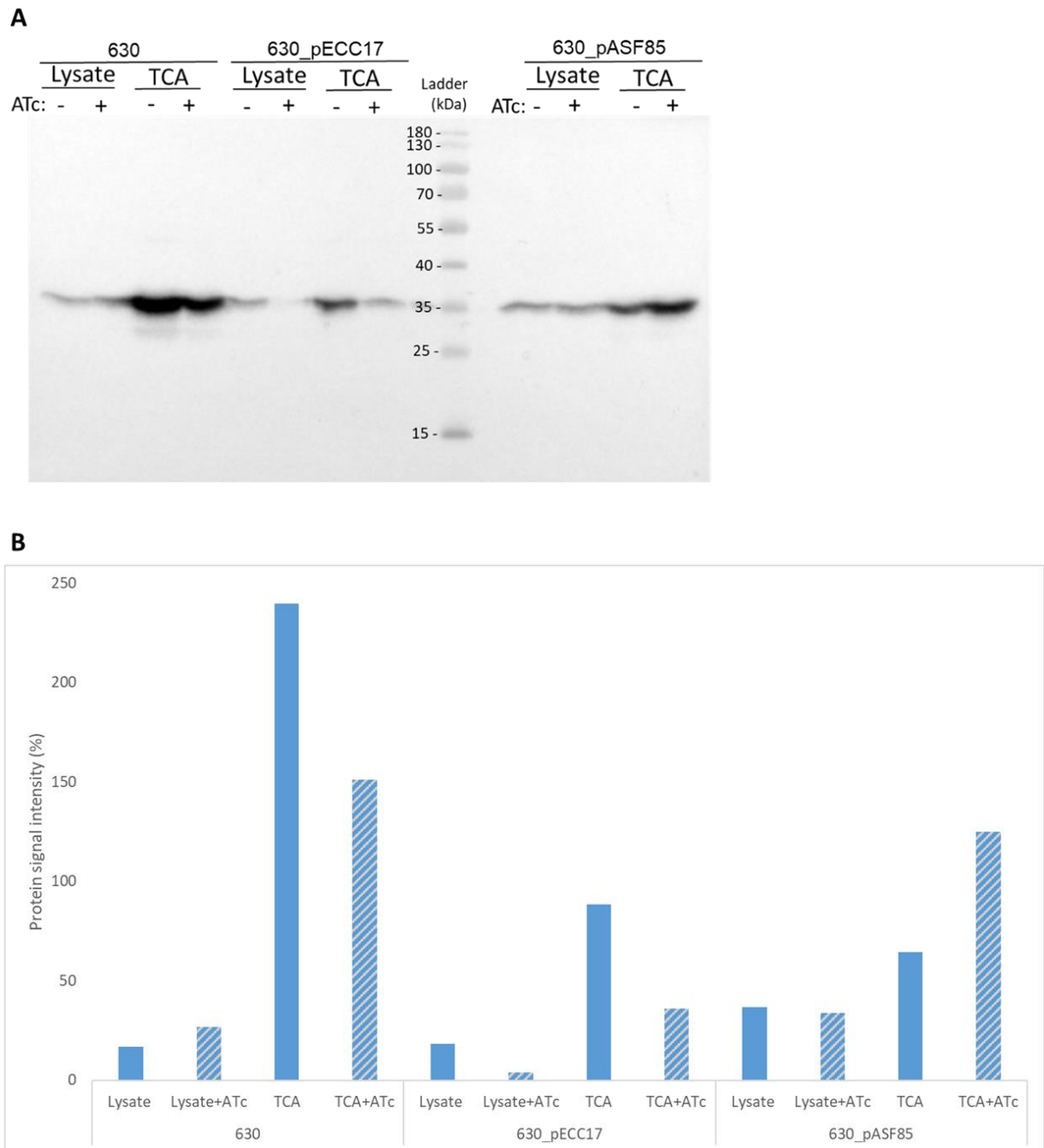


Figure 4-3. Immunoblot detection of FliC

FliC signal detected using anti-FliC antibodies on samples isolated from CD630, 630_pASF85 and 630_pECC17, grown on 1.8% agar either with (+) or without (-) ATc supplementation (A). Signal bands were quantified and plotted in (B). ATc supplementation is represented by slash in graph, quantification data can be found in Appendix E-5. Surface proteins were extracted by TCA precipitation, while cytosolic proteins were analysed from the cell lysates. Cathode/Anode buffers were applied in western blot, transfer was performed at 15V for 23 minutes onto nitrocellulose membranes. Predicted molecular weight of FliC is 30.8 kDa.

4.2.4. Swimming Motility of CD630

Next, we investigated motility in 0.3 % agar to see if the reduction of *fliC* expression leads to a decrease in *C. difficile* swimming motility. Samples were applied in the agar, as described in section 2.6.2 and the colony diameter was measured over time (Figure 4-4). In general, due to highly variable and uneven spread of the colonies in this semi-soft media, the experiments were stopped after 48h.

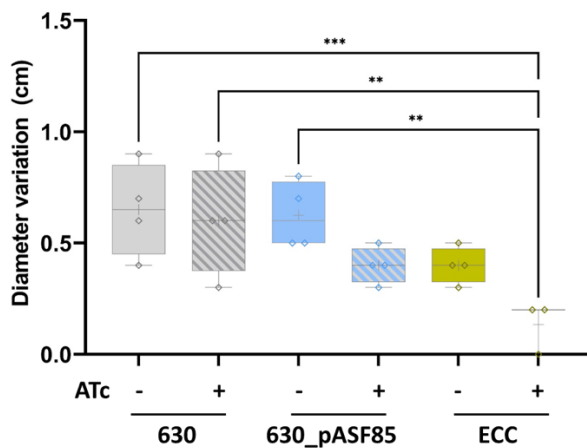


Figure 4-4. Colony diameter variation in 0.3% agar

Flagella-mediated swimming motility assay, performed on 0.3% agar, either with (+) or without (-) ATc supplementation. Changes in colony diameter from 24th to 48th hour of incubation were measured and analysed in CD630 (grey), 630_pASF85, (blue) and 630_pECC17 (ECC; yellow) strains. Strip shades indicated samples under *dccA* induction (+ ATc). Each replicate is represented as a diamond. ‘***’ indicates P value < 0.01. Significance analysed with one-way ANOVA in GraphPad Prism.

Measurements of colony diameter showed no significant differences in CD630 with and without ATc supplementation nor compared with the empty vector control (Figure 4-4). When *dccA* is induced in 630_pECC17, a significantly reduced diameter was observed as clearly seen in Figure 4-5 (bottom right), indicating reduced motility, as hypothesised.

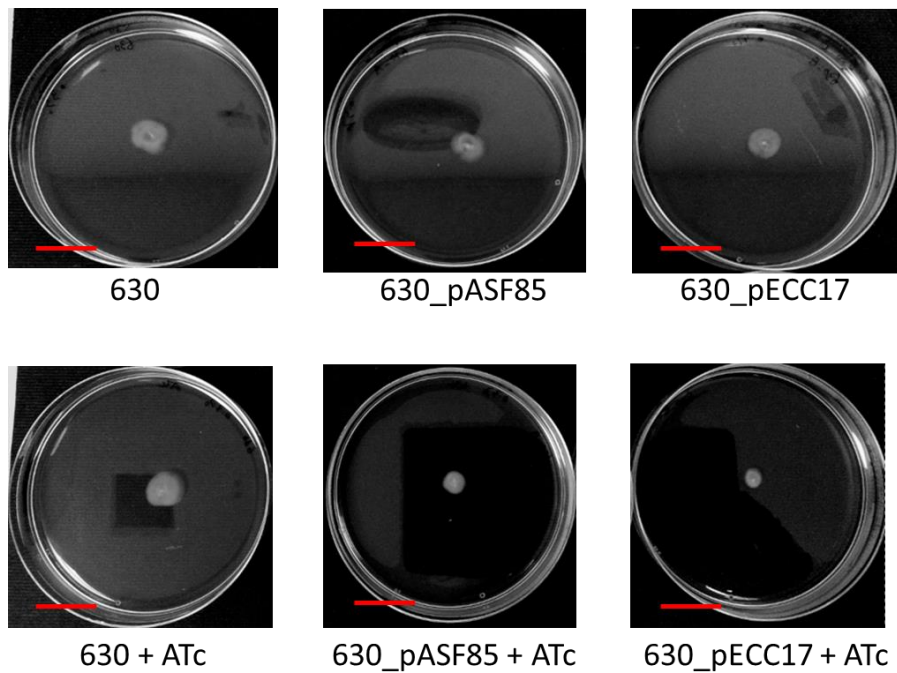


Figure 4-5. Colony morphology on 0.3% agar

CD630, 630_pASF85 and 630_pECC17 colonies inoculated into 0.3% agar and incubated for 48 hours with (+ ATc) or without (- ATc) 50 ng ml⁻¹ of ATc supplementation. The diameters were measured every 24 hours for statistical analysis. Red bars indicate 2.5 cm.

Since bacterial cultures disseminated into the semi-solid agar, it was not possible to extract cells from the 0.3% agar plates and perform western blots. However, taken all observations together, we can conclude that increased levels of c-di-GMP repress *fliC* expression, which leads to deficiency in flagella-mediated swimming motility.

4.3. Motility in CD630 $\Delta pilA1$ mutant

4.3.1. Effects of *PilA1* in CD630 Twitching Motility

Here, we investigated the twitching motility in $\Delta pilA1$ and complement strains as we hypothesised that the absence of *pilA1* would result in a deficiency in twitching motility. The strains were spotted on 1.8% agar with or without ATc and colony diameter monitored as described above.

Surprisingly, analysis of diameter changes over time suggests that $\Delta pilA1$ and complement strains show an increased diameter compared to 630_pECC17, regardless of *dccA* induction (Figure 4-6).

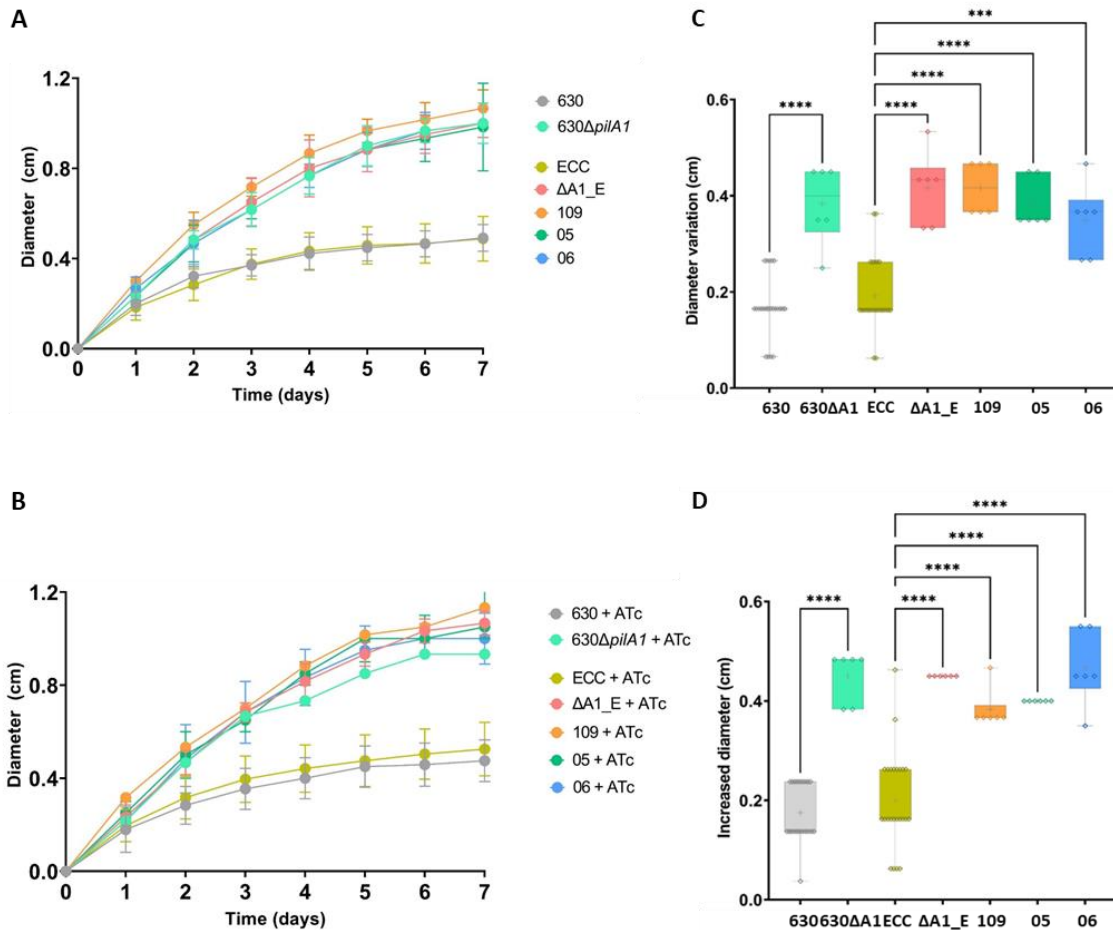


Figure 4-6. Effect of PilA1 on colony diameter in 1.8% agar

C. difficile CD630 (grey), 630 $\Delta pilA1$ (630 $\Delta A1$; cyan), 630_pECC17 (ECC; yellow), 630 $\Delta pilA1$ _pECC17 ($\Delta A1_E$; pink) and the complement strains 630 $\Delta pilA1$ _pECC109 (109; orange), 630 $\Delta pilA1$ _pZGW005 (05; green) and 630 $\Delta pilA1$ _pZGW006 (06; blue) samples were incubated on 1.8% agar plates. Colony diameter was measured every 24 hours for 7 days without (A) or with 50 ng ml⁻¹ of ATc supplementation (B). Changes in colony diameter between Day 1 and Day 3 post-inoculation in the absence (C) or presence (D) of ATc. Each replicate is represented as a diamond. One-way ANOVA analysis performed by Graphpad Prism. ‘***’ indicates P value < 0.001. ‘****’ indicates P value < 0.0001.

However, closer inspection of the colony morphology revealed that the increased diameter in $\Delta pilA1$ does not have the characteristic branching of twitching motility (Figure 4-7), suggesting this is more colony diffusion than active motility. Moreover, this lack of branching is also not

observed in the complement strains, which show a similar wider colony size, with only 630_pECC109 possibly showing some faint branching at the edges of the colony (Figure 4-7, right, bottom line).

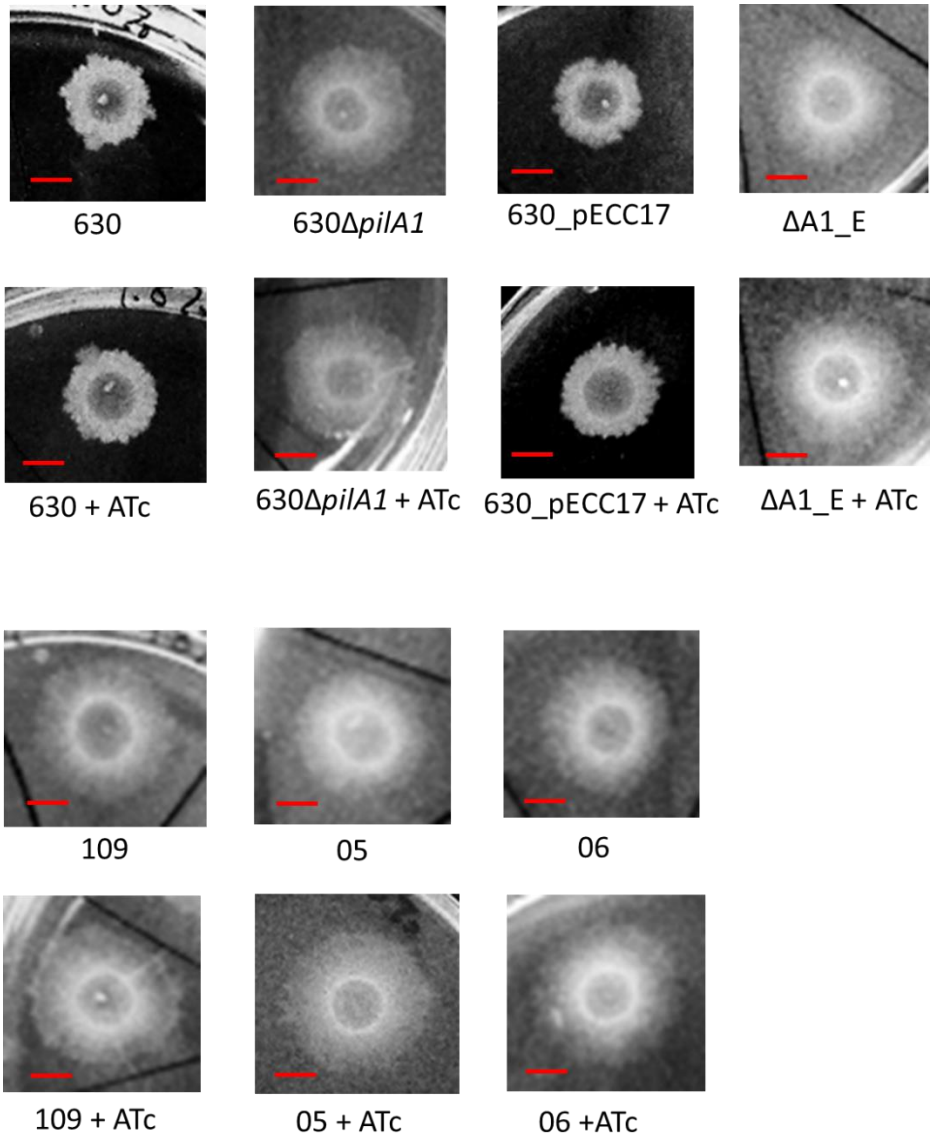


Figure 4-7. Effect of *pilA1* on colony morphology on 1.8% agar

Example of colonies from 630Δ*pilA1*, 630Δ*pilA1*_pECC17 (ΔA1_E) and complement strains 630Δ*pilA1*_pECC109 (109), 630Δ*pilA1*_pZGW005 (05) and 630Δ*pilA1*_pZGW006 (06) incubated for 7 days on 1.8% agar plates with (+ ATc) or without 50 ng ml⁻¹ of ATc supplementation, displayed and compared with CD630 and 630_pECC17 colonies. Red bars indicate 0.6 cm. Images of the entire plates are shown in Appendix B-10.

This suggests that, as hypothesised, PilA1 is essential for twitching motility but that our different complement constructs were not able to restore the phenotype under solid media growth.

4.3.2. TFP and flagella Expression in $\Delta pilA1$ mutant and complement strains grown on 1.8% agar

To further investigate if the diffuse growth observed for $\Delta pilA1$ and complemented strains correlated to changes in the expression of *pilA1* and *fliC*, samples collected 3 days post inoculation were examined by western blot as described above.

Interestingly, PilA1 signals were only detected in 630_pECC17 and 630 $\Delta pilA1$ _pZGW006, with a stronger signal detected in 630 $\Delta pilA1$ _pZGW006 under *dccA* induction (Figure 4-8). This strain also shows an accumulation of PilA1 in the cytosol.

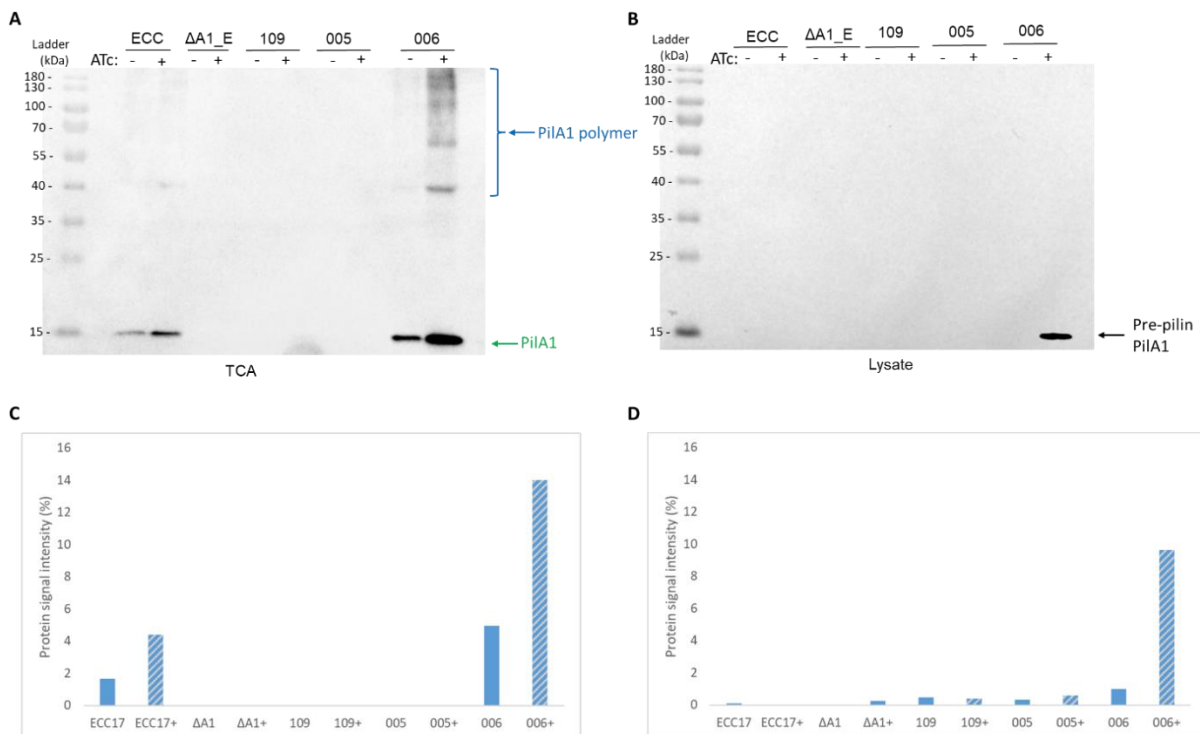


Figure 4-8. Immunoblot detection of PilA1 in $\Delta pilA1$ and complement strains on 1.8% agar

PilA1 signals from 630_pECC17 (ECC), 630 $\Delta pilA1$ _pECC17 ($\Delta A1_E$) 630 $\Delta pilA1$ _pECC109 (109), 630 $\Delta pilA1$ _pEZGW005 (005) and 630 $\Delta pilA1$ _pEZGW006 (006), either with (+) or without (-) ATc supplementation. (A) Surface proteins were extracted by TCA precipitation, signal bands were quantified and plotted in (C). (B) The cytosolic proteins analysed from the cell lysates, signal bands were quantified and plotted in (D). Cathode/Anode buffers were applied in western blot, transfer was performed at 15V for 23 minutes onto nitrocellulose membranes. Predicted molecular weight of pre-pilin PilA1 (black arrow) is 18.2 kD, mature pilin PilA1 (green arrow) is 17.2 kDa. Blue arrow indicates PilA1 polymers. ATc supplementation is represented by slash in graph, quantification data can be found in Appendix E-6.

The same set of samples extracted from 1.8% agar was then inspected using anti-FliC antibodies. We hypothesised that deleting and complementing *pilA1* would not affect *fliC* expression and no phenotype across strains would be observed, apart from a reduction in FliC signal under *dccA* induction, as observed in previous sections. Interestingly, only 630_pECC17 has FliC signals in the culture supernatant, while 630 Δ *pilA1*_pECC109 and 630 Δ *pilA1*_pZGW005 express FliC, but FliC is not exported to the cell surface. As flagella is not proposed to be involved in motility in 1.8 % agar, it is not surprising that there is no export of FliC in these strains and that any expressed protein accumulates in the cytoplasm. The presence of FliC in the supernatant but absence in the lysate observed in 630_pECC17 further confirms that induction of *dccA* inhibits expression of FliC and swimming motility.

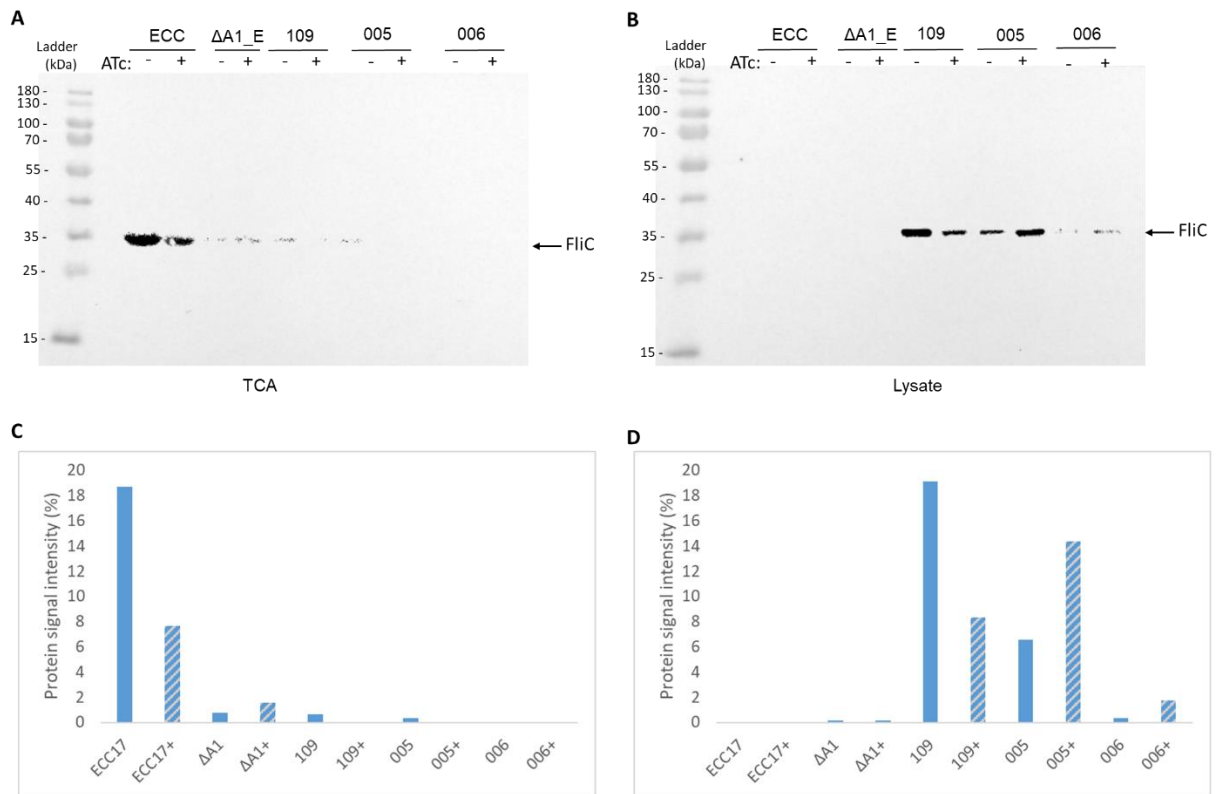


Figure 4-9. Immunoblot detection of FliC in 630 Δ *pilA1* mutant and complement strains on 1.8% agar

FliC signals from 630_pECC17 (ECC), 630 Δ *pilA1*_pECC17 (Δ A1_E), *pilA1* complement strains 630 Δ *pilA1*_pECC109 (109), 630 Δ *pilA1*_pEZGW005 (005) and 630 Δ *pilA1*_pZGW006 (006), either with (+) or without (-) ATC supplementation. (A) Surface proteins were extracted by TCA precipitation, signal bands were quantified and plotted in (C). (B) The cytosolic proteins analysed from the cell lysates, signal bands were quantified and plotted in (D). Cathode/Anode buffers were applied in western blot, transfer was performed at 15V for 23 minutes onto nitrocellulose membranes. Predicted molecular weight of FliC is 30.8 kDa. ATC supplementation is represented by slash in graph, quantification data can be found in Appendix E-7.

The absence of FliC in $\Delta pilA1$ mutant (Figure 4-9) is puzzling and further work is required to understand if a possible expression control loop exist between FliC and PilA1, beyond the c-di-GMP induced riboswitches.

4.3.3. Effects of PilA1 on Swimming Motility

We then investigated whether deleting *pilA1* affects swimming motility on 0.3% agar. From the previous result in CD630, a deficient swimming motility is observed under a higher level of c-di-GMP. If PilA1 is indeed not involved in swimming motility, there should be no phenotype in $\Delta pilA1$ or complement strains.

As expected, no changes in swimming motility were detected when comparing CD630 and 630_pECC17 or the $\Delta pilA1$ mutant or the complemented strains without ATc supplementation (Figure 4-10).

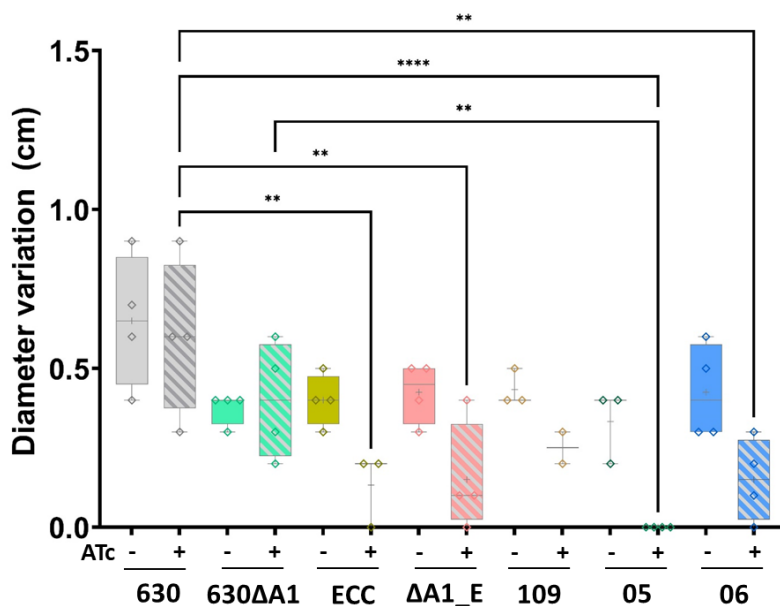


Figure 4-10. $\Delta pilA1$ and complement strains colony diameter variation in 0.3% agar

Flagella-mediated swimming motility assay, performed on 0.3% agar, either with (+) or without (-) ATc supplementation. CD630 (grey), 630 $\Delta pilA1$ (630 $\Delta A1$; cyan) 630_pECC17 (ECC; yellow), 630 $\Delta pilA1$ _pECC17 (ΔA_E ; pink), 630 $\Delta pilA1$ _pECC109 (109; orange), 630 $\Delta pilA1$ _pZGW005 (05; green) and 630 $\Delta pilA1$ _pZGW006 (06; blue). Strip shades indicated samples under *dccA* induction (+ ATc). Each replicate is represented as a diamond. Asterisks '**' indicate P value < 0.01, '****' indicate P value < 0.0001. Significance analysed with one-way ANOVA in GraphPad Prism.

Addition of ATc seems to lead to a small reduction in diameter in all strains containing an inducible *dccA*, due to repressed expression of *fliC* under a higher level of c-di-GMP, as described for wild type strains (section 4.2.3. above). However, this does not appear to be statistically significant, likely due to the considerable experimental variations associated with these measurements.

As expected from previous observations, all strains containing the plasmid showed significant reduction in swimming motility after induction of *dccA* when compared to CD630 (Figure 4-10). It is worth noting that this effect was most obvious when complementing with pZGW005, which does not contain the *pilA1* promoter region. Motility on 1.8 % and 0.3 % agar involving vector control strains can be found in Appendix Figure B-11 and B-12.

4.3.4. Flagella Expression in $\Delta pilA1$ mutant and complement strains

To confirm that the observed reduction in swimming motility was due to reduced FliC levels, immunoblotting with anti-FliC antibodies of $\Delta pilA1$ and complement strains was then performed. As 0.3% agar is semi-solid, extraction of bacterial cells from the plates was technically challenging. Therefore, the different strains were incubated in liquid media, prior to analysis as previously described (section 2.6.2).

A reduced level of FliC signal was detected when *dccA* was induced in strain 630_pECC17 with ATc supplementation. This is due to the regulation led by a class 1 riboswitch Cdi1_3, as explained before. We hypothesised that deleting and complementing *pilA1* would not affect the expression of *fliC*, nor the riboswitch regulation under increased levels of c-di-GMP.

As expected, reduced levels of FliC signal were observed in all strains upon induction of *dccA*. This confirms our hypothesis that deleting *PilA1* does not affect the expression of *fliC* or its regulation under higher levels of c-di-GMP (Figure 4-11).

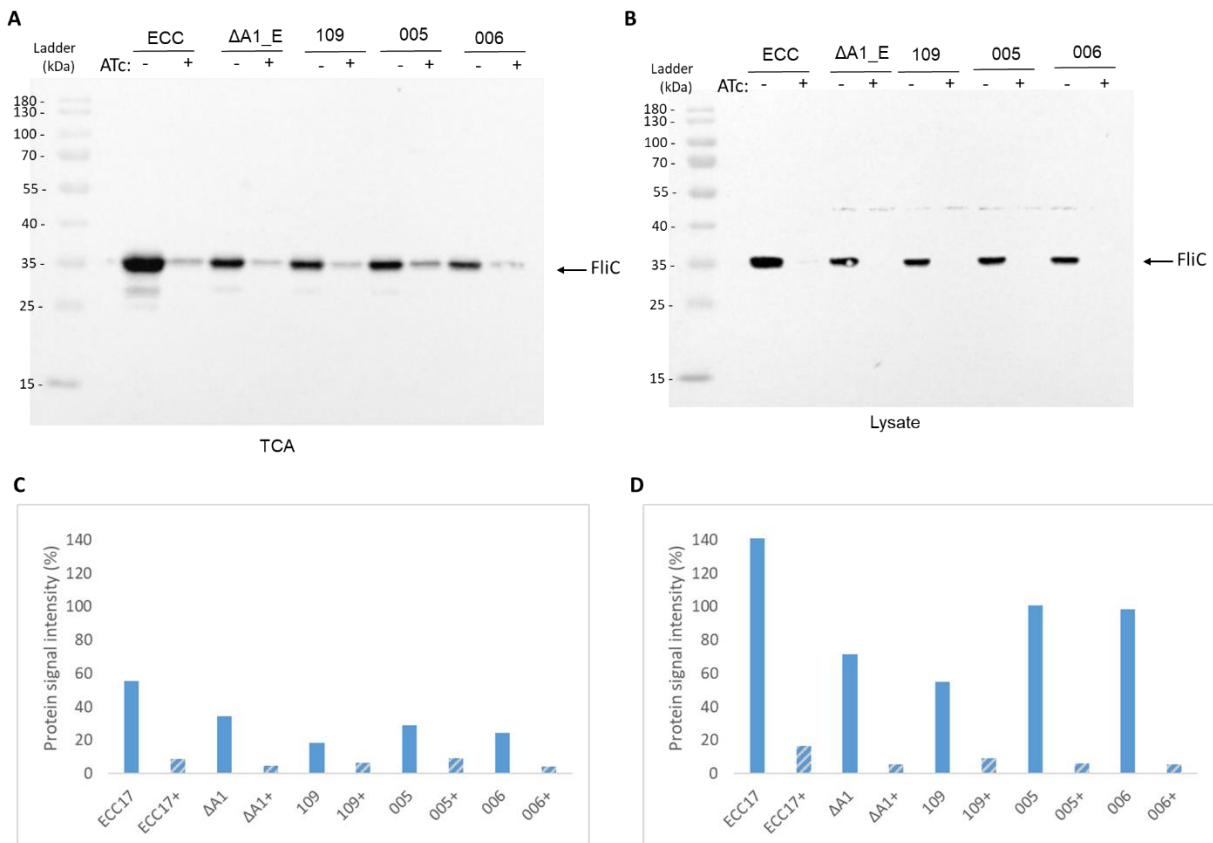


Figure 4-11. Immunoblot detection of FliC in $\Delta pilA1$ mutant and complement strains

FliC signals from *C. difficile* 630_pECC17 (ECC), 630 $\Delta pilA1$ _pECC17 ($\Delta A1_E$), 630 $\Delta pilA1$ _pECC109 (109), 630 $\Delta pilA1$ _pEZGW005 (005) and 630 $\Delta pilA1$ _pZGW006 (006), either with (+) or without (-) ATc supplementation. (A) Surface proteins were extracted by TCA precipitation, signal bands were quantified and plotted in (C). (B) Cytosolic proteins analysed from the cell lysates, signal bands were quantified and plotted in (D). Predicted molecular weight of FliC is 30.8 kDa. ATc supplementation is represented by slash in graph, quantification data can be found in Appendix E-8.

No FliC signal is detected in the cell lysates when *dccA* is induced in all strains, confirming that increased levels of c-di-GMP halt FliC expression, and any remaining protein has been exported to the cell surface.

4.4. Motility in CD630 $\Delta pilD1$ mutant

4.4.1. Effects of *PilD1* on Twitching Motility

In chapter 3, we showed that *PilD1* doesn't seem to be required for TFP biosynthesis, but that deletion of *pilD1* leads to long cell shapes. Here, we investigated the effects of lack of *pilD1* on

twitching motility by measuring the diameter of colonies over time, as well as the changes between day 1 and day 3, as described in section 2.6.3. above.

No statistically significant difference in colony diameter was observed among CD630 and $\Delta pilD1$ strains, regardless of the presence or even induction of *dccA* (Figure 4-12, compare 630 and 630_pECC17, with or without induction). Interestingly, complementation of *pilD1* deletion leads to increased colony diameter when compared to 630_pECC17, even without ATc, although the more significant changes are seen after *dccA* induction.

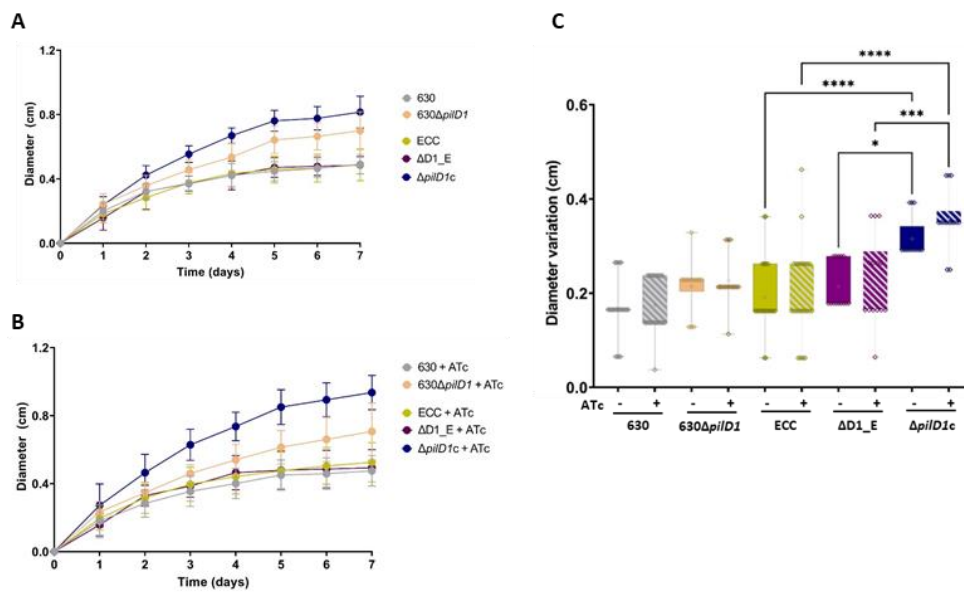


Figure 4-12. Effect of PilD1 in colony diameter in 1.8% agar

CD630 (grey), 630 $\Delta pilD1$ (orange), 630_pECC17 (ECC; yellow), 630 $\Delta pilD1$ _pECC17 ($\Delta D1_E$; purple) and 630 $\Delta pilD1$ _pZGW007 ($\Delta pilD1c$; navy) samples with (+ ATc) or without (-ATc) 50 ng ml⁻¹ of ATc supplementation on 1.8% agar plates and diameters measured every 24 h for 7 days. (A) Colony diameters in plates without ATc supplementation. (B) Colony diameters under ATc supplementation. (C) Changes in colony diameter between Day 1 and Day 3 post-inoculation. One-way ANOVA analysis performed by Graphpad Prism. Samples under ATc induction is shaded in strips. Each replicate is represented as diamonds. '*' indicates P value < 0.1. '***' indicates P value < 0.001. '****' indicates P value < 0.0001.

As described for $\Delta pilA1$ strains, measurement of colony diameter might lead to misinterpretations, as it can be a result of colony expansion/diffusion rather than twitching motility. We therefore examined colony morphology carefully (Figure 4-13). In this case, the characteristic branching was observed in all strains, with more pronounced branching in the complement strain, particularly after *dccA* induction. It should be noted that in this

complementation strain, *pilD1* is directly upregulated by ATc, together with *dccA*, which will also indirectly induce the primary gene cluster (see 1.3.1. for more details). Therefore, there is likely to be a significant higher level of D1 in the complement strain than in 630_pECC17, where only the indirect effect on expression of TFP is present.

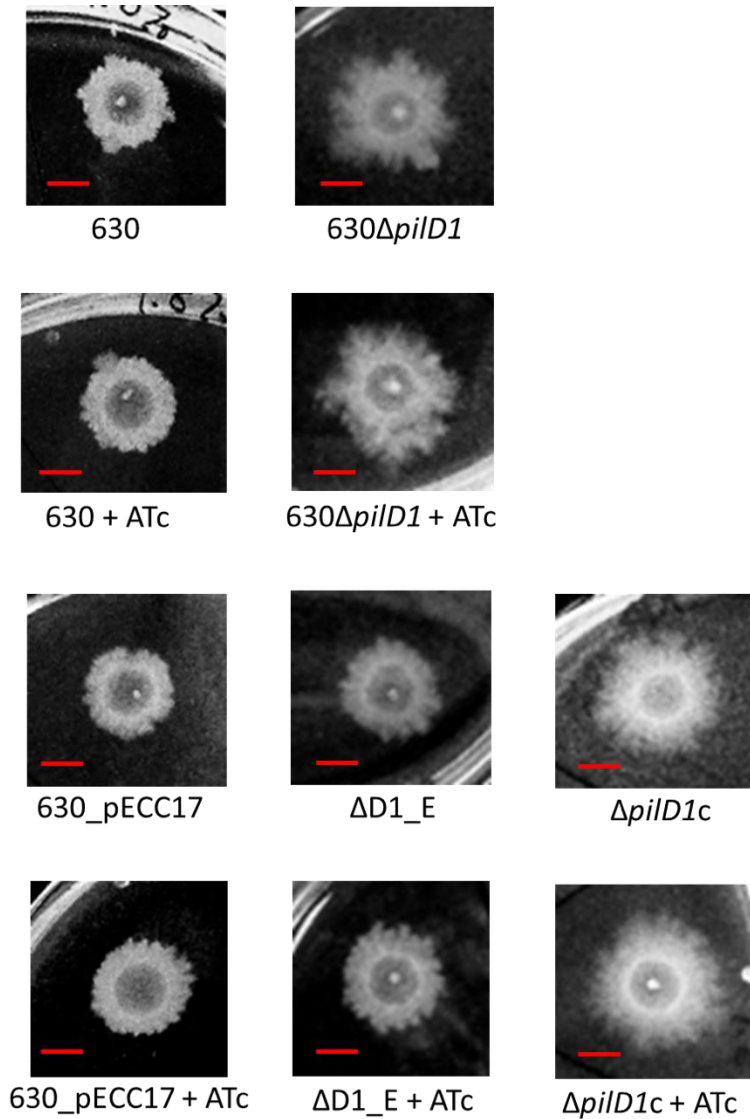


Figure 4-13. Effect of PilD1 and complement colonies on 1.8% agar 630*ΔpilD1*, 630*ΔpilD1*_pECC17 ($\Delta D1_E$) and 630*ΔpilD1*_pZGW007 ($\Delta pilD1c$) colonies incubated to 7 days on 1.8% agar plates with (+ ATc) or without 50 ng ml⁻¹ of ATc supplementation, displayed and compared with CD630 and 630_pECC17 colonies for comparison. Red bars indicate 0.6 cm. Images of the entire plates are shown in Appendix B-13.

These observations seem to suggest that, under normal circumstances, *pilD1* is not required for twitching motility, confirming our earlier result that it does not seem to be needed for PilA1 expression or assembly into pilin filaments (see section 3.3.3.).

4.4.2. Expression of *pilA1* in $\Delta pilD1$ and complement strains on 1.8% agar

We then examined if absence of *pilD1* affects expression of *pilA1* in cells growing on 1.8% agar. Surprisingly, and contrary to what was observed in liquid cultures in Chapter 4, PilA1 signal is detected in the wild type after induction of *dccA*, but not in $\Delta pilD1$ (Figure 4-14). This suggests, that under conditions that stimulate switching motility mediated by TFP (1.8% agar), *pilD1* might be required for expression and/or stability of PilA1.

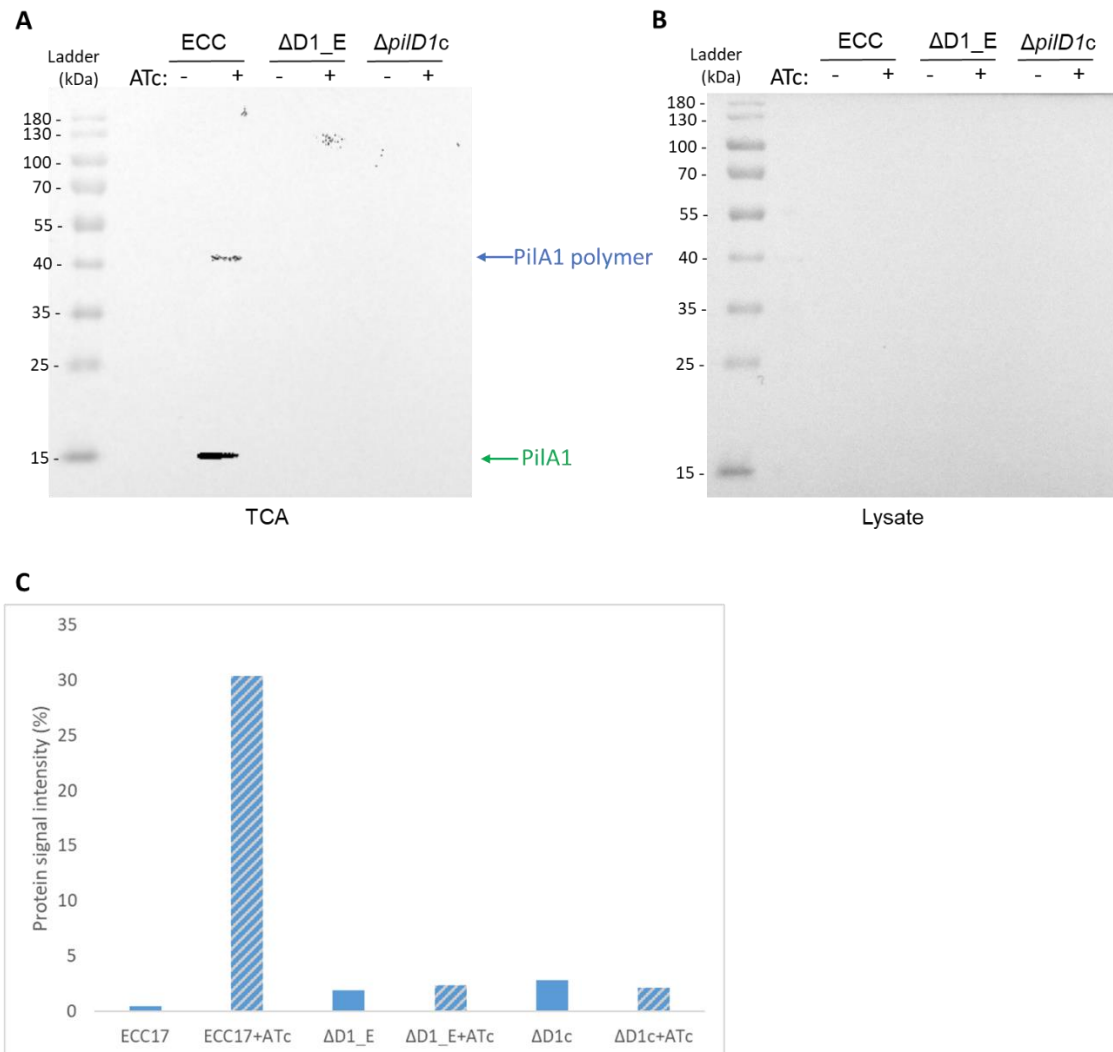


Figure 4-14. Immunoblot detection of PilA1 in 630 $\Delta pilD1$ and complement strains on 1.8% agar

PilA1 signals from *C. difficile* 630_pECC17 (ECC) and 630 $\Delta pilD1$ _pECC17 ($\Delta D1_E$) and 630 $\Delta pilD1$ _pZGW007 ($\Delta pilD1c$), either with (+) or without (-) ATc supplementation. (A) Surface proteins were extracted by TCA precipitation, signal bands were quantified and plotted in (C). (B) The cytosolic proteins analysed from the cell lysates. Cathode/Anode buffers were applied in western blot, transfer was performed at 15V for 23 minutes onto nitrocellulose membranes. Predicted molecular weight of pre-pilin PilA1 is 18.2 kDa (not detected), mature pilin (green arrow) PilA1 is 17.2 kDa. PilA1 polymer (blue arrow) is detected in the supernatant (TCA). ATc supplementation is represented by slash in graph, quantification data can be found in Appendix E-9.

Interestingly, complementation using a plasmid where both *dccA* and *pilD1* are under direct control of ATc does not seem to restore *pilA* expression, despite the observed branching of the colonies. This raises the possibility that the regulation mechanisms of the primary TFP cluster might be more complicated than previously proposed. Alternatively, PilD1 might be involved in stability of PilA1 or the filaments. It is also possible that there is more than one phenomenon being observed when growing *C. difficile* in 1.8% solid media, not just twitching motility.

These results suggest that the role of PilD1 could be different when *C. difficile* grows in liquid culture or on 1.8% agar. PilD1 seems to be required for the biosynthesis of PilA1 filament when cells grow on solid agar, but not when cells grow in liquid culture.

We also examined expression of *fliC* in (Figure 4-15) and a signal is detected in the cell supernatants in all strains, although the reduction observed in wild type upon *dccA* induction is not as obvious in the Δ *pilD* mutant or complement (Figure 4-15, panel A). Similarly, the levels of FliC in the cytosol are much lower in the wild type than in the other two strains without induction of *dccA*. Conversely, addition of ATc and subsequent increase in c-di-GMP levels leads to a halt in expression of FliC, as no protein is detected in the cytosol.

This confirms the previous observations that increased levels of c-di-GMP repress *fliC* expression and further suggests that TFP genes are not involved in this regulation.

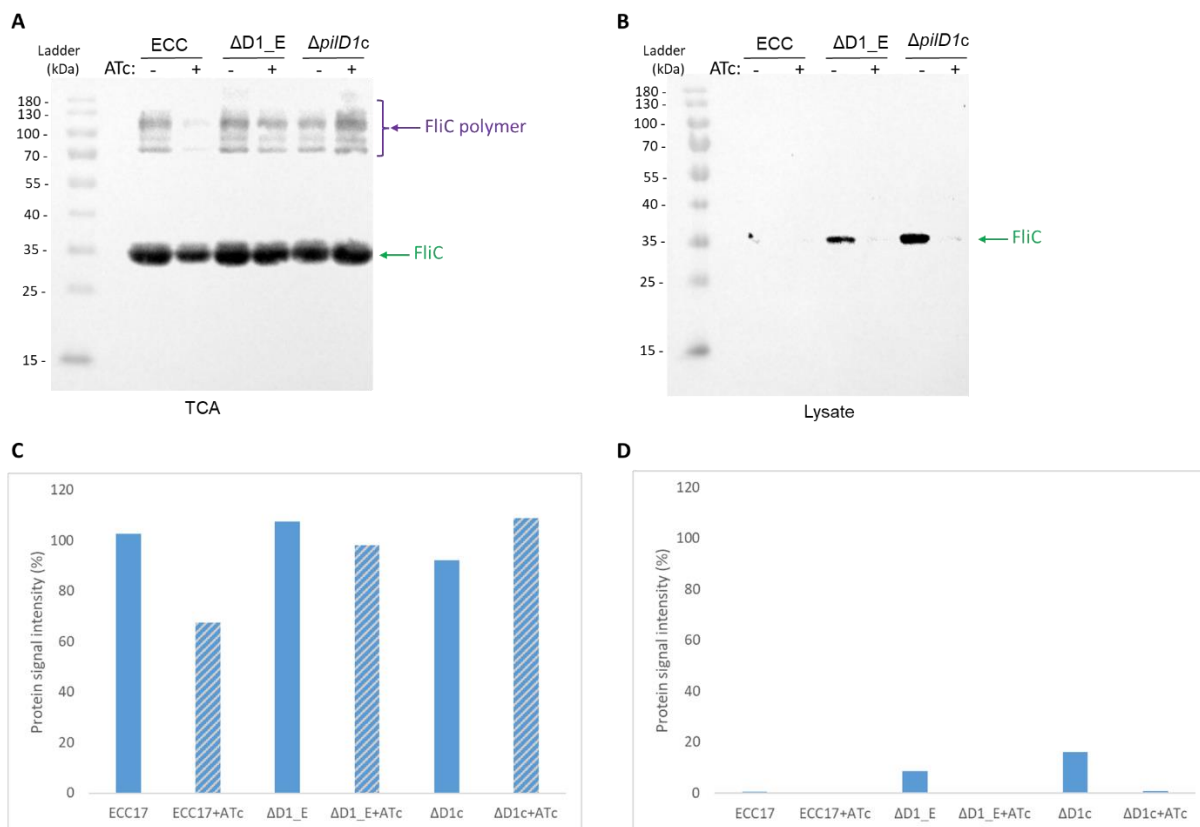


Figure 4-15. Immunoblot detection of FliC in *C. difficile* 630 $\Delta pilD1$ and complement strains on 1.8% agar

FliC signals from *C. difficile* 630_pECC17 (ECC) and 630 $\Delta pilD1$ _pECC17 ($\Delta D1_E$) and 630 $\Delta pilD1$ _pZGW007 (630 $\Delta pilD1c$), either with (+) or without (-) ATc supplementation. (A) Surface proteins were extracted by TCA precipitation, signal bands were quantified and plotted in (C). (B) Cytosolic proteins analysed from the cell lysates, signal bands were quantified and plotted in (D). Cathode/Anode buffers were applied in western blot, transfer was performed at 15V for 23 minutes onto nitrocellulose membranes. Predicted molecular weight of FliC (green arrow) is 30.8 kDa. Purple arrow indicates FliC polymers. ATc supplementation is represented by slash in graph, quantification data can be found in Appendix E-10.

4.4.3. Effects of *PilD1* on Swimming Motility

Flagella-mediated swimming motility was also examined in $\Delta pilD1$ and the complement strain and no statistically significant phenotype was observed, even after induction of *dccA* (Figure 4-16). Although it was expected to observe a deficient flagella-mediated motility in each strain under *dccA* induction, it should be noted that measurements are highly variable as colonies disseminate in 0.3% agar, which is also less stable. This gives rise to considerable experimental error, particularly evident in these experiments (Figure 4-16), that could mask biologically relevant differences. Due to these technical challenges, these plates were not

imaged after measurement. Motility on 1.8 % and 0.3 % agar involving vector control strains can be found in Appendix Figure B-14 and B-15.

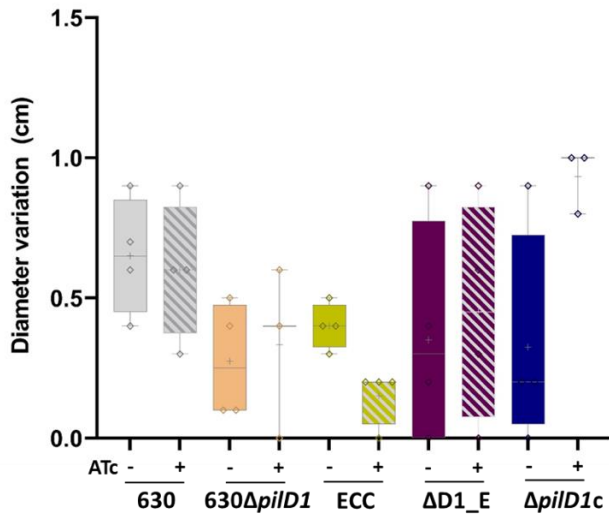


Figure 4-16. Variations in colony diameter for 630Δ*pilD1* and complement strains grown in 0.3 % agar

Flagella-mediated swimming motility is performed on 0.3% agar, either with (+) or without (-) 50ng ml⁻¹ of ATc supplementation. Changes in colony diameter between day 1 and day 2 post-inoculation for strains CD630 (grey), 630Δ*pilD1* (orange), 630_pECC17 (ECC; yellow), 630Δ*pilD1*_pECC17 (ΔD1_E; purple) and 630Δ*pilD1*_pZGW007 (Δ*pilD1c*; blue). Strip shades indicated samples under *dccA* induction (+ ATc) conditions performed by ATc supplementation. Each replicate is represented as a rectangle point. Significance analysed with one-way ANOVA in GraphPad Prism.

4.4.4. Flagella Expression in *pilD1* mutant and complement strains

Due to the technical challenges of accurately measuring swimming motility in 0.3 % agar, the level of *fliC* expression was analysed via immunoblotting from liquid cultures, as previously described (section 2.6.2.).

There is a clear reduction in FliC signal in the supernatant samples under *dccA* induction in all strains (Figure 4-17, panel A). In the cell lysates, there is no FliC signal detected in 630_pECC17 and 630Δ*pilD1*_pZGW007 (ΔD1_E) under *dccA* induction, and a very low level of FliC signal in 630Δ*pilD1*_pECC17 (Figure 4-17, panel B). It should be noted that higher bands of possible FliC polymers are detected, as well as possible partial degradation.

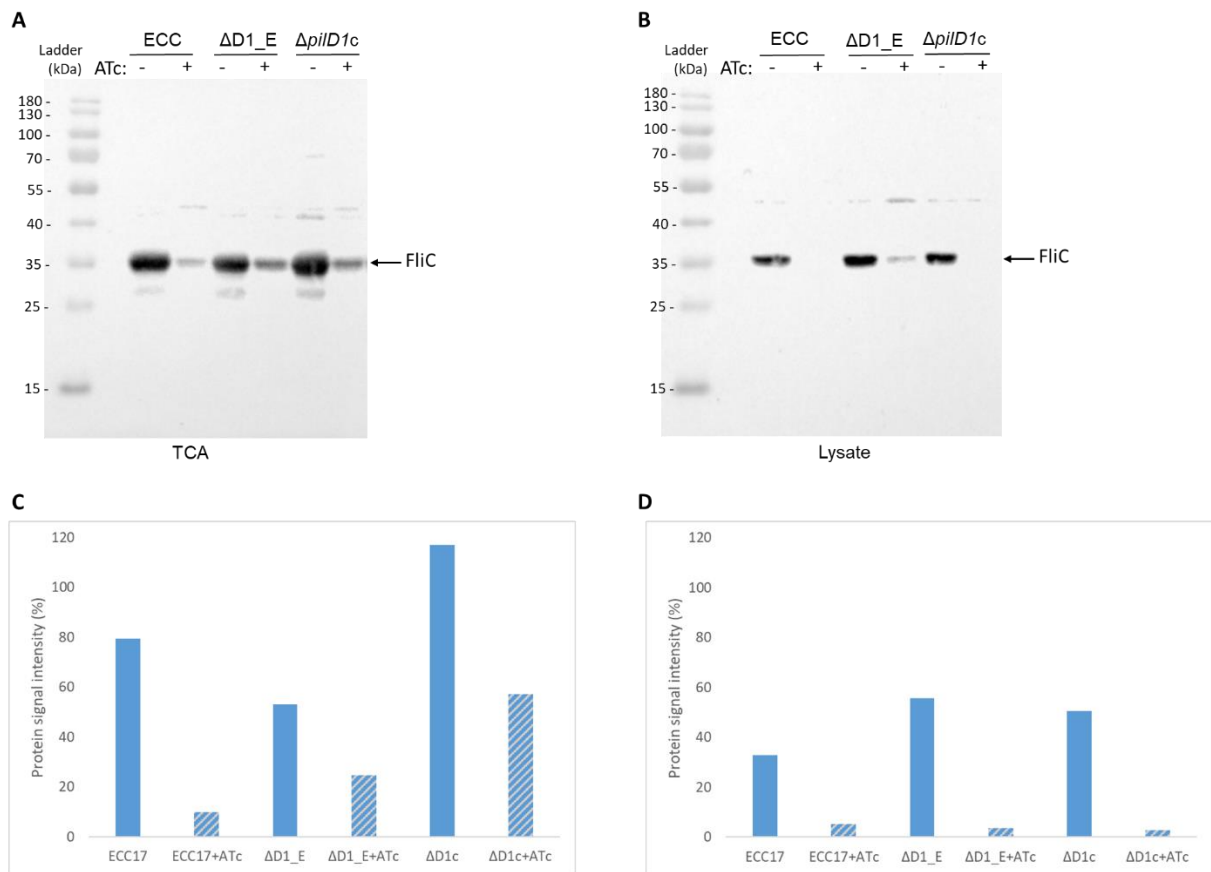


Figure 4-17. Immunoblot detection of FliC in *C. difficile* 630 Δ *pilD1* and complement strains

FliC signals from *C. difficile* with inducible *dccA*, 630_pECC17 (ECC) and 630 Δ *pilD1*_pECC17 (Δ D1_E), Δ *pilD1* complement strains 630 Δ *pilD1*_pZGW007 (Δ *pilD1c*), either with (+) or without (-) ATc supplementation. (A) Surface proteins were extracted by TCA precipitation, signal bands were quantified and plotted in (C). (B) Cytosolic proteins analysed from the cell lysates, signal bands were quantified and plotted in (D). Cathode/Anode buffers were applied in western blot, transfer was performed at 15V for 23 minutes onto nitrocellulose membranes. Predicted molecular weight of FliC is 30.8 kDa. ATc supplementation is represented by slash in graph, quantification data can be found in Appendix E-11.

Interestingly, although overall we see the expected effect of reduction of FliC expression at higher c-di-GMP levels, there are differences between liquid culture and 1.8 % plate samples, shown in the previous section (compare Figure 4-15 above with Figure 4-17). This suggests that the expression of FliC may also be affected by the incubation time and/or media type (solid vs liquid). Whether or not this is also related to the presence of *pilD1* is not clear, although it seems unlikely as no clear difference is observed between the mutant and the complemented strain.

4.5. Motility in CD630 $\Delta pilJ$ mutant

4.5.1. Effects of PilJ on Twitching Motility

Twitching motility and swimming motility were also investigated in our $\Delta pilJ$ mutagenesis study. In chapter 4, we showed that *pilJ* does not seem to be required for the assembly of the PilA1 filament and deleting *pilJ* does not affect the cell growth, morphology, and biofilm formation.

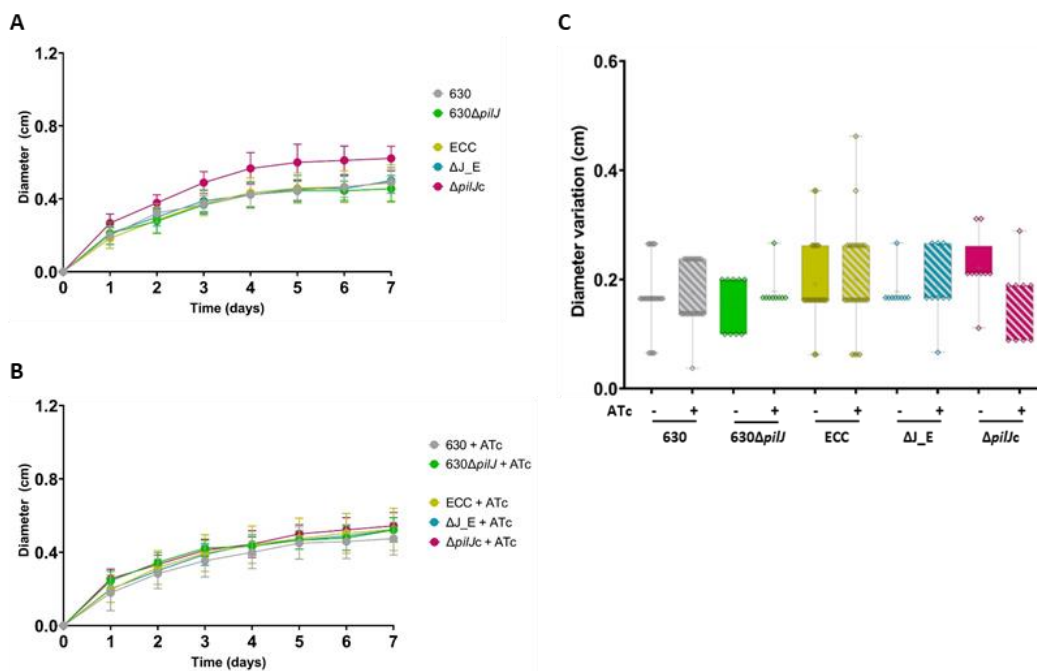


Figure 4-18. Effect of PilJ on colony diameter in 1.8 % agar

C. difficile CD630 (grey), 630 $\Delta pilJ$ (green), 630_pECC17 (ECC; yellow), 630 $\Delta pilJ$ _pECC17 (ΔJ_E ; blue) and 630 $\Delta pilJ$ _pZGW008 ($\Delta pilJc$; pink) samples were incubated with (+ ATc) or without (- ATc) 50 ng ml⁻¹ of ATc supplementation on 1.8% agar plates and diameters measured every 24h for 7 days. (A) Colony diameters without ATc supplementation. (B) Colony diameters under ATc supplementation. (C) Changes in colony diameters between Day 1 and Day 3 post-inoculation. Samples under ATc induction is shaded in strips. Each replicate is represented as diamonds. One-way ANOVA analysis performed by Graphpad Prism.

As expected, when analysing colony diameter and changes between day 1 and day 3 post-inoculation, neither the mutant itself nor strains with inducible *dccA* showed a significant difference (Figure 4-18).

Similarly, inspection of the colony morphology showed branching in all strains, regardless of mutation or *dccA* induction (Figure 4-19).

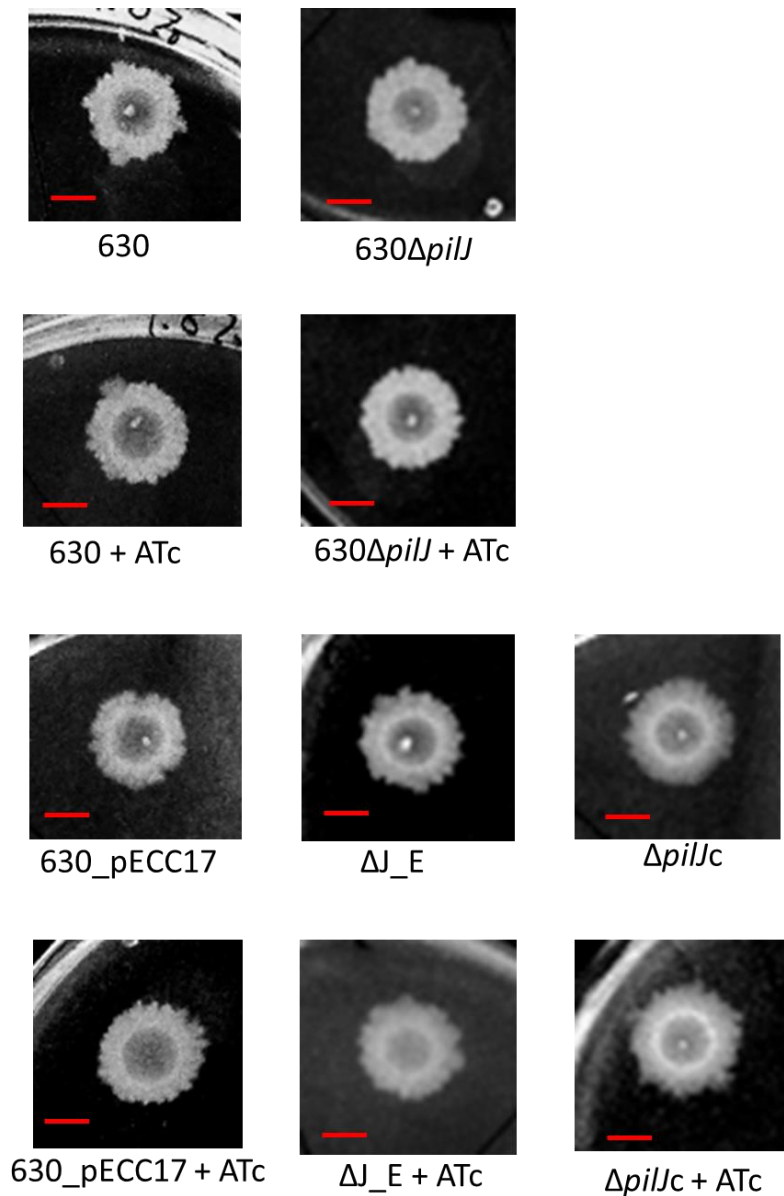


Figure 4-19. $\Delta pilJ$ and complement colonies on 1.8% agar plates

Examples of $630\Delta pilJ$, $630\Delta pilJ_pECC17$ and $630\Delta pilJ_pZGW008$ colonies incubated to 7 days on 1.8% agar plates with (+ ATc) or without (-ATc) 50 ng ml^{-1} of ATc supplementation, displayed and compared with CD630 and 630_pECC17 colonies. Red bars indicate 0.6 cm. Images of the entire plates are shown in Appendix B-16.

These results suggest that *pilJ* does not seem to have a noticeable effect on the ability of CD630 strain to expand on 1.8 % agar using twitching motility.

4.5.2. Expression of pilA1 in $\Delta pilJ$ and complement strains on 1.8% agar

To confirm the twitching motility result, anti-PilA1 and anti-FliC western blots were performed with samples incubated on 1.8 % agar plates (Figure 4-20). There is a similar level of PilA1 signal detected in the supernatants of 630_pECC17 and 630 $\Delta pilJ$ _pECC17 under *dccA* induction, with both PilA1 monomers and trimers. Interestingly, there is a lower level of PilA1 signal detected in 630 $\Delta pilJ$ _pZGW008 ($\Delta pilJc$) under *dccA* induction, with only monomers visible in the western blot.

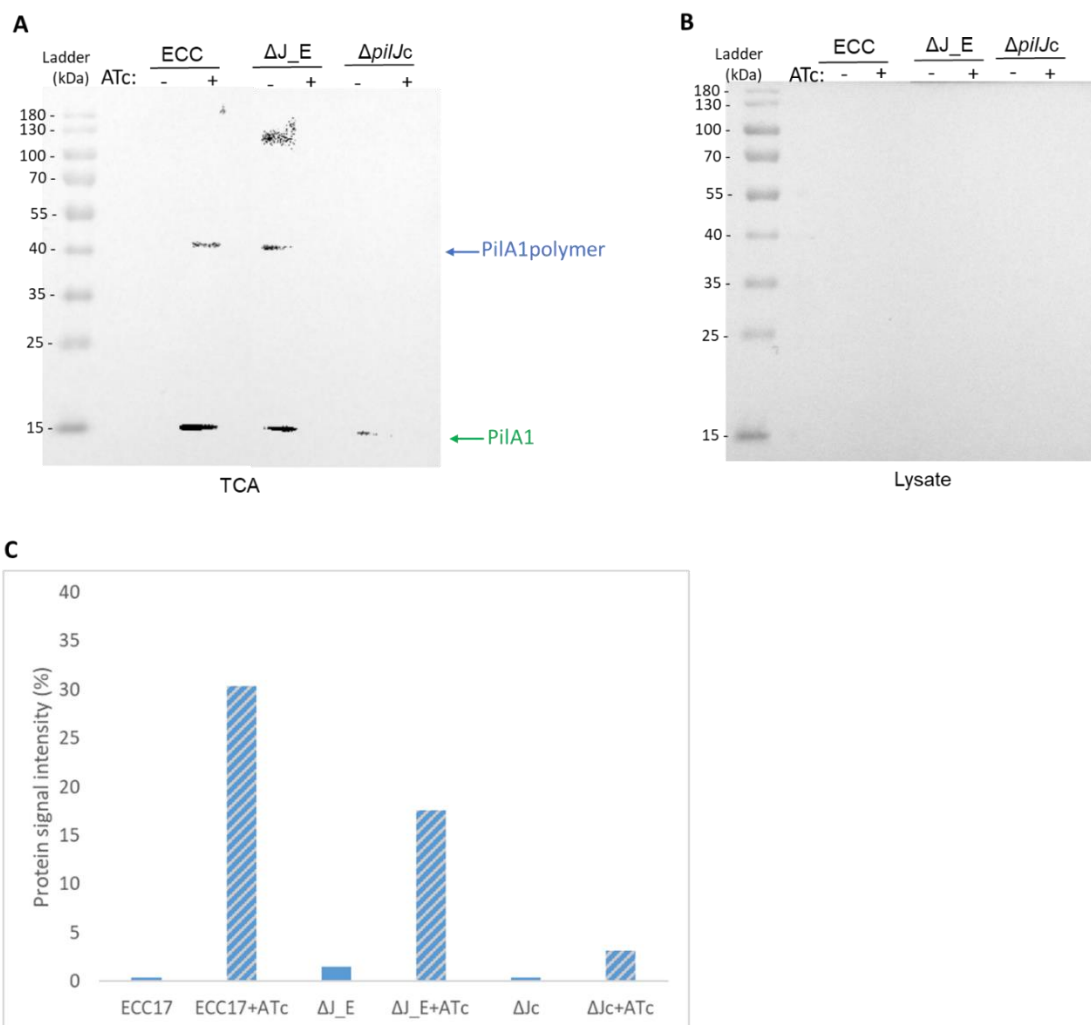


Figure 4-20. Immunoblot detection of PilA1 in 630 $\Delta pilJ$ and complement strains on 1.8% agar

PilA1 signals from *C. difficile* 630_pECC17 (ECC), 630 $\Delta pilJ$ _pECC17 (ΔJ_E) and 630 $\Delta pilJ$ _pZGW008 ($\Delta pilJc$), either with (+) or without (-) ATc supplementation. (A) Surface proteins were extracted by TCA precipitation, signal bands were quantified and plotted in (C). (B) The cytosolic proteins analysed from the cell lysates. Cathode/Anode buffers were applied in western blot, transfer was performed at 15V for 23 minutes onto nitrocellulose membranes. Predicted molecular weight of pre-pilin PilA1 is 18.2 kDa (not detected), mature pilin PilA1 (green arrow) is 17.2 kDa. PilA1 polymer (blue arrow) is detected in the supernatant (TCA). ATc supplementation is represented by slash in graph, quantification data can be found in Appendix E-12.

Similar to what was observed for $\Delta pilD1$, in $\Delta pilJ$ and complement strains, there is a less pronounced reduction of FliC in the supernatant when compared to wild type (Figure 4-21, panel A). Interestingly, FliC signals are detected, even though at low levels, in the cell lysates even after increasing c-di-GMP. However, it is hard to say if this is related to an effect of *pilJ* in FliC regulation. One possibility is that PilJ is somehow linked to export of FliC to the cell surface. However, considering the very subtle differences observed, it is possible that any variation is due to experimental conditions and variations. Further analysis, namely looking at PilJ levels both in these strains and in a $\Delta fliC$ mutant, could provide some new insights.

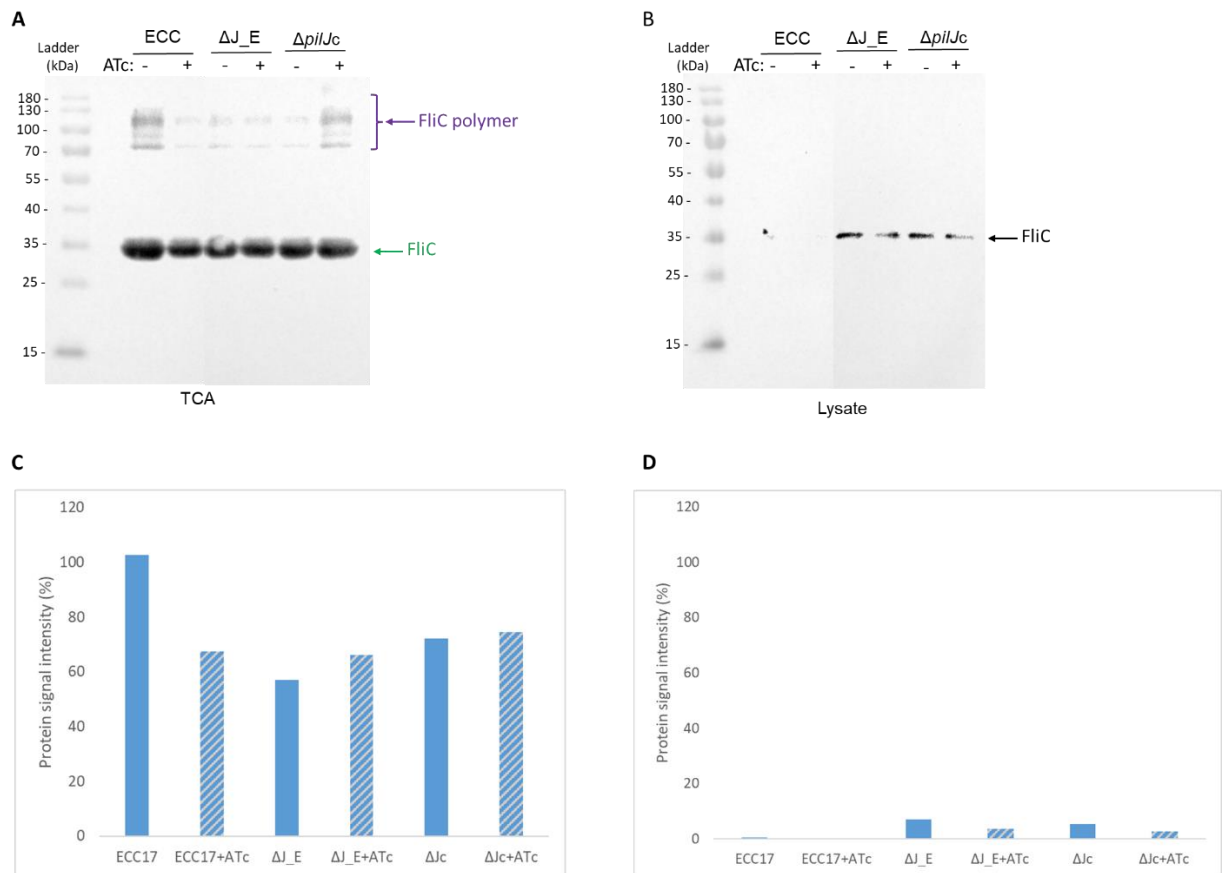


Figure 4-21. Immunoblot detection of FliC in 630 $\Delta pilJ$ and complement strains on 1.8% agar

FliC signals from *C. difficile* 630_pECC17 (ECC), 630 $\Delta pilJ$ _pECC17 (ΔJ_E) and 630 $\Delta pilJ$ _pZGW008 (630 $\Delta pilJc$), either with (+) or without (-) ATc supplementation. (A) Surface proteins were extracted by TCA precipitation, signal bands were quantified and plotted in (C). (B) Cytosolic proteins analysed from the cell lysates, signal bands were quantified and plotted in (D). Cathode/Anode buffers were applied in western blot, transfer was performed at 15V for 23 minutes onto nitrocellulose membranes. Predicted molecular weight of FliC (green arrow) is 30.8 kDa. Purple arrow indicates FliC polymers. PilA1 polymer (blue arrow) is detected in the supernatant (TCA). ATc supplementation is represented by slash in graph, quantification data can be found in Appendix E-13.

4.5.3. Effects of PilJ on Swimming Motility

We then investigated the flagella-mediated swimming motility in the $\Delta pilJ$ strains and found a reduced colony diameter upon deletion of *pilJ* when compared to wild type CD630 (Figure 4-22). In the presence of an inducible *dccA* gene (all ECC17 derived strains), there was a significant reduction of colony diameter, as expected from earlier observations that higher c-di-GMP leads to reduced swimming motility (section 4.2.4). Importantly, there is no significant difference between these strains, while they all differ from their wild type equivalent.

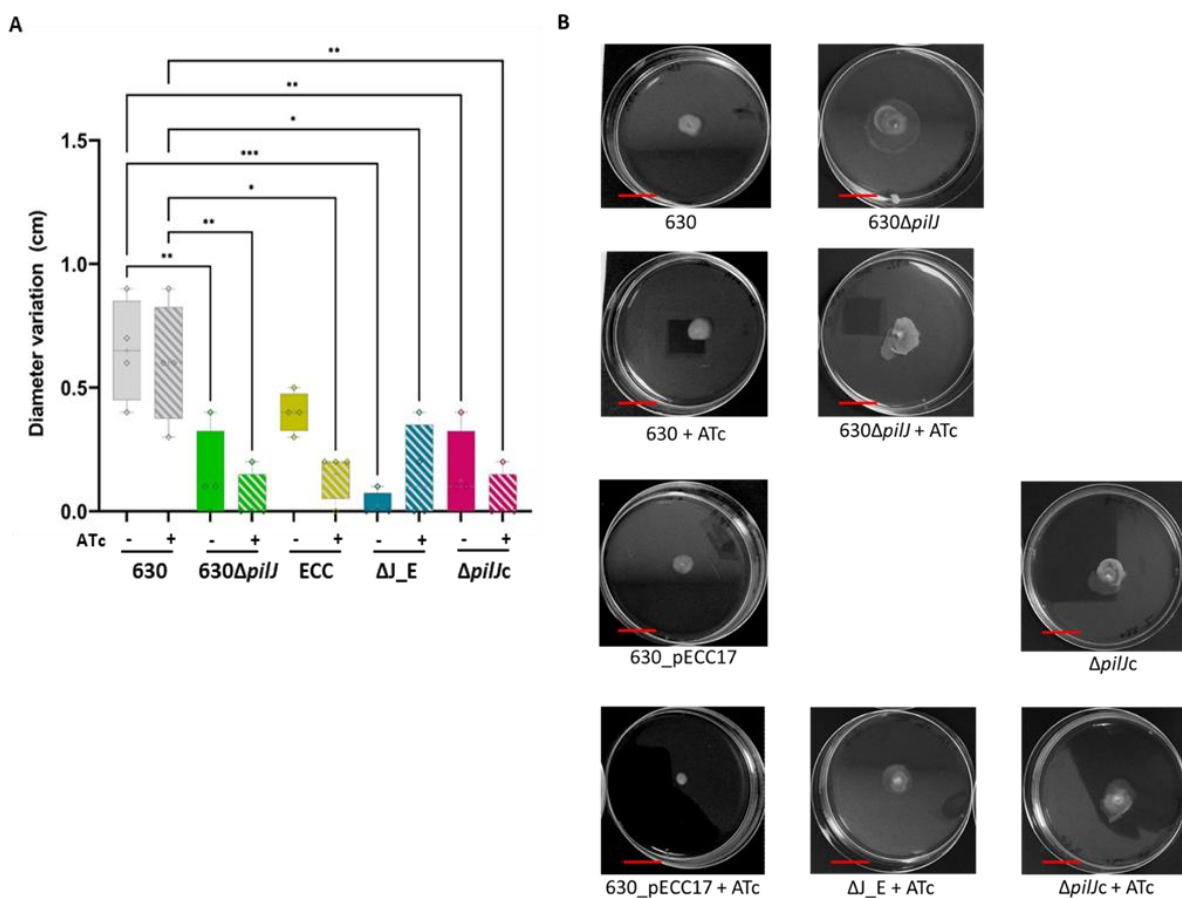


Figure 4-22. Effect of *pilJ* on colony diameter in 0.3 % agar

Colony diameter changes for strains grown in 0.3% agar, with (+) or without (-) ATc supplementation. (A) Changes in colony diameter between day 1 and day 2 post-inoculation for strains CD630 (grey), 630 $\Delta pilJ$ (green), 630_pECC17 (ECC; yellow), 630 $\Delta pilJ$ _pECC17 (ΔJ_E ; green) and 630 $\Delta pilJ$ _pZGW008 ($\Delta pilJc$; pink). Strip shades indicated samples under *dccA* induction (+ ATc). Each replicate is represented as diamonds. Significance analysed with one-way ANOVA by GraphPad Prism. ‘*’ indicates P value < 0.1, ‘**’ indicates P value < 0.01, ‘***’ indicates P value < 0.001. (B) Colony morphology in 0.3 % agar, with and without ATc, after 48h.

As previously discussed, the dissemination of the colonies in the soft agar led to considerable variation (Figure 4-22, B) and it is possible subtle biologically relevant effects are not easily detectable. Motility on 1.8 % and 0.3 % agar involving vector control strains can be found in Appendix Figure B-17 and B-18.

4.5.4. Flagella Expression in $\Delta pilJ$ mutant and complement strains

As in previous sections, anti-FliC immunoblotting could provide a more detailed analysis of how deleting *pilJ* affects the flagella. FliC signals detected in the cell lysates in $\Delta pilJ$ are similar and follow the pattern shown for 630_pECC17 (Figure 4-23, panel B): detectable without *dccA* induction, and not observed after increasing c-di-GMP levels. This confirms that a higher level of c-di-GMP represses the expression of *fliC* and this is not affected by the presence or absence of PilJ.

However, the complement strain 630 $\Delta pilJ$ _pZGW008 ($\Delta pilJc$) shows a lower level of FliC signal even without *dccA* induction, compared to the other two strains (Figure 4-23, panel A) and no FliC signal is detectable under *dccA* induction. This indicates that there might be differences related to the media used, as this is not what had been observed in samples recovered from cultures grown in 1.8 % agar (section 4.5.2 above).

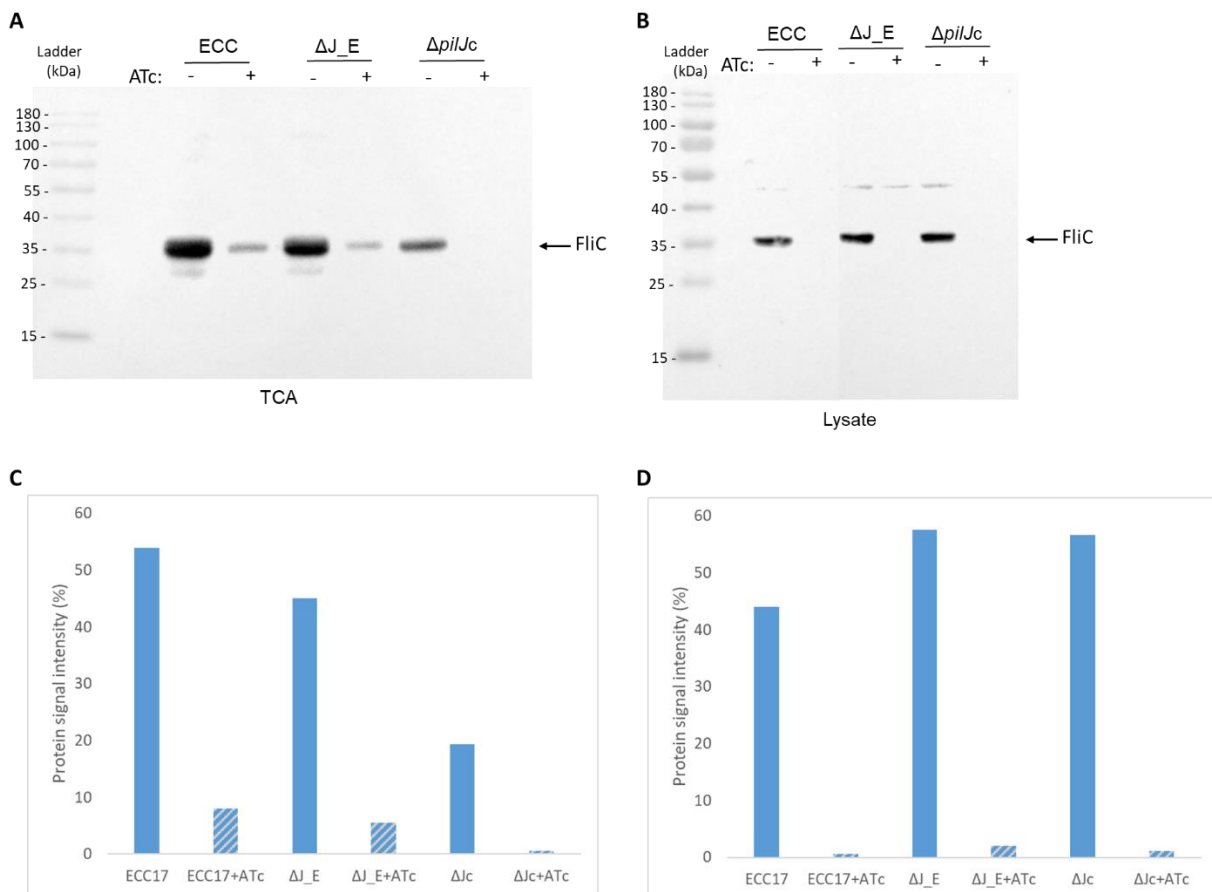


Figure 4-23. Immunoblot detection of FliC in *C. difficile* 630 Δ *pilJ* and complement strains

FliC signals from *C. difficile* 630_pECC17 (ECC), 630 Δ *pilJ*_pECC17 (Δ J_E) and 630 Δ *pilJ*_pZGW008 (Δ *pilJc*), either with (+) or without (-) ATc supplementation. (A) Surface proteins were extracted by TCA precipitation, signal bands were quantified and plotted in (C). (B) The cytosolic proteins analysed from the cell lysates, signal bands were quantified and plotted in (D). Cathode/Anode buffers were applied in western blot, transfer was performed at 15V for 23 minutes onto nitrocellulose membranes. Predicted molecular weight of FliC is 30.8 kDa. ATc supplementation is represented by slash in graph, quantification data can be found in Appendix E-14.

4.6. Discussion

In this chapter, the two different types of motility were studied in *C. difficile* 630 under different levels of c-di-GMP. The effects on motility of the main pilin, PilA1, one of the prepilin peptidases, PilD1 and a minor pilin, PilJ, were also investigated. Different media was used to assess two different types of motility, as previously described (Garrett et al., 2019; Purcell et al., 2016): 1.8% agar plates for twitching and 0.3 % agar for swimming motility. Additionally, the expression of PilA1 and FliC under different conditions was screened by immunoblotting.

Firstly, analysis of colony migration in 1.8 % agar clearly shows that CD630 twitching motility is less pronounced than in *C. difficile* R20291 strain (Purcell et al., 2016). Moreover, high levels of c-di-GMP seem to only result in a moderate motility increase.

As hypothesised, absence of *pilA1* seems to result in reduced twitching but this was only obvious upon careful inspection of the colony morphology as $\Delta pilA1$ produced more diffused colonies that lacked the characteristic branching seen upon twitching. Curiously, complementing the mutation with plasmids containing the promoter region or even the complete riboswitch did not seem to complement this phenotype, even when detectable levels of PilA1 were present (Figure 4-7).

From the previous studies on *cmr* genes discussed in chapter 3, *cmr* genes may not only influence cell shape, but also be relevant in colony morphology and motility. Colony morphology was examined in *cmr* gene mutants, and results show *cmrT* mutant loses rough-edge colony morphology (Garrett et al., 2019). Furthermore, to investigate whether swimming and surface motility were relevant to *cmr* genes, *cmrR* and *cmrT* mutants were investigated in motility tests. In their work, the twitching motility on 1.8% agar were referred as surface motility. The *cmrT* mutant loses surface motility on 1.8% agar, while *cmrR* mutant does not (Garrett et al., 2019). No phenotype was observed in swimming motility in 0.5% agar (Garrett et al., 2019). The results also indicated overexpression of either *cmrR* or *cmrT* leads to increased surface motility, even in *pilB1* mutants (Garrett et al., 2019). Overexpression also reduced swimming motility (Garrett et al., 2019). These results lead to a question whether the surface motility examined in this work is driven by *cmr* genes. This could be a possible explanation to the increased surface motility of *pilA1* and *pilD1* mutants in this study.

In twitching motility assays, we also observed a colony morphology phenotype in *pilA1* mutant, however, this was not observed in other mutants. *pilA1* mutant and complemented strains show larger and translucent colonies compared to wild strain and other mutants. This phenotype is also observed in an investigation on *Lysobacter enzymogenes* TFP. (Xia et al., 2017) while deleting each gene encoding TFP pilins and proteins. Similarly to what was seen in our work only the mutation of major pilin *pilA1* showed larger and translucent colonies compared to other mutant strains (Xia et al., 2017). It would be interesting to look at whether *pilA1* drives the aggregation on agar surface and the extracellular component changes under

deletion of *pilA1*. In the study by Xia *et al.*, twitching motility was also examined by colony microscopy. By looking at the edges and margins of the colonies, it is possible to distinguish rough and smooth colonies and the migration of bacteria on colony edges. This can be an efficient improvement for twitching motility examinations carried out here in future work.

Conversely, deletion of *PilD1* seemed to have a limited effect on twitching motility, with branching detected in all conditions (section 4.4.1.). Interestingly, complementation with a plasmid where *pilD1* is under direct induction by ATc seems to somewhat increase motility, despite no detectable *PilA1* levels. From the result discussed in chapter 4, deleting *pilD1* does not affect *PilA1* expression and export. However, based on results when analysing the sample collected from 1.8 % agar plates, *pilD1* could be essential for *PilA1* expression and/or stability, as levels of *PilA1* were not restored in the complement strain.

Similarly, no clear effect was observed in the absence of *pilJ*, neither on colony size and morphology, nor on detectable *PilA1* levels, suggesting twitching motility is not affected by the absence of the minor pilin. These results confirm previous observations that neither *PilD1* nor *PilJ* are essential for *PilA1* expression, export to the cell surface or assembly into filaments (Chapter 3).

Further investigation is required to fully understand the mechanisms regulating TFP gene expression, pili assembly and motility and how growth conditions affect these mechanisms. One key aspect would be to investigate levels of *PilD1* and *PilJ* in the strains studied, particularly to confirm that gene complementation is functional and that the proteins are indeed expressed, alongside *PilA1*.

Analysis of the effect of the three TFP genes under study in swimming motility was technically challenging, despite considerable optimisation attempts, due to the uneven and vary variable dissemination of the bacterial colonies in the semi-solid 0.3% agar. This also prevented investigation of pilin and flagellin expression in these growth conditions.

Despite these difficulties, combining analysis of colony morphology, diameter changes and *FliC* immunoblotting clearly shows repression of *FliC* expression when levels of c-di-GMP are elevated (Figures 4-3, 4-11, 4-13 and 4-23), as expected.

One of the most interesting observations is the fact that deleting *pilA1* might lead to a deficiency in the export of FliC when grown on 1.8 % agar plates, but not on liquid cultures. Surprisingly, complementation of *pilA1* does not restore the level of FliC export to the cell surface in these conditions. This suggests that there might be some interplay between TFP and flagella, not previously reported in *C. difficile*.

These results suggest that the expression of TFP and FliC, and the role of PilD1 can be affected by incubation time and/or on solid or liquid media. Although we cannot exclude that this is due to stability of ATc in solid plates over longer periods, it would be important to investigate this further. The effects on FliC export observed from plate samples, by deleting *pilA1*, *pilD1* and *pilJ*, raises several new possibilities. Is PilA1 required for FliC exportation? If *pilD1* becomes essential for PilA1 expression on 1.8 % agar, does the accumulation of cytosolic PilA1 increase FliC expression? And what is the role of PilJ in FliC expression and polymerisation? These are unanswered questions that raise interesting new possibilities that will require further investigation.

Chapter 5: Discussion and future work

C. difficile is a multi-drug resistant pathogen and healthcare burden, associated with hospital outbreaks. CDI treatments remain limited and antimicrobial resistance means they can potentially lose their efficiency over time. New therapeutic strategies are required, especially those that do not affect the rest of the microbiota.

TFP has been shown to contribute to adhesion and colonisation (Robert W McKee et al., 2018), motility (Garrett et al., 2019; Purcell et al., 2016) and biofilm formation (Brauer et al., 2021; Maldarelli et al., 2016; Purcell et al., 2016) during pathogenesis, and may be considered as a novel drug target to prevent and treat CDI. This work investigating TFP in *C. difficile* contributes to our further understanding of TFP and is a basis of future developments in this field.

5.1. c-di-GMP effects on pili, flagella and cell division

Interestingly, we also observed long cell morphology phenotypes in $\Delta pilD1$ mutant even in the absence of *dccA* induction to increase c-di-GMP (section 3.3.5.), but not when *pilA1* was deleted (section 3.3.2.). This suggests that the phenotype observed is not due to changes in CmrRST induced by c-di-GMP and that there might be other molecular pathways that involve crosstalk between TFP gene expression and cell division.

Studies suggest that pili, flagella and cell cycle are also regulated by c-di-GMP in other bacteria. In *Caulobacter crescentus*, phase switching between TFP and flagella motility are also reported but they are named 'swarmer' and 'stalked' (Duerig et al., 2009; Römling et al., 2013). *Caulobacter* pili are mainly observed in stalked cells, which are attached to surfaces by pili, whereas more flagella are observed in planktonic swarmer cells (Römling et al., 2013). Depending on the intracellular level of c-di-GMP, *C. crescentus* switches from swarmer cells to stalked cells and undergoes cell division (Duerig et al., 2009; Mignolet et al., 2018). In this bacterium, during cell division, c-di-GMP binds to an effector protein (PopA), which activates degradation of a replication initiation inhibitor (CtrA) and allows cells to enter S-phase and

undergo cell division (Duerig et al., 2009). It is also suggested some pili accessory proteins are responsible for flagella exportation in *C. crescentus* (Mignolet et al., 2018).

In our work, we suggest c-di-GMP represses flagella biosynthesis and swimming motility, but also observed a deficiency in flagella exportation from the $\Delta pilA1$ mutants when grown on 1.8 % agar. Would it be possible that some genes in the TFP gene cluster of *C. difficile* are also involved in flagella exporting pathways? There could be complex signal pathways and crosstalk between TFP and flagella in *C. difficile* beyond c-di-GMP. To our knowledge, this has not yet been reported and would be an interesting new research avenue.

To investigate the potential crosstalk between TFP and flagella and the differences depending on media type, our workflow using motility assays and immunoblotting, should be expanded to study mutants in other TFP genes as well as FliC and other genes in the flagella operon. Fluorescently labelling of PilA1, PilJ and/or FliC to detect localisation on the pilus and flagellum, respectively, would also provide important insight. This labelling strategy can also be expanded to other TFP and flagella genes to identify exporting sites of the target proteins.

Finally, electron microscopy and/or tomography could be used to directly observe pili filaments and flagella in the cells. Studying different mutant strains with these techniques would provide unique insights on assembly and organisation of the two motility filaments.

Additionally, a recent study shows that long cell chains, repressed flagella gene transcriptions, reduced motility, but increased adhesion and biofilm formation are detected under metronidazole antibiotic treatments to *C. difficile* (Doan et al., 2022). These biological changes are similar to the effect observed with higher levels of c-di-GMP. It has been demonstrated that some antibiotics can trigger c-di-GMP signalling pathways by the activation of an inner membrane phosphodiesterase (Hoffman et al., 2005). Therefore, it would be important to explore the mechanism that triggers c-di-GMP signalling pathways upon metronidazole treatment and if these relate to TFP and/or flagella as also observed here.

5.2. Genetic diversity of TFP genes in *C. difficile*

In our work, an increased level of c-di-GMP is shown to induce PilA1 expression. However, this did not lead to significant increase in twitching motility on agar surface, which was found to be limited in all conditions and strains tested. Previous studies suggested the c-di-GMP elevated twitching motility in R20291, while deleting *pilB1* results in loss of twitching motility (Purcell et al., 2016). However, it should be noted that strains CD630 used here and R20291 tested in previous work have significantly different characteristics and virulence, with R20291 being often classified as hypervirulent (Griffiths et al., 2010). Twitching motility could be one of the virulence traits that is significantly different in our lab strain CD630. Moreover, this could be related to sequence variation of *pilA1* across *C. difficile* strains, since PilA1 contains a hypervariable $\alpha\beta$ -loop, as discussed in Chapter 1.

To investigate if the different levels of twitching ability of CD630 and R20291 could relate to differences in sequence, we briefly analysed gene similarity of TFP in these strains. For completeness, we extended this analysis to include the TFP primary gene cluster from 47 isolates, using CD630 as the reference strain (Sebaihia et al., 2006).

From our analysis, *pilA1* shows the highest level of variation in the locus across isolates (Figure 5-1). Furthermore, there is considerable differentiation between CD630 *pilA1* and R20291 *pilA1* in the phylogenetic tree (Figure 5-2). As discussed in Chapter 1, R20291 is hypervirulent, while CD630 is a reference strain and they belong to different clades, 2 and 1, respectively.

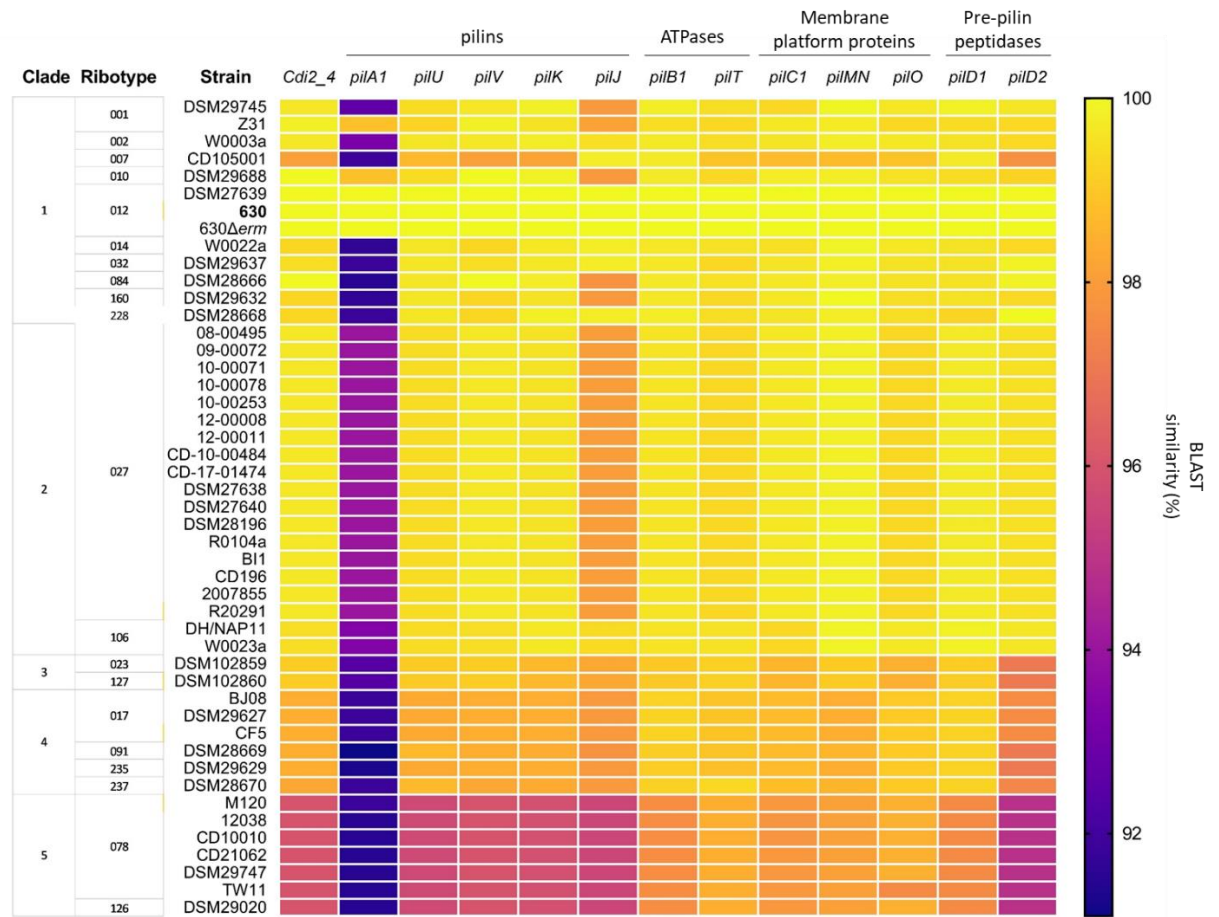


Figure 5-1. Sequence similarity of riboswitch Cdi2_4 and primary TFP cluster genes from 47 *C. difficile* isolates
 Sequence similarity is represented as a heat map, using CD630 as a reference. The gene names are labelled on the top of the heat map, isolates are listed on the left (strains) with the related MLST (Clade) and RT (Ribotype). Genes from CD630 (RT012, Clade 1) were used as template genes when analysed in BLAST. The BLAST data can be found in appendix table C-1.

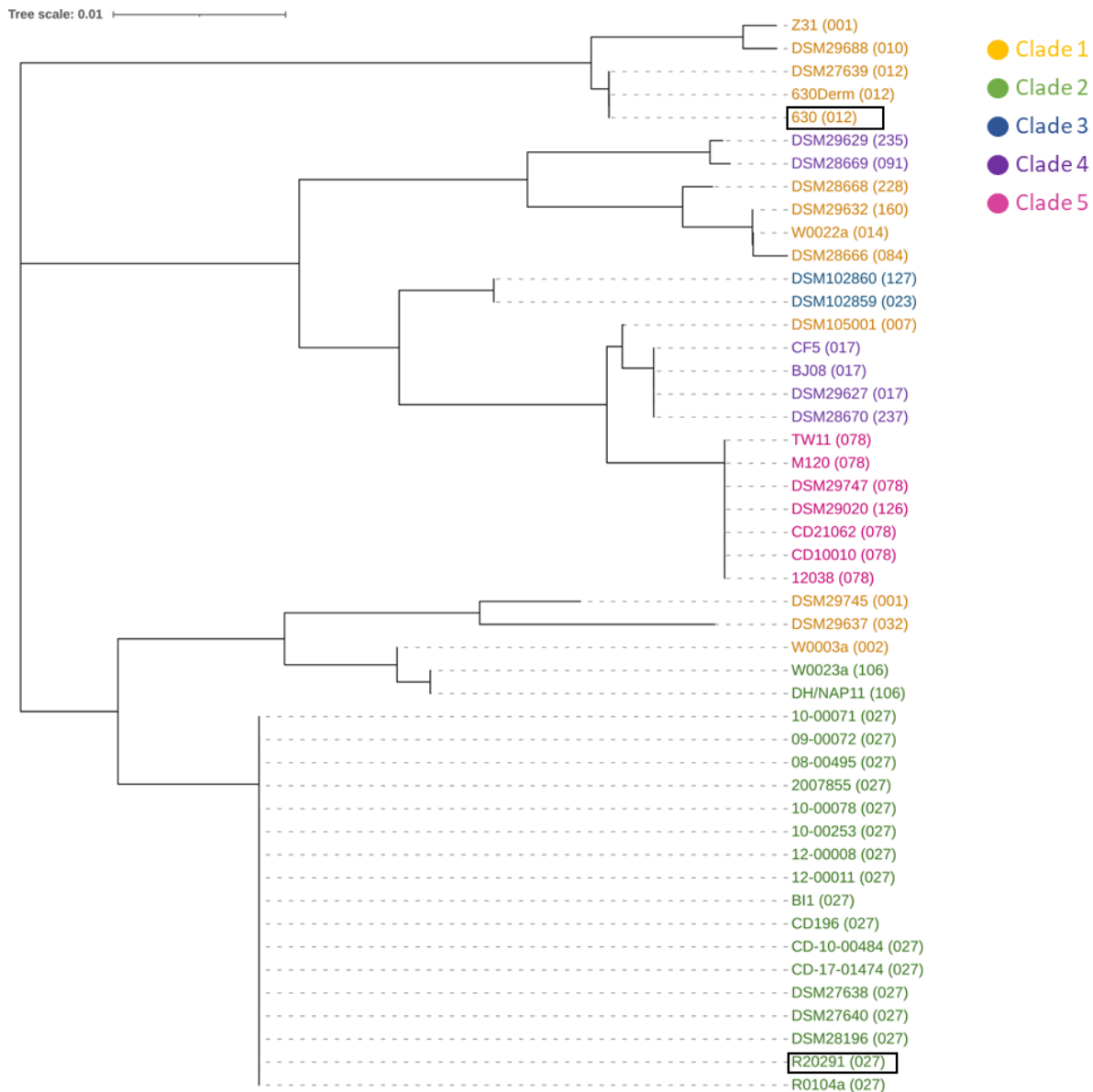


Figure 5-2. Phylogenetic tree of *C. difficile* *pilA1* genes

Neighbour-joining (N-J) tree of *pilA1* genes of 47 *C. difficile* isolates. The ribotype of strains are labelled in brackets. MLST is represented by colour codes: Clade 1 in yellow, Clade 2 in green, Clade 3 in blue, Clade 4 in purple and Clade 5 in pink. *C. difficile* isolate DH/NAP11/106/ST42 is represented by DH/NAP11. Isolate 630 Δ *erm* is represented by 630Derm. CD630 and R20291 are highlighted in boxes.

The genetic diversity of *pilA1* may explain the different phenotypes of twitching motility between CD630 and R20291. Additionally, a lower level of twitching motility is also observed in CD630 Δ *erm* compared to R20291 (Purcell et al., 2016). This is not surprising as CD630 Δ *erm* is derived from CD630 and they share 100% *pilA1* genetic similarity in our analysis. As TFP is one of virulent factors and has variable activation during infection, the different ability for

twitching motility *in vitro* observed between the hypervirulent R20291 and less virulent CD630 and CD630 Δ *erm* may also be relevant for pathogenicity of each strain.

Another interesting observation from the sequence analysis is that *pilA1* is highly conserved in the analysed isolates from Clade 5 (Figure 5-2, pink). All isolates correspond to RT078, a clinically relevant strain, also associated with animal infections that lacks a flagella operon and was therefore found to be non-motile in soft agar (Schwanbeck et al., 2021). We can speculate that TFP-mediated twitching motility could compensate for the lack of flagella-mediated swimming motility and it would be interesting to investigate twitching motility in this ribotype. A recent study suggests that the genes encoding FliC and two other flagella motility regulators, FliW and CsrA, are all conserved in other Clade 5 strains, while FliW plays a key role in virulence (Zhu and Britton, 2022). Comparing the TFP gene sequences in those strains in Clade 5 could also provide new insights on the variation of the two motility types across strains.

In order to further our understanding of TFP genes and their role in twitching motility, motility assays and immunoblotting of strains lacking the other TFP genes should be carried out.

5.3. Factors affecting colony and cell morphology

We observed that Δ *pilA1* shows a dimmer, thinner and larger colony than the wild type, but without branched and rough colony morphologies. This would indicate, that as predicted, Δ *pilA1* mutant loses twitching motility, and no branching was observed.

The study investigating CmrRST also reveals *C. difficile* cell morphology has impact on colony morphology (Garrett et al., 2019). Long cell chains were found in rough colonies, at the edge of colonies, whereas cells with normal cell morphology are found in smooth colonies (Garrett et al., 2019). This is also observed in *Listeria monocytogenes*, where long chain cells results in rough colonies (Kuhn and Goebel, 1989). In this work, long chain cell morphology was observed in CD630 under high level of c-di-GMP and Δ *pilD1* mutants, but not in Δ *pilA1*. This could explain the branchy and rough colonies observed in the former strains (section 4.2.1 and 4.4.1), while smooth colonies were observed in the later (section 4.3.1).

Similar observations have been seen in other bacteria, such as *Salmonella typhimurium* and *Vibrio* species where studies show that under a higher level of c-di-GMP, the signal triggers biofilm formation and secretion of adhesive extracellular matrix components, such as cellulose and curli fimbriae (Römling, 2005). The resulting bacterial cells have a firmer attachment to the surface than planktonic cells, which can lead to opaque and rugose colony morphologies, used to distinguish biofilm formation in *Vibrio* species (Beyhan et al., 2008; Römling, 2005; Yildiz and Visick, 2009).

Although there is no report observing whether biofilm affects colony morphologies in *C. difficile*, studies on *C. difficile* biofilm formation may provide a hint on the different colony morphology we observed in this work to previous twitching motility study in R20291 by Purcell and colleagues (2016). As discussed in section 1.3.3., c-di-GMP triggers biofilm formation, however, there are different phenotypes between CD630 and R20291 (Đapa et al., 2013). CD630 is suggested to show a better binding to extracellular matrix and biofilm formation than R20291 (Santos et al., 2022; Valiente et al., 2016), which may be a potential factor to observe a lower surface motility in CD630 than R20291. As $\Delta pilA1$ mutant shows deficiencies in biofilm formation, this could result in reduced attachment to the agar surface and therefore growth into larger, thinner but smoother colonies than the wild type on 1.8 % agar.

To further understand colony morphology and the effect of TFP, confocal microscopy can be used to study biofilm formation in more detail (Ronish et al., 2022).

5.4. The role of pre-pilin peptidases

Previous studies have shown that one of the pre-pilin peptidase, PilD2, is required for PilA1 biosynthesis when *C. difficile* is growing in liquid culture (Couchman, 2016). In this work, the other pre-pilin peptidase, PilD1, does not appear to be required for PilA1 biosynthesis in liquid culture. Interestingly, PilD1 becomes essential when growing on 1.8 % agar even though branchy colonies were observed in $\Delta pilD1$ mutant, which lacks PilA1 signal in western blot. Moreover, long-chain shapes in cell morphology were observed in PilD1 mutagenesis study, suggesting absence of the protein affects cell division (section 3.3.5.).

To complete the work presented here, it would be important to verify complementation of *pilD1* and *pilJ* by anti-PilD1 and anti-PilJ immunoblotting. The levels of these proteins, as well as the other TFP proteins in the strains described here, would provide important information on how c-di-GMP affects each TFP gene and might help explain the unexpected results observed.

The exact role and activation of the two pre-pilin peptidases remains unclear. In other species, PilD may contain a methyltransferase domain and act as a bi-functional peptidase and methylase enzyme, which may be involved in more molecular activities (Pepe and Lory, 1998; Strom et al., 1993). However, from protein domain prediction, neither PilD1 nor PilD2 contain additional enzymatic domain. One possibility is that PilD1 might work co-operatively with PilD2, depending on growth conditions. Another possibility is that the branched colonies may be due to twitching motility driven by PilA2 in the secondary TFP gene cluster to compensate for immaturity of PilA1 in the absence of PilD1.

To investigate the roles of PilD1 and PilD2, enzymatic assays can be carried out to confirm whether either of them cleaves prepilin into mature PilA1 and/or PilA2. Further, genes in the secondary TFP gene cluster can be investigated with the assays and analysis done in this work.

The key contributions of this work to our understanding of TFP and its role in *C. difficile* are the possibility of a novel crosstalk between TFP and flagella and a potential role of at least some TFP genes in cell division. These observations open a wider view of c-di-GMP signalling pathways and the switch between TFP and flagella phases in *C. difficile*, opening novel directions for future studies in *C. difficile* TFP, flagella, c-di-GMP riboswitches and signalling pathways.

References

- Alfa, M.J., Kabani, A., Lyerly, D., Moncrief, S., Neville, L.M., Al-Barrak, A., Harding, G.K.H., Dyck, B., Olekson, K., Embil, J.M., 2000. Characterization of a toxin A-negative, toxin B-positive strain of *Clostridium difficile* responsible for a nosocomial outbreak of Clostridium difficile-associated diarrhea. J. Clin. Microbiol. 38, 2706–2714. <https://doi.org/10.1128/JCM.38.7.2706-2714.2000>
- Anderson, D.M., Sheedlo, M.J., Jensen, J.L., Lacy, D.B., 2020. Structural insights into the transition of *Clostridioides difficile* binary toxin from prepore to pore. Nat. Microbiol. 5, 102–107. <https://doi.org/10.1038/S41564-019-0601-8>
- Anderson, T.F., 1949. In the Nature of the Bacterial Surface. Oxford Univ. Press.
- Anjuwon-Foster, B.R., Tamayo, R., 2017. A genetic switch controls the production of flagella and toxins in *Clostridium difficile*. PLOS Genet. 13, e1006701. <https://doi.org/10.1371/journal.pgen.1006701>
- Ayers, M., Sampaleanu, L.M., Tammam, S., Koo, J., Harvey, H., Howell, P.L., Burrows, L.L., 2009. PilM/N/O/P proteins form an inner membrane complex that affects the stability of the *Pseudomonas aeruginosa* type IV pilus secretin. J. Mol. Biol. 394, 128–142. <https://doi.org/10.1016/J.JMB.2009.09.034>
- Baban, S.T., Kuehne, S.A., Barketi-Klai, A., Cartman, S.T., Kelly, M.L., Hardie, K.R., Kansau, I., Collignon, A., Minton, N.P., 2013. The role of flagella in *Clostridium difficile* pathogenesis: comparison between a non-epidemic and an epidemic strain. PLoS One 8, e73026. <https://doi.org/10.1371/journal.pone.0073026>
- Bacci, S., Mølbak, K., Kjeldsen, M.K., Olsen, K.E.P., 2011. Binary toxin and death after *Clostridium difficile* infection. Emerg. Infect. Dis. 17, 976–982. <https://doi.org/10.3201/EID1706.101483>
- Barbut, F., Decré, D., Lalande, V., Burghoffer, B., Noussair, L., Gigandon, A., Espinasse, F., Raskine, L., Robert, J., Mangeol, A., Branger, C., Petit, J.C., 2005. Clinical features of *Clostridium difficile*-associated diarrhoea due to binary toxin (actin-specific ADP-ribosyltransferase)-producing strains. J. Med. Microbiol. 54, 181–185. <https://doi.org/10.1099/JMM.0.45804-0>
- Barra-Carrasco, J., Paredes-Sabja, D., 2014. *Clostridium difficile* spores: a major threat to the hospital environment. Future Microbiol. 9, 475–486. <https://doi.org/10.2217/FMB.14.2>
- Bauer, M.P., Notermans, D.W., Van Benthem, B.H., Brazier, J.S., Wilcox, M.H., Rupnik, M., Monnet, D.L., Van Dissel, J.T., Kuijper, E.J., 2011. *Clostridium difficile* infection in Europe: a hospital-based survey. Lancet (London, England) 377, 63–73. [https://doi.org/10.1016/S0140-6736\(10\)61266-4](https://doi.org/10.1016/S0140-6736(10)61266-4)
- Belete, B., Lu, H., Wozniak, D.J., 2008. *Pseudomonas aeruginosa* AlgR regulates type IV pilus biosynthesis by activating transcription of the fimU-pilVWXY1Y2E operon. J. Bacteriol. 190, 2023–2030. <https://doi.org/10.1128/JB.01623-07/ASSET/48671339-00D6-488C-8847-B99F142DD887/ASSETS/GRAPHIC/ZJB0060876410004.JPEG>
- Berry, J.L., Cehovin, A., McDowell, M.A., Lea, S.M., Pelicic, V., 2013. Functional Analysis of the Interdependence between DNA Uptake Sequence and Its Cognate ComP Receptor during Natural Transformation in *Neisseria* Species. PLOS Genet. 9, e1004014. <https://doi.org/10.1371/JOURNAL.PGEN.1004014>
- Berry, J.L., Pelicic, V., 2015. Exceptionally widespread nanomachines composed of type IV pilins: the prokaryotic Swiss Army knives. FEMS Microbiol. Rev. 39, 134–154.

- <https://doi.org/10.1093/FEMSRE/FUU001>
- Beyhan, S., Odell, L.S., Yildiz, F.H., 2008. Identification and Characterization of Cyclic Diguanylate Signaling Systems Controlling Rugosity in *Vibrio cholerae*. *J. Bacteriol.* 190, 7392. <https://doi.org/10.1128/JB.00564-08>
- Bidet, P., Barbut, F., Lalande, V., Burghoffer, B., Petit, J.-C., 1999. Development of a new PCR-ribotyping method for *Clostridium difficile* based on ribosomal RNA gene sequencing. *FEMS Microbiol. Lett.* 175, 261–266. <https://doi.org/10.1111/J.1574-6968.1999.TB13629.X>
- Bilverstone, T.W., Minton, N.P., Kuehne, S.A., 2019. Phosphorylation and functionality of CdtR in *Clostridium difficile*. *Anaerobe* 58, 103–109. <https://doi.org/10.1016/J.ANAEROBE.2019.102074>
- Bordeleau, E., Fortier, L.C., Malouin, F., Burrus, V., 2011. c-di-GMP turn-over in *Clostridium difficile* is controlled by a plethora of diguanylate cyclases and phosphodiesterases. *PLoS Genet.* 7. <https://doi.org/10.1371/JOURNAL.PGEN.1002039>
- Bordeleau, E., Purcell, E.B., Lafontaine, D.A., Fortier, L.C., Tamayo, R., Burrus, V., 2015. Cyclic di-GMP riboswitch-regulated type IV pili contribute to aggregation of *Clostridium difficile*. *J. Bacteriol.* 197, 819–832. <https://doi.org/10.1128/JB.02340-14>
- Brauer, M., Lassek, C., Hinze, C., Hoyer, J., Becher, D., Jahn, D., Sievers, S., Riedel, K., 2021. What's a Biofilm?—How the Choice of the Biofilm Model Impacts the Protein Inventory of *Clostridioides difficile*. *Front. Microbiol.* 12. <https://doi.org/10.3389/FMICB.2021.682111>
- Braun, V., Hundsberger, T., Leukel, P., Sauerborn, M., Von Eichel-Streiber, C., 1996. Definition of the single integration site of the pathogenicity locus in *Clostridium difficile*. *Gene* 181, 29–38. [https://doi.org/10.1016/S0378-1119\(96\)00398-8](https://doi.org/10.1016/S0378-1119(96)00398-8)
- Brinton, C.C., 1959. Non-flagellar appendages of bacteria. *Nature* 183, 782–786. <https://doi.org/10.1038/183782A0>
- Brown, D.R., Helaine, S., Carbonnelle, E., Pelicic, V., 2010. Systematic functional analysis reveals that a set of seven genes is involved in fine-tuning of the multiple functions mediated by type IV pili in *Neisseria meningitidis*. *Infect. Immun.* 78, 3053–3063. <https://doi.org/10.1128/IAI.00099-10>
- Buffie, C.G., Bucci, V., Stein, R.R., McKenney, P.T., Ling, L., Gobourne, A., No, D., Liu, H., Kinnebrew, M., Viale, A., Littmann, E., Van Den Brink, M.R.M., Jenq, R.R., Taur, Y., Sander, C., Cross, J.R., Toussaint, N.C., Xavier, J.B., Pamer, E.G., 2015. Precision microbiome restoration of bile acid-mediated resistance to *Clostridium difficile*. *Nature* 517, 205. <https://doi.org/10.1038/NATURE13828>
- Burrows, L.L., 2012a. Prime time for minor subunits of the type II secretion and type IV pilus systems. *Mol. Microbiol.* 86, 765–769. <https://doi.org/10.1111/MMI.12034>
- Burrows, L.L., 2012b. *Pseudomonas aeruginosa* twitching motility: type IV pili in action. *Annu. Rev. Microbiol.* 66, 493–520. <https://doi.org/10.1146/ANNUREV-MICRO-092611-150055>
- Carbonnelle, E., Hélaïne, S., Prouvensier, L., Nassif, X., Pelicic, V., 2005. Type IV pilus biogenesis in *Neisseria meningitidis*: PilW is involved in a step occurring after pilus assembly, essential for fibre stability and function. *Mol. Microbiol.* 55, 54–64. <https://doi.org/10.1111/J.1365-2958.2004.04364.X>
- Cehovin, A., Simpson, P.J., McDowell, M.A., Brown, D.R., Noschese, R., Pallett, M., Brady, J., Baldwin, G.S., Lea, S.M., Matthews, S.J., Pelicic, V., 2013. Specific DNA recognition mediated by a type IV pilin. *Proc. Natl. Acad. Sci. U. S. A.* 110, 3065–3070.

<https://doi.org/10.1073/PNAS.1218832110>

- Chilcott, G.S., Hughes, K.T., 2000. Coupling of flagellar gene expression to flagellar assembly in *Salmonella enterica* serovar typhimurium and *Escherichia coli*. *Microbiol. Mol. Biol. Rev.* 64, 694–708. <https://doi.org/10.1128/MMBR.64.4.694-708.2000>
- Chiumento, S., Roblin, C., Kieffer-Jaquinod, S., Tachon, S., Leprêtre, C., Basset, C., Adityarini, D., Olleik, H., Nicoletti, C., Bornet, O., Iranzo, O., Maresca, M., Hardré, R., Fons, M., Giardina, T., Devillard, E., Guerlesquin, F., Couté, Y., Atta, M., Perrier, J., Lafond, M., Duarte, V., 2019. Ruminococcin C, a promising antibiotic produced by a human gut symbiont. *Sci. Adv.* 5, 9969–9994. <https://doi.org/10.1126/SCIADV.AAW9969>
- Chou, S.H., Galperin, M.Y., 2016. Diversity of Cyclic Di-GMP-Binding Proteins and Mechanisms. *J. Bacteriol.* 198, 32–46. <https://doi.org/10.1128/JB.00333-15>
- Colland, F., Rain, J.C., Gounon, P., Labigne, A., Legrain, P., De Reuse, H., 2001. Identification of the *Helicobacter pylori* anti-sigma28 factor. *Mol. Microbiol.* 41, 477–487. <https://doi.org/10.1046/J.1365-2958.2001.02537.X>
- Collins, D.A., Hawkey, P.M., Riley, T. V., 2013. Epidemiology of *Clostridium difficile* infection in Asia. *Antimicrob. Resist. Infect. Control* 2. <https://doi.org/10.1186/2047-2994-2-21>
- Couchman, E., 2016. Investigating the Type IV pili of *Clostridium difficile* and *Clostridium sordellii*. PhD Thesis.
- Craig, L., Pique, M.E., Tainer, J.A., 2004. Type IV pilus structure and bacterial pathogenicity. *Nat. Rev. Microbiol.* 2, 363–378. <https://doi.org/10.1038/NRMICRO885>
- Crawshaw, A.D., 2016. Structural studies of pathogenicity-related proteins in *Clostridium difficile*. PhD Thesis.
- Crawshaw, A.D., Baslé, A., Salgado, P.S., 2020. A practical overview of molecular replacement: *Clostridioides difficile* PilA1, a difficult case study. *Acta Crystallogr. Sect. D Struct. Biol.* 76, 261–271. <https://doi.org/10.1107/S2059798320000467>
- Crowther, L.J., Anantha, R.P., Donnenberg, M.S., 2004. The inner membrane subassembly of the enteropathogenic *Escherichia coli* bundle-forming pilus machine. *Mol. Microbiol.* 52, 67–79. <https://doi.org/10.1111/J.1365-2958.2003.03963.X>
- Đapa, T., Dapa, T., Leuzzi, R., Ng, Y.K., Baban, S.T., Adamo, R., Kuehne, S.A., Scarselli, M., Minton, N.P., Serruto, D., Unnikrishnan, M., 2013. Multiple factors modulate biofilm formation by the anaerobic pathogen *Clostridium difficile*. *J. Bacteriol.* 195, 545–55. <https://doi.org/10.1128/JB.01980-12>
- Das, G., Varshney, U., 2006. Peptidyl-tRNA hydrolase and its critical role in protein biosynthesis. *Microbiology* 152, 2191–2195. <https://doi.org/10.1099/MIC.0.29024-0>
- Dawson, L.F., Valiente, E., Faulds-Pain, A., Donahue, E.H., Wren, B.W., 2012. Characterisation of *Clostridium difficile* biofilm formation, a role for Spo0A. *PLoS One* 7, e50527. <https://doi.org/10.1371/journal.pone.0050527>
- Dingle, K.E., Elliott, B., Robinson, E., Griffiths, D., Eyre, D.W., Stoesser, N., Vaughan, A., Golubchik, T., Fawley, W.N., Wilcox, M.H., Peto, T.E., Walker, A.S., Riley, T. V., Crook, D.W., Didelot, X., 2014. Evolutionary history of the *Clostridium difficile* pathogenicity locus. *Genome Biol. Evol.* 6, 36–52. <https://doi.org/10.1093/GBE/EVT204>
- Dingle, T.C., Mulvey, G.L., Armstrong, G.D., 2011. Mutagenic analysis of the *Clostridium difficile* flagellar proteins, FliC and FliD, and their contribution to virulence in hamsters. *Infect. Immun.* 79, 4061–7. <https://doi.org/10.1128/IAI.05305-11>
- Doan, T.H.D., Bernet-Camard, M.F., Hoÿs, S., Janoir, C., Péchiné, S., 2022. Impact of Subinhibitory Concentrations of Metronidazole on Morphology, Motility, Biofilm Formation and Colonization of *Clostridioides difficile*. *Antibiotics* 11.

- <https://doi.org/10.3390/ANTIBIOTICS11050624/S1>
- Drake, S.L., Sandstedt, S.A., Koomey, M., 1997. PilP, a pilus biogenesis lipoprotein in *Neisseria gonorrhoeae*, affects expression of PilQ as a high-molecular-mass multimer. *Mol. Microbiol.* 23, 657–668. <https://doi.org/10.1046/J.1365-2958.1997.2511618.X>
- Duerig, A., Abel, S., Folcher, M., Nicollier, M., Schwede, T., Amiot, N., Giese, B., Jenal, U., 2009. Second messenger-mediated spatiotemporal control of protein degradation regulates bacterial cell cycle progression. *Genes Dev.* 23, 93. <https://doi.org/10.1101/GAD.502409>
- Dyer, C., Hutt, L.P., Burky, R., Joshi, L.T., 2019. Biocide Resistance and Transmission of *Clostridium difficile* Spores Spiked onto Clinical Surfaces from an American Health Care Facility. *Appl. Environ. Microbiol.* 85. <https://doi.org/10.1128/AEM.01090-19>
- Eyre, D.W., Fawley, W.N., Best, E.L., Griffiths, D., Stoesser, N.E., Crook, D.W., Peto, T.E.A., Walker, A.S., Wilcox, M.H., 2013. Comparison of multilocus variable-number tandem-repeat analysis and whole-genome sequencing for investigation of *Clostridium difficile* transmission. *J. Clin. Microbiol.* 51, 4141–4149. <https://doi.org/10.1128/JCM.01095-13>
- Fives-Taylor, P.M., Thompson, D.W., 1985. Surface properties of *Streptococcus sanguis* FW213 mutants nonadherent to saliva-coated hydroxyapatite. *Infect. Immun.* 47, 752–759. <https://doi.org/10.1128/IAI.47.3.752-759.1985>
- Francetic, O., Buddelmeijer, N., Lewenza, S., Kumamoto, C.A., Pugsley, A.P., 2007. Signal recognition particle-dependent inner membrane targeting of the PulG Pseudopilin component of a type II secretion system. *J. Bacteriol.* 189, 1783–1793. <https://doi.org/10.1128/JB.01230-06>
- Frostid, L.R., Chengid, J.K.J., Unnikrishnanid, M., 2021. *Clostridioides difficile* biofilms: A mechanism of persistence in the gut? *PLOS Pathog.* 17, e1009348. <https://doi.org/10.1371/JOURNAL.PPAT.1009348>
- Gao, X., X, D., S, S., PM, M., CA, C., DB, K., CE, D., 2014. Engineering of *Bacillus subtilis* strains to allow rapid characterization of heterologous diguanylate cyclases and phosphodiesterases. *Appl. Environ. Microbiol.* 80, 6167–6174. <https://doi.org/10.1128/AEM.01638-14>
- Garrett, E.M., Sekulovic, O., Wetzal, D., Jones, J.B., Edwards, A.N., Vargas-Cuebas, G., McBride, S.M., Tamayo, R., 2019. Phase variation of a signal transduction system controls *Clostridioides difficile* colony morphology, motility, and virulence. *PLoS Biol.* 17, 1–28. <https://doi.org/10.1371/journal.pbio.3000379>
- Genisyuerk, S., Papatheodorou, P., Guttenberg, G., Schubert, R., Benz, R., Aktories, K., 2011. Structural determinants for membrane insertion, pore formation and translocation of *Clostridium difficile* toxin B. *Mol. Microbiol.* 79, 1643–1654. <https://doi.org/10.1111/J.1365-2958.2011.07549.X>
- Georgiadou, M., Castagnini, M., Karimova, G., Ladant, D., Pelicic, V., 2012. Large-scale study of the interactions between proteins involved in type IV pilus biology in *Neisseria meningitidis*: characterization of a subcomplex involved in pilus assembly. *Mol. Microbiol.* 84, 857–873. <https://doi.org/10.1111/J.1365-2958.2012.08062.X>
- Gerding, D.N., Johnson, S., Rupnik, M., Aktories, K., 2014. *Clostridium difficile* binary toxin CDT: mechanism, epidemiology, and potential clinical importance. *Gut Microbes* 5, 15–27. <https://doi.org/10.4161/GMIC.26854>
- Giltner, C.L., Habash, M., Burrows, L.L., 2010a. *Pseudomonas aeruginosa* minor pilins are incorporated into type IV pili. *J. Mol. Biol.* 398, 444–461. <https://doi.org/10.1016/J.JMB.2010.03.028>

- Giltner, C.L., Habash, M., Burrows, L.L., 2010b. *Pseudomonas aeruginosa* minor pilins are incorporated into type IV pili. *J. Mol. Biol.* 398, 444–461. <https://doi.org/10.1016/J.JMB.2010.03.028>
- Giltner, C.L., Nguyen, Y., Burrows, L.L., 2012. Type IV pilin proteins: versatile molecular modules. *Microbiol. Mol. Biol. Rev.* 76, 740–772. <https://doi.org/10.1128/MMBR.00035-12>
- Gold, V.A.M., Salzer, R., Averhoff, B., Kühlbrandt, W., 2015. Structure of a type IV pilus machinery in the open and closed state. *Elife* 4. <https://doi.org/10.7554/ELIFE.07380>
- Goorhuis, A., Bakker, D., Corver, J., Debast, S.B., Harmanus, C., Notermans, D.W., Bergwerff, A.A., Dekker, F.W., Kuijper, E.J., 2008. Emergence of *Clostridium difficile* infection due to a new hypervirulent strain, polymerase chain reaction ribotype 078. *Clin. Infect. Dis.* 47, 1162–1170. <https://doi.org/10.1086/592257>
- Govind, R., Dupuy, B., 2012. Secretion of *Clostridium difficile* toxins A and B requires the holin-like protein TcdE. *PLoS Pathog.* 8. <https://doi.org/10.1371/JOURNAL.PPAT.1002727>
- Griffiths, D., Fawley, W., Kachrimanidou, M., Bowden, R., Crook, D.W., Fung, R., Golubchik, T., Harding, R.M., Jeffery, K.J.M., Jolley, K.A., Kirton, R., Peto, T.E., Rees, G., Stoesser, N., Vaughan, A., Walker, A.S., Young, B.C., Wilcox, M., Dingle, K.E., 2010. Multilocus sequence typing of *Clostridium difficile*. *J. Clin. Microbiol.* 48, 770–778. <https://doi.org/10.1128/JCM.01796-09>
- Hammond, G.A., Johnson, J.L., 1995. The toxigenic element of *Clostridium difficile* strain VPI 10463. *Microb. Pathog.* 19, 203–213. [https://doi.org/10.1016/S0882-4010\(95\)90263-5](https://doi.org/10.1016/S0882-4010(95)90263-5)
- Hanawalt, P.C., Spivak, G., 2008. Transcription-coupled DNA repair: two decades of progress and surprises. *Nat. Rev. Mol. Cell Biol.* 9, 958–970. <https://doi.org/10.1038/NRM2549>
- Hartman, A.H., Liu, H., Melville, S.B., 2011. Construction and characterization of a lactose-inducible promoter system for controlled gene expression in *Clostridium perfringens*. *Appl. Environ. Microbiol.* 77, 471–478. <https://doi.org/10.1128/AEM.01536-10>
- Hélaïne, S., Carbonnelle, E., Prouvensier, L., Beretti, J.L., Nassif, X., Pelicic, V., 2005. PilX, a pilus-associated protein essential for bacterial aggregation, is a key to pilus-facilitated attachment of *Neisseria meningitidis* to human cells. *Mol. Microbiol.* 55, 65–77. <https://doi.org/10.1111/J.1365-2958.2004.04372.X>
- Helmann, J.D., Chamberlin, M.J., 1987. DNA sequence analysis suggests that expression of flagellar and chemotaxis genes in *Escherichia coli* and *Salmonella typhimurium* is controlled by an alternative sigma factor. *Proc. Natl. Acad. Sci. U. S. A.* 84, 6422–6424. <https://doi.org/10.1073/PNAS.84.18.6422>
- Hendrick, W.A., Orr, M.W., Murray, S.R., Lee, V.T., Melville, S.B., 2017. Cyclic Di-GMP Binding by an Assembly ATPase (PilB2) and Control of Type IV Pilin Polymerization in the Gram-Positive Pathogen *Clostridium perfringens*. *J. Bacteriol.* 199. <https://doi.org/10.1128/JB.00034-17>
- Hengge, R., 2009. Principles of c-di-GMP signalling in bacteria. *Nat. Rev. Microbiol.* 7, 263–273. <https://doi.org/10.1038/NRMICRO2109>
- Hodgkinson, J.L., Horsley, A., Stabat, D., Simon, M., Johnson, S., Da Fonseca, P.C.A., Morris, E.P., Wall, J.S., Lea, S.M., Blocker, A.J., 2009. Three-dimensional reconstruction of the *Shigella* T3SS transmembrane regions reveals 12-fold symmetry and novel features throughout. *Nat. Struct. Mol. Biol.* 16, 477–485. <https://doi.org/10.1038/NSMB.1599>
- Hoffman, L.R., D’Argenio, D.A., MacCoss, M.J., Zhang, Z., Jones, R.A., Miller, S.I., 2005. Aminoglycoside antibiotics induce bacterial biofilm formation. *Nature* 436, 1171–1175.

- <https://doi.org/10.1038/NATURE03912>
- Horvat, S., Rupnik, M., 2018. Interactions between *Clostridioides difficile* and fecal microbiota in in vitro batch model: Growth, sporulation, and microbiota changes. *Front. Microbiol.* 9. <https://doi.org/10.3389/FMICB.2018.01633/FULL>
- Huang, B., Whitchurch, C.B., Mattick, J.S., 2003. FimX, a multidomain protein connecting environmental signals to twitching motility in *Pseudomonas aeruginosa*. *J. Bacteriol.* 185, 7068–7076. <https://doi.org/10.1128/JB.185.24.7068-7076.2003>
- Hyyryläinen, H.L., Marciniak, B.C., Dahncke, K., Pietiäinen, M., Courtin, P., Vitikainen, M., Seppala, R., Otto, A., Becher, D., Chapot-Chartier, M.P., Kuipers, O.P., Kontinen, V.P., 2010. Penicillin-binding protein folding is dependent on the PrsA peptidyl-prolyl cis-trans isomerase in *Bacillus subtilis*. *Mol. Microbiol.* 77, 108–127. <https://doi.org/10.1111/J.1365-2958.2010.07188.X>
- Indra, A., Blaschitz, M., Kernbichler, S., Reischl, U., Wewalka, G., Allerberger, F., 2010. Mechanisms behind variation in the *Clostridium difficile* 16S-23S rRNA intergenic spacer region. *J. Med. Microbiol.* 59, 1317–1323. <https://doi.org/10.1099/JMM.0.020792-0>
- Janezic, S., Mlakar, S., Rupnik, M., 2018. Dissemination of *Clostridium difficile* spores between environment and households: Dog paws and shoes. *Zoonoses Public Health* 65, 669–674. <https://doi.org/10.1111/ZPH.12475>
- Janezic, S., Rupnik, M., 2015. Genomic diversity of *Clostridium difficile* strains. *Res. Microbiol.* 166, 353–360. <https://doi.org/10.1016/J.RESMIC.2015.02.002>
- Janezic, S., Rupnik, M., 2010. Molecular typing methods for *Clostridium difficile*: pulsed-field gel electrophoresis and PCR ribotyping. *Methods Mol. Biol.* 646, 55–65. https://doi.org/10.1007/978-1-60327-365-7_4
- Janvilisri, T., Scaria, J., Thompson, A.D., Nicholson, A., Limbago, B.M., Arroyo, L.G., Songer, J.G., Gröhn, Y.T., Chang, Y.F., 2009. Microarray identification of *Clostridium difficile* core components and divergent regions associated with host origin. *J. Bacteriol.* 191, 3881–3891. <https://doi.org/10.1128/JB.00222-09>
- Kabała, M., Gofron, Z., Aptekorz, M., Sacha, K., Harmanus, C., Kuijper, E., Martirosian, G., 2021. *Clostridioides difficile* Ribotype 027 (RT027) Outbreak Investigation Due to the Emergence of Rifampicin Resistance Using Multilocus Variable-Number Tandem Repeat Analysis (MLVA). *Infect. Drug Resist.* 14, 3247–3254. <https://doi.org/10.2147/IDR.S324745>
- Karasawa, T., Ikoma, S., Yamakawa, K., Nakamura, S., 1995. A defined growth medium for *Clostridium difficile*. *Microbiology* 141 (Pt 2), 371–375. <https://doi.org/10.1099/13500872-141-2-371>
- Karuppiyah, V., Derrick, J.P., 2011. Structure of the PilM-PilN inner membrane type IV pilus biogenesis complex from *Thermus thermophilus*. *J. Biol. Chem.* 286, 24434–24442. <https://doi.org/10.1074/JBC.M111.243535>
- Knight, D.R., Putsathit, P., Elliott, B., Riley, T. V., 2016. Contamination of Australian newborn calf carcasses at slaughter with *Clostridium difficile*. *Clin. Microbiol. Infect.* 22, 266.e1–266.e7. <https://doi.org/10.1016/J.CMI.2015.11.017>
- Koo, J., Tammam, S., Ku, S.Y., Sampaleanu, L.M., Burrows, L.L., Howell, P.L., 2008. PilF is an outer membrane lipoprotein required for multimerization and localization of the *Pseudomonas aeruginosa* Type IV pilus secretin. *J. Bacteriol.* 190, 6961–6969. <https://doi.org/10.1128/JB.00996-08>
- Krantz, B.A., Melnyk, R.A., Zhang, S., Juris, S.J., Lacy, D.B., Wu, Z., Finkelstein, A., Collier, R.J., 2005. A phenylalanine clamp catalyzes protein translocation through the anthrax toxin

- pore. *Science* 309, 777–781. <https://doi.org/10.1126/SCIENCE.1113380>
- Krogh, A., Larsson, B., Von Heijne, G., Sonnhammer, E.L.L., 2001. Predicting transmembrane protein topology with a hidden Markov model: application to complete genomes. *J. Mol. Biol.* 305, 567–580. <https://doi.org/10.1006/JMBI.2000.4315>
- Kuchma, S.L., O’Toole, G.A., 2022. Surface-Induced cAMP Signaling Requires Multiple Features of the *Pseudomonas aeruginosa* Type IV Pili. *J. Bacteriol.* <https://doi.org/10.1128/JB.00186-22>
- Kuhn, M., Goebel, W., 1989. Identification of an Extracellular Protein of *Listeria monocytogenes* Possibly Involved in Intracellular Uptake by Mammalian Cells. *Infect. Immun.* 57, 55–61.
- Kuijper, E., Weerd, J., Kato, H., Kato, N., Dam, A., Vorm, E., Weel, J., Rheenen, C., Dankert, J., 2001. Nosocomial outbreak of *Clostridium difficile*-associated diarrhoea due to a clindamycin-resistant enterotoxin A-negative strain. *Eur. J. Clin. Microbiol. Infect. Dis.* 20, 528–534. <https://doi.org/10.1007/S100960100550>
- Kuijper, E.J., Barbut, F., Brazier, J.S., Kleinkauf, N., Eckmanns, T., Lambert, M.L., Drudy, D., Fitzpatrick, F., Wiuff, C., Brown, D.J., Coia, J.E., Pituch, H., Reichert, P., Even, J., Mossong, J., Widmer, A.F., Olsen, K.E., Allerberger, F., Notermans, D.W., Delmée, M., Coignard, B., Wilcox, M., Patel, B., Frei, R., Nagy, E., Bouza, E., Marin, M., Akerlund, T., Virolainen-Julkunen, A., Lyytikäinen, O., Kotila, S., Ingebretsen, A., Smyth, B., Rooney, P., Poxton, I.R., Monnet, D.L., 2008. Update of *Clostridium difficile* infection due to PCR ribotype 027 in Europe, 2008. *Euro Surveill.* 13. <https://doi.org/10.2807/ese.13.31.18942-en>
- Kuijper, E.J., Coignard, B., Brazier, J.S., Suetens, C., Drudy, D., Wiuff, C., Pituch, H., Reichert, P., Schneider, F., Widmer, A.F., Olsen, K.E., Allerberger, F., Notermans, D.W., Barbut, F., Delmée, M., Wilcox, M., Pearson, A., Patel, B.C., Brown, D.J., Frei, R., Akerlund, T., Poxton, I.R., Tüll, P., 2007. Update of *Clostridium difficile*-associated disease due to PCR ribotype 027 in Europe. *Euro Surveill.* 12. <https://doi.org/10.2807/ESM.12.06.00714-EN>
- LaFrance, M.E., Farrow, M.A., Chandrasekaran, R., Sheng, J., Rubin, D.H., Lacy, D.B., 2015. Identification of an epithelial cell receptor responsible for *Clostridium difficile* TcdB-induced cytotoxicity. *Proc. Natl. Acad. Sci. U. S. A.* 112, 7073–7078. <https://doi.org/10.1073/PNAS.1500791112>
- LaPointe, C.F., Taylor, R.K., 2000. The type 4 prepilin peptidases comprise a novel family of aspartic acid proteases. *J. Biol. Chem.* 275, 1502–1510. <https://doi.org/10.1074/JBC.275.2.1502>
- Lawler, A.J., Lambert, P.A., Worthington, T., 2020. A Revised Understanding of *Clostridioides difficile* Spore Germination. *Trends Microbiol.* 28, 744–752. <https://doi.org/10.1016/j.tim.2020.03.004>
- Lee, E.R., Baker, J.L., Weinberg, Z., Sudarsan, N., Breaker, R.R., 2010. An allosteric self-splicing ribozyme triggered by a bacterial second messenger. *Science* 329, 845–848. <https://doi.org/10.1126/SCIENCE.1190713>
- Leighton, T.L., Buensuceso, R.N.C., Howell, P.L., Burrows, L.L., 2015. Biogenesis of *Pseudomonas aeruginosa* type IV pili and regulation of their function. *Environ. Microbiol.* 17, 4148–4163. <https://doi.org/10.1111/1462-2920.12849>
- Lieberman, J.A., Petro, C.D., Thomas, S., Yang, A., Donnenberg, M.S., 2015. Type IV pilus secretins have extracellular C termini. *MBio* 6. <https://doi.org/10.1128/MBIO.00322-15>
- Lim, S.K., Stuart, R.L., MacKin, K.E., Carter, G.P., Kotsanas, D., Francis, M.J., Easton, M., Dimovski, K., Elliott, B., Riley, T. V., Hogg, G., Paul, E., Korman, T.M., Seemann, T.,

- Stinear, T.P., Lyras, D., Jenkin, G.A., 2014. Emergence of a ribotype 244 strain of *Clostridium difficile* associated with severe disease and related to the epidemic ribotype 027 strain. *Clin. Infect. Dis.* 58, 1723–1730. <https://doi.org/10.1093/CID/CIU203>
- Linke, C., Young, P.G., Kang, H.J., Bunker, R.D., Middleditch, M.J., Caradoc-Davies, T.T., Proft, T., Baker, E.N., 2010. Crystal structure of the minor pilin FctB reveals determinants of Group A *streptococcal* pilus anchoring. *J. Biol. Chem.* 285, 20381–20389. <https://doi.org/10.1074/JBC.M109.089680>
- Loo, V.G., Poirier, L., Miller, M.A., Oughton, M., Libman, M.D., Michaud, S., Bourgault, A.-M., Nguyen, T., Frenette, C., Kelly, M., Vibien, A., Brassard, P., Fenn, S., Dewar, K., Hudson, T.J., Horn, R., René, P., Monczak, Y., Dascal, A., 2005. A predominantly clonal multi-institutional outbreak of *Clostridium difficile*-associated diarrhea with high morbidity and mortality. *N. Engl. J. Med.* 353, 2442–2449. <https://doi.org/10.1056/NEJMOA051639>
- Lukaszczuk, M., Pradhan, B., Remaut, H., 2019. The Biosynthesis and Structures of Bacterial Pili. *Subcell. Biochem.* 92, 369–413. https://doi.org/10.1007/978-3-030-18768-2_12
- Lyon, S.A., Hutton, M.L., Rood, J.I., Cheung, J.K., Lyras, D., 2016. CdtR Regulates TcdA and TcdB Production in *Clostridium difficile*. *PLoS Pathog.* 12. <https://doi.org/10.1371/JOURNAL.PPAT.1005758>
- Maldarelli, G.A., De Masi, L., von Rosenvinge, E.C., Carter, M., Sonnenberg, M.S., 2014. Identification, immunogenicity, and cross-reactivity of type IV pilin and pilin-like proteins from *Clostridium difficile*. *Pathog. Dis.* 71, 302–14. <https://doi.org/10.1111/2049-632X.12137>
- Maldarelli, G.A., Matz, H., Gao, S., Chen, K., Hamza, T., Yfantis, H.G., Feng, H., Sonnenberg, M.S., 2016. Pilin Vaccination Stimulates Weak Antibody Responses and Provides No Protection in a C57Bl/6 Murine Model of Acute *Clostridium difficile* Infection. *J. Vaccines Vaccin.* 7. <https://doi.org/10.4172/2157-7560.1000321>
- Mani, N., Dupuy, B., 2001. Regulation of toxin synthesis in *Clostridium difficile* by an alternative RNA polymerase sigma factor. *Proc. Natl. Acad. Sci. U. S. A.* 98, 5844–5849. <https://doi.org/10.1073/PNAS.101126598>
- Martens, E.C., Chiang, H.C., Gordon, J.I., 2008. Mucosal Glycan Foraging Enhances Fitness and Transmission of a Saccharolytic Human Gut Bacterial Symbiont. *Cell Host Microbe* 4, 447. <https://doi.org/10.1016/J.CHOM.2008.09.007>
- Martin, P.R., Watson, A.A., McCaul, T.F., Mattick, J.S., 1995. Characterization of a five-gene cluster required for the biogenesis of type 4 fimbriae in *Pseudomonas aeruginosa*. *Mol. Microbiol.* 16, 497–508. <https://doi.org/10.1111/J.1365-2958.1995.TB02414.X>
- Matamouros, S., England, P., Dupuy, B., 2007. *Clostridium difficile* toxin expression is inhibited by the novel regulator TcdC. *Mol. Microbiol.* 64, 1274–1288. <https://doi.org/10.1111/J.1365-2958.2007.05739.X>
- Mathur, H., Fallico, V., O'Connor, P.M., Rea, M.C., Cotter, P.D., Hill, C., Ross, R.P., 2017. Insights into the Mode of Action of the Sactibiotic Thuricin CD. *Front. Microbiol.* 8. <https://doi.org/10.3389/FMICB.2017.00696>
- McCallum, M., Tammam, S., Khan, A., Burrows, L.L., Lynne Howell, P., 2017. The molecular mechanism of the type IVa pilus motors. *Nat. Commun.* 8. <https://doi.org/10.1038/ncomms15091>
- McDonald, L.C., Killgore, G.E., Thompson, A., Owens, R.C., Kazakova, S. V., Sambol, S.P., Johnson, S., Gerding, D.N., 2005. An epidemic, toxin gene-variant strain of *Clostridium difficile*. *N. Engl. J. Med.* 353, 2433–2441. <https://doi.org/10.1056/NEJMOA051590>

- McKee, Robert W, Aleksanyan, N., Garrett, E.M., Tamayo, R., 2018. Type IV Pili Promote *Clostridium difficile* Adherence and Persistence in a Mouse Model of Infection. *Infect. Immun.* 86, e00943-17. <https://doi.org/10.1128/IAI.00943-17>
- McKee, Robert W., Harvest, C.K., Tamayo, R., 2018. Cyclic Diguanylate Regulates Virulence Factor Genes via Multiple Riboswitches in *Clostridium difficile*. *mSphere* 3. <https://doi.org/10.1128/MSPHERE.00423-18>
- McKee, R.W., Mangalea, M.R., Purcell, E.B., Borchardt, E.K., Tamayo, R., 2013. The second messenger cyclic Di-GMP regulates *Clostridium difficile* toxin production by controlling expression of sigD. *J. Bacteriol.* 195, 5174–5185. <https://doi.org/10.1128/JB.00501-13>
- Mehner-Breitfeld, D., Rathmann, C., Riedel, T., Just, I., Gerhard, R., Overmann, J., Brüser, T., 2018. Evidence for an Adaptation of a Phage-Derived Holin/Endolysin System to Toxin Transport in *Clostridioides difficile*. *Front. Microbiol.* 9. <https://doi.org/10.3389/FMICB.2018.02446>
- Melville, S., Craig, L., 2013. Type IV pili in Gram-positive bacteria. *Microbiol. Mol. Biol. Rev.* 77, 323–341. <https://doi.org/10.1128/MMBR.00063-12>
- Mendez, M., Huang, I.-H., Ohtani, K., Grau, R., Shimizu, T., Sarker, M.R., 2008. Carbon catabolite repression of type IV pilus-dependent gliding motility in the anaerobic pathogen *Clostridium perfringens*. *J. Bacteriol.* 190, 48–60. <https://doi.org/10.1128/JB.01407-07>
- Metcalf, D.S., Scott Weese, J., 2011. Binary toxin locus analysis in *Clostridium difficile*. *J. Med. Microbiol.* 60, 1137–1145. <https://doi.org/10.1099/JMM.0.028498-0>
- Mignolet, J., Panis, G., Viollier, P.H., 2018. More than a Tad: spatiotemporal control of *Caulobacter* pili. *Curr. Opin. Microbiol.* 42, 79–86. <https://doi.org/10.1016/J.MIB.2017.10.017>
- Moloney, G., Eyre, D.W., Aogáin, M. Mac, McElroy, M.C., Vaughan, A., Peto, T.E.A., Crook, D.W., Rogers, T.R., 2021. Human and Porcine Transmission of *Clostridioides difficile* Ribotype 078, Europe. *Emerg. Infect. Dis.* 27, 2294–2300. <https://doi.org/10.3201/EID2709.203468>
- Morand, P.C., Drab, M., Rajalingam, K., Nassif, X., Meyer, T.F., 2009. *Neisseria meningitidis* differentially controls host cell motility through PilC1 and PilC2 components of type IV Pili. *PLoS One* 4. <https://doi.org/10.1371/JOURNAL.PONE.0006834>
- Na, X., Kim, H., Moyer, M.P., Pothoulakis, C., LaMont, J.T., 2008. gp96 is a human colonocyte plasma membrane binding protein for *Clostridium difficile* toxin A. *Infect. Immun.* 76, 2862–2871. <https://doi.org/10.1128/IAI.00326-08>
- Ng, Y.K., Ehsaan, M., Philip, S., Collery, M.M., Janoir, C., Collignon, A., Cartman, S.T., Minton, N.P., 2013. Expanding the repertoire of gene tools for precise manipulation of the *Clostridium difficile* genome: allelic exchange using pyrE alleles. *PLoS One* 8, e56051. <https://doi.org/10.1371/journal.pone.0056051>
- O'Connor, J.R., Johnson, S., Gerding, D.N., 2009. *Clostridium difficile* infection caused by the epidemic BI/NAP1/027 strain. *Gastroenterology* 136, 1913–1924. <https://doi.org/10.1053/J.GASTRO.2009.02.073>
- Pelvic, V., 2008. Type IV pili: e pluribus unum? *Mol. Microbiol.* 68, 827–837. <https://doi.org/10.1111/J.1365-2958.2008.06197.X>
- Pepe, J.C., Lory, S., 1998. Amino acid substitutions in PilD, a bifunctional enzyme of *Pseudomonas aeruginosa*. Effect on leader peptidase and N-methyltransferase activities in vitro and in vivo. *J. Biol. Chem.* 273, 19120–19129. <https://doi.org/10.1074/JBC.273.30.19120>

- Pépin, J., Valiquette, L., Alary, M.E., Villemure, P., Pelletier, A., Forget, K., Pépin, K., Chouinard, D., 2004. *Clostridium difficile*-associated diarrhea in a region of Quebec from 1991 to 2003: a changing pattern of disease severity. *CMAJ* 171, 466–472. <https://doi.org/10.1503/CMAJ.1041104>
- Perelle, S., Gibert, M., Bourlioux, P., Corthier, G., Popoff, M.R., 1997. Production of a complete binary toxin (actin-specific ADP-ribosyltransferase) by *Clostridium difficile* CD196. *Infect. Immun.* 65, 1402–1407. <https://doi.org/10.1128/IAI.65.4.1402-1407.1997>
- Persat, A., Inclan, Y.F., Engel, J.N., Stone, H.A., Gitai, Z., 2015. Type IV pili mechanochemically regulate virulence factors in *Pseudomonas aeruginosa*. *Proc. Natl. Acad. Sci. U. S. A.* 112, 7563–7568. <https://doi.org/10.1073/PNAS.1502025112>
- Popoff, M.R., Rubin, E.J., Gill, D.M., Boquet, P., 1988. Actin-specific ADP-ribosyltransferase produced by a *Clostridium difficile* strain. *Infect. Immun.* 56, 2299–2306. <https://doi.org/10.1128/IAI.56.9.2299-2306.1988>
- Pothoulakis, C., Gilbert, R.J., Cladaras, C., Castagliuolo, I., Semenza, G., Hitti, Y., Montcrief, J.S., Linevsky, J., Kelly, C.P., Nikulasson, S., Desai, H.P., Wilkins, T.D., Lamont, J.T., 1996. Rabbit sucrase-isomaltase contains a functional intestinal receptor for *Clostridium difficile* toxin A. *J. Clin. Invest.* 98, 641–649. <https://doi.org/10.1172/JCI118835>
- Pratt, J.T., Tamayo, R., Tischler, A.D., Camilli, A., 2007. PilZ domain proteins bind cyclic diguanylate and regulate diverse processes in *Vibrio cholerae*. *J. Biol. Chem.* 282, 12860–70. <https://doi.org/10.1074/jbc.M611593200>
- Prouty, M.G., Correa, N.E., Klose, K.E., 2001. The novel sigma54- and sigma28-dependent flagellar gene transcription hierarchy of *Vibrio cholerae*. *Mol. Microbiol.* 39, 1595–1609. <https://doi.org/10.1046/J.1365-2958.2001.02348.X>
- Purcell, E.B., McKee, R.W., Bordeleau, E., Burrus, V., Tamayo, R., 2016. Regulation of Type IV Pili Contributes to Surface Behaviors of Historical and Epidemic Strains of *Clostridium difficile*. *J. Bacteriol.* 198, 565–77. <https://doi.org/10.1128/JB.00816-15>
- Purcell, E.B., McKee, R.W., Bordeleau, E., Burrus, V., Tamayo, R., 2015. Regulation of Type IV Pili Contributes to Surface Behaviors of Historical and Epidemic Strains of *Clostridium difficile*. *J. Bacteriol.* 198, 565–577. <https://doi.org/10.1128/JB.00816-15>
- Purcell, E.B., McKee, R.W., Courson, D.S., Garrett, E.M., McBride, S.M., Cheney, R.E., Tamayo, R., 2017. A Nutrient-Regulated Cyclic Diguanylate Phosphodiesterase Controls *Clostridium difficile* Biofilm and Toxin Production during Stationary Phase. *Infect. Immun.* 85. <https://doi.org/10.1128/IAI.00347-17>
- Purcell, E.B., McKee, R.W., McBride, S.M., Waters, C.M., Tamayo, R., 2012. Cyclic diguanylate inversely regulates motility and aggregation in *Clostridium difficile*. *J. Bacteriol.* 194, 3307–3316. <https://doi.org/10.1128/JB.00100-12>
- Purdy, D., O’Keeffe, T.A.T., Elmore, M., Herbert, M., McLeod, A., Bokori-Brown, M., Ostrowski, A., Minton, N.P., 2002. Conjugative transfer of clostridial shuttle vectors from *Escherichia coli* to *Clostridium difficile* through circumvention of the restriction barrier. *Mol. Microbiol.* 46, 439–452. <https://doi.org/10.1046/J.1365-2958.2002.03134.X>
- Quigley, B.R., Zähler, D., Hatkoff, M., Thanassi, D.G., Scott, J.R., 2009. Linkage of T3 and Cpa pilins in the *Streptococcus pyogenes* M3 pilus. *Mol. Microbiol.* 72, 1379–1394. <https://doi.org/10.1111/J.1365-2958.2009.06727.X>
- Rakotoarivonina, H., Jubelin, G., Hebraud, M., Gaillard-Martinie, B., Forano, E., Mosoni, P., 2002. Adhesion to cellulose of the Gram-positive bacterium *Ruminococcus albus*

- involves type IV pili. *Microbiology* 148, 1871–1880. <https://doi.org/10.1099/00221287-148-6-1871>
- Roelofs, K.G., Jones, C.J., Helman, S.R., Shang, X., Orr, M.W., Goodson, J.R., Galperin, M.Y., Yildiz, F.H., Lee, V.T., 2015. Systematic Identification of Cyclic-di-GMP Binding Proteins in *Vibrio cholerae* Reveals a Novel Class of Cyclic-di-GMP-Binding ATPases Associated with Type II Secretion Systems. *PLoS Pathog.* 11. <https://doi.org/10.1371/JOURNAL.PPAT.1005232>
- Rohlfing, A.E., Eckenroth, B.E., Forster, E.R., Kevorkian, Y., Donnelly, M.L., Benito de la Puebla, H., Doublé, S., Shen, A., 2019. The CspC pseudoprotease regulates germination of *Clostridioides difficile* spores in response to multiple environmental signals. *PLoS Genet.* 15. <https://doi.org/10.1371/JOURNAL.PGEN.1008224>
- Römling, U., 2005. Characterization of the rdar morphotype, a multicellular behaviour in Enterobacteriaceae. *Cell. Mol. Life Sci.* 62, 1234–1246. <https://doi.org/10.1007/S00018-005-4557-X/METRICS>
- Römling, U., Galperin, M.Y., Gomelsky, M., 2013. Cyclic di-GMP: the first 25 years of a universal bacterial second messenger. *Microbiol. Mol. Biol. Rev.* 77, 1–52. <https://doi.org/10.1128/MMBR.00043-12>
- Ronish, L.A., Sidner, B., Yu, Y., Piepenbrink, K.H., 2022. Recognition of extracellular DNA by type IV pili promotes biofilm formation by *Clostridioides difficile*. *J. Biol. Chem.* 298. <https://doi.org/10.1016/J.JBC.2022.102449>
- Rosa, R., Donskey, C.J., Munoz-Price, L.S., 2018. The Intersection Between Colonization Resistance, Antimicrobial Stewardship, and *Clostridium difficile*. *Curr. Infect. Dis. Rep.* 20. <https://doi.org/10.1007/S11908-018-0631-Z>
- Ryjenkov, D.A., Tarutina, M., Moskvina, O. V., Gomelsky, M., 2005. Cyclic diguanylate is a ubiquitous signaling molecule in bacteria: insights into biochemistry of the GGDEF protein domain. *J. Bacteriol.* 187, 1792–1798. <https://doi.org/10.1128/JB.187.5.1792-1798.2005>
- Sampaleanu, L.M., Bonanno, J.B., Ayers, M., Koo, J., Tammam, S., Burley, S.K., Almo, S.C., Burrows, L.L., Howell, P.L., 2009. Periplasmic domains of *Pseudomonas aeruginosa* PilN and PilO form a stable heterodimeric complex. *J. Mol. Biol.* 394, 143–159. <https://doi.org/10.1016/J.JMB.2009.09.037>
- Santos, M.G. de C., Trindade, C.N.D.R., Vommaro, R.C., Domingues, R.M.C.P., Ferreira, E. de O., 2022. Binding of the extracellular matrix laminin-1 to *Clostridioides difficile* strains. *Mem. Inst. Oswaldo Cruz* 117. <https://doi.org/10.1590/0074-02760220035>
- Satyshur, K.A., Worzalla, G.A., Meyer, L.S., Heiniger, E.K., Aukema, K.G., Misic, A.M., Forest, K.T., 2007. Crystal structures of the pilus retraction motor PilT suggest large domain movements and subunit cooperation drive motility. *Structure* 15, 363–376. <https://doi.org/10.1016/J.STR.2007.01.018>
- Sayed, L., Kothari, D., Richards, R.J., 2010. Toxic megacolon associated *Clostridium difficile* colitis. *World J. Gastrointest. Endosc.* 2, 293. <https://doi.org/10.4253/WJGE.V2.I8.293>
- Scaria, J., Ponnala, L., Janvilisri, T., Yan, W., Mueller, L.A., Chang, Y.F., 2010. Analysis of ultra low genome conservation in *Clostridium difficile*. *PLoS One* 5. <https://doi.org/10.1371/JOURNAL.PONE.0015147>
- Schmidt, A.J., Ryjenkov, D.A., Gomelsky, M., 2005. The ubiquitous protein domain EAL is a cyclic diguanylate-specific phosphodiesterase: enzymatically active and inactive EAL domains. *J. Bacteriol.* 187, 4774–4781. <https://doi.org/10.1128/JB.187.14.4774-4781.2005>

- Schwanbeck, J., Oehmig, I., Groß, U., Zautner, A.E., Bohne, W., 2021. *Clostridioides difficile* Single Cell Swimming Strategy: A Novel Motility Pattern Regulated by Viscoelastic Properties of the Environment. *Front. Microbiol.* 12. <https://doi.org/10.3389/FMICB.2021.715220>
- Sebahia, M., Wren, B.W., Mullany, P., Fairweather, N.F., Minton, N., Stabler, R., Thomson, N.R., Roberts, A.P., Cerdeño-Tárraga, A.M., Wang, H., Holden, M.T.G., Wright, A., Churcher, C., Quail, M.A., Baker, S., Bason, N., Brooks, K., Chillingworth, T., Cronin, A., Davis, P., Dowd, L., Fraser, A., Feltwell, T., Hance, Z., Holroyd, S., Jagels, K., Moule, S., Mungall, K., Price, C., Rabinowitsch, E., Sharp, S., Simmonds, M., Stevens, K., Unwin, L., Whithead, S., Dupuy, B., Dougan, G., Barrell, B., Parkhill, J., 2006. The multidrug-resistant human pathogen *Clostridium difficile* has a highly mobile, mosaic genome. *Nat. Genet.* 38, 779–786. <https://doi.org/10.1038/NG1830>
- Sekulovic, O., Mathias Garrett, E., Bourgeois, J., Tamayo, R., Shen, A., Camilli, A., 2018. Genome-wide detection of conservative site-specific recombination in bacteria. *PLoS Genet.* 14, e1007332. <https://doi.org/10.1371/journal.pgen.1007332>
- Setlow, P., 2007. I will survive: DNA protection in bacterial spores. *Trends Microbiol.* 15, 172–180. <https://doi.org/10.1016/J.TIM.2007.02.004>
- Setlow, P., 2003. Spore germination. *Curr. Opin. Microbiol.* 6, 550–556. <https://doi.org/10.1016/j.mib.2003.10.001>
- Setlow, P., Wang, S., Li, Y.Q., 2017. Germination of Spores of the Orders Bacillales and Clostridiales. *Annu. Rev. Microbiol.* 71, 459–477. <https://doi.org/10.1146/ANNUREV-MICRO-090816-093558>
- Sheedlo, M.J., Anderson, D.M., Thomas, A.K., Borden Lacy, D., 2020. Structural elucidation of the *Clostridioides difficile* transferase toxin reveals a single-site binding mode for the enzyme. *Proc. Natl. Acad. Sci. U. S. A.* 117, 6139–6144. <https://doi.org/10.1073/PNAS.1920555117>
- Sheetz, M.P., Merz, A.J., So, M., 2000. Pilus retraction powers bacterial twitching motility. *Nature* 407, 98–102. <https://doi.org/10.1038/35024105>
- Sherwood, A. V., Henkin, T.M., 2016. Riboswitch-Mediated Gene Regulation: Novel RNA Architectures Dictate Gene Expression Responses. *Annu. Rev. Microbiol.* 70, 361–374. <https://doi.org/10.1146/ANNUREV-MICRO-091014-104306>
- Simm, R., Morr, M., Kader, A., Nimtz, M., Römling, U., 2004. GGDEF and EAL domains inversely regulate cyclic di-GMP levels and transition from sessility to motility. *Mol. Microbiol.* 53, 1123–1134. <https://doi.org/10.1111/J.1365-2958.2004.04206.X>
- Skarin, H., Håfström, T., Westerberg, J., Segerman, B., 2011. *Clostridium botulinum* group III: a group with dual identity shaped by plasmids, phages and mobile elements. *BMC Genomics* 12. <https://doi.org/10.1186/1471-2164-12-185>
- Smith, W.D., Pointon, J.A., Abbot, E., Kang, H.J., Baker, E.N., Hirst, B.H., Wilson, J.A., Banfield, M.J., Kehoe, M.A., 2010. Roles of minor pilin subunits Spy0125 and Spy0130 in the serotype M1 *Streptococcus pyogenes* strain SF370. *J. Bacteriol.* 192, 4651–4659. <https://doi.org/10.1128/JB.00071-10>
- Soncini, S.R., Hartman, A.H., Gallagher, T.M., Camper, G.J., Jensen, R. V., Melville, S.B., 2020. Changes in the expression of genes encoding type IV pili-associated proteins are seen when *Clostridium perfringens* is grown in liquid or on surfaces. *BMC Genomics* 21. <https://doi.org/10.1186/S12864-020-6453-Z>
- Song, J.H., Kim, Y.S., 2019. Recurrent *Clostridium difficile* Infection: Risk Factors, Treatment, and Prevention. *Gut Liver* 13, 16. <https://doi.org/10.5009/GNL18071>

- Sorg, J.A., Sonenshein, A.L., 2010. Inhibiting the initiation of *Clostridium difficile* spore germination using analogs of chenodeoxycholic acid, a bile acid. *J. Bacteriol.* 192, 4983–4990. <https://doi.org/10.1128/JB.00610-10>
- Sorg, J.A., Sonenshein, A.L., 2009. Chenodeoxycholate is an inhibitor of *Clostridium difficile* spore germination. *J. Bacteriol.* 191, 1115–1117. <https://doi.org/10.1128/JB.01260-08>
- Soutourina, O.A., Monot, M., Boudry, P., Saujet, L., Pichon, C., Sismeiro, O., Semenova, E., Severinov, K., Le Bouguenec, C., Coppée, J.Y., Dupuy, B., Martin-Verstraete, I., 2013. Genome-wide identification of regulatory RNAs in the human pathogen *Clostridium difficile*. *PLoS Genet.* 9. <https://doi.org/10.1371/JOURNAL.PGEN.1003493>
- Stabler, R.A., Dawson, L.F., Valiente, E., Cairns, M.D., Martin, M.J., Donahue, E.H., Riley, T. V., Songer, J.G., Kuijper, E.J., Dingle, K.E., Wren, B.W., 2012. Macro and micro diversity of *Clostridium difficile* isolates from diverse sources and geographical locations. *PLoS One* 7. <https://doi.org/10.1371/JOURNAL.PONE.0031559>
- Stabler, R.A., Gerding, D.N., Songer, J.G., Drudy, D., Brazier, J.S., Trinh, H.T., Witney, A.A., Hinds, J., Wren, B.W., 2006. Comparative phylogenomics of *Clostridium difficile* reveals clade specificity and microevolution of hypervirulent strains. *J. Bacteriol.* 188, 7297–7305. <https://doi.org/10.1128/JB.00664-06>
- Stabler, R.A., He, M., Dawson, L., Martin, M., Valiente, E., Corton, C., Lawley, T.D., Sebahia, M., Quail, M.A., Rose, G., Gerding, D.N., Gibert, M., Popoff, M.R., Parkhill, J., Dougan, G., Wren, B.W., 2009. Comparative genome and phenotypic analysis of *Clostridium difficile* 027 strains provides insight into the evolution of a hypervirulent bacterium. *Genome Biol.* 10. <https://doi.org/10.1186/GB-2009-10-9-R102>
- Stevenson, E., Minton, N.P., Kuehne, S.A., 2015. The role of flagella in *Clostridium difficile* pathogenicity. *Trends Microbiol.* 23, 275–282. <https://doi.org/10.1016/J.TIM.2015.01.004>
- Stewart, D.B., Berg, A., Hegarty, J., 2013. Predicting recurrence of *C. difficile* colitis using bacterial virulence factors: binary toxin is the key. *J. Gastrointest. Surg.* 17, 118–125. <https://doi.org/10.1007/S11605-012-2056-6>
- Strom, M.S., Nunn, D.N., Lory, S., 1993. A single bifunctional enzyme, PilD, catalyzes cleavage and N-methylation of proteins belonging to the type IV pilin family. *Proc. Natl. Acad. Sci. U. S. A.* 90, 2404–2408. <https://doi.org/10.1073/PNAS.90.6.2404>
- Studer, N., Desharnais, L., Beutler, M., Brugiroux, S., Terrazos, M.A., Menin, L., Schürch, C.M., McCoy, K.D., Kuehne, S.A., Minton, N.P., Stecher, B., Bernier-Latmani, R., Hapfelmeier, S., 2016. Functional intestinal bile acid 7 α -dehydroxylation by *Clostridium scindens* associated with protection from *Clostridium difficile* infection in a gnotobiotic mouse model. *Front. Cell. Infect. Microbiol.* 6, 191. <https://doi.org/10.3389/FCIMB.2016.00191/FULL>
- Sudarsan, N., Lee, E.R., Weinberg, Z., Moy, R.H., Kim, J.N., Link, K.H., Breaker, R.R., 2008. Riboswitches in eubacteria sense the second messenger cyclic di-GMP. *Science* 321, 411–413. <https://doi.org/10.1126/SCIENCE.1159519>
- Sundriyal, A., Roberts, A.K., Shone, C.C., Acharya, K.R., 2009. Structural basis for substrate recognition in the enzymatic component of ADP-ribosyltransferase toxin CDTa from *Clostridium difficile*. *J. Biol. Chem.* 284, 28713–28719. <https://doi.org/10.1074/JBC.M109.043018>
- Suo, J., Yan, Z., Wu, Y., Li, W.G., Zhang, W.Z., Liu, X.S., Liu, Y., Lu, J., 2017. *Clostridium difficile* RT 078/ST11: A Threat to Community Population and Pigs Identified in Elder Hospitalized Patients in Beijing, China. *Infect. Control Hosp. Epidemiol.* 38, 1383–1385.

- <https://doi.org/10.1017/ICE.2017.206>
- Tamayo, R., Tischler, A.D., Camilli, A., 2005. The EAL domain protein VieA is a cyclic diguanylate phosphodiesterase. *J. Biol. Chem.* 280, 33324–33330. <https://doi.org/10.1074/JBC.M506500200>
- Tammam, S., Sampaleanu, L.M., Koo, J., Manoharan, K., Daubaras, M., Burrows, L.L., Howell, P.L., 2013. PilMNOPQ from the *Pseudomonas aeruginosa* type IV pilus system form a transenvelope protein interaction network that interacts with PilA. *J. Bacteriol.* 195, 2126–2135. <https://doi.org/10.1128/JB.00032-13>
- Tammam, S., Sampaleanu, L.M., Koo, J., Sundaram, P., Ayers, M., Andrew Chong, P., Forman-Kay, J.D., Burrows, L.L., Howell, P.L., 2011. Characterization of the PilN, PilO and PilP type IVa pilus subcomplex. *Mol. Microbiol.* 82, 1496–1514. <https://doi.org/10.1111/J.1365-2958.2011.07903.X>
- Tao, L., Zhang, J., Meraner, P., Tovaglieri, A., Wu, X., Gerhard, R., Zhang, X., Stallcup, W.B., Miao, J., He, X., Hurdle, J.G., Breault, D.T., Brass, A.L., Dong, M., 2016. Frizzled proteins are colonic epithelial receptors for *C. difficile* toxin B. *Nature* 538, 350–355. <https://doi.org/10.1038/NATURE19799>
- Tap, J., Mondot, S., Levenez, F., Pelletier, E., Caron, C., Furet, J.P., Ugarte, E., Muñoz-Tamayo, R., Paslier, D.L.E., Nalin, R., Dore, J., Leclerc, M., 2009. Towards the human intestinal microbiota phylogenetic core. *Environ. Microbiol.* 11, 2574–2584. <https://doi.org/10.1111/J.1462-2920.2009.01982.X>
- Tickler, I.A., Goering, R. V., Whitmore, J.D., Lynn, A.N.W., Persing, D.H., Tenover, F.C., 2014. Strain types and antimicrobial resistance patterns of *Clostridium difficile* isolates from the United States, 2011 to 2013. *Antimicrob. Agents Chemother.* 58, 4214–4218. <https://doi.org/10.1128/AAC.02775-13>
- Turner, L.R., Lara, J.C., Nunn, D.N., Lory, S., 1993. Mutations in the consensus ATP-binding sites of XcpR and PilB eliminate extracellular protein secretion and pilus biogenesis in *Pseudomonas aeruginosa*. *J. Bacteriol.* 175, 4962–4969. <https://doi.org/10.1128/JB.175.16.4962-4969.1993>
- Twine, S.M., Reid, C.W., Aubry, A., McMullin, D.R., Fulton, K.M., Austin, J., Logan, S.M., 2009. Motility and flagellar glycosylation in *Clostridium difficile*. *J. Bacteriol.* 191, 7050–62. <https://doi.org/10.1128/JB.00861-09>
- Valiente, E., Bouché, L., Hitchen, P., Faulds-Pain, A., Songane, M., Dawson, L.F., Donahue, E., Stabler, R.A., Panico, M., Morris, H.R., Bajaj-Elliott, M., Logan, S.M., Dell, A., Wren, B.W., 2016. Role of Glycosyltransferases Modifying Type B Flagellin of Emerging Hypervirulent *Clostridium difficile* Lineages and Their Impact on Motility and Biofilm Formation. *J. Biol. Chem.* 291, 25450–25461. <https://doi.org/10.1074/jbc.M116.749523>
- Varga, J.J., Nguyen, V., O'Brien, D.K., Rodgers, K., Walker, R.A., Melville, S.B., 2006a. Type IV pili-dependent gliding motility in the Gram-positive pathogen *Clostridium perfringens* and other Clostridia. *Mol. Microbiol.* 62, 680–694. <https://doi.org/10.1111/j.1365-2958.2006.05414.x>
- Varga, J.J., Therit, B., Melville, S.B., 2008. Type IV pili and the CcpA protein are needed for maximal biofilm formation by the gram-positive anaerobic pathogen *Clostridium perfringens*. *Infect. Immun.* 76, 4944–51. <https://doi.org/10.1128/IAI.00692-08>
- Vincent, C., Manges, A.R., 2015. Antimicrobial Use, Human Gut Microbiota and *Clostridium difficile* Colonization and Infection. *Antibiot. (Basel, Switzerland)* 4, 230–253. <https://doi.org/10.3390/ANTIBIOTICS4030230>
- Wang, S., Liu, X., Xu, X., Yang, D., Wang, D., Han, X., Shi, Y., Tian, M., Ding, C., Peng, D., Yu, S.,

2016. *Escherichia coli* Type III Secretion System 2 ATPase EivC Is Involved in the Motility and Virulence of Avian Pathogenic *Escherichia coli*. *Front. Microbiol.* 7. <https://doi.org/10.3389/FMICB.2016.01387>
- Waterfield, S., Ahmed, H., Jones, I.A., Burky, R., Joshi, L.T., 2022. Isolation of *Clostridioides difficile* PCR Ribotype 027 from single-use hospital gown ties. *J. Med. Microbiol.* 71. <https://doi.org/10.1099/JMM.0.001550>
- Wegner, A., Aktories, K., 1988. ADP-ribosylated actin caps the barbed ends of actin filaments. *J. Biol. Chem.* 263, 13739–13742. [https://doi.org/10.1016/s0021-9258\(18\)68303-6](https://doi.org/10.1016/s0021-9258(18)68303-6)
- Wioland, L., Dupont, J.L., Bossu, J.L., Popoff, M.R., Poulain, B., 2013. Attack of the nervous system by *Clostridium perfringens* Epsilon toxin: from disease to mode of action on neural cells. *Toxicon* 75, 122–135. <https://doi.org/10.1016/J.TOXICON.2013.04.003>
- Wu, Y., Yang, L., Li, W.G., Zhang, W.Z., Liu, Z.J., Lu, J.X., 2019. Microevolution within ST11 group *Clostridioides difficile* isolates through mobile genetic elements based on complete genome sequencing. *BMC Genomics* 20, 796. <https://doi.org/10.1186/s12864-019-6184-1>
- Xia J, Chen J, Chen Y, Qian G, Liu F. Type IV pilus biogenesis genes and their roles in biofilm formation in the biological control agent *Lysobacter enzymogenes* OH11. *Appl Microbiol Biotechnol.* 2018 Jan 1;102(2):833–46. Available from: <https://link.springer.com/article/10.1007/s00253-017-8619-4>
- Yamagata, A., Milgotina, E., Scanlon, K., Craig, L., Tainer, J.A., Donnenberg, M.S., 2012. Structure of an essential type IV pilus biogenesis protein provides insights into pilus and type II secretion systems. *J. Mol. Biol.* 419, 110–124. <https://doi.org/10.1016/J.JMB.2012.02.041>
- Yildiz, F.H., Visick, K.L., 2009. Vibrio biofilms: so much the same yet so different. *Trends Microbiol.* 17, 109. <https://doi.org/10.1016/J.TIM.2008.12.004>
- Yuan, P., Zhang, H., Cai, C., Zhu, S., Zhou, Y., Yang, X., He, R., Li, C., Guo, S., Li, S., Huang, T., Perez-Cordon, G., Feng, H., Wei, W., 2015. Chondroitin sulfate proteoglycan 4 functions as the cellular receptor for *Clostridium difficile* toxin B. *Cell Res.* 25, 157–168. <https://doi.org/10.1038/CR.2014.169>
- Zhu, D., Britton, R., 2022. Flagellin modulates regulation of *Clostridioides difficile* pathogenesis in the absence of motility. *bioRxiv* 2022.11.08.515568. <https://doi.org/10.1101/2022.11.08.515568>

Appendix A

Cloning

Table A-1. Primers used in this study

Primer	Sequence 5'to3'	Description
oZGW001	GAATTGATAAATAGTTAACTTCAGGTTTG	pMTL-SC7315 sequencing primer F
oZGW002	AGAAGATCCTTTGATCTTTTCTACG	pMTL-SC7315 sequencing primer R
oZGW003	AAACTCCTTTTGGATAATCTCATGAC	pMTL-SC7315 linearisation primer F
oZGW004	AAACTTAGGGTAACAAAAACACC	pMTL-SC7315 linearisation primer R
oZGW005	TAGGGTAACAAAAACACCG	To amplify pMTL-SC7315 from pJAK080 (without restriction sites)
oZGW006	CCTTTTGGATAATCTCATGACC	To amplify pMTL-SC7315 from pJAK080 (without restriction sites)
oZGW011	cggtgtttttgttacctaGGAGTAACTACAATGGATATTATAATC	Gibson Assembly: pMTL-SC7315 (from pJAK080) -> pilD1 LHR
oZGW012	taaataatattataCATAGTTTGTAGCACTTAGTAATAG	Gibson Assembly: pilD1 RHR -> pilD1 LHR
oZGW013	acaaactatgTATAATATATTTAATTTTTATTATAATTTGTTATACAAATTTATATAAC	Gibson Assembly: pilD1 LHR -> pilD1 RHR
oZGW014	tcatgagattatcaaaaaggAAATATCTTGAAAACCTAAATATTTCAAC	Gibson Assembly: pilD1 RHR -> pMTL-SC7315 (from pJAK080)
oZGW015	cggtgtttttgttacctaGGTCCTTTAAATTAATATATCATGTTTATTAATC	Gibson Assembly: pMTL-SC7315 (from pJAK080) -> pilJ RHR
oZGW016	taaaaagggtCCTAAACTCTGGAAACTTTG	Gibson Assembly: pilJ LHR -> pilJ RHR
oZGW017	agagtttaggACCTTTTTATTTCATAATAATCATTTC	Gibson Assembly: pilJ RHR -> pilJ LHR
oZGW018	tcatgagattatcaaaaaggAGTTAAAATAAAGTGCGAATAC	Gibson Assembly: pMTL-SC7315 (from pJAK080) -> pilJ LHR
oZGW021	CAAAGTTTCCAGAGTTTAGGCCTTTTTGATAATCTCATGACCA	Gibson Assembly: pMTL-SC7315 linearisation primer with pilJ LHR flank
oZGW022	TTTTAACTTCTGGATTTCTTTAGGGTAACAAAAACACCGTATTTTC	Gibson Assembly: pMTL-SC7315 linearisation primer with pilJ RHR flank
oZGW023	CGGTGTTTTTTGTTACCCTAAAGAAATCCAGAAGTTAAAAATAAG	Gibson Assembly: pMTL-SC7315 (from pJAK080) -> pilJ LHR
oZGW024	TTAAAGGACATAATAATCATTCCCATTAATAAAATTATAG	Gibson Assembly: pilJ RHR -> pilJ LHR
oZGW025	GATTATTATGTCCTTTAAATTAATATATCATGTTTTATTAAATC	Gibson Assembly: pilJ LHR -> pilJ RHR
oZGW026	TCATGAGATTATCAAAAAGGCCTAAACTCTGGAAACTTTG	Gibson Assembly: pilJ RHR -> pMTL-SC7315 (from pJAK080)
oZGW027	TAATGGGAATGATTATTATGGAGGGATGGGGTCTTTAAATA	Gibson Assembly: pilJ LHR -> pilJ RHR
oZGW028	AACGAGTAGTGATTTAGAAGCCTTTTTGATAATCTCATGACCAAAAATC	Gibson Assembly: pMTL-SC7315 Linearisation primer with PilD1 link
oZGW029	TATCCATTGTAGTTTACTCCTAGGGTAACAAAAACACCGTATTTTC	Gibson Assembly: pMTL-SC7315 Linearisation primer with PilD1 link

Primer	Sequence 5'to3'	Description
oZGW030	CGGTGTTTTTTGTTACCCTAGGAGTAACTACAATGGATA TTATAATC	Gibson Assembly: pMTL-SC7315 ->pilD1 LHR
oZGW031	AATTTGCTTTCTTATATCTACCATAGTTTGTAGCACTTTAG TAATAG	Gibson Assembly: pilD1 RHR -> pilD1 LHR
oZGW032	TAAAGTGCTACAACTATGGTAGATATAAGAAAGCAAAT TCC	Gibson Assembly: pilD1 LHR -> pilD1 RHR
oZGW033	TCATGAGATTATCAAAAAGGCTTCTAAATCACTACTCGTT ATAAAAATC	Gibson Assembly: pilD1 RHR -> pMTL- SC7315
oZGW036	GAAAACCTAAATATTCAACTTTATCTTCCATATA	PilD1 630 gDNA Screening Primer
oZGW037	CTGACCAAGAGTTTATGACAAGAATG	PilD1 630 gDNA Screening Primer
oZGW038	GATGTAAGAAATCCAGAAGTTAAAATAAAG	pilJ screening F
oZGW039	CTTGCAACTTTTATCCTAAACTCTG	pilJ screening R
oZGW040	GATCCGCGAGCTCAGAAATCCAGAAGTAAAATAAAG	to amplify PilJ LHR from gDNA with SacI restriction site (for pJAK112 construct and SOE PCR)
oZGW041	GATATATTAATTTAAAGGACCCCATCCCTC TCATAATAATCATTCCATTAATAAAA	to amplify PilJ LHR from gDNA with flank binding to RHR (for pJAK112 construct)
oZGW042	AATTTTATTTAATGGGAATGATTATTATGA GAGGGATGGGGTCTTTAAA	to amplify PilJ RHR from gDNA with flank binding to LHR (for pJAK112 construct)
oZGW043	GATCCGCGGATCCCCTAAACTCTGAAACTTTG	to amplify PilJ RHR from gDNA with BamHI restriction site (for pJAK112 construct and SOE PCR)
oZGW048	GATCGAGCTCTAGGGTAACAAAAACACCG	RF1065 To amplify pMTL-SC7315 from pJAK080 (with restriction sites)
oZGW049	GATCGGATCCCCTTTTGGATAATCTCATGACC	RF1066 To amplify pMTL-SC7315 from pJAK080 (with restriction sites)
oZGW052	GATCGCATGCATAAACTTTAAATAGAAAAAGGCT	To amplify pECC109 with SphI restriction sites at both ends
oZGW053	GATCGCATGCACCACCACCAAGAGCTCCTTGTGATCCAT TACAATATTAT	To amplify pECC109 with SphI restriction sites at both ends
oZGW055	CACCTCCTTTTACTTTAAGCCTACGAATACC	NF793; pECC109 screening primer, upstream of Ptet promoter
oZGW056	CTGGACTTCATGAAAACTAAAAAATATTG	NF1323; pECC109 screening primer, downstream of Ptet promoter
oZGW057	CACCGACGAGCAAGGCAAGACCG	NF794; pECC109 screening primer
oZGW058	GATCGGATCCATTATTATTAACCTATTACT	to amplify pilD1 from 630 and insert into pECC76 for constructing complement strain
oZGW059	GATCGCATGCTTATATAAATTTGTATAACAAATTAT	to amplify pilD1 from 630 and insert into pECC76 for constructing complement strain
oZGW060	GATCGGATCCTTTTATTAATGGGAATGATTAT	to amplify pilJ from 630 and insert into pECC76 for constructing complement strain
oZGW061	GATCGCATGCTTAATTTAAAGGACCCC	to amplify pilJ from 630 and insert into pECC76 for constructing complement strain

Primer	Sequence 5'to3'	Description
oZGW062	GAT <u>CGCATGC</u> ATAAACTTTAAATAGAAAAAGGCTTCTCT C	NF3180; amplify pECC76 for constructing pilin complement strains
oZGW063	GAT <u>CGGATC</u> CTTAATGGTGATGGTGATGGTGCT	amplify pECC76 for constructin pilin complement strains
oZGW064	TTCATACTCTATAGGGTCTTCTATTG	NF3091; pilA1 gDNA screening (2925bp)
oZGW065	AGTTAATAGTTCTTGATACTATACAACTTC	NF3092; pilA1 gDNA screening (2925bp)
oZGW066	GAT <u>CGGATC</u> CTAGAAGATATGGAGAGTAAATATTAT	to amplify pilT from 630 and insert into pECC76 for constructing complement strain
oZGW067	GAT <u>CGCATGC</u> CTTAACGATTATAATATCCATTGTAGT	to amplify pilT from 630 and insert into pECC76 for constructing complement strain
oZGW068	CGATGCCCTGGACTTCATGAAAACTAAAAAATATTG	PilA1 complement plasmids (pZGW005, pZGW006) screening primer
oZGW069	CGACGAGCAAGGCAAGACCG	PilA1 complement plasmids (pZGW005, pZGW006) screening primer
oZGW070	GGATCCCCTAGCGCTACA	Bind to downstream of dccA on pilA1 complement plasmids (pZGW005, pZGW006)
oZGW071	GGATCCTATGTTCTGTAATGTGGCA	Bind to upstream of pilA1 on pZGW005
oZGW072	GGATCCTTTTTGTATAGCATAATTTTCTAGAAATTCTGTT TCAATATGAAAAAG	Bind to upstream of cdi2_4 riboswitch on pZGW006
oZGW073	GGTATTCGTAGGCTTAAAGTCAAAAAGGA	Reverse primer binding upstream of Ptet, to sequence pZGW005/006 backbone, pair with No.495
oZGW074	TTTTAACTTGTTTTAAAAAAGCACCTACTAATTAGGATT	Forward primer binding downstream of oriV, to sequence pZGW005/006 backbone, pair with No.494
oZGW075	AATCCTAATTAGTAGGTGCTTTTTTAAACAAGTTAAAA	Reverse primer binding downstream of oriV, to sequence pZGW005/006 backbone, pair with No.497
oZGW076	CTTGCCTTGCTCGTCGGTGAT	Forward primer binding upstream of inserted terminator, to sequence pZGW005/006 backbone, pair with No.496
oZGW077	GCTTGATCGTAGCGTTAACAGAT	pilA1 complement plasmid screening primer
oZGW078	CCTACTACTGACAGCTTCAA	pilA1 complement plasmid screening primer

Underlined bases indicate restriction sites. Capital and lower cases distinguish aliments to the plasmid or genomic DNA.

Table A-2. Plasmids used in this study

Plasmid name	Descriptive name	Description	Source
pMTL-SC7315	pMTL8000-pCB102- <i>catP</i> -ColeE1+tra-T1- <i>codA</i> -T2	used to introduce deletions into <i>C. difficile</i> 630 via <i>codA</i> -based ACE	(Cartman et al., 2012)
pJAK112	pMTL8000-pCB102- <i>catP</i> -ColeE1+tra-T1- <i>codA</i> -T2	BamHI/SacI restriction sites into pMTL-SC7315	Dr J Kirk
pASF85	pMTL960- <i>Ptet</i>	<i>Ptet</i> empty vector. Derived from pPRF185	Dr R Fagan
pECC17	pMTL960- <i>Ptet</i> -CD630_ <i>dccA</i> -His	CD630_ <i>dccA</i> -His regulated by <i>Ptet</i> promoter, derived from pPRF185	Dr E Couchman
pECC76	pMTL960- <i>Ptet</i> -CD630_ <i>dccA</i> -His-Strep	Strep-tag, SphI/SalI restriction sites inserted into pECC17	Dr E Couchman
pZGW001	pMTL-SC7315- Δ <i>pilD1</i>	used to introduce a 528 bp deletion (aa 6-181) in <i>C. difficile pilD1</i> (CD3503)	This work
pZGW002	pJAK112- Δ <i>pilJ</i>	used to introduce a 776 bp deletion (aa 2-261) in <i>C. difficile pilD1</i> (CD0755)	This work
pECC109	pMTL960- <i>Ptet</i> - <i>dccA</i> -His- <i>pilA1</i>	<i>pilA1</i> cloned into the second site of pECC76 (BamHI/SphI) (3298/3299)	Dr E Couchman
pZGW005	pMTL960- <i>Ptet</i> - <i>dccA</i> -His-Term- <i>Ppila1</i> - <i>pilA1</i>	<i>pilA1</i> complement: Promoter- <i>pilA1</i>	This work
pZGW006	pMTL960- <i>Ptet</i> - <i>dccA</i> -His-Term-Cdi2_4- <i>Ppila1</i> - <i>pilA1</i>	<i>pilA1</i> complement: Cdi2_4-promoter- <i>pilA1</i>	This work
pZGW007	pMTL960- <i>Ptet</i> - <i>dccA</i> - <i>pilD1</i>	to complement <i>pilD1</i> in 630 Δ <i>pilD1</i>	This work
pZGW008	pMTL960- <i>Ptet</i> - <i>dccA</i> - <i>pilJ</i>	to complement <i>pilJ</i> in 630 Δ <i>pilJ</i>	This work

Table A-3. Antibodies used in this study

Antibody	Host	Working dilution	Source
Anti-Cd3513 (<i>PilA1</i>)	Rabbit	1:2,000	Prof. N Fairweather
Anti-CdFliC	Chicken	1:100,000	Dr. G Armstrong
Anti-rabbit IgG (H+L)-HRP conjugate	Goat	1:30,000	Promega
Anti-chicken IgY-HRP conjugate	Goat	1:10,000	Fisher

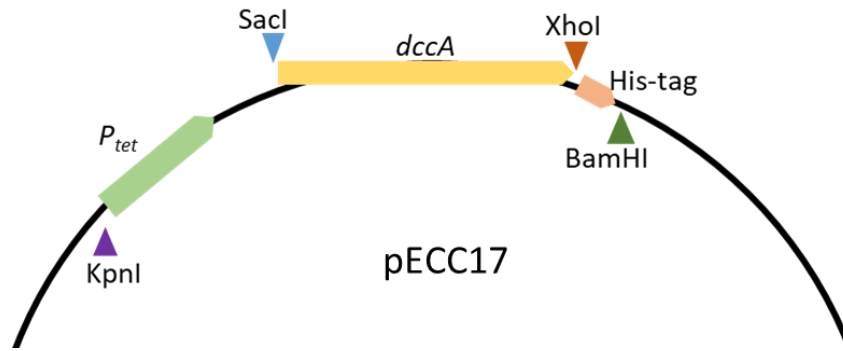


Figure A-1. Plasmid map of pECC17 containing inducible region

Figure represents plasmid pECC17 containing an inducible *dccA* (yellow) controlled by P_{tet} promoter (green). Restriction enzyme BamHI (green triangle) allows insert TFP genes during TFP gene complementation.

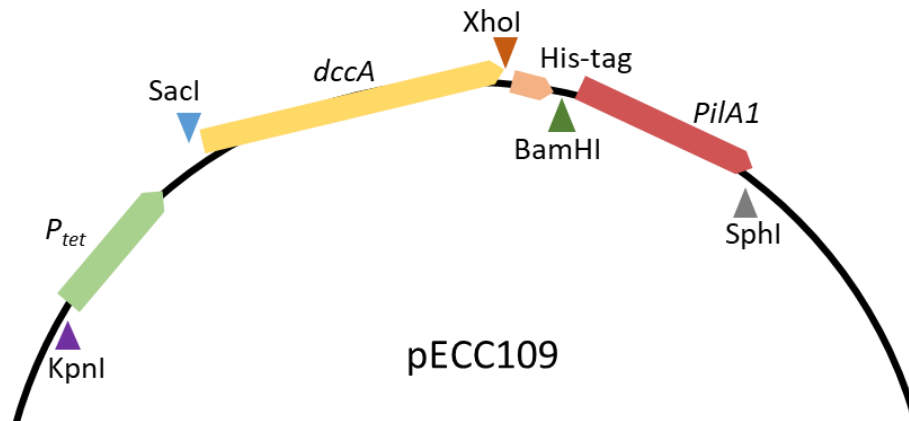


Figure A-2. Plasmid map of pECC109 containing inducible region

Figure represents plasmid pECC109 containing an inducible *dccA* (yellow) controlled by P_{tet} promoter (green). Restriction enzymes BamHI (green triangle) and SphI (grey triangle) were used to insert *pilA1* (red) as a complementation of $\Delta pilA1$ mutant.

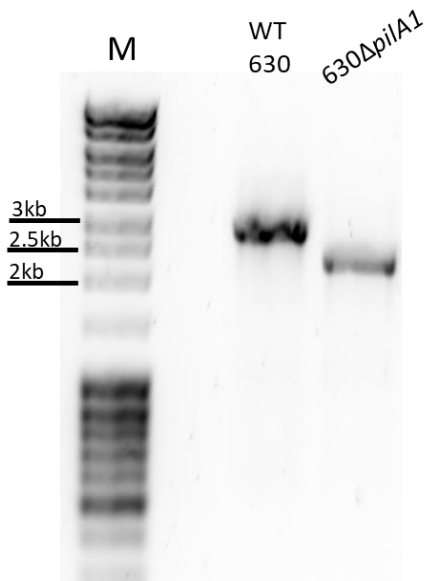


Figure A-3. Screening of putative $\Delta pilA1$ mutant

Colony PCR using primers oZGW064/oZGW065. Lane 'M' indicates marker. PCR product band size of wild-type (WT) *C. difficile* 630 strains is 2921bp. A smaller band is seen in 630 $\Delta pilA1$ (2389bp). 630 $\Delta pilA1$ strain was constructed by Dr E Couchman (Couchman, 2016).

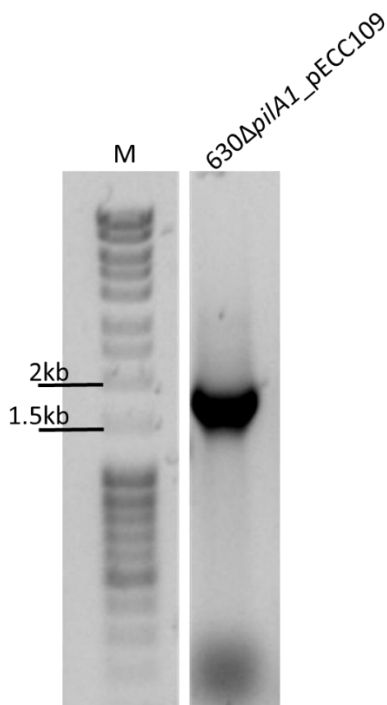


Figure A-4. Screening of pECC109 in $\Delta pilA1$ mutant

Colony PCR using primers oZGW077/oZGW078. Lane 'M' indicates marker. PCR product band size of pECC109 is 1693bp. 630 $\Delta pilA1$ strain and pECC109 is constructed by Dr E Couchman (Couchman, 2016).

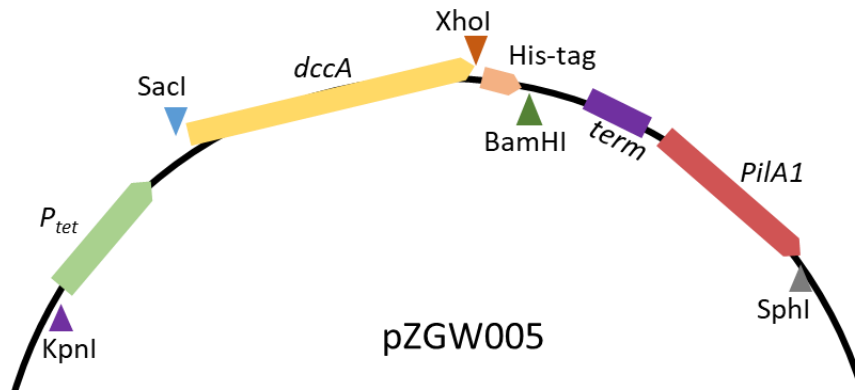


Figure A-5. Plasmid map of pZGW005 containing inducible region

Figure represents plasmid pZGW005. Based on pECC109, a terminator (purple) is inserted upstream of *pilA1* (red), yielding pZGW005 as a control complementation of $\Delta pilA1$ mutant missing Cdi2_4 riboswitch. *dccA* in yellow controlled by P_{tet} promoter (green).

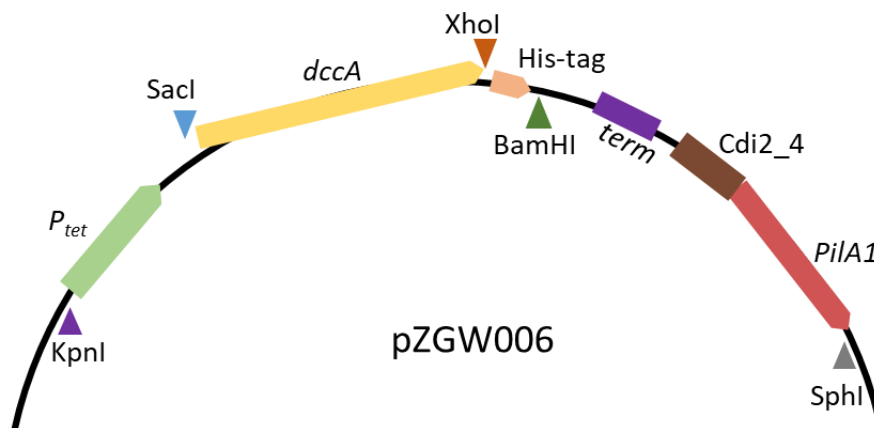


Figure A-6. Plasmid map of pZGW006 containing inducible region

Figure represents plasmid pZGW006. Based on pECC109, a terminator (purple) and Cdi2_4 riboswitch (brown) is inserted upstream of *pilA1* (red), yielding pZGW006 as an additional complementation of $\Delta pilA1$ mutant. *dccA* in yellow controlled by P_{tet} promoter (green).

Appendix B

Biological assays with vector controls and mutants

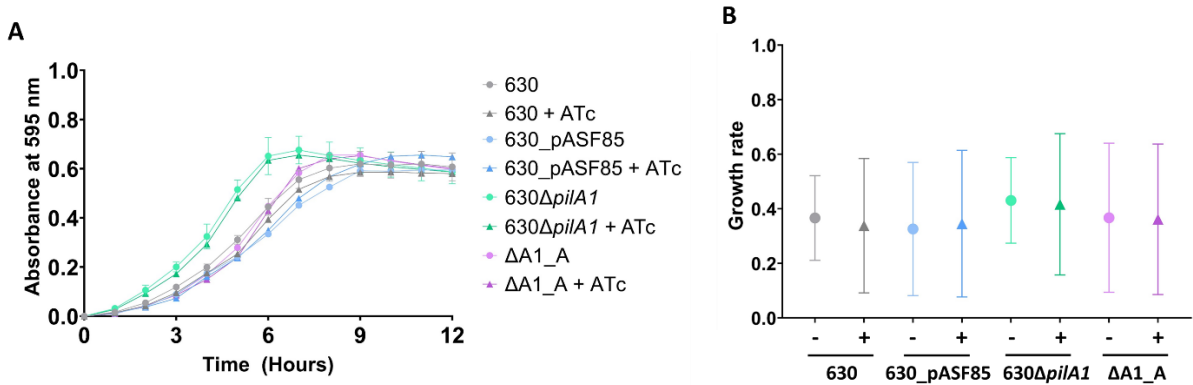


Figure B-1. Δ *pilA1* growth curves and rates with vector control

The growth of CD630 (grey), 630_pASF85 (blue), 630 Δ *pilA1* (cyan), 630 Δ *pilA1*_pASF85 (Δ A1_A; pink) was measured hourly by spectrometry absorbance at 595 nm in a plater reader during 12 hour incubation in BHIS. (A) Growth curves under (+ ATc; triangle dots) or without (round dots) 50 ng ml⁻¹ of ATc supplementation. (B) Growth rates of all strains under either 0 (-, dots) or 50 ng ml⁻¹ (+, triangles) of ATc supplementation. No significant difference reported after one-way ANOVA analysis performed by GraphPad Prism.

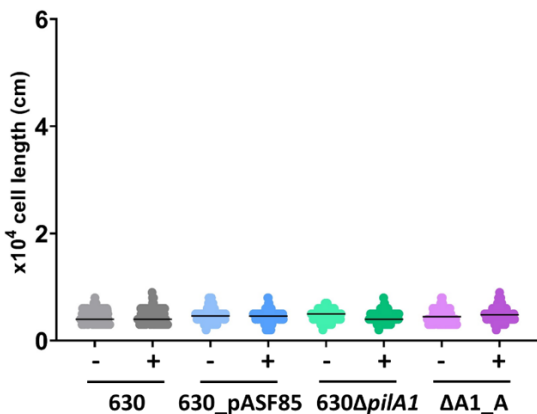


Figure B-2. Δ *pilA1* cell morphology with vector control

CD630 (grey), 630_pASF85 (blue), 630 Δ *pilA1* (cyan), 630 Δ *pilA1*_pASF85 (Δ A1_A; pink) incubated either with (+) or without (-) ATc supplementation. Samples were collected after incubating in BHIS for 7 hours. Dot plots show the data of measured cell length. 120 cells were randomly picked and measured. Data from samples under ATc supplementation is coloured in darker shades. Horizontal lines indicate the median. Figure generated and one-way ANOVA analysis performed by GraphPad Prism.

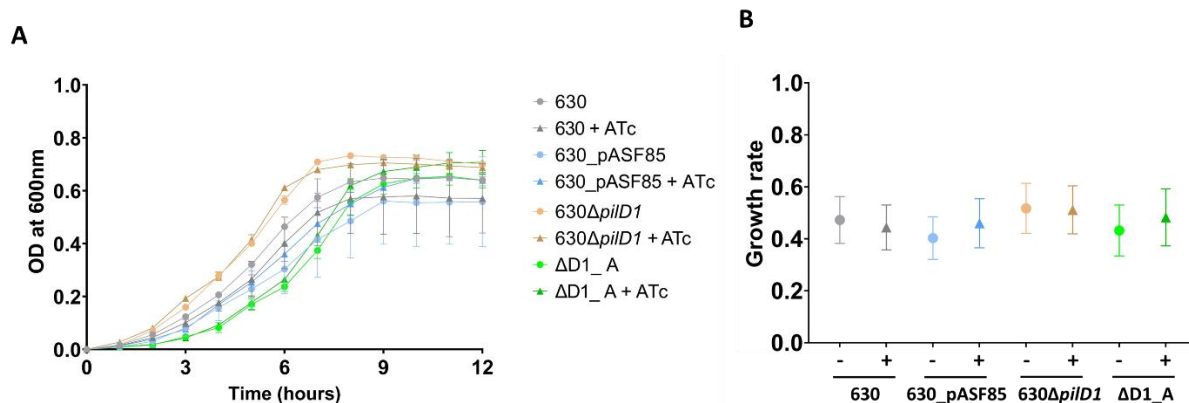


Figure B-3. *ΔpilD1* growth curves and rates with vector control

The growth of CD630 (grey), 630_pASF85 (blue), 630Δ*pilD1* (orange), 630Δ*pilD1*_pASF85 (ΔD1_A; green) was measured hourly by spectrometry absorbance at 595 nm in a plater reader during 12 hour incubation in BHIS. (A) Growth curves under (+ ATc; triangle dots) or without (round dots) 50 ng ml⁻¹ of ATc supplementation. (B) Growth rates of all strains under either 0 (-, dots) or 50 ng ml⁻¹ (+, triangles) of ATc supplementation. No significant difference reported after one-way ANOVA analysis performed by GraphPad Prism.

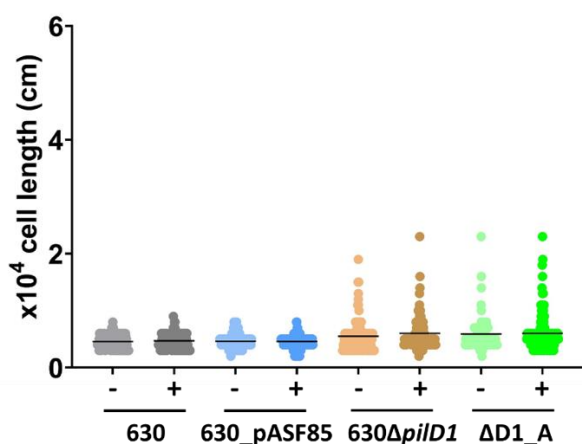


Figure B-4. *ΔpilD1* cell morphology with vector control

CD630 (grey), 630_pASF85 (blue), 630Δ*pilD1* (orange), 630Δ*pilD1*_pASF85 (ΔD1_A; green) incubated either with (+) or without (-) ATc supplementation. Samples were collected after incubating in BHIS for 7 hours. Dot plots show the data of measured cell length. 120 cells were randomly picked and measured. Data from samples under ATc supplementation is coloured in darker shades. Horizontal lines indicate the median. Figure generated and one-way ANOVA analysis performed by GraphPad Prism.

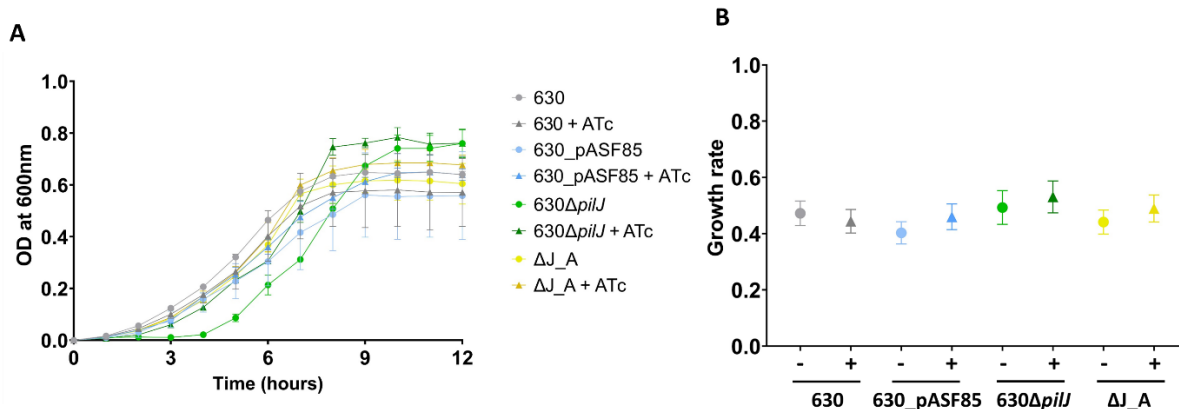


Figure B-5. *ΔpilJ* growth curves and rates with vector control

Growth of CD630 (grey), 630_pASF85 (blue), 630Δ*pilJ* (green), 630Δ*pilJ*_pASF85 (ΔJ_A; yellow) was measured hourly by spectrometry absorbance at 595 nm in a plater reader during 12 hour incubation in BHIS. (A) Growth curves under (+ ATc; triangle dots) or without (round dots) 50 ng ml⁻¹ of ATc supplementation. (B) Growth rates of all strains under either 0 (-, dots) or 50 ng ml⁻¹ (+, triangles) of ATc supplementation. No significant difference reported after one-way ANOVA analysis performed by GraphPad Prism.

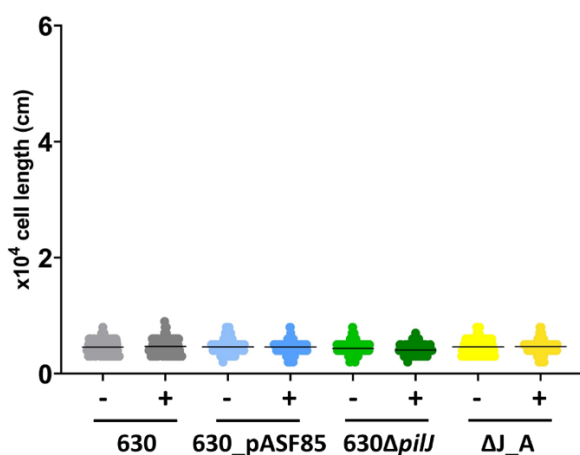


Figure B-6. *ΔpilJ* cell morphology with vector control

CD630 (grey), 630_pASF85 (blue), 630Δ*pilJ* (green), 630Δ*pilJ*_pASF85 (ΔJ_A; yellow) incubated either with (+) or without (-) ATc supplementation. Samples were collected after incubating in BHIS for 7 hours. Dot plots show the data of measured cell length. 120 cells were randomly picked and measured. Data from samples under ATc supplementation is coloured in darker shades. Horizontal lines indicate the median. Figure generated and one-way ANOVA analysis performed by GraphPad Prism.

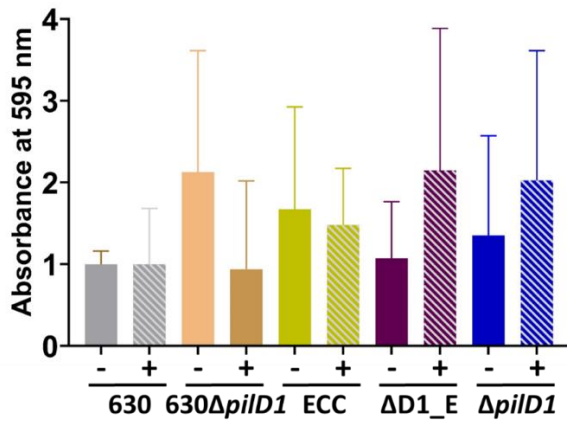


Figure B-7. $\Delta pilD1$ biofilm formation

Biofilm formation is quantified by absorbance at 595 nm of CD630 (grey), 630 $\Delta pilD1$ (orange), 630_pECC17 (ECC; yellow), 630 $\Delta pilD1$ _pECC17 ($\Delta D1_E$; yellow) and 630 $\Delta pilD1$ _pZGW007 ($\Delta pilD1$; blue) cultures after 7-day incubation in 24-well plates either without (- ATc) or without (+ ATc, strips) 50 ng ml⁻¹ of ATc supplementation. No significant phenotype reported. Significance analysed with one-way ANOVA in GraphPad Prism.

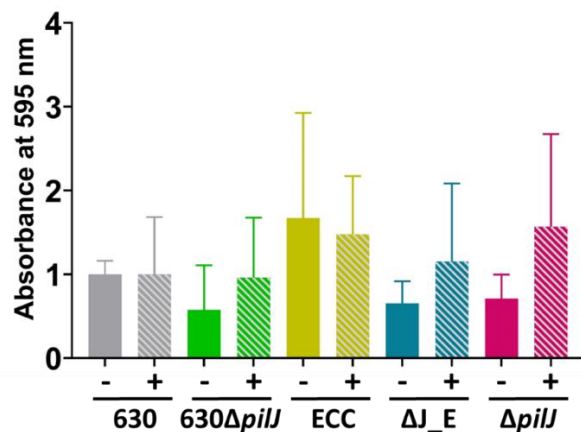


Figure B-8. $\Delta pilJ$ biofilm formation

Biofilm formation is quantified by absorbance at 595 nm of CD630 (grey), 630 $\Delta pilJ$ (orange), 630_pECC17 (ECC; yellow), 630 $\Delta pilJ$ _pECC17 (ΔJ_E ; yellow) and 630 $\Delta pilD1$ _pZGW008 ($\Delta pilJ$; blue) cultures after 7-day incubation in 24-well plates either without (- ATc) or without (+ ATc, strips) 50 ng ml⁻¹ of ATc supplementation. No significant phenotype is reported. Significance analysed with one-way ANOVA in GraphPad Prism.

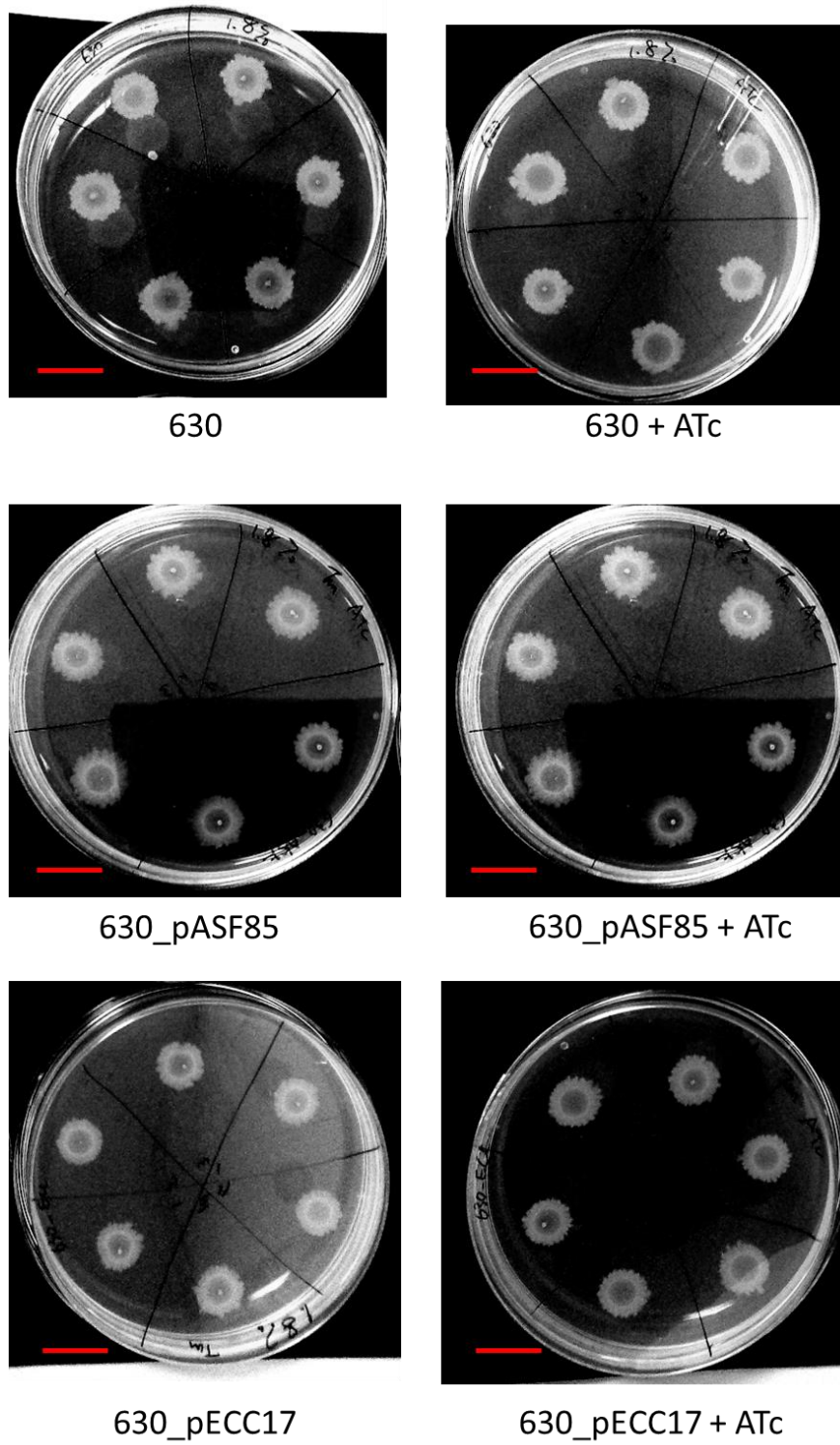


Figure B-9. *C. difficile* 630 colony size and morphology on 1.8 % agar

CD630 (top row), vector control 630_pASF85 (middle row) and 630_pECC17 (bottom row) samples were incubated with (+ATc) or without 50 ng ml⁻¹ of ATc on 1.8% agar plates. Red bars indicate 1.6 cm.

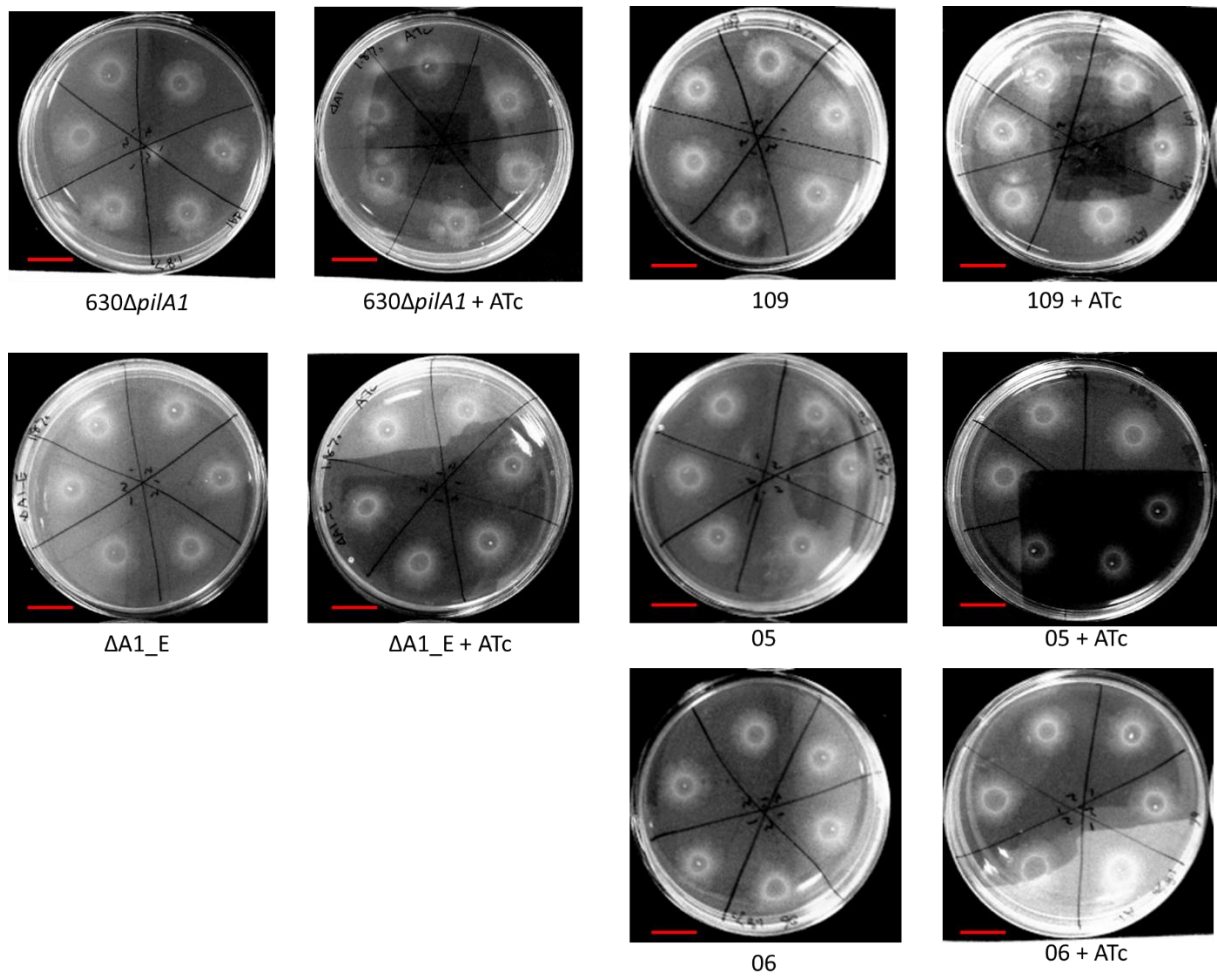


Figure B-10. *ΔpilA1* and complement colonies on 1.8 % agar plates

Example of colonies from 630*ΔpilA1*, 630*ΔpilA1*_pECC17 (*ΔA1_E*) and complement strains 630*ΔpilA1*_pECC109 (009), 630*ΔpilA1*_pZGW005 (05) and 630*ΔpilA1*_pZGW006 (06) incubated for 7 days on 1.8% agar plates with (+ ATc) or without 50 ng ml⁻¹ of ATc supplementation. Red bars indicate 1.6 cm.

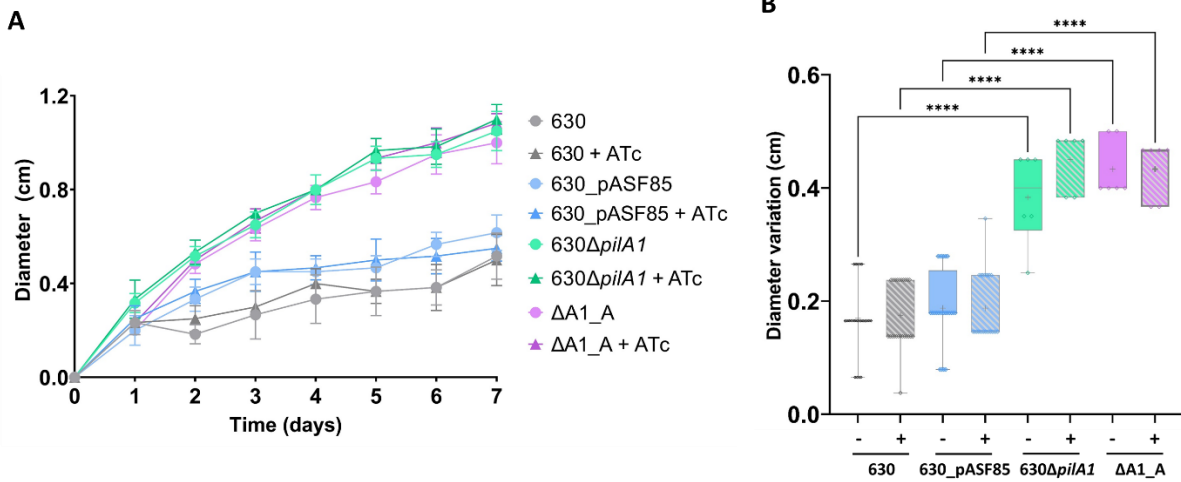


Figure B-11. Colony diameter in 1.8% agar of 630ΔpilA1 and vector control

C. difficile CD630 (grey), 630_pASF85 (blue), 630ΔpilA1 (cyan) and 630ΔpilA1_pASF85 (ΔA1_A; pink) samples were incubated on 1.8% agar plates. (A) Colony diameter was measured every 24 hours for 7 days without or with 50 ng ml⁻¹ of ATc supplementation. (B) Changes in colony diameter between Day 1 and Day 3 post-inoculation in the absence or supplementation (strip-shades) of ATc. Each replicate is represented as a diamond. One-way ANOVA analysis performed by Graphpad Prism. '****' indicates P value < 0.0001. No significant phenotype when introducing vector pASF85, but observing an increased motility when deleting *pilA1* as described in section 4.3.1.

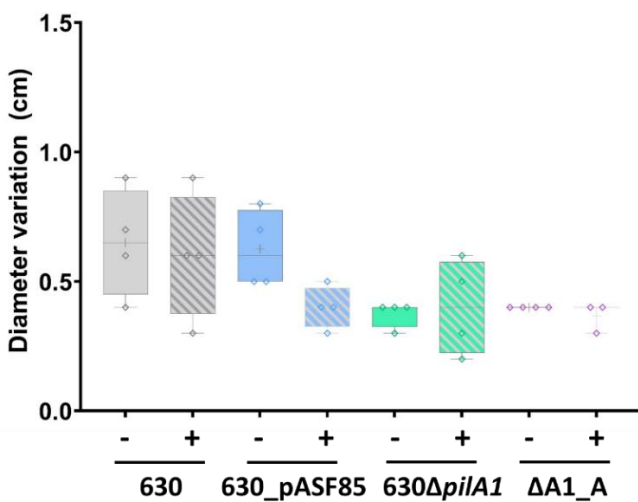


Figure B-12. Colony diameter variation in 0.3% agar of ΔpilA1 and complement strains

Flagella-mediated swimming motility assay, performed on 0.3% agar, either with (+) or without (-) ATc supplementation. CD630 (grey), 630_pASF85 (blue), 630ΔpilA1 (cyan) and 630ΔpilA1_pASF85 (ΔA1_A; pink). Strip shades indicated samples under *dccA* induction (+ ATc). Each replicate is represented as a diamond. Significance analysed with one-way ANOVA in GraphPad Prism. No significant phenotype is reported.

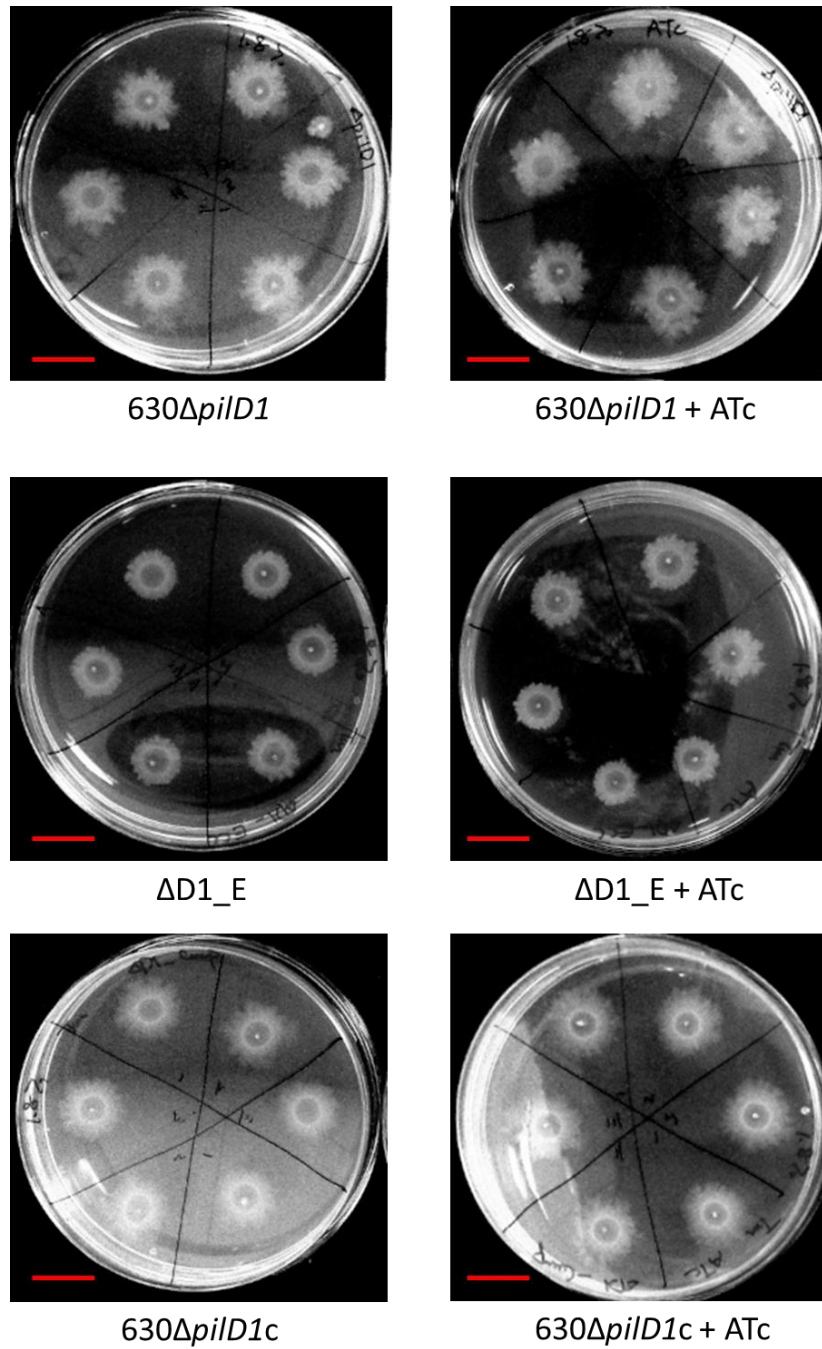


Figure B-13. $\Delta pilD1$ and complement colonies on 1.8 % agar plates

630ΔpilD1, *630ΔpilD1_pECC17* ($\Delta D1_E$) and *630ΔpilD1_pZGW007* ($\Delta pilD1c$) colonies incubated to 7 days on 1.8% agar plates with (+ ATc) or without 50 ng ml⁻¹ of ATc supplementation. Red bars indicate 1.6 cm.

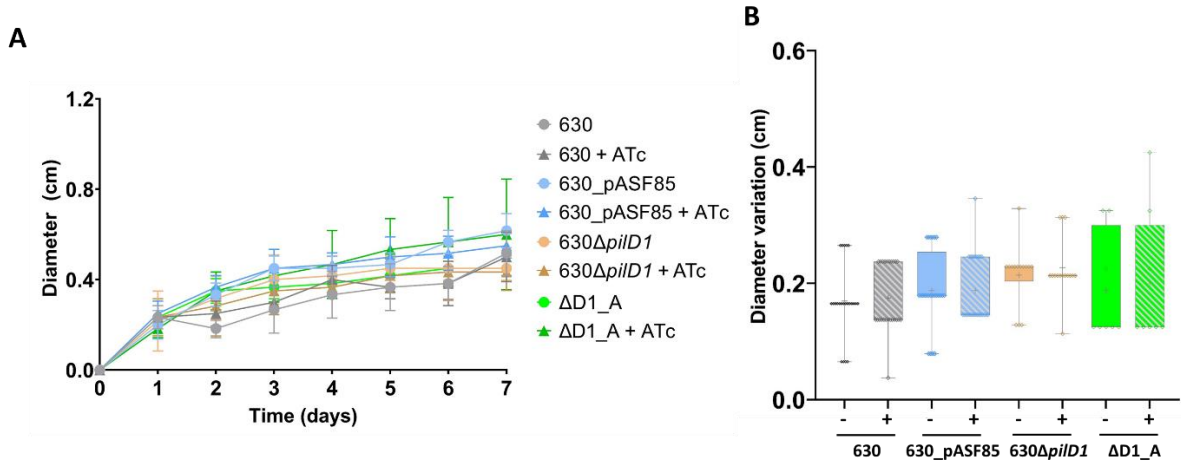


Figure B-14. Colony diameter in 1.8 % agar of 630Δ*pilD1* and vector controls

C. difficile CD630 (grey), 630_pASF85 (blue), 630Δ*pilD1* (orange) and 630Δ*pilD1*_pASF85 (ΔD1_A; green) samples were incubated on 1.8% agar plates. (A) Colony diameter was measured every 24 hours for 7 days without or with 50 ng ml⁻¹ of ATc supplementation. (B) Changes in colony diameter between Day 1 and Day 3 post-inoculation in the absence or supplementation (strip-shades) of ATc. Each replicate is represented as a diamond. One-way ANOVA analysis performed by Graphpad Prism. No significant phenotype is reported.

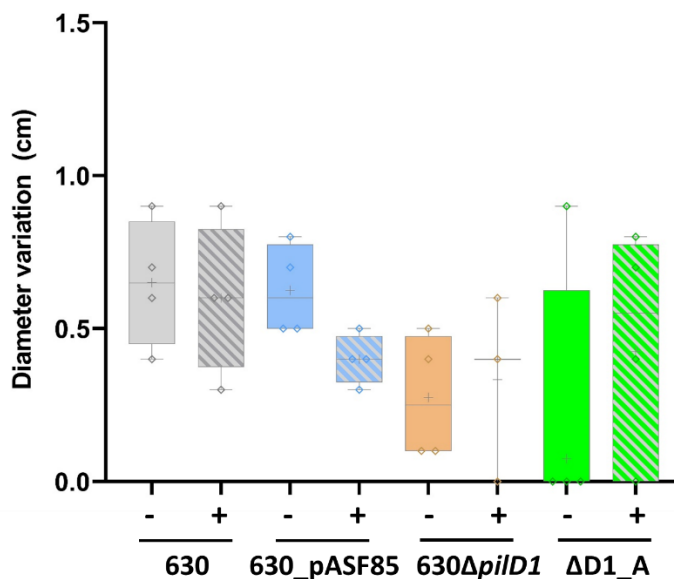
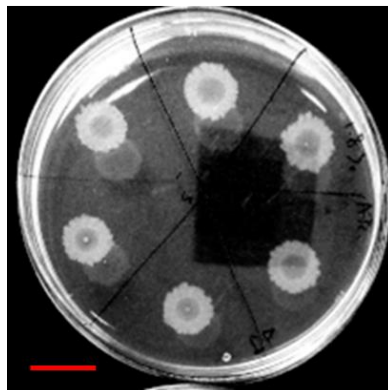
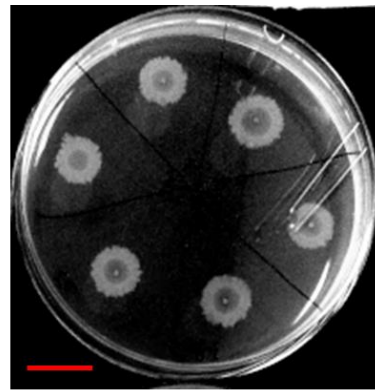


Figure B-15. Colony diameter variation in 0.3 % agar of Δ*pilD1* and complement strains

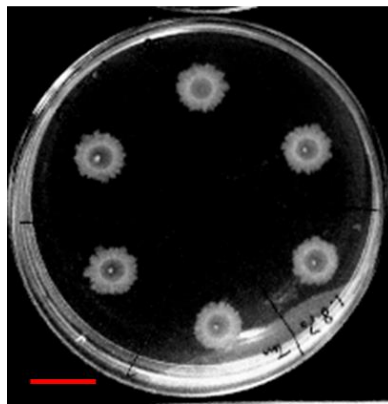
Flagella-mediated swimming motility assay, performed on 0.3% agar, either with (+) or without (-) ATc supplementation. CD630 (grey), 630_pASF85 (blue), 630Δ*pilD1* (orange) and 630Δ*pilD1*_pASF85 (ΔD1_A; green). Strip shades indicated samples under *dccA* induction (+ ATc). Each replicate is represented as a diamond. Significance analysed with one-way ANOVA in GraphPad Prism. No significant phenotype is reported.



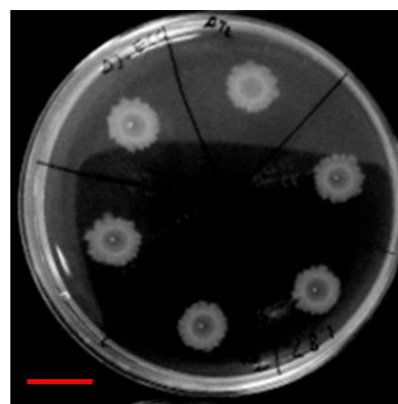
630 Δ *pilJ*



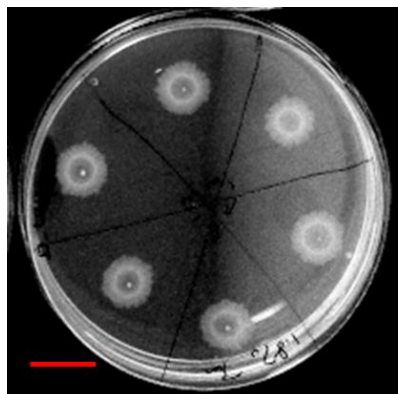
630 Δ *pilJ* + ATc



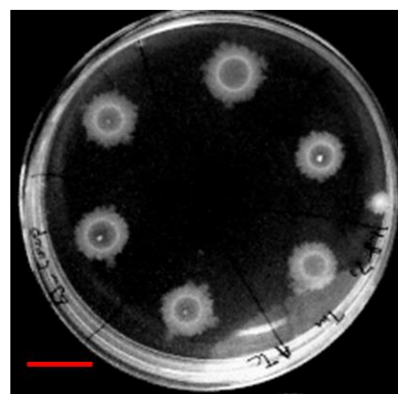
Δ J_E



Δ J_E + ATc



630 Δ *pilJc*



630 Δ *pilJc* + ATc

Figure B-16. Δ *pilJ* and complement colonies on 1.8 % agar plates

630 Δ *pilJ*, 630 Δ *pilJ*_pECC17 (Δ J_E) and 630 Δ *pilJ*_pZGW007 (Δ *pilJc*) colonies incubated to 7 days on 1.8% agar plates with (+ ATc) or without 50 ng ml⁻¹ of ATc supplementation. Red bars indicate 1.6 cm.

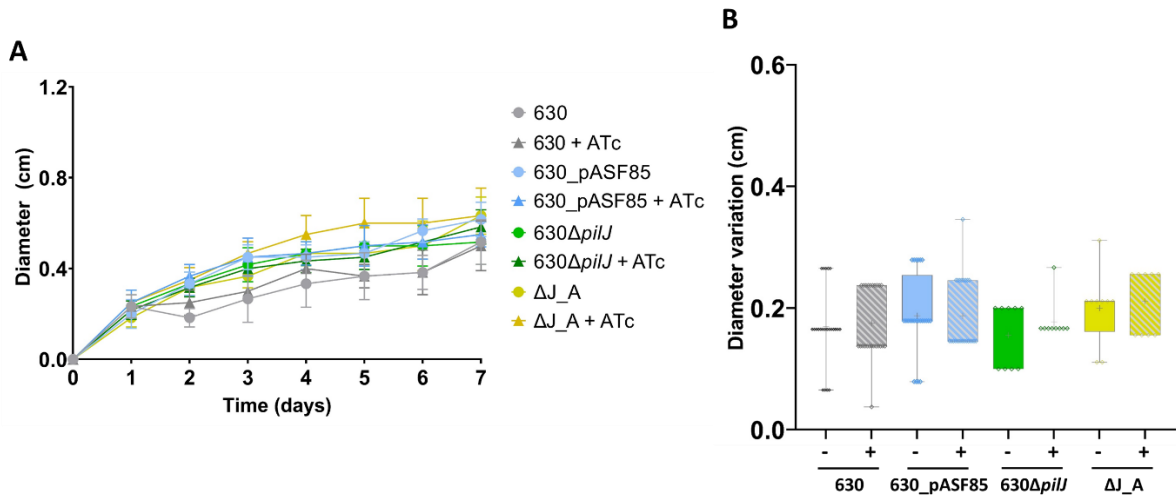


Figure B-17. Colony diameter in 1.8 % agar of 630ΔpilJ and vector controls

C. difficile CD630 (grey), 630_pASF85 (blue), 630ΔpilJ (green) and 630ΔpilJ_pASF85 (ΔJ_A; yellow) samples were incubated on 1.8% agar plates. (A) Colony diameter was measured every 24 hours for 7 days without or with 50 ng ml⁻¹ of ATc supplementation. (B) Changes in colony diameter between Day 1 and Day 3 post-inoculation in the absence or supplementation (strip-shades) of ATc. Each replicate is represented as a diamond. One-way ANOVA analysis performed by Graphpad Prism. No significant phenotype is reported.

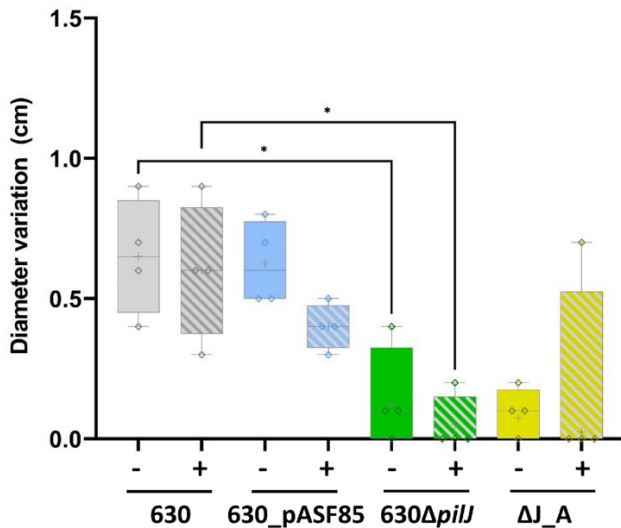


Figure B-18. Colony diameter variation in 0.3% agar of ΔpilJ and complement strains

Flagella-mediated swimming motility assay, performed on 0.3% agar, either with (+) or without (-) ATc supplementation. CD630 (grey), 630_pASF85 (blue), 630ΔpilJ (green) and 630ΔpilJ_pASF85 (ΔJ_A; green). Strip shades indicated samples under *dccA* induction (+ ATc). Each replicate is represented as a diamond. Asterisks '*' indicate P value < 0.1. Significance analysed with one-way ANOVA in GraphPad Prism.

Appendix C

Sequence variation analysis

Table C-1. Nucleotide similarities of 47 *C.difficile* isolates by BLAST

Strain	Gene	Cdi2_4	pilA1	pilU	pilV	pilK	pilJ	pilB1	pilT	pilC1	pilMN	pilO	pilD1	pilD2
DSM29745		99.65	92.65	99.43	99.65	99.81	97.89	99.76	99.45	99.34	99.94	99.67	99.85	99.62
Z31		99.82	98.84	99.24	99.82	99.55	98.13	99.46	99.35	99.67	99.71	99.34	99.4	99.36
W0003a		99.65	93.23	99.62	99.65	99.74	99.5	99.7	99.45	99.59	99.77	99.67	99.55	99.36
CD105001		98.07	91.9	98.67	98.07	98.18	99.75	99.7	98.89	98.68	98.72	98.9	99.7	97.7
DSM29688		100	98.84	99.43	100	99.87	97.89	99.7	99.35	99.75	99.77	99.56	99.4	99.23
DSM27639		100	100	100	100	100	100	100	100	100	100	100	100	100
630		100	100	100	100	100	100	100	100	100	100	100	100	100
630Aerm		100	100	100	100	100	100	100	100	100	100	100	100	100
W0022a		99.3	91.68	99.62	99.3	99.68	99.75	99.64	99.54	99.5	99.88	99.67	99.55	99.36
DSM29637		99.47	91.88	99.62	99.47	99.68	99.75	99.64	99.35	99.59	99.82	99.56	99.55	99.87
DSM28666		100	91.49	99.62	100	99.74	97.76	99.7	99.54	99.67	99.77	99.56	99.55	99.87
DSM29632		99.3	91.68	99.62	99.3	99.55	97.89	99.64	99.35	99.67	100	99.45	99.55	99.36
DSM28668		99.3	91.88	99.62	99.3	99.81	99.75	99.76	99.45	99.59	99.77	99.45	99.25	100
08-00495		99.65	94	99.43	99.65	99.55	98.01	99.58	99.35	99.67	99.82	99.34	99.7	99.49
09-00072		99.65	94	99.43	99.65	99.55	98.01	99.58	99.35	99.67	99.82	99.34	99.7	99.49
10-00071		99.65	94	99.43	99.65	99.55	98.01	99.58	99.35	99.67	99.82	99.34	99.7	99.49
10-00078		99.65	94	99.43	99.65	99.55	98.01	99.58	99.35	99.67	99.82	99.34	99.7	99.49
10-00253		99.65	94	99.43	99.65	99.55	98.01	99.58	99.35	99.67	99.82	99.34	99.7	99.49
12-00008		99.65	94	99.43	99.65	99.55	98.01	99.58	99.35	99.67	99.82	99.34	99.7	99.49
12-00011		99.65	94	99.43	99.65	99.55	98.01	99.58	99.35	99.67	99.82	99.34	99.7	99.49
CD-10-00484		99.65	94	99.43	99.65	99.55	98.01	99.58	99.35	99.67	99.82	99.34	99.7	99.49
CD-17-01474		99.65	94	99.43	99.65	99.55	98.01	99.58	99.35	99.67	99.82	99.34	99.7	99.49
DSM27638		99.65	94	99.43	99.65	99.55	98.01	99.58	99.35	99.67	99.82	99.34	99.7	99.49
DSM27640		99.65	94	99.43	99.65	99.55	98.01	99.58	99.35	99.67	99.82	99.34	99.7	99.49
DSM28196		99.65	94	99.43	99.65	99.55	98.01	99.58	99.35	99.67	99.82	99.34	99.7	99.49
RO104a		99.65	94	99.43	99.65	99.55	98.01	99.58	99.35	99.67	99.82	99.34	99.7	99.49
BI1		99.65	94	99.43	99.65	99.55	98.01	99.58	99.35	99.67	99.82	99.34	99.7	99.49
CD196		99.65	94	99.43	99.65	99.55	98.01	99.58	99.35	99.67	99.82	99.34	99.7	99.49
2007855		99.65	94	99.43	99.65	99.55	98.01	99.58	99.35	99.67	99.82	99.34	99.7	99.49
R20291		99.65	94	99.43	99.65	99.55	98.01	99.58	99.35	99.67	99.82	99.34	99.7	99.49
DH/NAP11		99.47	93.42	99.43	99.47	99.68	99.38	99.58	99.54	99.34	99.88	99.67	99.85	99.62
W0023a		99.47	93.42	99.43	99.47	99.68	99.38	99.58	99.54	99.34	99.88	99.67	99.85	99.62
DSM102859		99.12	92.44	99.05	99.12	98.64	98.26	98.99	99.17	98.59	99.07	98.46	99.1	97.06
DSM102860		99.12	92.44	99.05	99.12	98.64	98.26	98.99	99.17	98.59	99.07	98.46	99.1	97.06
BJ08		98.42	91.88	98.3	98.42	98.44	97.89	99.22	98.89	98.68	98.42	99.01	99.23	97.57
DSM29627		98.42	91.88	98.3	98.42	98.44	97.89	99.22	98.89	98.68	98.42	99.01	99.23	97.57
CF5		98.42	91.88	98.3	98.42	98.44	97.89	99.22	98.89	98.68	98.42	99.01	99.23	97.57
DSM28669		98.42	91.1	98.67	98.42	98.38	97.76	99.11	98.89	98.68	98.6	99.01	99.23	97.06
DSM29629		98.42	91.3	98.3	98.42	98.44	97.89	99.11	98.8	98.68	98.42	99.01	99.23	97.06
DSM28670		98.25	91.88	98.67	98.25	98.31	97.89	99.17	99.35	98.76	98.54	99.01	99.23	97.45
M120		95.96	91.88	95.64	95.96	95.84	95.52	97.61	98.43	97.85	98.07	98.46	97.54	94.89
12038		95.96	91.49	95.64	95.96	95.84	95.52	97.61	98.43	97.77	98.07	98.46	97.54	94.89
CD10010		95.96	91.49	95.64	95.96	95.84	95.52	97.61	98.43	97.77	98.07	98.46	97.54	94.89
CD21062		95.96	91.49	95.64	95.96	95.84	95.52	97.61	98.43	97.85	98.07	98.46	97.54	94.89
DSM29747		95.96	91.49	95.64	95.96	95.84	95.52	97.61	98.43	97.85	98.07	98.46	97.54	94.89
TW11		95.96	91.49	95.64	95.96	95.84	95.52	97.61	98.43	97.85	98.07	97.53	97.54	94.89
DSM29020		95.96	91.49	95.64	95.96	95.84	95.52	97.61	98.43	97.85	98.07	98.46	97.54	94.89

TFP genes in *C. difficile* 630 (CD630; Sebahia et al, 2006) were used as template for nucleotide similarity alignments in this study, which are listing in Appendix Table C-2. References of the 47 isolates can be found in Appendix Table C-3.

Table C-2. Template genes for nucleotide similarity BLAST

GENE	LOCUS TAG
<i>Cdi2_4</i>	170 bp from 4,105,967 to 4, 105,798
<i>pilA1</i>	CD630_35130
<i>pilB1</i>	CD630_35120
<i>pilC1</i>	CD630_35110
<i>pilMN</i>	CD630_35100
<i>pilO</i>	CD630_35090
<i>pilV</i>	CD630_35080
<i>pilU</i>	CD630_35070
<i>pilK</i>	CD630_35060
<i>pilT</i>	CD630_35050
<i>pilD2</i>	CD630_35040
<i>pilD1</i>	CD630_35030

Table C-3. References of isolates used in nucleotide similarity analysis

Clade	Ribotype	Strain name	Genome in GenBank	Genome Reference	PCR-ribotyping Reference
1	001	DSM29745	CP019857.1	Riedel et al., 2017	Riedel et al., 2017
		Z31	CP013196.1	Pereira et al., 2017	Pereira et al., 2016
	002	W0003a	CP025047.1	Yin et al., 2017	Yin et al., 2017
	007	DSM105001	CP028361.1	Schwanbeck et al., 2019	Schwanbeck et al., 2018
	010	DSM29688	CP019858.1	Riedel et al., 2017	Riedel et al., 2017
	012	DSM27639	CP011847.1	Gross et al., 2018	Gross et al., 2017
		630	AM180355.1	Sebahia et al., 2006	Riedel et al., 2017
		630Δerm	LN614756.1	Aslett and De Silva, 2014	Riedel et al., 2017
	014	W0022a	CP025046.1	Yin et al., 2017	Yin et al., 2017
	032	DSM29637	CP016106.1	Riedel et al., 2016	Riedel et al., 2017
	084	DSM28666	CP012321.1	Riedel et al., 2015	Riedel et al., 2017
	160	DSM29632	CP019860.1	Riedel et al., 2017	Riedel et al., 2017
228	DSM28668	CP012309.1	Riedel et al., 2015	Riedel et al., 2017	
2	027	08-00495	CP026594.1	Steglich et al., 2018	Steglich et al., 2018
		09-00072	CP026599.1	Steglich et al., 2018	Steglich et al., 2018
		10-00071	CP026596.1	Steglich et al., 2018	Steglich et al., 2018
		10-00078	CP026597.1	Steglich et al., 2018	Steglich et al., 2018
		10-00253	CP026598.1	Steglich et al., 2018	Steglich et al., 2018
		12-00008	CP026593.1	Steglich et al., 2018	Steglich et al., 2018
		12-00011	CP026595.1	Steglich et al., 2018	Steglich et al., 2018
		CD-10-00484	CP026592.1	Steglich et al., 2018	Steglich et al., 2018
		CD-17-01474	CP026591.1	Steglich et al., 2018	Steglich et al., 2018
		DSM27638	CP011846.1	Gross et al., 2018	Gross et al., 2017
		DSM27640	CP011848.1	Gross et al., 2018	Gross et al., 2017
		DSM28196	CP012320.1	Riedel et al., 2015	Riedel et al., 2017
		R0104a	CP025044.1	Yin et al., 2017	Yin et al., 2017
		BI1	NC_017179.1	He et al., 2010	Kurka et al., 2014
		CD196	CP059592.1	Masklanka et al., 2020	Gross et al., 2017
		2007855	FN665654.1	He et al., 2010	Gross et al., 2017
	R20291	CP029423.1	Riedel et al., 2018	Gross et al., 2017	
	106	DH/NAP11/106/ST-42	CP022524.1	Kocielek et al., 2017	Kocielek et al., 2017
		W0023a	CP025045.1	Yin et al., 2017	Yin et al., 2017
3	023	DSM102859	CP020378.1	Riedel et al., 2017	Riedel et al., 2017
	127	DSM102860	CP020379.1	Riedel et al., 2017	Riedel et al., 2017
4	017	BJ08	CP003939.1	Cheng et al., 2012	Wu et al., 2019
		DSM29627	CP016102.1	Riedel et al., 2017	Riedel et al., 2017
		CF5	NC_017173.1	He et al., 2010	Gross et al., 2017
	091	DSM28669	CP012323.1	Riedel et al., 2017	Riedel et al., 2017
	235	DSM29629	CP016104.1	Riedel et al., 2016	Riedel et al., 2017
	237	DSM28670	CP012312.1	Riedel et al., 2015	Riedel et al., 2017
5	078	M120	CP068555.1	te Vrugt and Minton, 2021	Gross et al., 2017
		12038	CP033214.1	Wu, 2018	Wu et al., 2019
		CD10010	CP033213.1	Wu, 2018	Wu et al., 2019
		CD21062	CP033216.1	Wu, 2018	Wu et al., 2019
		DSM29747	CP019864.1	Riedel et al., 2017	Riedel et al., 2017
		TW11	CP045224.1	Li, 2019	Li et al., 2020
	126	DSM29020	CP012325.1	Riedel et al., 2017	Riedel et al., 2017

Appendix D

C. difficile TFP predicted protein structures

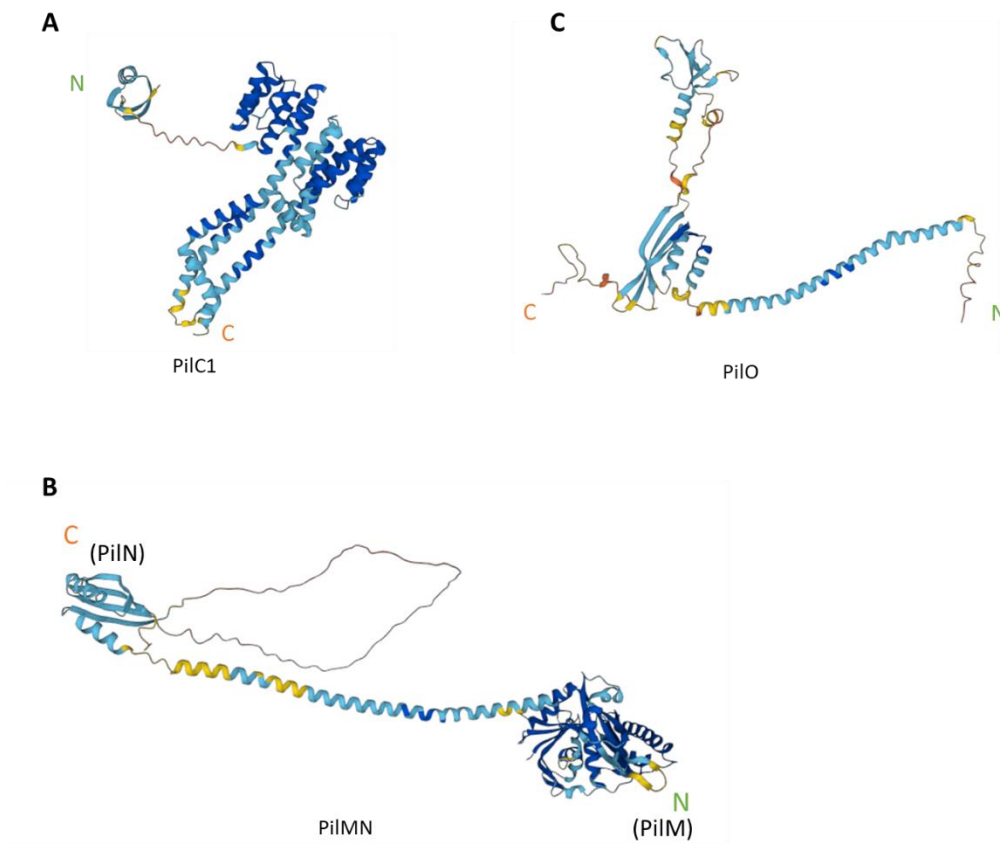


Figure D-1. *C. difficile* TFP platform proteins

Predicted TFP platform protein structures generated by AlphaFold (alphafold.ebi.ac.uk). (A) FliC1 according to gene CD3511, core protein. (B) FilMN according to gene CD3510. (C) FliO according to gene CD3509. C-termini are labelled in orange, N-termini are labelled in green.

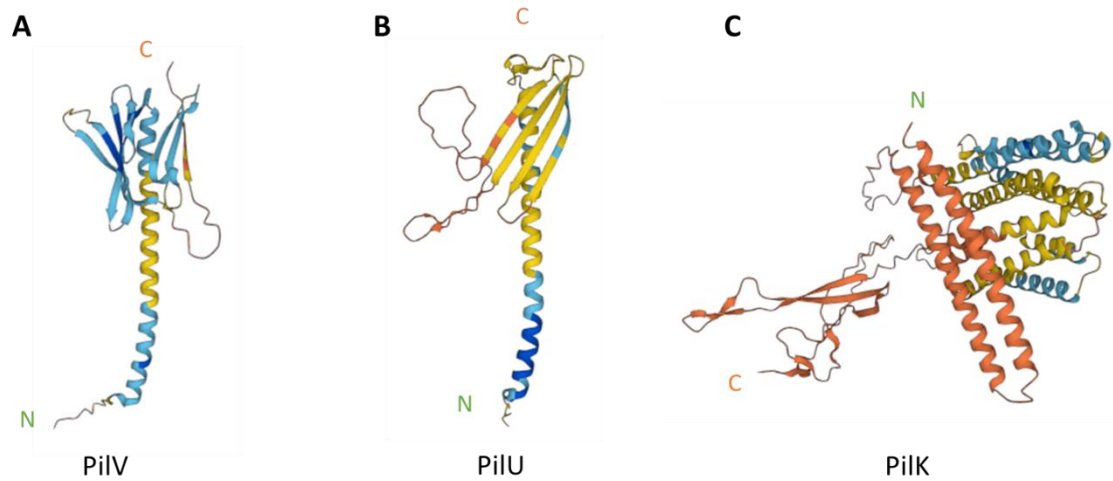


Figure D-2. *C. difficile* TFP minor pilins

Predicted protein structures of TFP minor pilins generated by AlphaFold (alphafold.ebi.ac.uk). (A) PilV according to gene CD3508, core protein. (B) PilU according to gene CD3507. (C) PilK according to gene CD3506, different shape to other pilins, suggested to be the cap of TFP filament. C-termini are labelled in orange, N-termini are labelled in green.

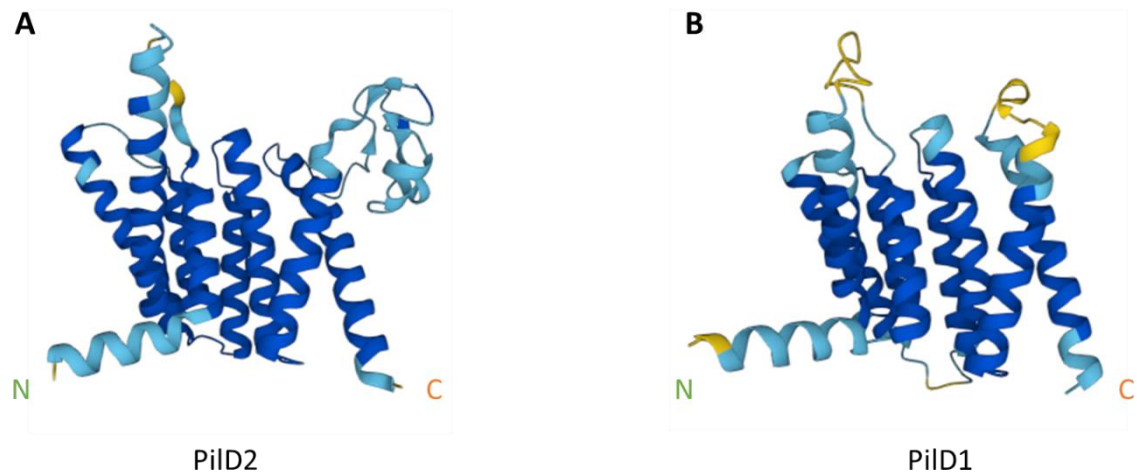


Figure D-3. *C. difficile* TFP pre-pilin peptidases

Predicted protein structures of TFP pre-pilin peptidases generated by AlphaFold (alphafold.ebi.ac.uk). (A) PilD2 according to gene CD3504. (B) PilD1 according to gene CD3503. C-termini are labelled in orange, N-termini are labelled in green.

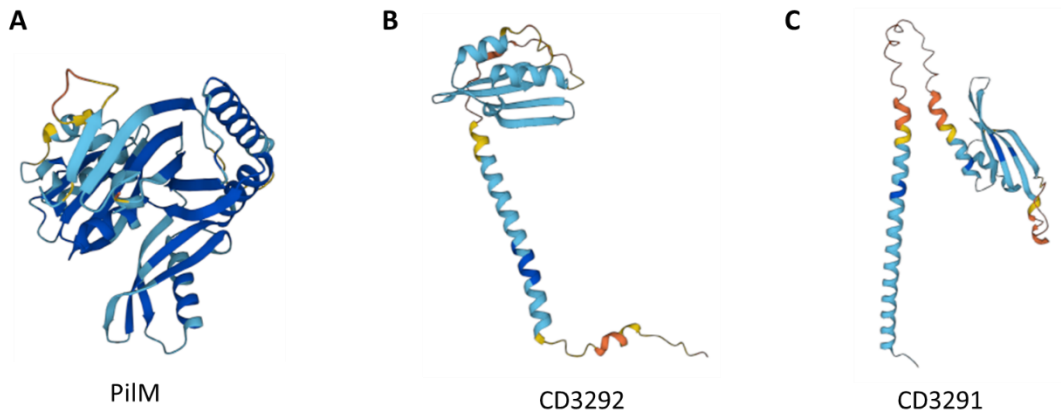


Figure D-4. *C. difficile* predicted TFP platform proteins on the secondary gene cluster

Predicted protein structures of PiIM (CD3293; A), CD3292 (B) and CD3291 (C) by AlphaFold

(alphafold.ebi.ac.uk). The three proteins are encoded in the TFP secondary gene cluster. CD3292 and CD3291 are analogous to PiIN and PiIO.

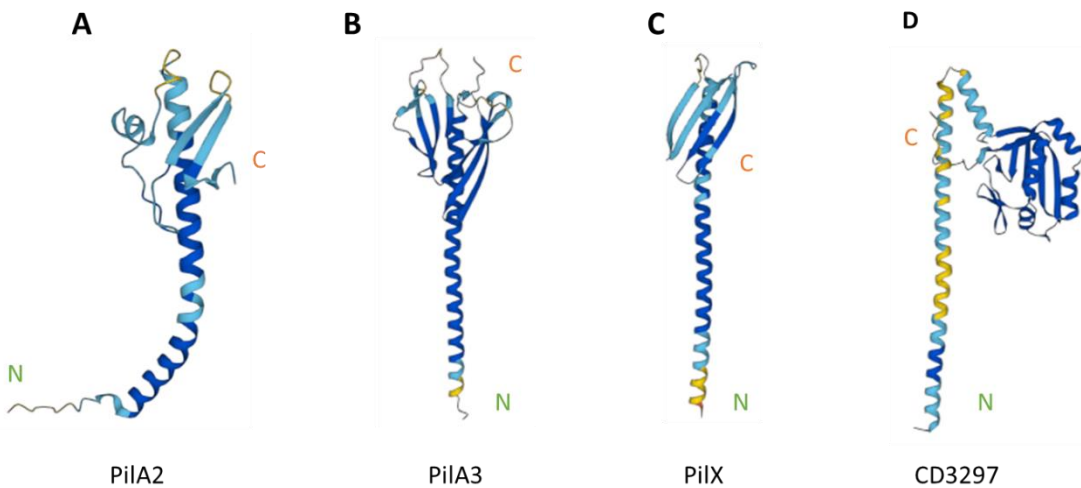


Figure D-5. *C. difficile* TFP minor pilins on other gene loci

Predicted protein structures of TFP minor pilins found in other gene loci by AlphaFold (alphafold.ebi.ac.uk). (A) PiIA2 (encoded by CD3294) in TFP secondary gene cluster. (B) PiIA3 encoded by CD1245. (C) PiIX encoded by CD1242. (D) CD3297 in TFP secondary gene cluster shows extending out C-terminal domain like PiIJ. C-termini are labelled in orange, N-termini are labelled in green.

Appendix E

Quantification data of western blots

Table E-1. Quantified band intensity of PilA1 signals from *C. difficile* 630 in Figure 3-7

630			
Lysate	Lysate + ATc	TCA	TCA + ATc
-0.38987	-0.303715374	0	-0.06392

630_pASF85			
Lysate	Lysate + ATc	TCA	TCA + ATc
1.960884	1.784698	0	-0.34878

630_pECC17			
Lysate	Lysate + ATc	TCA	TCA + ATc
37.17204	127.8184	27.04593	154.3028

Table E-2. Quantified band intensity of PIIA1 signals in figure 3-9

TCA										
	ECC17	ECC17+ATc	$\Delta A1_E$	$\Delta A1_E+ATc$	109	109+ATc	005	005+ATc	006	006+ATc
Repeat 1	-0.17725	4.005121	1.276948	1.74857	1.740306	5.630576	3.251881	3.486516	-0.77181	57.58548
Repeat 2	-0.87981	-0.74332	-0.53386	-0.43117	-0.17211	6.749089	0.258314	0.217752	0.288864	34.03223
Repeat 3	0.348109	2.916009	-0.02483	0.438631	0.122581	0.190372	0.353978	0.320045	1.076227	38.11607
Average	-0.23632	2.059269	0.239418	0.585343	0.563592	4.190012	1.288058	1.341438	0.19776	43.24459
Standard Deviation	0.616087	2.487455	0.933879	1.097251	1.029661	3.508648	1.701393	1.858397	0.927381	12.58631

Lysate										
	ECC17	ECC17+ATc	$\Delta A1_E$	$\Delta A1_E+ATc$	109	109+ATc	005	005+ATc	006	006+ATc
Repeat 1	0.238479	3.334029	0.448674	0.611862	0.581215	0.519018	0.200412	0.134305	-0.16102	17.83902
Repeat 2	2.516395	12.5085	-0.14026	-0.00184	0.297488	0.765215	0.523612	0.259024	14.5684	30.93358
Average	1.377437	7.921263	0.154207	0.305009	0.439351	0.642116	0.362012	0.196664	7.20369	24.3863
Standard Deviation	1.61073	6.487329	0.41644	0.433956	0.200625	0.174088	0.228538	0.08819	10.41527	9.259252

Table E-3. Quantified band intensity of PilA1 signals from *C. difficile* 630 *pilD1* mutant and complement strains in Figure 3-13

	Lysate					
	ECC17	ECC17+ATc	$\Delta D1_E$	$\Delta D1_E+ATc$	$\Delta D1c$	$\Delta D1c+ATc$
Repeat 1	15.46083	72.66799	0.65714	40.77377	0.311315	20.60001
Repeat 2	43.54502	70.02167	6.749749	80.8521	7.52114	97.44957
Repeat 3	19.14812	29.69838	5.90366	59.39542	7.70336	36.07402
Average	26.05132	57.46268	4.43685	60.34043	5.178605	51.37453
Standard deviation	15.26175	24.08097	3.300549	20.05587	4.216181	40.64533

	Lysate					
	ECC17	ECC17+ATc	$\Delta D1_E$	$\Delta D1_E+ATc$	$\Delta D1c$	$\Delta D1c+ATc$
Repeat 1	15.46083	72.66799	0.65714	40.77377	0.311315	20.60001
Repeat 2	43.54502	70.02167	6.749749	80.8521	7.52114	97.44957
Repeat 3	19.14812	29.69838	5.90366	59.39542	7.70336	36.07402
Average	26.05132	57.46268	4.43685	60.34043	5.178605	51.37453
Standard deviation	15.26175	24.08097	3.300549	20.05587	4.216181	40.64533

Table E-4. Quantified band intensity of PilA1 signals from *C. difficile* 630 *pilJ* mutant and complement strains in Figure 3-17

	TCA					
	ECC17	ECC17+ATc	ΔJ_E	ΔJ_E+ATc	ΔJc	$\Delta Jc+ATc$
Repeat 1	-0.36674962	24.50580814	1.557772	33.15101	5.462294	36.61605
Repeat 2	5.630597315	38.74126549	18.20894	50.94874	22.03172	0.671678
Repeat 3	-0.33608596	22.4323035	1.898378	16.01204	0.96965	16.17986
Average	1.642587246	28.55979238	7.221696	33.3706	9.487889	17.82253
Standard deviation	3.453752061	8.878155857	9.516755	17.46938	11.0931	18.0284

	Lysate					
	ECC17	ECC17+ATc	ΔJ_E	ΔJ_{E+ATc}	ΔJ_c	ΔJ_{c+ATc}
Repeat 1	15.46083	72.66799	3.628826	67.788	10.32917	40.65084
Repeat 2	43.54502	70.02167	42.74904	40.01397	140.9399	142.0474
Repeat 3	19.14812	29.69838	25.61719	28.77176	43.1161	44.53114
Average	26.05132	57.46268	23.99835	45.52458	64.79506	75.74312
Standard deviation	15.26175	24.08097	19.61029	20.08337	67.95053	57.45395

Table E-5. Quantified band intensity of FliC signals from *C. difficile* 630 in Figure 4-3

630			
Lysate	Lysate+ATc	TCA	TCA+ATc
16.76793	26.90838	239.5154	151.0097

630_pECC17			
Lysate	Lysate+ATc	TCA	TCA+ATc
18.41759	3.970845	88.32045	36.13717

630_pASF85			
Lysate	Lysate+ATc	TCA	TCA+ATc
36.62907	33.90446	64.30581	124.9761

Table E-6. Quantified band intensity of PliA1 signals from *C. difficile* 630 *pilA1* mutant and complement strains on 1.8% agar in Figure 4-8

TCA									
ECC17	ECC17+	$\Delta A1$	$\Delta A1+$	109	109+	005	005+	006	006+
1.661042	4.412146	-0.66176	-0.81524	-0.80674	-0.44813	-0.69576	-0.75637	4.945753	14.00752

Lysate									
ECC17	ECC17+	$\Delta A1$	$\Delta A1+$	109	109+	005	005+	006	006+
0.092483	-0.35676	-0.22287	0.237532	0.486502	0.385361	0.33106	0.603543	0.990539	9.621572

Table E-7. Quantified band intensity of FliC signals from *C. difficile* 630 *pilA1* mutant and complement strains on 1.8% agar in Figure 4-9

TCA									
ECC17	ECC17+	$\Delta A1$	$\Delta A1+$	109	109+	005	005+	006	006+
18.69386	7.628018	0.794656	1.540288	0.620295	-0.08721	0.313527	-0.34699	-0.50357	-0.61095

Lysate									
ECC17	ECC17+	$\Delta A1$	$\Delta A1+$	109	109+	005	005+	006	006+
-0.46285	-0.25777	0.152801	0.183122	19.12579	8.304736	6.562867	14.37959	0.322614	1.755337

Table E-8. Quantified band intensity of FliC signals from *C. difficile* 630 *pilA1* mutant and complement strains in culture in figure 4-11

TCA										
	ECC17	ECC17+ATc	$\Delta A1_E$	$\Delta A1_E+ATc$	109	109+ATc	005	005+ATc	006	006+ATc
Repeat 1	106.4727	9.46452	50.42834	6.094954	45.44083	7.007266	50.3637	13.70387	34.0662	4.376653
Repeat 2	40.72369	9.133421	51.67854	6.738566	8.596597	12.10834	35.5467	14.44593	39.68899	8.641503
Repeat 3	18.69386	7.628018	0.794656	1.540288	0.620295	-0.08721	0.313527	-0.34699	-0.50357	-0.61095
Average	55.29674	8.741987	34.30051	4.791269	18.21924	6.342799	28.74131	9.267603	24.41721	4.135733
Standard deviation	45.66793	0.978826	29.02365	2.833764	23.90955	6.124869	25.70972	8.334741	21.76437	4.630931

Lysate										
	ECC17	ECC17+ATc	$\Delta A1_E$	$\Delta A1_E+ATc$	109	109+ATc	005	005+ATc	006	006+ATc
Repeat 1	183.7623	4.474001	91.53466	4.601136	91.0443	9.126141	100.6205	6.122332	91.35725	5.400546
Repeat 2	98.35359	28.73546	51.23127	6.866932	18.56682	9.162305	100.8209	5.997691	105.1667	6.220128
Average	141.0579	16.60473	71.38296	5.734034	54.80556	9.144223	100.7207	6.060011	98.26195	5.810337
Standard deviation	60.39305	17.15544	28.4988	1.60216	51.24932	0.025572	0.141691	0.088134	9.764729	0.579532

Table E-9. Quantified band intensity of PilA1 signals from *C. difficile* 630 *pilD1* mutant and complement strains on 1.8% agar in Figure 4-14

TCA					
ECC17	ECC17+ATc	$\Delta D1_E$	$\Delta D1_E+ATc$	$\Delta D1c$	$\Delta D1c+ATc$
0.427917997	30.37966533	1.908226	2.329779	2.785328	2.140006

Table E-10. Quantified band intensity of FliC signals from *C. difficile* 630 *pilD1* mutant and complement strains on 1.8% agar in Figure 4-15

	TCA					
	ECC17	ECC17+ATc	$\Delta D1_E$	$\Delta D1_E+ATc$	$\Delta D1c$	$\Delta D1c+ATc$
Repeat 1	132.090662	86.90169	138.6683	126.0894	118.6876	140.538
Repeat 2	73.23884593	48.10833	76.58822	70.15286	65.81629	77.23274
Average	102.664754	67.50501	107.6283	98.12114	92.25193	108.8854
Standard deviation	41.61451822	27.43105	43.89725	39.55312	37.38564	44.76358

	Lysate					
	ECC17	ECC17+ATc	$\Delta D1_E$	$\Delta D1_E+ATc$	$\Delta D1c$	$\Delta D1c+ATc$
Repeat 1	0.50029	-0.24692	8.549593	0.255614	15.9121	0.722686
Repeat 2	0.541152	-0.2435	8.766568	0.177931	16.32862	0.777639
Average	0.520721	-0.24521	8.65808	0.216772	16.12036	0.750162
Standard deviation	0.028894	0.002417	0.153425	0.05493	0.294518	0.038858

Table E-11. Quantified band intensity of FliC signals from *C. difficile* 630 *pilD1* mutant and complement strains in culture in Figure 4-17

	TCA					
	ECC17	ECC17+ATc	$\Delta D1_E$	$\Delta D1_E+ATc$	$\Delta D1c$	$\Delta D1c+ATc$
Repeat 1	134.5783663	13.41398	105.0823	41.26198	148.8135	36.69209
Repeat 2	24.57124274	6.272277	1.387554	8.278343	85.14714	77.35874
Average	79.5748045	9.84313	53.23495	24.77016	116.9803	57.02541
Standard deviation	77.78678303	5.049949	73.32329	23.32295	45.01892	28.75566

	Lysate					
	ECC17	ECC17+ATc	Δ D1_E	Δ D1_E+ATc	Δ D1c	Δ D1c+ATc
Repeat 1	43.95171	0.571784	64.64387	7.561388	50.53087	3.29301
Repeat 2	38.8656	9.94323	74.93056	1.41401	69.99616	2.365498
Repeat 3	16.04677	5.401347	27.57822	1.572735	30.95413	2.47518
Average	32.95469	5.305454	55.71755	3.516044	50.49372	2.711229
Standard deviation	14.86189	4.686459	24.90623	3.504269	19.52104	0.506813

Table E-12. Quantified band intensity of PliA1 signals from *C. difficile* 630 *pilJ* mutant and complement strains on 1.8% agar in Figure 4-20

TCA					
ECC17	ECC17+ATc	Δ J_E	Δ J_E+ATc	Δ Jc	Δ Jc+ATc
0.427917997	30.37966533	1.52287	17.62749	0.361925	3.114677

Table E-13. Quantified band intensity of FliC signals from *C. difficile* 630 *pilJ* mutant and complement strains on 1.8% agar in Figure 4-21

	TCA					
	ECC17	ECC17+ATc	Δ J_E	Δ J_E+ATc	Δ Jc	Δ Jc+ATc
Repeat 1	132.090662	86.90169	73.21785	84.99064	93.08594	95.90019
Repeat 2	73.23884593	48.10833	40.65883	47.06261	51.40426	53.19844
Average	102.664754	67.50501	56.93834	66.02662	72.2451	74.54932
Standard deviation	41.61451822	27.43105	23.0227	26.81917	29.4734	30.1947

	Lysate					
	ECC17	ECC17+ATc	Δ J_E	Δ J_E+ATc	Δ Jc	Δ Jc+ATc
Repeat 1	0.50029	-0.24692	6.952651	3.58399	5.352984	2.768154
Repeat 2	0.541152	-0.2435	6.936625	3.645961	5.446271	2.832067
Average	0.520721	-0.24521	6.944638	3.614976	5.399627	2.800111
Standard deviation	0.028894	0.002417	0.011332	0.04382	0.065964	0.045193

Table E-14. Quantified band intensity of FliC signals from *C. difficile* 630 *pilJ* mutant and complement strains in culture agar in Figure 4-21

TCA					
ECC17	ECC17+ATc	Δ J_E	Δ J_E+ATc	Δ Jc	Δ Jc+ATc
53.90293377	8.030018	45.11092	5.559198	19.29806	0.591999

Lysate					
ECC17	ECC17+ATc	ΔJ_E	ΔJ_E+ATc	ΔJc	$\Delta Jc+ATc$
43.95171	0.571784	57.57256	2.09089	56.63493	1.10291